



THE UNIVERSITY OF
WAIKATO
Te Whare Wānanga o Waikato

Research Commons

<http://researchcommons.waikato.ac.nz/>

Research Commons at the University of Waikato

Copyright Statement:

The digital copy of this thesis is protected by the Copyright Act 1994 (New Zealand).

The thesis may be consulted by you, provided you comply with the provisions of the Act and the following conditions of use:

- Any use you make of these documents or images must be for research or private study purposes only, and you may not make them available to any other person.
- Authors control the copyright of their thesis. You will recognise the author's right to be identified as the author of the thesis, and due acknowledgement will be made to the author where appropriate.
- You will obtain the author's permission before publishing any material from the thesis.

Supercapacitor Assisted LED (SCALED) Converter Technique for Solar Powered DC-Microgrids

A thesis

submitted in fulfilment

of the requirements for the degree

of

Doctor of Philosophy in Electronics Engineering

at

The University of Waikato

by

Udathenne Gedara Dilini Udeshika Kumari Jayananda



THE UNIVERSITY OF
WAIKATO
Te Whare Wānanga o Waikato

October 2020

Abstract

Designing electronic products and systems with high energy efficiency is a major challenge for electronic power circuit designers. Almost all residential and industrial buildings are presently AC powered. However, they contain electronic equipment that is internally dependent on a bulk DC power rail with multiple DC-DC converters or DC-AC converters to supply motors controlled by variable speed drives. The overall efficiency of an electronic device with multiple voltage converters is determined by the product of the efficiencies of the individual conversion stages. Thus, overall efficiency drops drastically with the number of converter stages. However, with renewable energy sources such as photovoltaic solar cells generating DC electricity, we can eliminate the first AC-DC converter and reduce the number of converter stages, to achieve a significant rise in end-to-end efficiency. This is the motivation for the DC-microgrid concept. DC-microgrids are local energy networks consisting of renewable energy sources and storage systems.

Although power generation using solar energy is economical, designers have to cope with frequent fluctuations in irradiance and temperature and the non-availability of solar energy at night. Accordingly, there is a need for energy storage for reliable operation. The most common energy storage device used in solar power-based systems is the rechargeable battery pack, typically based on lead-acid and lithium-ion chemistries. However, all rechargeable batteries have limited charge-discharge life cycles as well as calendar lives, and are environmentally unfriendly. With the continuous developments of supercapacitor materials and manufacturing techniques over the last decade, it is now possible to adopt supercapacitors as short-term energy storage devices in solar powered DC-microgrids to replace electrochemical battery packs. When supercapacitors are used in solar power-based DC-microgrid environments, there is the possibility of directly operating “white goods” (such as washing machines, refrigerators, dishwashers and air conditioners) and lighting. However, if a supercapacitor bank is used as the sole energy storage, existing maximum power point tracking schemes are no longer appropriate. This is because the storage bank acts as a near-ideal capacitor, so its impedance depends on its state of charge, unlike a rechargeable battery pack with internal resistance.

The supercapacitor assisted LED lighting (SCALED) converter is a new circuit topology that can be applied to solar powered DC-microgrids. This topology has been developed specially for low voltage LED lighting systems where a supercapacitor bank is used as an efficient energy storage device instead of a battery bank. The SCALED converter is another extension of the supercapacitor assisted loss management concept developed by the Power Electronics research team at the University of Waikato. This thesis presents details of this SCALED conversion system, developed for the Ports of Auckland DC-microgrid lighting systems, including theory and experimental efficiency measurements.

Preface

The power electronic research team at The University of Waikato uses supercapacitors in non-traditional applications. Rather than using a supercapacitor as a complement to conventional energy storage media, the research team lead by the Associate Professor Nihal Kularatna employs supercapacitors in applications such as (a) high-efficiency and extra-low-frequency DC-DC converters (SCALDO); (b) high performance surge protector circuits (SCASA); (c) Water heating apparatus (SCATMA); and (d) high performance inverters (SCADHI). These circuits are currently known as supercapacitor assisted (SCA) circuits. All these applications are based on the Supercapacitor Assisted Loss Management (SCALOM) concept. In 2014, the research team identified that the SCALOM concept can be extended to PV based DCMG area. This research is based on the extension of SCALOM concept to DC-microgrid.

This thesis is submitted in partial fulfilment of the requirement for obtaining the PhD degree at the University of Waikato, Hamilton, New Zealand. The work was carried out during the period from September 2016 until June 2020 and was supervised by Associate Professors Nihal Kularatna and D. Alistair Steyn-Ross. This work was supported by the Ports of Auckland Limited DC-microgrid research.

Thesis Structure

This thesis outlines the design and the analysis of the supercapacitor assisted LED lighting (SCALED) converter. The chapters as follows.

- Chapter 1 presents a general overview of renewable energy sources and the state of the art in DC-microgrids, solar photovoltaic-based systems, electrochemical batteries and maximum power point tracking techniques used in photovoltaic systems.
- Chapter 2 provides an overview of the electrical double layer concept, commercially available supercapacitors and non-traditional applications of supercapacitors (supercapacitor assisted techniques).
- Chapter 3 introduces the fundamentals of the loss circumvention concept applied to an RC charging loop and how it is extended to the SCALED technique.
- Chapter 4 presents an overview of different lighting technologies and operational details of LED lamps.
- Chapter 5 introduces the basic concept of the SCALED technique, implementation details of the SCALED converter and its application in a Ports of Auckland DC-microgrid container. This chapter also provides the experimental results for the SCALED converter and the overall performance of the converter in terms of efficiency.

- Chapter 6 explains the essential theory of supercapacitor energy circulation in a SCALED converter,an presents the analytical and experimental results. This chapter also discusses the reasons why existing maximum power point tracking (MPPT) controllers cannot be used with the SCALED converter and the remedy for these issues.
- Chapter 7 discusses the extended applications of the SCALED concept.
- The conclusion summarises the results of this research and provides suggestions for future research.

Original Contributions

I consider myself lucky to have been part of such a brilliant research team! Listed below are the publications made as a part of this research i.e. conference papers and journal papers. These are the original contributions by the author during the course of the PhD study.

Journal papers

- D. Jayananda, N. Kularatna, and D.A. Steyn-Ross, “Supercapacitor Assisted LED (SCALED) technique for renewable energy systems: A very low frequency design approach with short-term DC-UPS capability eliminating battery banks”, IET Renewable Power Generation Journal, vol.14, issue 9, pp. 1559-1570, July 2020.
- N. Kularatna, D. Jayananda, “Supercapacitor Based Long Time Constant Circuits: A Unique Design Opportunity for New Power Electronic Circuit Topologies”, in IEEE Industrial Electronics Magazine, vol.14, no.2, pp. 40-56, June 2020.

Peer-reviewed conference papers

- D. Jayananda, N. Kularatna, and D. A. Steyn-Ross, “A Validity of MPPT Technique Using Supercapacitors as Energy Storage Devices: Example of the SCALED converter technique,”, in 45th Annual Conference of the IEEE Industrial Electronics Society 2019 (IECON), Lisbon, Portugal, 2019, pp. 2301-2306.
- D. Jayananda, N. Kularatna, and D. A. Steyn-Ross, “Supercapacitor Assisted LED lighting (SCALED) for DC-micro grids,”, in 2019 IEEE Third International Conference on DC Microgrids (ICDCM), 2019 to be published.
- D. Jayananda, N. Kularatna, and D. A. Steyn-Ross, “Performance Characteristics of Energy Efficient LED Lamps Leading to Supercapacitor Assisted LED (SCALED) Technique for DC-microgrid Applications,”, in 20th IEEE International conference on Industrial Technology 2019 (ICIT), Feb 2019, pp. 515-520.
- D. Jayananda, N. Kularatna, and D. A. Steyn-Ross, “Powering 12-V LED luminaries with supercapacitor-based energy storage in DC-microgrid systems,”, in 44th Annual Conference of the IEEE Industrial Electronics Society 2018 (IECON), Oct 2018, pp. 1922-1927.
- D. Jayananda, N. Kularatna, and D. A. Steyn-Ross, “Design Approach for Supercapacitor Assisted LED lighting (SCALED) technique for DC-microgrids”, in 2018 IEEE International Conference on Industrial Electronics for Sustainable Energy Systems (IESES), Jan 2018, pp. 27-31.
- T. Ariyaratna, D. Jayananda, N. Kularatna and D. A. Steyn-Ross, “Potential of supercapacitors in novel power converters as semi-ideal lossless voltage droppers”, IECON 2017 - 43rd Annual Conference of the IEEE Industrial Electronics Society, Beijing, 2017, pp. 1429-1434.

Acknowledgements

I wish to express my utmost gratitude for the help and guidance I received from my supervisory panel, Associate Professor Nihal Kularatna and Associate Professor D. Alistair Steyn-Ross, throughout this project.

My special thanks and appreciation also go to:

- Prof Jonathan Scott and all the technical and administration staff of the School of Engineering at the University of Waikato
- The team led by the sustainability manager of Ports of Auckland Ltd (POAL), Rosie Mercer
- WaikatoLink Ltd staff
- My colleagues in the power electronics research group
- All my other friends and family in Hamilton

Dedication

I dedicate this thesis—

To my husband Thilina

To my daughter Rinee

To my mother Mrs Chandani Gawarathenna

To my father Mr U.G. Jayananda

And to my brother Dinuka Jayananda

You have all been most patient...

Contents

Abstract	i
Preface	iii
Original Contributions	v
Acknowledgements	vi
Dedication	vii
List of Figures	xiii
List of Tables	xvii
Acronyms and Abbreviations	xix
Chapter 1 Introduction	1
1.1 Solar Energy	2
1.1.1 Photovoltaic (PV) Cell Model: Approximation of PV cell V-I characteristics	5
1.2 Motivation for DC-Microgrids	9
1.2.1 DC Microgrid Reference Architectures	10
1.3 Photovoltaic (PV) Systems	13
1.3.1 Grid-connected PV systems	14
1.3.2 Off-Grid PV systems	15
1.4 Energy Storage Devices (ESDs) in PV Systems	15
1.4.1 Overview of Electrochemical Batteries	16
1.4.2 Ragone Plot	18
1.5 Maximum Power Transfer Techniques	19
1.5.1 A review of the Maximum Power Transfer concept	20
1.5.2 Summary of Existing Maximum Power Point Tracking (MPPT) Techniques	21
1.6 Chapter Summary	24
Chapter 2 Overview of Supercapacitors and Supercapacitor Assisted (SCA) Techniques	27
2.1 Electrical Double Layer concept leading to Supercapacitor Technology	27
2.2 Supercapacitor (SC) Fundamentals	28
2.3 Comparison of Commercially Available Supercapacitors	32
2.3.1 Constant resistance discharge	33

2.3.2	Constant current discharge	33
2.4	Traditional Applications of Supercapacitors	35
2.5	Non-Traditional Applications of Supercapacitors: SCA Techniques from an Application viewpoint	37
2.5.1	Supercapacitor assisted low drop-out (SCALDO) regulator	38
2.5.2	Supercapacitor assisted surge absorber (SCASA)	39
2.5.3	Supercapacitor assisted temperature modification apparatus (SCATMA)	41
2.5.4	Supercapacitor assisted high density inverter (SCADHI)	42
2.5.5	Supercapacitor assisted LED (SCALED) lighting converter	43
2.6	Supercapacitor models and equivalent circuits	43
2.7	Chapter Summary	44
Chapter 3 Generalized Loss Circumvention Concept Applied to RC Charging Circuit Leading to SCA Techniques		45
3.1	Analysis of a modified RC charging loop and the supercapacitor assisted loss management concept (SCALOM)	45
3.1.1	Capacitor charging behaviour of an RC circuit leading to the loss circumvention concept (LCC)	45
3.1.2	Capacitor charging behaviour of a modified RC loop	47
3.2	Applications of the SCALOM concept	52
3.2.1	Supercapacitor assisted low drop-out (SCALDO) regulator	52
3.2.2	Supercapacitor assisted surge absorber (SCASA) technique	52
3.2.3	Supercapacitor assisted temperature modification apparatus (SCATMA) technique to provide rapid hot-water at domestic water faucets	53
3.2.4	Supercapacitor assisted high density inverter (SCAHDI)	53
3.3	Supercapacitor assisted loss circumvention concept leading to supercapacitor assisted LED (SCALED) lighting converter	53
3.4	Chapter Summary	54
Chapter 4 Operational Details of commercial LED lamps		55
4.1	Comparison of lighting technologies	55
4.1.1	Incandescent lamps	55
4.1.2	Halogen lamps	56
4.1.3	Fluorescent lamps (FL)	56
4.1.4	LED lamps	57
4.2	LED luminaires	58
4.2.1	Line voltage operable LED lamps	60
4.2.2	Low voltage LED luminaires	62
4.3	Practical operational region of low voltage LED luminaires	62
4.3.1	Current-voltage characteristics	62
4.3.2	Luminance-voltage characteristics	64
4.3.3	Power-voltage characteristics	65
4.4	Chapter Summary	66

Chapter 5	Supercapacitor assisted LED lighting (SCALED) converter for DC-microgrids	67
5.1	Basic concept	67
5.2	Design considerations	68
5.2.1	SCALED converter: Proof-of-concept	69
5.2.2	Design of a prototype SCALED system	75
5.2.3	Initial charging phase of the supercapacitor banks	77
5.2.4	Power supply design for SCALED controller	81
5.3	Remedy for MOSFET body diode effect in SCALED converter	87
5.3.1	Possible solutions and limitations	87
5.4	Application of SCALED in POAL DC-Microgrid container	90
5.4.1	Field results of SCALED converter	91
5.5	Loss estimation of SCALED implementation	94
5.5.1	Equivalent series resistance (ESR) and leakage current losses in the supercapacitors	94
5.5.2	Losses due to switches	95
5.5.3	Losses of the parasitics in the circuit	95
5.5.4	Control circuit power consumption	95
5.6	SCALED loss measurement	97
5.7	Efficiency comparison	98
5.8	SCALED Advantages	99
5.9	Chapter Summary	99
Chapter 6	Theoretical foundation, analysis and simulation of the SCALED converter	101
6.1	Analysis of the charging phase of a SCALED converter	101
6.1.1	Case A: Neglecting parasitic resistance r_{Pc}	102
6.1.2	Case B: Including parasitic resistance r_{Pc}	103
6.2	Analysis of the discharging phase of a SCALED converter	103
6.3	Simulation of SCALED converter	107
6.4	Feasibility of replacing a battery pack with supercapacitors	109
6.4.1	Input impedance of switch mode DC-DC converters	109
6.5	SCALED converter with battery bank and MPPT charge controller	118
6.6	MATLAB Simulink simulation of SCALED converter with battery bank and MPPT controller	120
6.7	Chapter Summary	124
Chapter 7	Extended application of SCALED concept	125
7.1	24 V LED luminaires	126
7.2	Flood lights	127
7.3	Extension of the SCALED concept into white goods	127
7.4	Chapter Summary	130

Chapter 8	Conclusions and Recommendation	131
8.1	Summary	131
8.2	Conclusions	132
8.3	Recommendations and Future work	133
Appendix A	Schematic, PCB layouts and PIC codes of SCALED converter prototypes	135
A.1	Schematic and PCB Layout for SCALED Converter Power Stage	135
A.2	Schematic and PCB Layout for SCALED Converter controller	138
A.3	PIC code for SCALED controller	141
A.4	PIC code for SCALED start-up circuit	145
Appendix B	MATLAB and Spice Simulation of SCALED converter	147
B.1	Curve fitting for LED characteristics	147
B.2	MATLAB Script for Charging Loop of SCALED converter	150
B.3	MATLAB Script for Charging Loop of SCALED converter with parasitic resistance	152
B.4	MATLAB Script for Charging Loop of SCALED converter with parasitic resistance and solar panel	154
B.5	MATLAB Script for Discharging Loop of SCALED converter	156
B.6	MATLAB Script for Discharging Loop of SCALED converter with parasitic resistance	158
B.7	MATLAB Script for SCALED converter	160
B.8	Simulink model of SCALED converter with battery bank and MPPT controller .	162
B.9	MATLAB Script for MPPT controller in Simulink model	164
B.10	MATLAB Script for SCALED controller in Simulink model	165
B.11	Spice Net list for SCALED converter	166
	B.11.1 Voltage-controlled switch in LTSpice	166
	B.11.2 Net list for SCALED converter with solar model	170
Appendix C	MATLAB codes	173
C.1	Loss circumvention concept	173
References		175

List of Figures

1.1	Linear concentrator systems	3
1.2	Power tower systems	3
1.3	Solar dish system	4
1.4	Inside of a PV cell	5
1.5	Simplified equivalent circuit of solar cell	6
1.6	Solar cell model with series ohmic losses	7
1.7	Model with ohmic losses	9
1.8	Energy flow within a typical electronic product or system	11
1.9	Microgrid reference architectures	12
1.10	Existing PV systems: (a) Typical grid-connected PV system; (b) Off-grid PV AC-system; (c) Off-grid PV DC-system	14
1.11	Midpoint voltage and the voltage plateau for a rechargeable battery	18
1.12	Ragone plot of batteries and supercapacitors	19
1.13	Characteristics curves of a solar PV panel	20
1.14	DC supply with external load connected	21
1.15	Flow chart for constant voltage (CV) method	22
1.16	Flow chart for the perturb and observe (P&O) method	23
1.17	Flow chart for the incremental conductance (IC) method	25
2.1	Concept of an EDLC capacitor formed by double layers at each electrode: (a) Conceptual electrochemical capacitor; (b) Charged and discharged condition	28
2.2	Cross-section of a porous carbon electrode	29
2.3	Multilayer cylindrical LSmttron supercapacitor	30
2.4	Variation of internal resistance of a 3000 F, 2.7 V EDLC supercapacitor and an Energizer 6 V battery with percentage discharge	31
2.5	Comparison of electrolytic capacitors and supercapacitors	32
2.6	Three different supercapacitor families	33
2.7	Discharge curves for different SC technologies - Under constant resistance (Devices tested were 3000 F , 2.7 V ELDC SC, 7000 F, 2.7 V Hybrid SC and 40000 F, 2.8 V CAPAbattery respectively)	34
2.8	Constant current discharge curve for hybrid and CAPAbattery SCs	36
2.9	Variation of Average life cycle for batteries and SCs with Depth of Discharge	37

2.10	SCALDO converter: (a) SC bank charging while minimizing series dissipation; (b) Releasing stored energy in the SC bank	38
2.11	The simplified version of SCASA	40
2.12	Comparison of energy lost and stored for electrolytic capacitors and SCs subjected to a 6 kV, 50 μ s pulse	40
2.13	The implementation block diagram of the SCATMA technique	41
2.14	The simplified concept of the SCADHI technique: (a) overall inverter block; (b) block diagram of SCADHI	43
2.15	Supercapacitor models: (a) simplified first order model; (b) First order model; (c) RC equivalent circuit of a supercapacitor to illustrate the basic operation of a single cell	44
3.1	<i>RC</i> charging loop: (a) Basic <i>RC</i> loop; (b) Modified <i>RC</i> loop with loss circumvention concept (LCC)	46
3.2	<i>RC</i> circuit with pre-charged capacitor and over-rated DC voltage source	47
3.3	Variation of charging efficiency with over-rated factor m and pre-charged factor k	49
3.4	Modified case of <i>RC</i> circuit with pre-charged capacitor and over-rated DC voltage source	49
3.5	Graphical representation of circuit behaviour in terms of efficiency versus m (over-rated or over-voltage factor) and k (pre-charged factor)	51
3.6	Variation of charging efficiency	51
3.7	Modified <i>RC</i> charging loop with LED lamp	53
4.1	Types of solid-state lightings and their applications	56
4.2	Energy saving vs consumption for common lighting technologies	58
4.3	Simple structure of an LED device	59
4.4	Typical residential LED lamp construction	60
4.5	Generalized line voltage operable LED luminaire driver circuit with transient and surge protection devices	61
4.6	Typical low voltage operable LED luminaire internal circuitry	63
4.7	Test set-up used for the experiment	63
4.8	Current-voltage characteristics for 5 commercially available LED lamps	64
4.9	Variation of illuminance with voltage for 5 commercially available LED lamps	64
4.10	Power-voltage characteristics for 5 commercially available LED lamps	65
4.11	DC voltage reversal capability of Philips 5:5 W LED lamps	65
5.1	Concept of proposed SCALED converter: (a) Modified <i>RC</i> charging loop with LED lamp; (b) Voltage waveforms for SC bank and LED lamp load	68
5.2	Existing solar-powered LED lighting systems	69
5.3	Proposed concept of SCALED converter for solar-powered DC microgrids: Simplified block diagram	69
5.4	Current-voltage characteristics for Philips 5.5 W LED lamp in the constant brightness region	70

5.5	Basic SCALED converter (proof of concept)	70
5.6	Proof of concept: (a) Schematic diagram of basic SCALED converter; (b) Oscilloscope waveforms of the basic SCALED converter at input of 22 V	72
5.7	Brightness of the Philips 5.5 W LED lamp during SCALED operation	73
5.8	Basic SCALED converter (proof of concept)	73
5.9	The proposed SCALED converter with three operational configurations	76
5.10	<i>CSUN250 – 60P</i> PV panel characteristics curves [103]	77
5.11	Initial charging phase of the SCALED converter	78
5.12	High side switching of a MOSFET	79
5.13	P-channel MOSFET driver circuit	80
5.14	A compact version of SCALED converter: (a) Power stage circuit board; (b) Control circuit board	80
5.15	The flow-chart of the PIC algorithm	82
5.16	Circuit diagram of 10 V SCALDO regulator	83
5.19	5 V transformer isolated power supply test results at a load current of 100 mA	87
5.20	MOSFET body diode effect on SCALED converter	88
5.21	N-channel MOSFET blocking the body-diode effect	88
5.22	Laboratory test results of modified SCALED converter: (a) With 11 W LED lamp load; (b) With 22 W LED load	89
5.23	Operational behaviour of SCALED converter with PV panel connection	91
5.24	Simplified block diagram of implemented SCALED converter	92
5.25	Operational behaviour of SCALED converter installed in POAL DC microgrid container	93
5.26	Comparison of measured and estimated power losses of the SCALED prototype	97
5.27	Comparison of charging efficiency between direct SC bank replacing battery pack and SCALED converter	98
6.1	Basic configurations of the SCALED converter: (a) SC charging phase; (b) SC discharging phase	101
6.2	Simulation results for the charging phase of a SCALED converter	105
6.3	Simulation results for the discharging phase of a SCALED converter	106
6.4	LTSpice model of SCALED converter used for simulation	107
6.5	Simulation results for SCALED converter: (a) MATLAB simulation results; (b) Spice simulation results	108
6.6	Block diagram of loaded switched mode DC-DC converter	109
6.7	Variation of input resistance r_{in} of a switching converter with duty cycle ratio D	110
6.8	Buck converter with resistive load is buffered by a battery bank	110
6.9	Buck converter with a capacitor at the output: (a) Parallel connection; (b) Series connection	111
6.10	Variation of r_{in} for a buck converter with a capacitor at the output	114
6.11	Series connection of pre-charged capacitor	115

6.12	Variation in r_{in} for buck converter with SCALED converter (for different duty cycles)	117
6.13	5 W LED PHILIPS lamp characteristics	117
6.14	Buck converter with SCALED circuit buffered by a battery	118
6.15	Variation of r_{in} for buck converter with SCALED circuit buffered by a battery pack	119
6.16	Variation of voltages and currents of two SC banks (MATLAB Simulink results of SCALED converter with battery bank and MPPT controller)	121
6.17	Variation of voltages and currents of two LED lamp banks (MATLAB Simulink results of SCALED converter with battery bank and MPPT controller)	122
6.18	Behaviour of the PV panel (MATLAB Simulink results of SCALED converter with battery bank and MPPT controller)	123
6.19	Comparison of estimated and measured output power levels of PV panels	124
7.1	Extension of SCALED concept to other applications	125
7.2	Variation of brightness and current of a 24 V PHILIPS with applied voltage	126
7.3	Variation of brightness in flood lamps with applied voltage	128
7.4	Current voltage characteristics of the compressor	129
7.5	Basic circuit designed based on SCALED concept to power up DC refrigerator	129
A.1	Schematic for SCALED Power Stage	136
A.2	PCB layout for SCALED Power Stage	137
A.3	Schematic for SCALED control circuit	139
A.4	PCB layout for SCALED control circuit	140
B.1	Simulink model of SCALED converter with battery bank and MPPT controller	163
B.2	Schematic diagram for example 1	167
B.3	Voltage source characteristics	167
B.4	Volatge across R1	168
B.5	Schematic diagram for example 2	169
B.6	Voltage waveforms for example 2	169

List of Tables

1.1	PV module efficiencies under the global AM1.5 spectrum (1000 W/m ²) at cell temperature of 24 °C (IEC 60904 – 3: 2008, ASTM <i>G – 173 – 03</i> global)	5
1.2	Benefits and limitations of solar energy systems	9
1.3	Summary of the metrics for DC-microgrid architectures over AC-microgrid	13
1.4	Comparison between Grid connected and Off-grid PV systems	16
1.5	Secondary battery chemistry characteristics	18
1.6	Major characteristics of MPPT algorithms	26
2.1	A comparison of energy storage technologies	31
2.2	Comparison of commercially available supercapacitors	33
2.3	C-rate calculation for supercapacitors	35
2.4	Comparison of DC-DC converter techniques	39
2.5	Essential specifications for fast-heating solutions based on energy storage	42
4.1	Comparison of different lighting technologies	57
4.2	Cost comparison between different lighting technologies (Note: cost of electricity and bulbs vary, and bulb replacement cost is not considered in this comparison)	60
5.1	Summary of Components used for basic SCALED converter	71
5.2	Switching arrangement of proposed SCALED converter	77
5.3	Control sequence of SCALDO regulator	83
5.4	Summary of components used for SCALED converter	92
5.5	Summary of experimental results of SCALED converter	94
5.6	Copper resistance versus copper weight	95
5.7	Theoretical estimation of power/energy losses for SCALED converter	96
5.8	Measured power losses for SCALED converter	97
6.1	Component data used for MATLAB simulations	104
6.2	Transformation coefficient n for switched mode converter (D is the duty ratio of the converter)	109
6.3	Component data used for MATLAB simulations	116
6.4	Input impedance of switch mode DC-DC converter	118
6.5	Comparison between estimated and measured MPP power of PV panels	124

8.1 Comparison of engineering specifications of supercapacitor families compared with rechargeable batteries 133

B.1 Model parameters 166

B.2 Three operating models of voltage controlled switch 167

B.3 Appropriate scale suffix 170

Acronyms and Abbreviations

AC	Alternating current
CSP	Concentration solar power
DC	Direct current
DoD	Depth of Discharge
EDLC	Electrochemical Double Layer Capacitor
EIA	Energy Information Administration
EMI	Electromagnetic Interference
ESD	Energy Storage Device
ESR	Equivalent Series Resistance
ESS	Energy Storage Systems
IEEE	Institute of Electronics and Electrical Engineers
ISDM	Ideal single diode model
LCC	Loss Circumvention Concept
LDO	Low Drop-out Regulator
LED	Light Emitting Diode
MPP	maximum power point
MPPT	maximum power point tracking
MOSFET	Metal Oxide Semiconductor Field Effect Transistor
NIWA	National Institute of Water and Atmospheric Research
NMOS	n-type Metal Oxide Semiconductor
PCB	Printed Circuit Board
PIC	Peripheral Interface Controller
PMOS	p-type Metal Oxide Semiconductor
PSD	Pore size distribution
PV	Photovoltaic
RFI	Radio Frequency Interference
RES	Renewable Energy Sources
SC	Supercapacitor
SCADHI	Supercapacitor Assisted high density inverter
SCALDO	Supercapacitor Assisted low drop-out regulator
SCALEL	Supercapacitor Assisted LED Lighting
SCALOM	Supercapacitor Assisted Loss Management
SCASA	Supercapacitor Assisted Surge absorber
SCATMA	Supercapacitor Assisted Temperature Modification Apparatus
SDM	Single diode model
SOC	State of Charge
STC	Standard test conditions
UPS	Interruptible Power Supply

Introduction

The 20th century began with a crucial debate on the fundamental aspects of electricity delivery. This debate was known as the “current war”, in which George Westinghouse and Nicola Tesla supported alternating current (AC) and their opponent Thomas Edison supported direct current (DC).

Edison designed his utility based on a relatively low 110 V DC supply to power a high resistance incandescent lamp which he had invented for the system. His system was sold to cities throughout the United States, making it a standard. Edison’s DC system originally focused on distributed generation operating within DC-grids. His system had a favoured position in the society back then because [1–5];

1. DC system could be easily used to power incandescent lamps and DC motors.
2. DC generators could be easily paralleled, allowing economical operation by using smaller machines during periods of light load and improving reliability.
3. DC system could be used with battery storages directly.
4. He had invented a meter to allow customers to be billed for energy proportional to consumption, but this meter worked only with DC.
5. DC system could provide load-levelling (usually involves storing power during periods of light loading on the system and delivering it during periods of high demand) and backup power during interruptions of generator operation

However, the primary drawbacks of Edison’s DC system was that it used 110 V from generation to its final destination giving it a relatively short useful transmission range because there was no way to step up or step down the DC voltages in order to minimize the transmission losses. Therefore, the generating plants had to be situated in the middle of population centres and could only supply customers less than a kilometre or two from the generating plant.

Aware of the problems associated with DC transmission, Tesla and his team saw an opportunity to create an electric distribution system using AC which could travel much longer distances with much lower transmission loss. The challenge was to find a way to step up and step down the voltages. However, with the development of the transformer, it was possible to step up and step down the voltages. The high voltages allowed a central generating station to supply a large area, up to 11 km long circuits. However, the main problem with high voltage AC was the risk of death by electric shock.

At the end of the “Current War” AC power won for three main reasons: (i) AC voltage could be easily stepped up to facilitate power transfer over long distances and then stepped down for delivery to the end users; (ii) the invention of the transformer; and (iii) the invention of the

AC induction motor. Therefore, AC power has been the primary form of electricity generation and delivery for the last 130 years. Currently, about 2% of installed global generating capacity is transferred to other locations by high voltage DC transmission [6]. Due to local generation of DC power using solar or wind energy and the availability of power electronics to step up or step down DC voltages, Thomas Edison's original concept of local DC power generation has now become practically applicable in the 21st century.

Since this thesis is focused on photovoltaic (PV) panel based DC power generation, details of electricity generation using solar energy will be discussed in the next section.

1.1 Solar Energy

The sun is the ultimate source for all the energy sources and fuels that are used today. The amount of solar energy received by the earth in one day is many times greater than the total amount of energy consumed by people in one day. However, solar energy is a variable and intermittent energy source. Over time, many technologies have been developed to collect solar energy for heat and to convert it into electricity. The use of solar energy, especially for power generation, has increased significantly in the United States and around the world in the past 30 years.

There are two ways to use solar energy to generate electricity:

1. ***Solar thermal power generation:*** Concentrated solar energy is used to generate electricity. These systems collect and concentrate sunlight to produce the high-temperature heat needed to generate electricity. These plants contain collectors with two main parts; *reflectors*(mirrors) that capture and focus sunlight onto a *receiver*. In most systems, a heat transfer fluid is circulated and heated in the receiver to produce steam. This steam is used to drive a turbine, which powers the generator to generate electricity. These plants have tracking systems to track the sunlight onto the receiver throughout the day.

There are three main types of concentrating solar thermal power plants: (i) linear concentrating systems; (ii) solar power towers; and (iii) solar dish/engines.

Linear concentrating systems capture solar energy using long, rectangular, U-shaped mirrors that reflect and focus the sunlight onto a linear receiver tube that runs the length of the mirrors as shown in Figure 1.1. The concentrated sunlight heats a fluid flowing through the receiver tubes. This heated fluid is sent to a heat exchanger to boil water in a conventional steam-turbine generator to produce electricity. Alternatively, steam can be generated directly in the solar field, eliminating the need for costly heat exchangers. There are two major types of linear concentrator systems: parabolic trough systems, where receiver tubes are positioned along the focal line of each parabolic mirror, and linear Fresnel reflector systems, where one receiver tube is positioned above several mirrors to allow the mirrors greater mobility in tracking the sun [7]. Currently, this type of individual system can generate about 80 MW of electricity [8].

Solar power tower systems consist of a large field of flat, sun-tracking mirrors known as heliostats, which reflect and concentrate the sunlight onto a receiver on top of a tower as shown in Figure 1.2. The heated fluid in the receiver is used to generate vapour, which

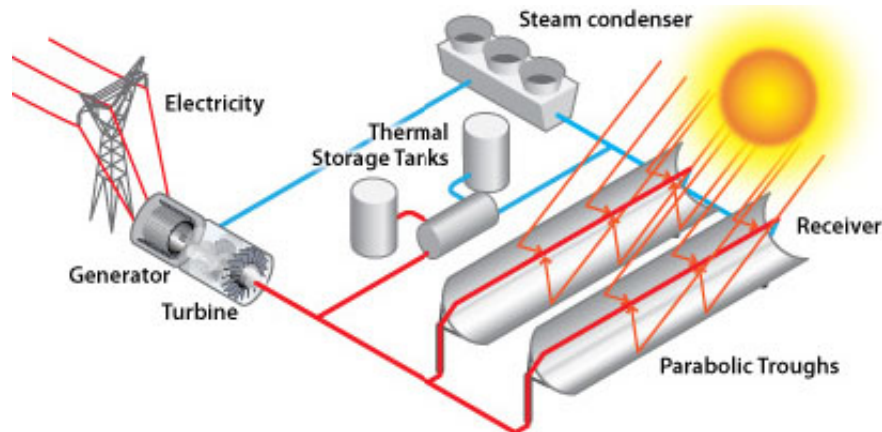


Figure 1.1: Linear concentrator systems [8]

spins a turbine generator to produce electricity. Some of these systems use water/steam as their heat-transfer fluid. Individual commercial plants of this type can be sized to produce up to 200 MW of electricity [8]. Using this kind of system, sunlight can be concentrated as much as 1500 times more than in other systems [7].

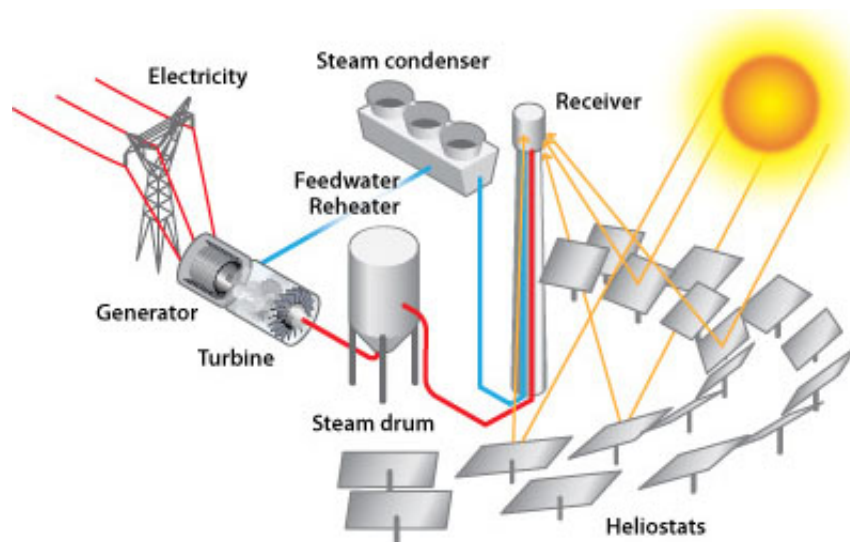


Figure 1.2: Power tower system [8]

Solar dish/engine systems use parabolic mirrored dishes, similar to very large satellite dishes and concentrate sunlight onto a central engine that generates electricity as depicted in Figure 1.3. To reduce the cost, these mirrored dishes are usually composed of many small flat mirrors. Solar dish/engine systems always point straight at the sun and concentrate the solar energy at the focal point of the dish. A solar dish's concentration ratio is much higher than those of linear concentrating systems. These systems produce relatively small amounts of electricity compared to other concentrated solar power (CSP) technologies—typically; in the range of 3 kW to 25 kW [7,8].

2. **Photovoltaic cell/panel based power generation:** Uses semiconductor-based devices to generate electricity.

Since this thesis is focused on photovoltaic panel-based power generation, more details of electricity generation using photovoltaic cells will be presented throughout the thesis.

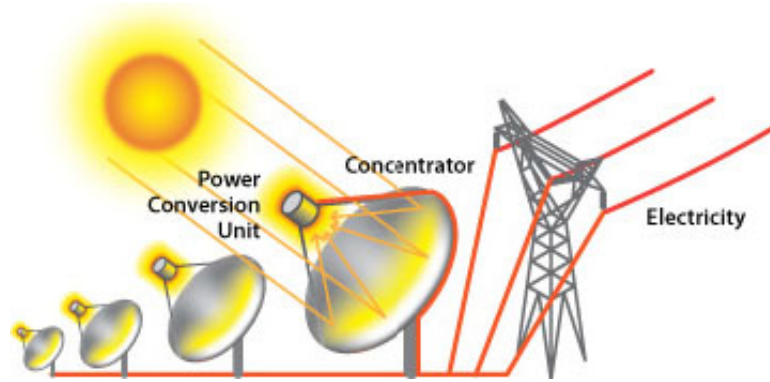


Figure 1.3: Solar dish system [8]

Sunlight is composed of photons or particles of radiant solar energy. These photons contain various amounts of energy depending on the wavelength of the solar spectrum, and can be used to generate electricity. The device used to convert solar energy into electricity is known as a photovoltaic (PV) cell. A PV cell, commonly known as a solar cell, is a non-mechanical device which is made of semiconductor material. The first practical PV cell was developed in 1954 by Bell Telephone researchers. PV cells were used to power US space satellites in the late 1950s. By the late 1970s, PV panels were providing electricity in remote, or off-grid, locations that did not have electric power lines.

When photons hit a PV cell, some are reflected or passed through the cell while others are absorbed by the semiconductor material. The atoms within the material absorb energy from the photons and release electrons in the outer-most orbit. These free electrons naturally migrate to the front surface (n-type layer) of the cell, which is manufactured to be receptive to free electrons. This movement of electrons results in an imbalance of electric charge between the cell's front (n-type layer) and back (p-type layer) surfaces, which in turn creates a potential difference between the two surfaces, because, now the n-type layer has more electrons (and thus a negative charge) while the p-type layer has more holes (and thus a positive charge). When a PV cell is connected to an external load, free electrons in the n-type layer flow to the p-type layer to engage with the holes in the p-type layer, through the external connection, creating an electric current [7, 9, 10] as shown in Figure 1.4. However, PV cells generate direct current (DC) electricity. In a typical home solar installation, this DC power is converted to AC using an inverter.

A typical silicon-based solar cell produces a maximum open-circuit voltage of 0.5 to 0.6 V. Therefore, cells are connected in series and parallel to achieve higher voltages and currents respectively. Even-though a solar cell seems to be the ideal solution to convert solar energy to electricity, one of the major drawbacks of these cells is the relatively low conversion efficiency. The two main factors deciding this are: (i) the type of semiconductor material; and (ii) the PV technology. Recently developed photovoltaic technologies have demonstrated efficiencies of 20 to 28%, but most existing systems have conversion efficiencies of 9 to 20% [11]. However, with the development of multi-junction solar cells based on Indium Gallium Phosphide (InGaP), Gallium Arsenide (GaAs) and Indium Gallium Arsenide (InGaAs) chemistries, now it possible to achieve $\approx 30\%$ cell efficiency [12]. Table 1.1 compares commercially available PV cell efficiencies which

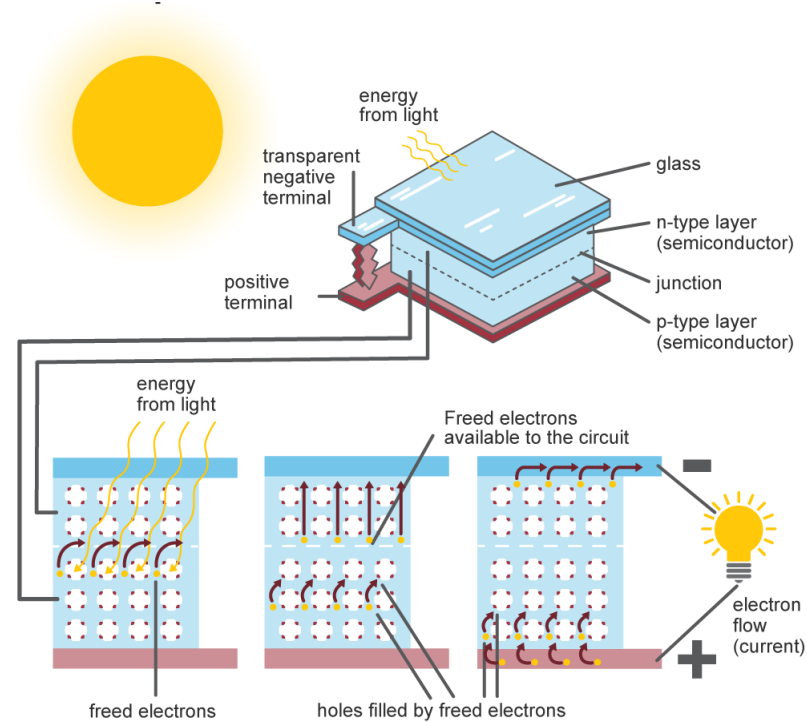


Figure 1.4: Inside of a PV cell [7]

were tested according to IEC standards. Despite the low efficiency of solar cells, their popularity and usage continue to experience tremendous growth.

According to the US Energy Information Administration (EIA), electricity generated at utility-scale PV power plants increased from 76 million kWh in 2008 to 63 billion kWh in 2018 [7]. These utility-scale power plants have at least 1 MW of electricity generating capacity. Also, EIA estimates that 30 billion kWh were generated by small-scale grid-connected PV systems in 2018, up from 11 billion kWh in 2014. The world's largest solar market, China, had an installed capacity of 154.1 GW as of August 2018. As of January 2019, New Zealand had 90.1 MW of installed PV systems, which is only 0.1% of total renewable energy generation [10].

Table 1.1: PV module efficiencies under the global AM1.5 spectrum (1000 W/m^2) at cell temperature of $24 \text{ }^\circ\text{C}$ (IEC 60904 – 3: 2008, ASTM $G - 173 - 03$ global) [12]

Classification	Efficiency (%)
Si(Crystalline)	23.8 ± 0.5
Si(multi-crystalline)	19.5 ± 0.4
GaAs (thin film)	24.1 ± 1
CdTe (thin film)	18.6 ± 0.6
CIGS (Cd free)	17.5 ± 0.5
CIGS (large)	15.7 ± 0.5
a-Si/nc-Si (tandem)	12.3 ± 0.6
Organic	8.7 ± 0.3
InGaP/GaAs/InGaAs	31.2 ± 1.2

1.1.1 Photovoltaic (PV) Cell Model: Approximation of PV cell V-I characteristics

In the existing literature, several mathematical models describe the operation and behaviour of photovoltaic cells/arrays. These models differ from each other in accuracy and number of

parameters used in the calculation of current and voltage of the PV cell.

(A) Ideal Single Diode Model (ISDM)

The simplest model of a solar cell consists of a diode and current source connected in parallel as shown in Figure 1.5. Here, current generated by a current source I_{ph} is a function of solar irradiance G and temperature T . The short-circuit current (I_{SC}) and open-circuit voltage (V_{OC}) are the two key parameters generally used to characterize a PV cell. Typically, these parameters can be extracted from the manufacturer's data-sheet.

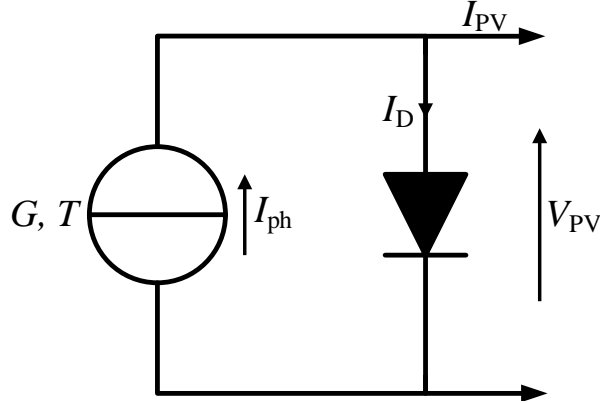


Figure 1.5: Simplified equivalent circuit of solar cell

Using Figure 1.5, output current I_{PV} can be written in terms of photo current I_{ph} and diode current I_D as;

$$I_{PV} = I_{ph} - I_D \quad (1.1)$$

where

$$I_D = I_S \left[\exp \left(\frac{qV_{PV}}{nk_B T} \right) - 1 \right] \quad (1.2)$$

For a forward biased condition of the diode Eq. 1.2 can be simplified as;

$$I_D = I_S \left[\exp \left(\frac{qV_{PV}}{nk_B T} \right) \right] \quad (1.3)$$

where I_S is the reverse saturation current of the diode, q is the electron charge (1.602×10^{-19} C), V_{PV} is the voltage across the PV cell, k_B is Boltzmann's constant (1.3819×10^{-23} J/K), n is an ideality factor and T is the junction temperature of the cell in Kelvin.

Thus,

$$I_{PV} = I_{ph} - I_S \left[\exp \left(\frac{qV_{PV}}{nk_B T} \right) \right] \quad (1.4)$$

by setting I_{PV} to zero (no load connected) it is possible to find the diode saturation current I_S as;

$$I_S = \frac{I_{ph}}{\exp \left(\frac{qV_{OC}}{nk_B T} \right)} = I_{SC} \left[\exp \left(\frac{-V_{OC}}{V_T} \right) \right] \quad (1.5)$$

where $V_T = nk_B T/q$ is the thermal voltage of the diode. With this model it is assumed that the short circuit current (I_{SC}) is equal to the photo current.

Using Eq. 1.5 we can re-write Eq. 1.4 as:

$$I_{PV} = I_{SC} \left[1 - \exp \left(\frac{V_{PV} - V_{OC}}{V_T} \right) \right] \quad (1.6)$$

Also, at the maximum power point (MPP), the cell voltage and current are available from the manufacturer's data sheet as V_{MPP} and I_{MPP} respectively. Using these values in Eq. 1.6:

$$I_{MPP} = I_{SC} \left[1 - \exp \left(\frac{V_{MPP} - V_{OC}}{V_T} \right) \right] \quad (1.7)$$

Re-arranging the above equation it is possible to find V_T as;

$$V_T = \frac{V_{MPP} - V_{OC}}{\ln \left(1 - \frac{I_{MPP}}{I_{SC}} \right)} \quad (1.8)$$

Finally using Eq. 1.6 and Eq. 1.8, the $V - I$ characteristics of PV cell can be derived as:

$$I_{PV} = I_{SC} \left[1 - \exp \left(\frac{(V_{PV} - V_{OC}) \ln \left(1 - \frac{I_{MPP}}{I_{SC}} \right)}{V_{MPP} - V_{OC}} \right) \right] \quad (1.9)$$

(B) Model with series ohmic losses

To obtain a better representation of the electrical behaviour of the solar cell, the material resistivity and ohmic losses in the cell are taken into account in this model. These losses are represented by a series resistance R_S in the equivalent circuit as shown in Figure 1.6.

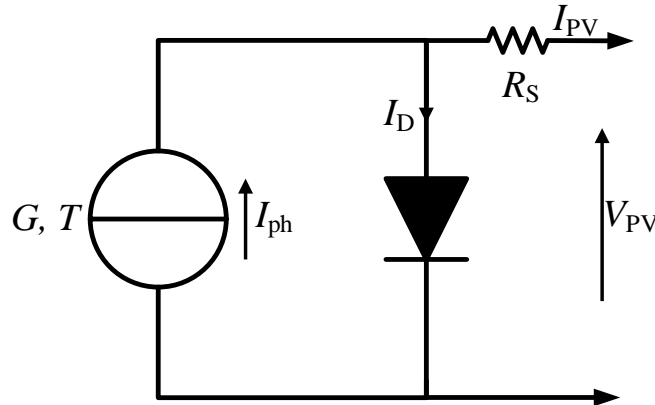


Figure 1.6: Solar cell model with series ohmic losses

The current voltage equation for this model is given as follows:

$$I_{PV} = I_{ph} - I_S \left[\exp \left(\frac{q(V_{PV} + I_{PV}R_S)}{nk_B T} \right) - 1 \right] \quad (1.10)$$

The open circuit voltage at any temperature can be written as;

$$V_{OC} = V_{OC(STC)} [1 - k_v(T - T_{STC})] \quad (1.11)$$

where $V_{OC(STC)}$ is the open circuit voltage at standard test conditions (STC) [at 1000 Wm^{-2} , $25 \text{ }^\circ\text{C}$], k_v is the voltage temperature coefficient (K^{-1}), T is the junction temperature in Kelvin and T_{STC} is the reference temperature ($25 \text{ }^\circ\text{C}$ or 298 K).

The photo current I_{ph} at a given temperature and irradiance can be calculated using [13–17]:

$$I_{ph} = [I_{SC(STC)} + k_i(T - T_{STC})] \frac{G}{G_{ref}} \quad (1.12)$$

where $I_{SC(STC)}$ is the short circuit current at standard test conditions (STC) [at 1000 Wm^{-2} , $25 \text{ }^\circ\text{C}$], G is the irradiance, G_{ref} is the STC irradiance (1000 Wm^{-2}) and k_i is the current temperature coefficient (A/K).

Using Eq. 1.10 and Eq. 1.12 the reverse saturation current of the diode I_{rs} in open circuit condition under STC can be found as:

$$I_{rs} = \frac{I_{SC(STC)}}{\exp\left(\frac{qV_{OC(STC)}}{nk_B T_{STC}}\right)} \quad (1.13)$$

The module saturation current at any temperature can be found as [13–17]:

$$I_S = I_{rs} \left(\frac{T}{T_{STC}}\right)^{3/n} \exp\left[\frac{qE_{go}}{nk_B} \left(\frac{1}{T_{STC}} - \frac{1}{T}\right)\right] \quad (1.14)$$

where E_{go} represents the band gap energy of the semiconductor material.

The value of R_S can be obtained as [13–16]:

$$R_S = -\frac{dV_{PV}}{dI_{PV}} \Big|_{V_{PV}=V_{OC}} - \frac{nk_B T}{qI_{SC}} \quad (1.15)$$

Using the Newton-Raphson method it is possible to find the I_{PV} for a given solar cell voltage.

(C) Model with ohmic losses

This model consists of a single diode for the phenomenon of cell polarization and two resistors (series and shunt) for the losses as shown in Figure 1.7. Thus, is described as a “single diode model (SDM)”. This model is used by manufacturers to provide the technical characteristics of their solar cells (data sheets).

$I_{PV} = f(V_{PV})$ characteristic of this model is given by the following equation [13, 14, 17]:

$$I_{PV} = I_{ph} - I_S \left[\exp\left(\frac{q(V_{PV} + I_{PV}R_S)}{nk_B T}\right) - 1 \right] - \frac{V_{PV} + I_{PV}R_S}{R_{Sh}} \quad (1.16)$$

where R_{Sh} is the shunt resistance.

There are different approaches to solving Eq. 1.16, resulting in various approximated mathematical models. These models generally include constraints that are provided by photovoltaic module manufacturers. These approaches are typically approximations of the SDM with assumptions made to establish a final current-voltage relationship which is somewhat traceable. By assuming $R_S = 0$ and R_{Sh} is infinite at operating points near the maximum

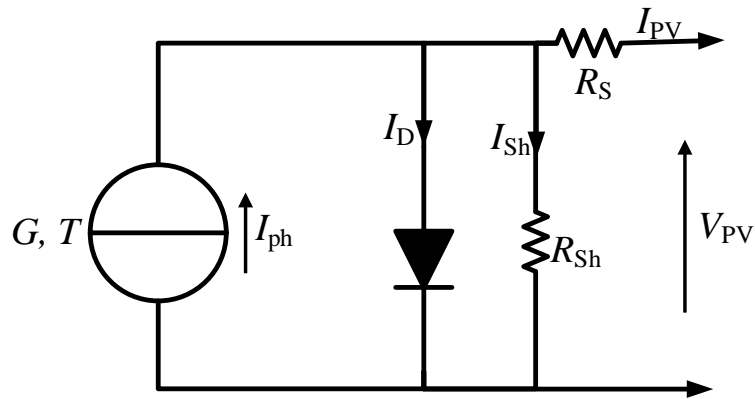


Figure 1.7: Model with ohmic losses

power point it is possible to derive an ideal single diode model (ISDM) discussed in (A) and by assuming R_{Sh} is infinite it is possible to derive the model discussed in (B).

Wolf and Rauschenbach [18] suggest that the current-voltage characteristics of photovoltaic cells can be determined using three different methods: (i) photovoltaic output characteristics; (ii) $p-n$ junction characteristics; and (iii) forward characteristics of the diode. These methods give different results because of the effects of the cell internal series resistance R_S .

Table 1.2: Benefits and limitations of solar energy systems

Benefits	Limitations
Do not produce air pollutants or CO ₂	The amount of sunlight that arrives at the earth's surface is not constant
Solar energy systems on buildings have minimal environmental effects	Since, the amount of sunlight reaching a square meter (m ²) of earth is relatively small, a large surface area is necessary to absorb or collect an useful amount of energy

Even though solar energy systems seem to be the ideal solution for electricity generation, they have benefits and limitations as discussed in Table 1.2. More details of PV-based electricity generation will be discussed in section 1.3.

1.2 Motivation for DC-Microgrids

With renewable energy sources proliferating, governments are encouraging end-users and product developers to reduce their carbon footprints and their dependency on fossil fuels to keep our planet's environment clean for future generations. In this regard designing products and systems with high end-to-end efficiency (E_{TEE}) is a priority for both power electronic product designers and the research community. As shown in Figure 1.8 (a), most electrical consumer products have electronic modules powered by a cascade of converters, typically starting with an AC-DC converter followed by multiple DC-DC converters. With the E_{TEE} effectively controlled by the multiplication of the individual efficiencies of the converter stages, E_{TEE} drastically drops with the number of converter stages. If the energy source is a 230 V AC, 50 Hz household power supply, with an AC-DC converter followed by other DC-DC converters, E_{TEE} could be as low

as 73%, if each of the three converters comes with acceptably high efficiencies around of 90%. With renewable energy sources (RES) such as photovoltaic energy, providing DC outputs, we have the option of eliminating the first AC-DC converter and achieving a significant rise in the ETEE as depicted in Figure 1.8 (b).

In 2014, the IEEE Committee on DC Energy Efficiency [19], [20] decided to promote the DC-Microgrid-based households as a novel approach to energy efficiency. Given the case of renewable sources such as photovoltaic (PV) solar cells providing a DC output, with very short connections from the energy source to the load, Thomas Edison's concept of local DC power generation and distribution is quite practicable today using renewable sources. To conserve energy, ideally, the distance between power generating sources and loads must be at a minimum and minimum conversion stages must take place [20,21].

According to the US EIA, local power generation can be defined as:

1. self-generated
2. generated by either the same entity that consumes power or an affiliate
3. used in the direct support of a service or industrial process located within the same facility or group of facilities that contain the generating equipment.

As evidenced by the contributions to three biennial conferences IEEE-ICDCM (IEEE-International Conference on DC microgrids) from 2015 to 2019 on DC microgrid applications, the direct use of DC has been claimed as a key strategy for improving reliability and saving energy in buildings [22–25]. Though many components are driving the growth of local DC electricity, some key points are listed in the literature [6] :

- (i) Traditional AC centralized electrical power systems lose approximately 70% of the bulk generated electricity produced in transmission, distribution and conversion [19];
- (ii) Most consumer loads operate internally using DC power and the relative proportion of AC loads is decreasing over time;
- (iii) DC power locally generated by renewable energy sources, such as solar panels and wind-mills, can reduce energy losses by as much as 30% compared with AC power systems;
- (iv) DC-based PV and wind power systems are more resilient than AC-based systems.

1.2.1 DC Microgrid Reference Architectures

Microgrid developments are expanding around the world. Although goals are specific to each site, microgrid architectures have demonstrated the ability to provide improved energy utilization, higher power quality and reliability than utility power systems [21,23–26]. However, the vast majority of these microgrids are based on AC because traditionally power is delivered using AC. Figure 1.9 (a) and (c) depicts two different AC microgrid reference architectures. However, manufacturers, researchers and power system engineers are using DC distribution systems for end-user loads that are natively DC. These DC applications provide higher efficiency, and flexibility, and reduced capital costs compared to their AC counterparts [21,23].

DC-microgrids are local DC energy networks consisting of RES and storage systems, with advanced capabilities that enable control of DC network resources for higher operational performance and/or the ability to operate independently of the primary AC system for enhanced

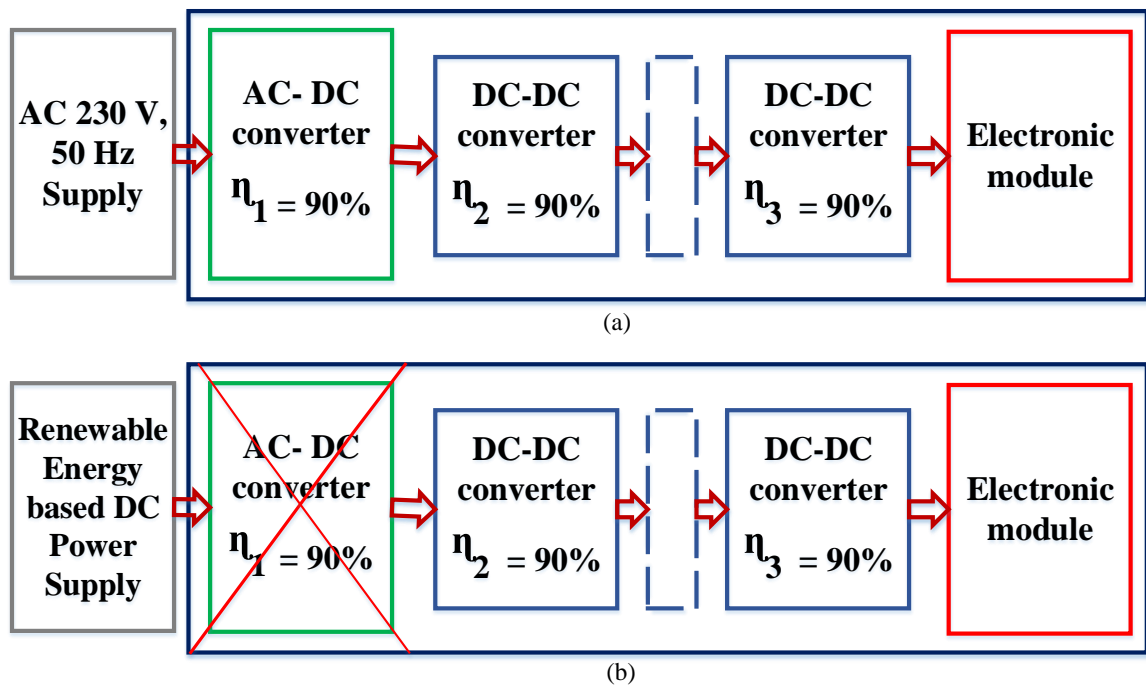


Figure 1.8: Energy flow within a typical electronic product or system: (a) with AC-power supply showing an end-to-end efficiency of $0.9^3 \approx 0.73$; (b) with renewable energy based DC-power supply showing an end-to-end efficiency of $0.9^2 \approx 0.81$;

reliability [21, 23, 26]. A residential building powered by a DC-microgrid uses 3% less electricity compared to a residential building powered by an AC supply [25]. In addition, the use of DC provides higher efficiency, flexibility and sustainability. If on-site renewable generation is used as the energy source for DC-microgrids it may offer additional benefits for electric vehicles and storage systems. Figure 1.9 (b) and (d) depicts two different power system reference architectures available in a DC-microgrid environment. These two are claimed to be the simplest architectures in DC-microgrid [23].

Figure 1.9 shows that both AC-microgrid and DC-microgrid include a switch at the point of common coupling (PCC) to disconnect the microgrid from the AC grid.

The **firm generation subsystems** for both AC and DC microgrids are depicted in Figure 1.9 (c) and (d). These subsystems are assumed to be composed of some form of fuel-driven rotating machinery (e.g. a natural gas-fired combined heat and power engine). Therefore, the DC system requires an additional AC-DC converter to interface the firm generation with the DC bus. For a failure of this converter to count against the reliability of service to the loads, the DC microgrid would have to be in an N-2 state; i.e. the AC grid has failed and the AC-DC converter has also failed [23]. The likelihood of such a failure is very low, and will not count against the reliability of a DC microgrid with firm generation.

However, in the **PV and battery subsystem**, the AC-microgrid has two DC-AC inverters and one DC-DC converter versus three DC-DC converters in DC-microgrid. These three converters in this integrated subsystem are often lumped together as a “charge controller” in real-world applications. For the AC-microgrid and DC-microgrid shown in Figure 1.9 (a) and

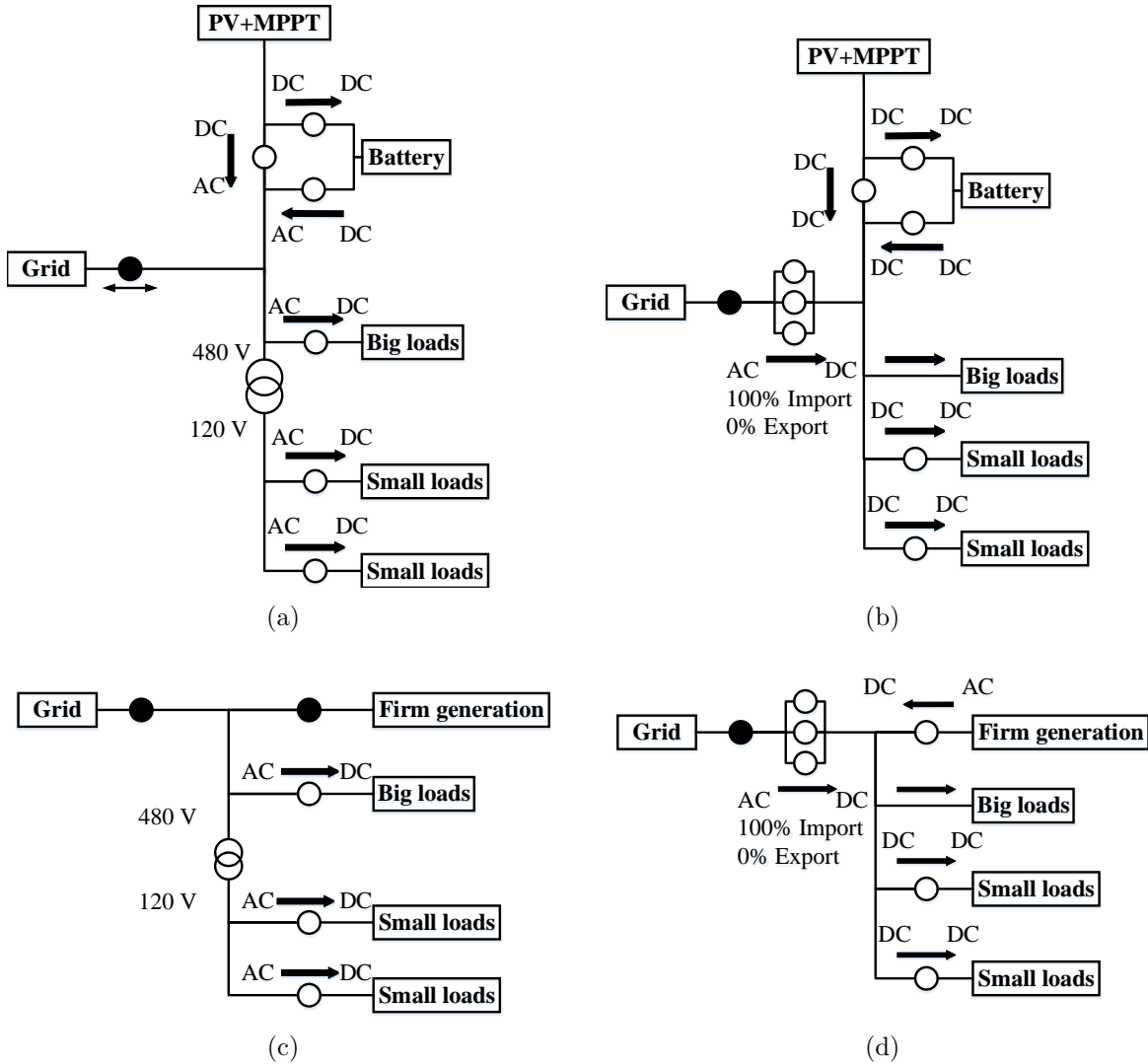


Figure 1.9: Microgrid reference architectures: (a) AC microgrid, PV + storage; (b) DC microgrid, PV + Storage; (c) AC microgrid, firm generation (d) DC microgrid, firm generation (Open circle: voltage converters, rectifiers, or inverters; Filled circle: switch. Arrows: direction of power flow. All loads are assumed to be native DC. The percentages listed under the power electronic interface at the AC grid/DC microgrid point of common coupling indicate the capacities of the importing and export electronics relative to the peak microgrid load.) Redrawn from: [23]

(b), instead of PV it is possible to include wind or another form of intermittent generation as the energy source.

According to Figure 1.9 (b) and (d), it is obvious that DC systems require a large number of power electronic devices at their interface to the AC grid. These bi-directional converters/inverters (for both import and export) have been appropriately sized in coordination with the other energy resources in the microgrid to ensure that these architectures have a reliability nearly the same as their AC grid (N-1 reliability). This is achieved by setting the AC-DC import capacity to 100% of the microgrid load.

However, determining the DC-AC export capacity of these converters is difficult because it depends on the excess electricity generation of the DC-microgrid. For an example, in DC-microgrid with firm generation, the reasons for running firm generation may go beyond the need

for electrical power in the microgrid, (e.g. if combined heat power (CHP) is used as the firm generation, the thermal loads do not overlap with the electrical loads) [21, 23]. In the case of DC-microgrid with PV generation, it is not possible to predict the generation since solar energy is an intermittent energy source. Therefore, it is challenging to decide the export capacity of the bi-directional converter at the interface of the DC-microgrid to main AC grid.

Table 1.3 provides a summary of the metrics for DC-microgrid architectures over AC-microgrid in a study done by Los Alamos National laboratory on DC-microgrids.

Table 1.3: Summary of the metrics for DC-microgrid architectures over AC-microgrid [23]. +(-) indicates an advantage (disadvantage) for the DC architecture over its related AC architecture. 0 indicates no perceived advantage for either architecture. Multiple rankings are given if there are differences between the microgrid configurations in Figure 1.9.

Metric	Rank	DC relative to AC architectures
Safety & protection	0	Both AC and DC have adequate protection devices
Reliability	0	Assuming power electronics at AC/DC interface are sized appropriately to account for potential failures
Capital cost	+/-	DC architecture for a PV+Battery microgrid enjoys lower cost for power electronics if the energy assets are sized so that power export is not required while N-1 reliability is maintained. However DC-microgrid with firm generation has a higher cost for power electronics under similar reliability and sizing assumptions
Energy efficiency	+	DC-microgrid architectures have 2-3 % efficiency increase assuming that the DCMG energy assets are sized so that power export is not required.
Engineering cost	+	Distributed control systems for DC architectures are potentially more universal, making engineering costs lower.
Power quality	+	Power electronics at the AC/DC interface provides a buffer against external disturbances
Resilience	0	Both AC and DC-microgrid have similar properties

In this thesis, a DC microgrid architecture with PV generation was considered. Therefore further details of PV generation-based DC-microgrids are discussed in the rest of this chapter.

1.3 Photovoltaic (PV) Systems

When considering solar and wind energy there is no competition between these two. However, solar energy is more uniformly distributed throughout the world than wind energy; 98% of the world's population receives more than 3 kWh/m² solar insolation per day [6]. Since 2008, PV panel prices have dropped more than 70%, while the cost of wind turbines decreased by 40% during that time [20]. With a similar experience in semiconductor products, the experts in the renewable energy field believe that the cost of PV systems will continue to decrease in coming years. All of these reasons make PV-based DC microgrids popular and convenient.

About 89 PW (1 PW = 10¹⁵ W) of solar energy is received by the earth's surface per year. According to data published by EIA, global energy consumption in 2013 was around 18 TW (1 TW = 10¹² W) which is about 0.021% of the solar energy received on the earth's surface. However, the challenge is to convert that enormous amount of energy into electricity at a lower cost than any other traditional electricity-generating techniques. Using either concentrated solar power (CSP) or PV technology, solar energy can be converted into electricity. In 2016, the installed capacity of CSP worldwide was 4.8 GW, compared to 300 GW of solar PV capacity. Although, initially more interest was shown in CSP than PV technology due to the advantage of

intrinsic cost reductions, the situation has changed and companies, organizations and individuals are more interested in using PV.

PV panels can be easily installed on the rooftop or walls of commercial and residential buildings, giving customers the choice of using either grid-connected or off-grid PV systems. Also, PV technology can be used to generate electricity for remote communities where the national grid is not accessible. Therefore, the use of a PV system is the most common local energy generation technique where no fossil-fuel-based rotating machinery is used. US companies are increasingly turning to solar PV-based DC microgrids to offset energy costs. For example, in Minnesota, roof-top PV electricity costs 36% to 75% less than natural gas-based electricity during peak hours of the day [22].

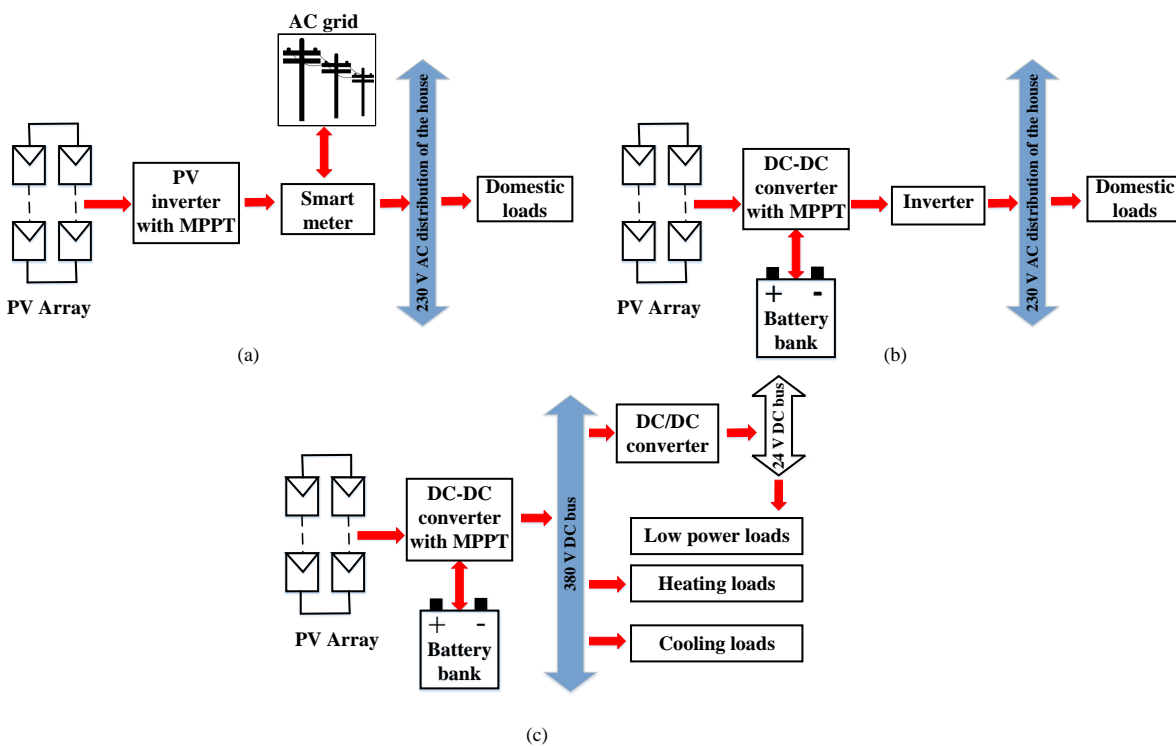


Figure 1.10: Existing PV systems: (a) Typical grid-connected PV system; (b) Off-grid PV AC-system; (c) Off-grid PV DC-system

Basically there are two kinds of PV systems, as depicted in Figure 1.10. They are as follows:

1. Grid-connected PV systems
2. Off-grid (or stand-alone) PV systems

1.3.1 Grid-connected PV systems

In Figure 1.10(a) block diagram of a typical grid-connected PV system is shown. The DC power generated by the PV panels is converted to AC and fed to the grid via a PV inverter. Grid-connected PV systems can be found in different sizes and power levels according to requirements, and applications, ranging from 200 W to over 100 MW [27]. Hence, for simplicity, this system can be categorized into three subcategories as follows:

1. small scale - from a few watts to a few 10s of kW
2. medium-scale - 10s of kW to a few 100s of kW
3. large scale - a few 100s of kW to several 100s of MW

In addition to these subcategories, grid-connected PV systems can be classified depending on the PV module arrangement: a single module, a string of modules, multiple strings and arrays [27].

1.3.2 Off-Grid PV systems

Figure 1.10(b),(c) depicts an off-grid PV system, which is designed to operate independently of the utility grid and is commonly designed and sized to supply certain DC and/or AC electrical loads. In an energy storage device (ESD), electrochemical batteries are used to store the DC power generated by the PV panels. When using batteries, a charge controller is needed to switch off the PV modules when the batteries are fully charged and switch off the load when the batteries become discharged below a certain limit. The use of off-grid PV systems is not limited only to remote areas. Stand-alone PV systems can be divided into two varieties:

1. A simple DC PV system with batteries
2. A large PV system with both DC and AC loads

Both grid-connected and off-grid PV systems comprise a battery bank with a maximum power point tracking (MPPT) charge controller as depicted in Figure 1.10. Use of the battery bank requires an MPPT charge controller which consists of a switch-mode DC-DC converter to adjust the current and voltage to the battery bank to optimize charging while protecting the battery from overcharging. In a typical domestic AC mains supply related inverter system, with its few hundred volts solar array based DC source, MPPT charge controller typically provides end to end efficiency in nineties [28]. When considering the grid-connected PV system depicted in Figure 1.10(a), each power conversion stage in this system wastes energy, leading to unavoidable reduction of ETEE. A typical solar energy supply installed by commercial organizations is typically based on an inverter feeding the DC energy supply via the DC to AC converter on to the AC mains supply. This simple approach is disadvantaged by low conversion efficiency in the range of mid eighties to low nineties, and low rebate rates for the energy fed to the grid via the inverter during the day time. With ageing of the system and deterioration of energy storage devices such as batteries, the ETEE could drop to much lower figures. Accordingly, increasing the efficiency even by as little as a few percent is economically worthwhile, and this motivates researchers to investigate new circuit topologies and techniques to boost efficiency levels. Figure 1.10(b) depicts a typical off-grid DCMG system where the inverter is eliminated for higher ETEE. Table 1.4 shows the advantages and disadvantages of the PV systems represented in Figure 1.10.

1.4 Energy Storage Devices (ESDs) in PV Systems

When DC loads are powered by a renewable energy source (RES) such as solar, ESDs becomes essential for reliable operation due to the fluctuating nature of the energy source. Even though there are two main types of ESDs batteries and capacitors, the most common energy storage system (ESS) used in renewable energy-based systems is the rechargeable battery pack, typically

Table 1.4: Comparison between Grid connected and Off-grid PV systems

Grid-connected PV system	Off-grid PV system
Availability of offset in customer electricity usage cost through net metering and feed in tariff	Can be cheaper than extending power line in remote areas
Utility grid can be used as virtual battery allowing to remove the ESD requirement	Can become energy self-sufficient
E _{TEE} is low	High E _{TEE} because additional DC-AC converter can be eliminated
Can cause voltage regulation issues	No voltage regulation issues since system is not connected to grid
Grid connection poses many protection related challenges	Fewer protection related challenges
Can compromise the power quality due to intermittency causing voltage flickers	Power quality is high in comparison with grid-connected system

based on lead-acid (Pb-acid) or lithium-ion (Li-ion) chemistries. However, all rechargeable battery chemistries have limited charge-discharge life cycles and calendar lives. The charge-discharge life cycle of these chemistries is typically a few thousand and it varies with the depth of discharge (DoD).

1.4.1 Overview of Electrochemical Batteries

The demand for smaller, lightweight portable electronic equipment has drastically increased research interest in battery chemistries and the markets for the batteries. Electrochemical battery chemistries come in two different forms:

1. Disposable batteries
2. Rechargeable batteries

The growth in electric vehicles, portable consumer electronic products and PV systems has had a huge impact on the development of battery technology. More interest has been paid to rechargeable batteries because of their higher energy density, superior life cycle and environmental friendliness compared to disposable batteries. Also, primary batteries have a reasonably mature market and product chemistry range. However, researchers are still attempting to increase the energy density, reduce the self-discharge rate and improve the usable temperature range of disposable batteries. In order to complement these developments in battery technologies, many semiconductor manufacturers continue to introduce new integrated circuit families for battery management [29].

When considering rechargeable batteries, there are several matured chemistries:

- (i) Lead acid
- (ii) Nickel cadmium
- (iii) Nickel metal hydride
- (iv) Lithium-ion
- (v) Lithium-polymer/Lithium metal
- (vi) Lithium-iron phosphate

Battery Terminology

Several terminologies are used to identify the parameters of batteries. More details on this can be found in the literature [29].

(A) Capacity

The capacity of a battery or a cell is defined as follows:

$$\text{Capacity} = \int_0^t i(t) dt \quad (1.17)$$

This relationship can be used to either charge or discharge of the battery to obtain the capacity added or capacity removed from a battery or a cell. The capacity of a battery is typically given in ampere-hours [Ah] or milliamper-hour [mAh].

(B) Rated capacity

This is defined as the minimum expected capacity when a new battery is measured under standard conditions. This is the basis for the C rate and depends on the standard conditions used, which may vary with the battery manufacturer.

(C) C rate

This is defined as the rate in amperes or milliamperes that is numerically equal to the capacity of the battery given in Ah or mAh. For an example, a battery with 10 Ah capacity has a C rate of 10 A. At a low discharge rate the actual capacity of the battery is higher than that at high discharge rates.

(D) Power density

This is the amount of power that a battery can deliver per unit volume at a specified state of charge (SOC), usually 20% [29]. This is usually measured in watts per litre [W/L].

(E) Cycle life

This is a measure of a battery's ability to withstand repetitive deep discharging and recharging. Typically cycle life has an inverse logarithmic relationship to depth of discharge (DoD).

(F) Depth of discharge (DoD)

DoD is defined as follows:

$$\text{DoD} = \frac{\text{Capacity removed from a battery}}{\text{Actual capacity of the battery}} \quad (1.18)$$

(G) State of charge (SOC)

SOC can be defined as:

$$\text{SOC} = \frac{\text{Saved energy in the battery}}{\text{Total energy that can be saved in the battery}} \quad (1.19)$$

Basically SOC is a measure of the state of a battery, which can be used to safely charge and discharge the battery at a level suitable for enhancing the life of the battery.

Figure 1.11 depicts the typical discharge curve of a rechargeable battery, which is applicable for in general to all types. Normally, a fully charged battery has a higher open-circuit voltage than the nominal terminal voltage (relatively flat area in the discharge curve). However, when

a battery is discharged up to about 80% of its rated capacity, this voltage drops drastically, as shown in Figure 1.11. This is due to the increase in its internal resistance.

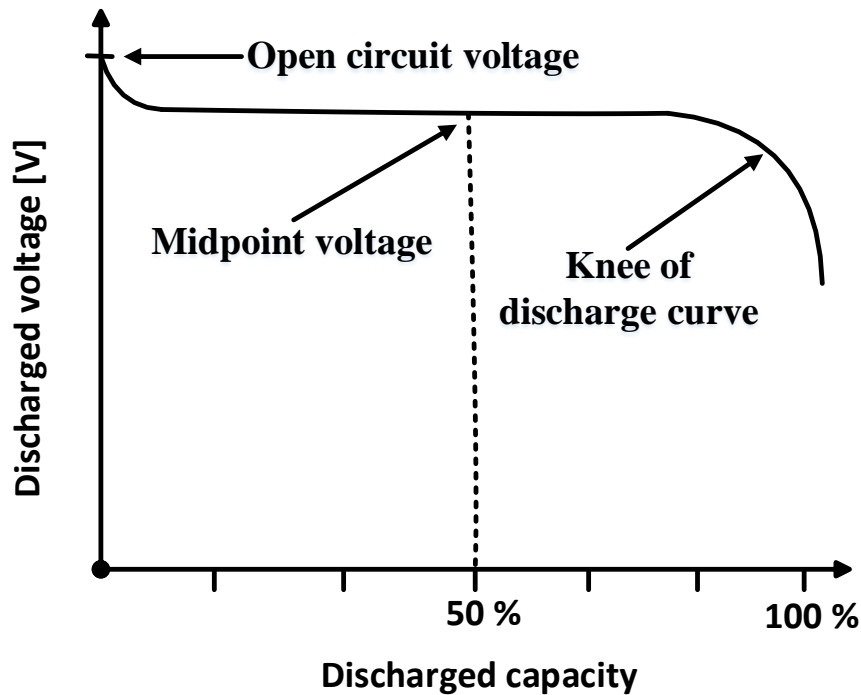


Figure 1.11: Midpoint voltage and the voltage plateau for a rechargeable battery

Some characteristics of the above-mentioned rechargeable battery chemistries are listed in Table 1.5.

Table 1.5: Secondary battery chemistry characteristics [29–32]

Parameter	Pb-acid	NiCd	NiMH	Li-ion	Li-polymer	Li-iron phosphate
Average cell voltage [V]	2	1.2	1.2	3.6	1.8 – 3	3.2 – 3.3
Internal resistance	Low	Very low	Moderate	High	High	High
Gravimetric energy density [Whkg ⁻¹]	30 – 50	40 – 60	60 – 120	170 – 250	120 – 250	90 – 160
Cycle life	500 – 2000	500 – 1000	500 – 800	1000 – 1200	500 – 1000	1500 – 2000
Self-discharge % per month	2 – 4	15 – 25	20 – 25	< 10	< 10	< 10

1.4.2 Ragone Plot

The performance of ESDs can be compared using their energy storage and power delivery capability. A Ragone plot, as shown in Figure 1.12, is the most convenient tool for this comparison. This is a plot between specific energy density [Whkg⁻¹] vs specific power density [Wkg⁻¹] or alternatively a plot of energy density [WhL⁻¹] vs power density [WL⁻¹]. These plots can be used to characterise the trade-off between energy storage and power delivery capabilities in

ESDs. As seen in Figure 1.12, conventional batteries have a high energy and low power density, making them ideal for long-term energy storage options. Supercapacitors (SCs) have medium energy and high power density compared with batteries and capacitors, which makes SCs an ideal short-term energy storage option for applications such as wind turbine pitch control systems and vehicle brake energy recovery systems. Further, SCs can be coupled with conventional batteries to deliver extraordinary power and energy performance without having to sacrifice the service life of the battery. Photovoltaic systems are one example of such applications.

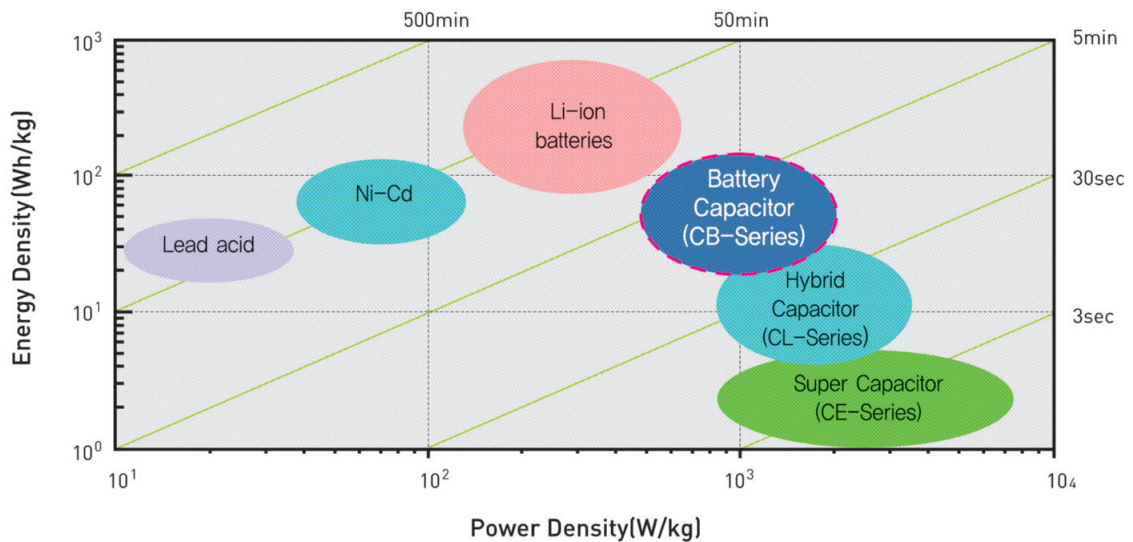


Figure 1.12: Ragone plot of batteries and supercapacitors [33] Source: SAMWHA Electric

1.5 Maximum Power Transfer Techniques

Despite all the advantages related to energy generation using PV technology, the conversion efficiency still has a very low value in the range of 9-20%. Also, a PV module inherits non-linear characteristics as shown in Figure 1.13, which vary with temperature and solar irradiation levels. Figure 1.13(a) shows the typical characteristics of a solar panel including its near-constant current region (A-B), the narrow maximum power point (MPP) area of operation (B-C) and the typical voltage-source type operational region (C-D). It is vital to operate at the MPP in order to achieve maximum efficiency for the overall system (which includes the PV array, and converters, and loads). Also, it is obvious from Figure 1.13(d) that the power generated by the PV module varies with irradiance and temperature. Therefore it is necessary to use a technique that can extract maximum power from the PV panels and deliver it to the connected load. Several methods to extract maximum power have been proposed in the literature [28, 34–39]. Each of these tracking techniques has different efficiencies [39]. Theoretically, the maximum possible load power occurs when the source resistance matches the load resistance [28]. This is achieved by changing the duty cycle of the switch-mode DC-DC converter in the MPPT charge controller.

If a PV array is directly connected to a load (i.e. direct-coupled systems), the operating point of the overall system will be at the intersection of the DC load line and the I-V curve

of the PV array, as shown in Figure 1.13(a). This operating point is not the MPP for the PV array, therefore it is not possible to extract the maximum power from the PV array. Thus, for a direct-coupled system, it must use an oversized PV array in order to ensure the load's power requirements can be matched.

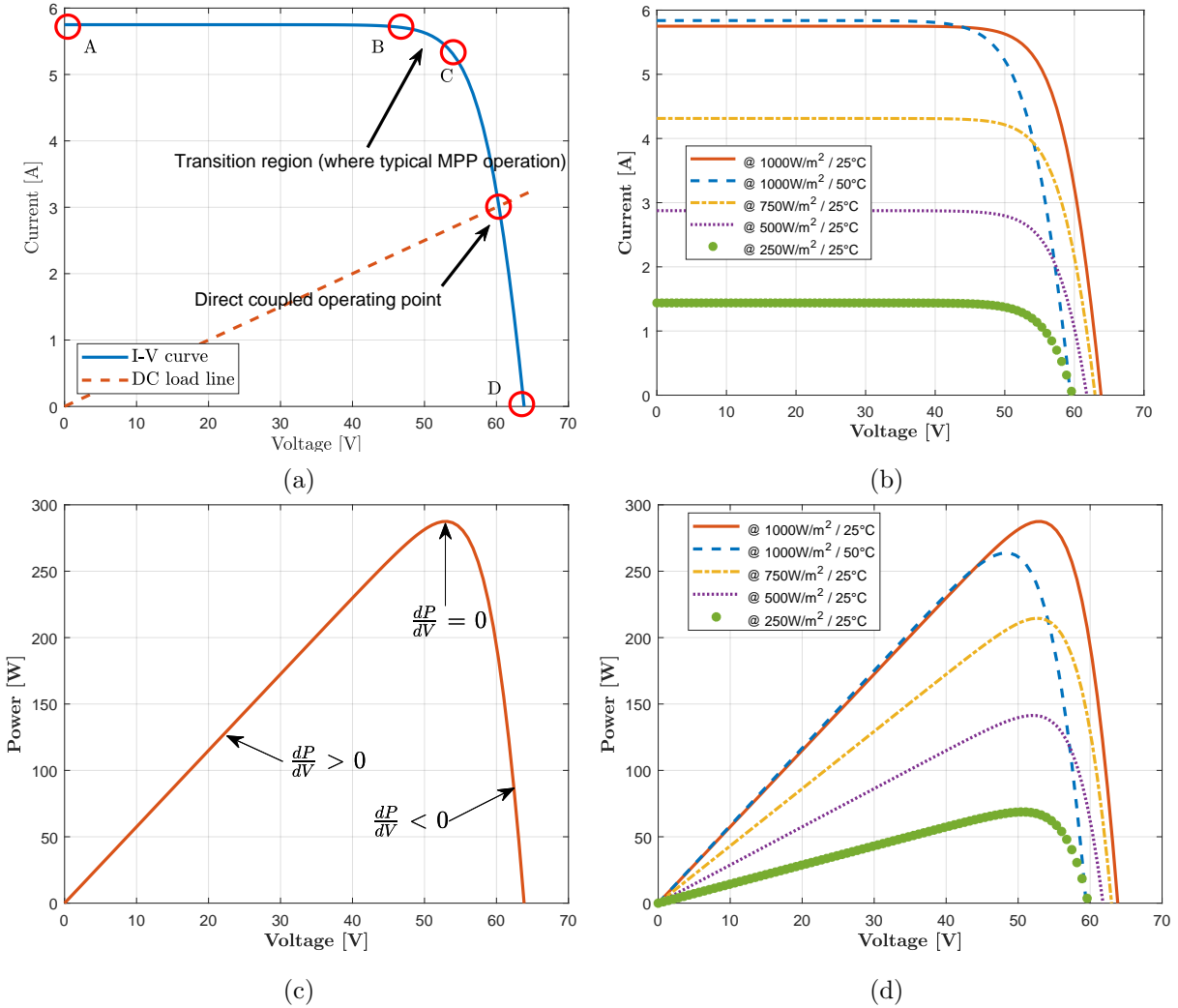


Figure 1.13: Characteristics curves of a solar PV panel: (a) PV current versus voltage characteristics with directly coupled operating point; (b) Current-voltage variations with irradiance and temperature; (c) Power vs voltage curve; (d) Power-voltage variation with irradiance and temperature

1.5.1 A review of the Maximum Power Transfer concept

There are several techniques or algorithms available for maximum power point tracking. Ultimately all these methods use maximum power transfer theory. Let's consider the circuit shown in Figure 1.14, where r_{in} , R_L is internal resistance of DC source and load connected.

Based on Ohm's law, the loop current i_0 is given by,

$$i_0 = \frac{V_{in}}{r_{in} + R_L} \tag{1.20}$$

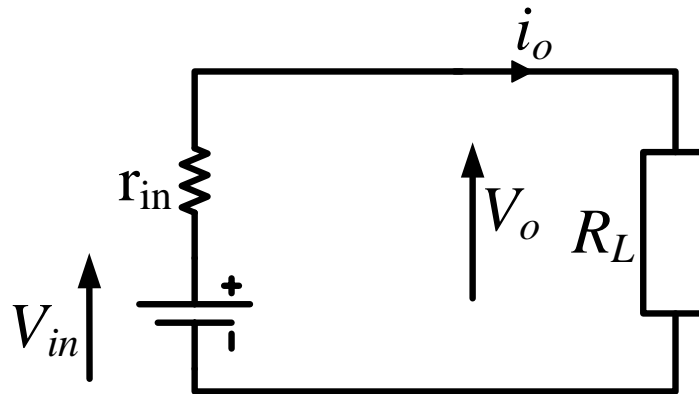


Figure 1.14: DC supply with external load connected

where V_{in} is the source voltage, r_{in} is the internal resistance of the source and R_L is the load resistance.

The terminal voltage at the load, V_o can be written as:

$$V_o = \frac{V_{in} R_L}{r_{in} + R_L} \quad (1.21)$$

using Eq.1.20 and 1.21 the power delivered to the load can be derived as:

$$P_L = \frac{V_{in}^2}{R_L} \left[\frac{1}{\left(1 + \frac{r_{in}}{R_L}\right)^2} \right] \quad (1.22)$$

Differentiating Eq. 1.22 with respect to R_L maximum power delivery to the connected loads can be achieved when $r_{in} = R_L$.

1.5.2 Summary of Existing Maximum Power Point Tracking (MPPT) Techniques

This fundamental theory of maximum power transfer is used in every technique or algorithm used for MPPT controllers. The impedance of the PV system must match that of the load in order to deliver maximum power to the connected load. The main commercially available MPPT techniques are:

Fixed Duty Cycle [28]

This is the simplest method available and does not require any feedback. Load impedance is adjusted to match with the PV module resistance only once to extract maximum power from the panel, and is classified as an off-line method. Variations in MPP due to temperature and irradiance are disregarded in this method.

Constant Voltage (CV) method [39]

In this method it is assumed that $V_{MPP} = kV_{OC}$ where V_{MPP} is the MPP voltage, $0.7 \leq k \leq 0.8$ and V_{OC} is the open-circuit voltage of the PV module under standard test conditions (1000 Wm^{-2} , 25°C). Since the value of k is based on an approximation, it does not always give the correct MPP. This results in poor performance as the linear relationship is unable to capture the complexities of shading. Also, the open-circuit voltage of the PV module varies a little with the

level of solar radiation, and can change significantly due to temperature variations. Therefore, this method is good in regions where the temperature does not vary widely. A flowchart for this method is provided in Figure 1.15.

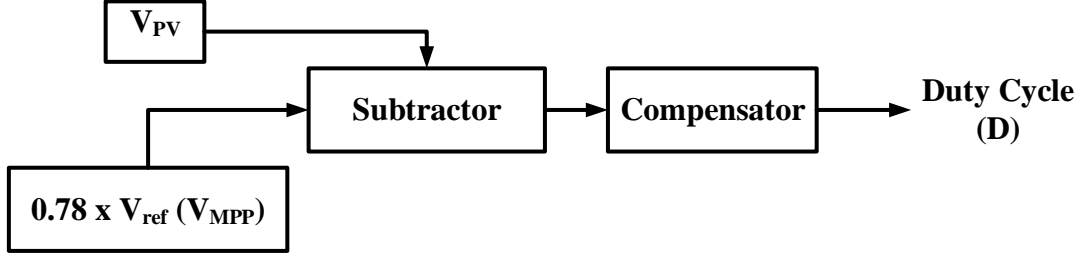


Figure 1.15: Flow chart for constant voltage (CV) method [39]

MPP locus Characterization [39]

The objective of this method is to establish a linear relationship between the current in the PV array and the voltage at MPP. Eq. 1.23 is used in this method. This relationship is given by the tangent to the MPP locus curve for the PV current in which the minimum irradiation condition satisfies the sensitivity of this method. The mathematical derivation of this method is discussed in [39]. As the MPP locus varies with irradiance and temperature, continuous updating of the model for the tangent line is required. This is achieved by measuring the V_{OC} of the array periodically and inserting the measured value in Eq. 1.23. The PV module must be disconnected from the load during these measurements, which results in power loss to the load.

$$T_L = \left(\frac{\eta V_T}{I_{MPP}} - N R_S \right) I_{MPP} + (V_{OC} - \eta [V D_o + V_T]) \quad (1.23)$$

where T_L is the tangent line, N is the number of cells, R_S is the series resistance of the PV module, V_{OC} is the open-circuit voltage, I_{MPP} is the current at the MPP, V_T is the thermal voltage, and $V D_o$ is differential voltage [39].

Perturb and Observe (P&O) [39]

According to Figure 1.13(c) it is obvious that the power produced by the PV module increases with the panel voltage before MPP and decreases after reaching MPP with an increase in voltage. The algorithm compares the power of the previous step ($P[k-1]$) with that of the next step ($P[k]$), so that it can increase or decrease the reference voltage (V_{ref}) of the switched DC-DC converter; i.e., if the current operating point is left of the MPP an increase in voltage will result in an increase in power. Therefore further voltage perturbation (increasing V_{ref}) is needed to reach the MPP. If the current operating point is to the right of the MPP an increase in voltage will result in a decrease in power. Hence, a reduction of V_{ref} is needed to reach the MPP. Therefore, the operating point is aligned towards the MPP by either increasing or decreasing the PV array voltage. The flowchart representation for this method is depicted in Figure 1.16

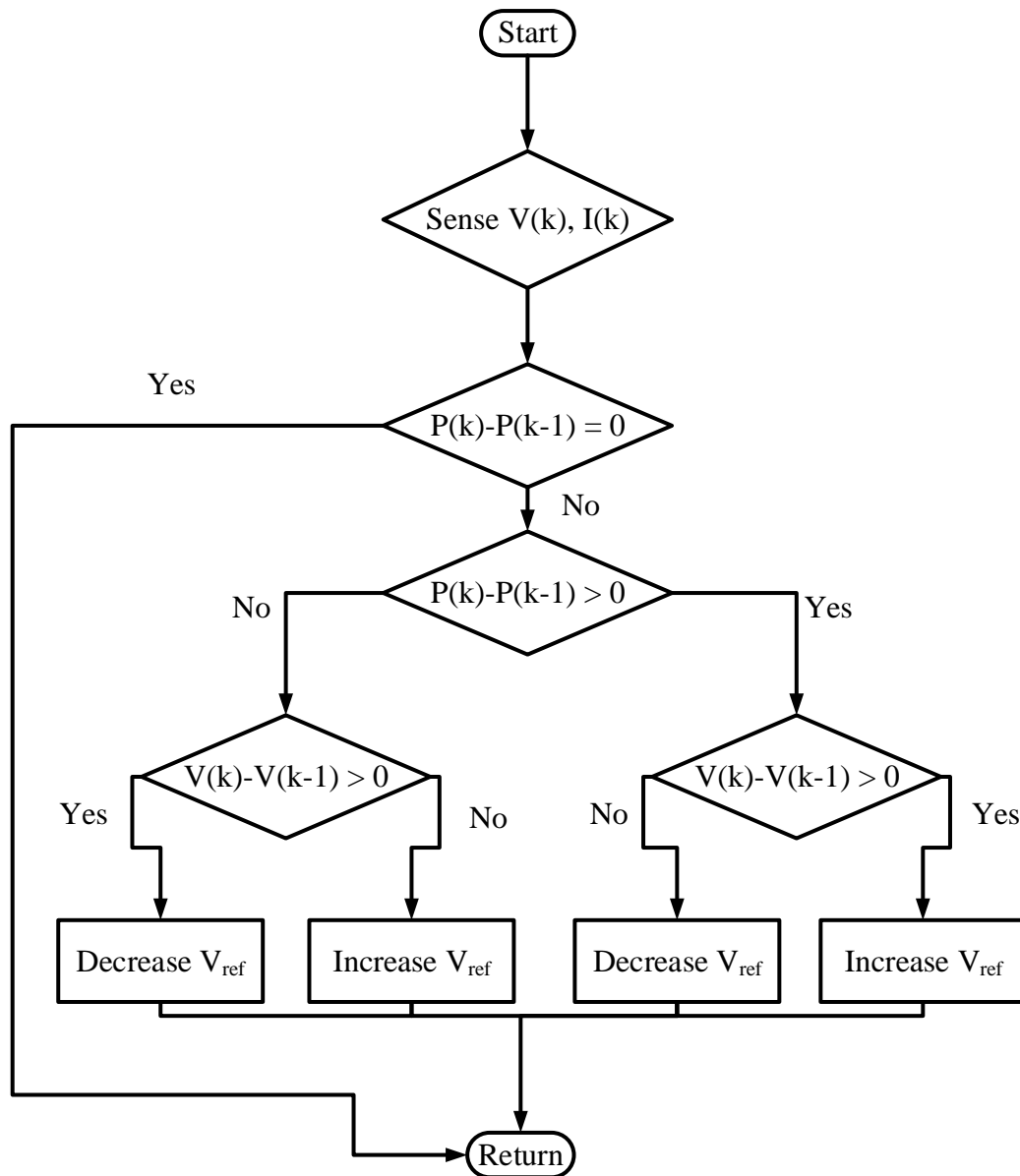


Figure 1.16: Flow chart for the perturb and observe (P&O) method

Incremental Conductance (IC) [39]

This method was proposed to overcome some limitations of the P&O method. This is based on the fact that the slope of the P-V characteristics curve is zero at MPP $\left(\frac{dP}{dV} = 0\right)$, positive to the left, and negative to the right, as shown in Figure 1.13 (c). Therefore the MPP is related to the incremental change in the conductance of the PV array, and by manipulating Eq. 1.24 and 1.25, the peak power delivery point can be located. The flow chart for the algorithm used in this method is provided in Figure 1.17.

$$\frac{dp}{dv} = \frac{d(vi)}{dv} = i + v \frac{di}{dv} = 0 \quad (1.24)$$

$$\frac{di}{dv} = -\frac{i}{v} \quad (1.25)$$

Based on the results of the comparison given below, the algorithm provides a decision to either increase or decrease the voltage across the PV array by changing the V_{ref} to the switched mode DC-DC converter.

- (a) $\Delta v/\Delta i = -i/v$: operating point at the MPP
- (b) $\Delta v/\Delta i < -i/v$: operating point lies to the left of the MPP
- (c) $\Delta v/\Delta i > -i/v$: operating point lies to the right of the MPP

Beta method [39]

The beta method provides an approximation of the MPP using an intermediate variable β [39]. The following equation is used to calculate this variable, in which the value of β at the optimum operating point remains constant. Therefore, β can be continuously calculated using the panel voltage and current.

$$\beta(V_{\text{PV}}, I_{\text{PV}}) = \ln\left(\frac{I_{\text{PV}}}{V_{\text{PV}}}\right) - cV_{\text{PV}}$$

where c is a constant depending on the electron charge (q), temperature (T), quality factor (η), Boltzmann constant (K_{B}) and the number of series cells (N_{s}). β can be continuously calculated using the voltage and current of the panel. However, the electrical parameters of the PV module should be known to estimate the optimal performance point.

Temperature method

For this technique a low-cost temperature sensor is used to modify the MPP algorithm function, because MPP varies with temperature. However, irregular temperature distribution on a PV array can cause practical implementation problems. The following equation is used:

$$V_{\text{MPP}}(T) = V_{\text{MPP}}(T_{\text{ref}}) + T_{\text{Kvoc}}(T - T_{\text{ref}})$$

where V_{MPP} is the MPP voltage, T is the panel temperature, T_{Kvoc} is the temperature coefficient of V_{MPP} and T_{ref} is the standard test condition temperature.

All these methods are used to match the load impedance with the resistance of the solar panel. The major characteristics of the above-mentioned methods are described in Table 1.6. More details can be found in the literature [39].

1.6 Chapter Summary

This chapter has provided an overview of renewable energy sources and the state of the art in DC microgrids, PV-based systems, batteries and the maximum power point tracking techniques used in PV systems. Even though there are many renewable energy sources that can be used to generate electricity, solar energy is the most popular choice. The two methods used to produce electricity from solar energy can be summarized as: (i) PV cell/ panel based power generation and (ii) Solar thermal power generation. In PV panel-based systems there are two categories: (i) grid-connected and (ii) off-grid. In each case, a rechargeable battery bank is used to achieve

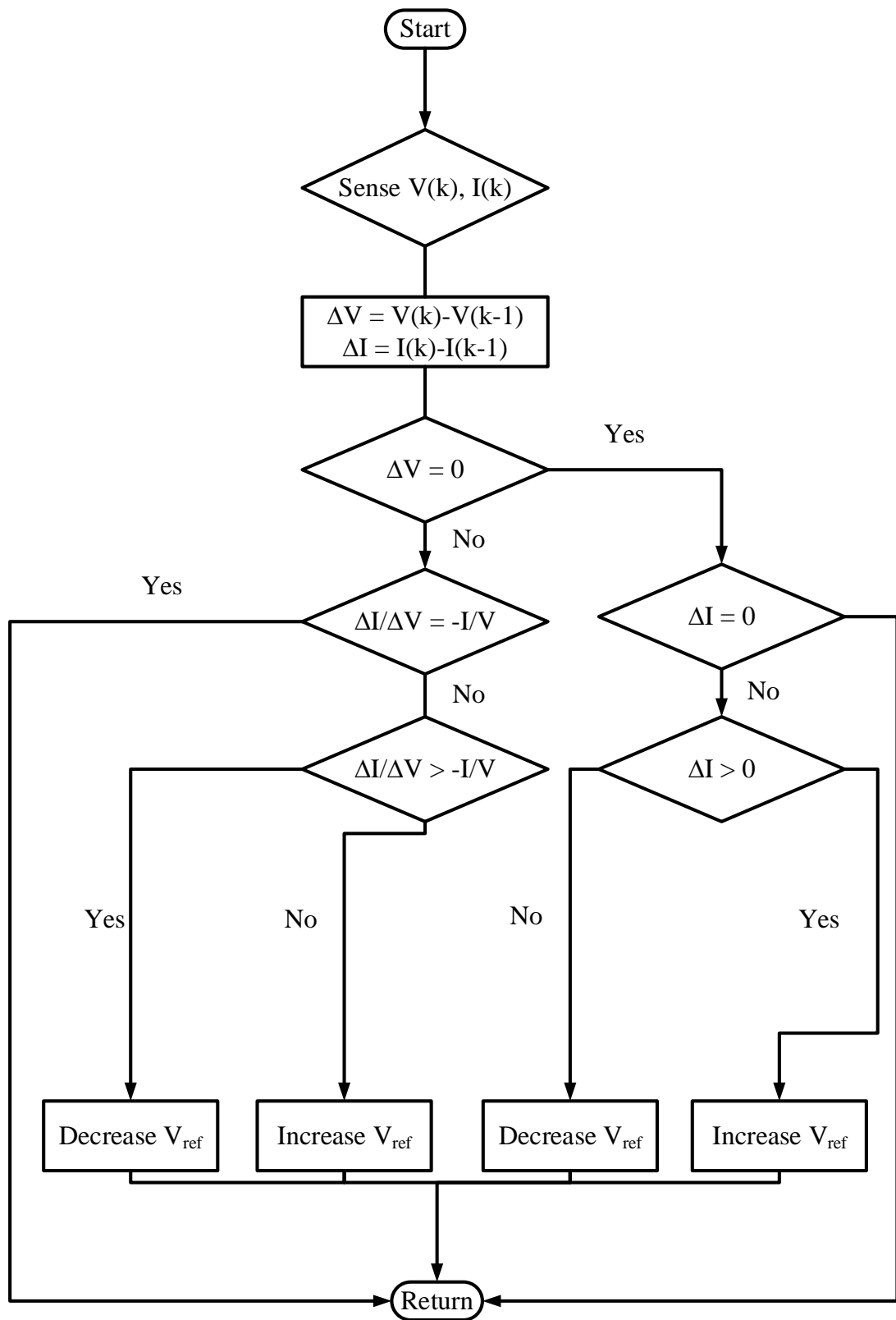


Figure 1.17: Flow chart for the incremental conductance (IC) method

Table 1.6: Major characteristics of MPPT algorithms [39]

Method	Dependency of PV array	Tracking Factor (TF)	Implementation complexity	Accuracy	Sensors
Fixed Duty	No	0.87	Very simple	Very low	None
Constant voltage	Yes	0.92	Simple	Low	V
P&O	No	0.96	Simple	Very High	V, I
IC	No	0.96	Medium	Very High	V, I
P&O based on PI controller	No	0.98	Medium	Very High	V, I
IC based on PI controller	No	0.98	Medium	Very High	V, I
Beta	Yes	0.99	Medium	Very High	V, I
Temperature	Yes	0.98	Simple	Very High	V, Temp

reliable operation. In a PV-battery-based DC microgrid, it is essential to use the maximum power point transfer technique to deliver maximum power to the load to achieve high overall efficiency. However, with the development of supercapacitors, it is now possible to use them as energy storage devices in PV-based DC microgrids.

The next chapter, will discuss supercapacitor technology and supercapacitor-assisted techniques.

Overview of Supercapacitors and Supercapacitor Assisted (SCA) Techniques

Supercapacitors (also known as ultra-capacitors or electrochemical double-layer capacitors (EDLC)) represent a newer energy storage device (ESD) family, that has excellent life-cycling but lower energy density than electrochemical batteries. With the ongoing development of supercapacitor (SC) technology, materials and manufacturing, it is now possible to use SCs as short-term ESDs in electronic systems with the advantages of low maintenance, extended life cycling and constant equivalent series resistance (ESR) with depth of discharge (DoD).

Early versions of supercapacitors were in the range of a few Farads only, with internal resistances of fractional ohms to a few ohms, aimed at simple applications such as powering memory modules for short to medium-term backup. With the device capacitances subsequently entering the range of 100 F to a few 1000 F, they were hybridized with battery packs, to make use of their high power density compared to batteries.

Over the last two decades, supercapacitors have emerged with single-cell capacitance values from 0.2 F to 5000 F within the same canister sizes used to package electrolytic capacitors and film capacitors. This means a million-times greater capacitance, despite their well-known limitation of less than 5.0 V DC voltage rating [40–46].

With over 100 worldwide manufacturers manufacturing these devices [47], today there are two new variations: the hybrid types and CAPAbatteries, in which the electro-chemistry of rechargeable Li-ion batteries is mixed with the electric double layer effect, to produce single-cell devices of capacitance up-to 70,000 F [33] with improved energy density.

2.1 Electrical Double Layer concept leading to Supercapacitor Technology

Supercapacitors are based on the same principles applicable to electrostatic capacitors, where two larger area plates and a shorter distance between plates can produce a higher effective capacitance. In SCs, the electrical double layer is formed next to a large area electrode and an electrolyte is effectively used. Therefore, these devices are known as electrical double-layer capacitors (EDLC).

Figure 2.1 illustrates the basics concept of an EDLC, where two electrodes are immersed in an ionic electrolyte with a separator located between the two electrodes. Double-layer capacitance is one of the most important characteristics of an electrical double layer that is formed at the interface between a conductive electrode and the adjacent liquid electrolyte. When an external electric field is applied to the two electrodes, they are electrically charged and ions in the electrolyte move towards the electrode of opposite charge [29, 40, 41, 48–52]. Typically, electrons in the electrode and ions in the electrolyte are separated by a single layer of solvent molecules that adheres to the surface of the electrode and acts as a dielectric in a conventional capacitor.

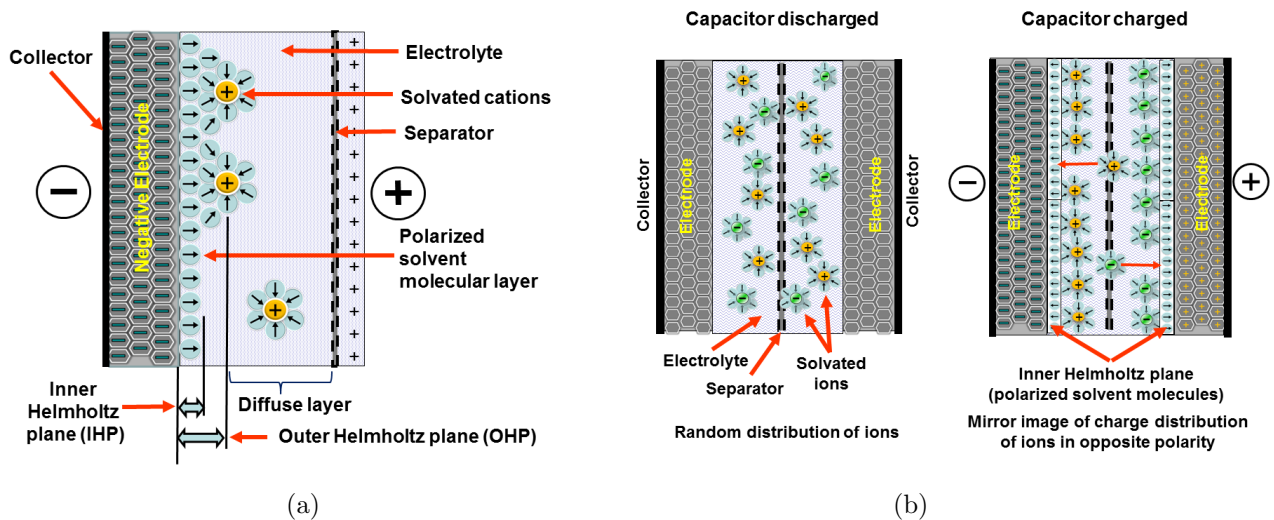


Figure 2.1: Concept of an EDLC capacitor formed by double layers at each electrode: (a) Conceptual electrochemical capacitor; (b) Charged and discharged condition [Source: European Passive-Components Institute]

As shown in Figure 2.1(b), during the charging state, the anions and cations are located in the electrolyte next to the electrode such that they balance the excess charge on the electrically conducting side of the phase boundary. Hence, there will be two layers of excess charge of opposite polarity across each phase boundary. Thus, the electrode-electrolyte interface represents a capacitor, so the complete cell can be represented as two capacitors in series. Therefore, for a symmetrical capacitor, the cell capacitance can be written as,

$$\frac{1}{C_{\text{cell}}} = \frac{1}{C_1} + \frac{1}{C_2} \quad (2.1)$$

where C_1 and C_2 are the capacitances of the first and second electrode-electrolyte interfaces respectively. This electrical double layer effect was the key to SC technology.

2.2 Supercapacitor (SC) Fundamentals

SCs are electrical double-layer capacitors where two electrodes (often made from activated carbon) are immersed in an organic, aqueous, solid state/quasi solid state, or redox active electrolyte [53] separated by non-conducting layer to separate charges as depicted in Figures 2.1 and 2.3. As shown in Figure 2.1(b), when an EDLC discharges, the charges at the boundary of

the electrode move to the electrolyte and at the same time positive and negative charges on the electrode are neutralized by the current through the external circuit. Figure 2.1(b) shows the behaviour of the capacitor during the discharging and charging process.

The use of porous carbon, such as active carbon, as electrodes, is motivated by its high electrical conductivity, low cost and high chemical stability with a large specific surface area (or large surface area per gram). Figure 2.2 shows an expanded view of the cross-section of a porous electrode, where the electrode surface is composed of multiple diameter pores with different pore size distribution (PSD). In a given particle of the porous material, different pore sizes are mixed and in each of these randomly distributed pores an electrical double layer is formed, creating capacitor plates with a very high surface area. Depending on the diameter of the pores they can be categorized as macro-pores, mesopores and micro-pores. This means that porous carbon electrodes can have a very large effective area creating a large capacitor at each electrode. To improve performance, various porous carbon materials, such as active carbons, carbide-derived carbons, zeolite-templated carbons, carbon nanotubes (CNTs), onion-like carbon, carbon aerogels, and graphene have been studied extensively as electrodes in EDLCs [54]. Although carbide-derived carbons and zeolite-templated carbons offer tight pore size control, high specific surface area and high conductivity, these techniques are yet to be commercialized [54].

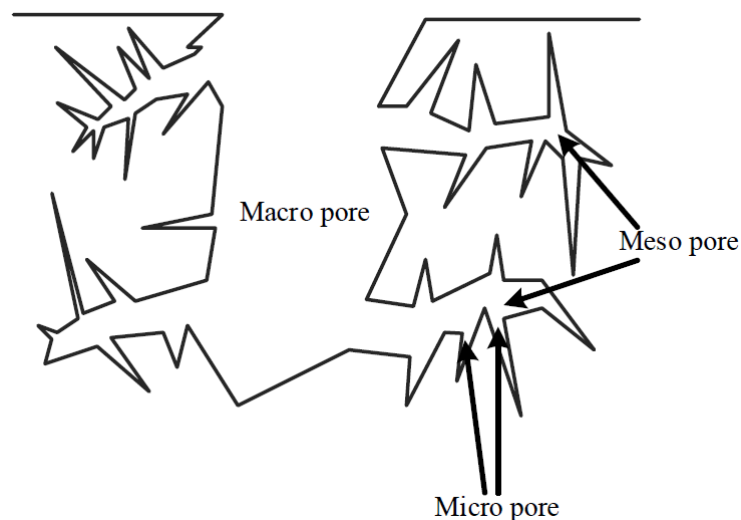


Figure 2.2: Cross-section of a porous carbon electrode [55]

Due to the micro-pores in a carbon-based material, the surface area of a carbon-based electrode can reach up to $3000 \text{ m}^2/\text{g}$ [56]. By combining this property with the short distance between opposite charges (typically less than 1 nm) it is possible to achieve high capacitance, of up to 5000 F per SC cell [40]. Since the separation process is purely physical (no redox reaction involved), an SC can undergo many more charge-discharge cycles than any other energy storage devices. Therefore, SCs have a longer life cycle than other energy storage devices such as batteries and normal capacitors. However, the power density of EDLCs depends on the pore size distribution and specific surface area of the electrode [54].

The capacitance of an SC can be very large (one million times larger than the typical μF electrolytic or film capacitor), in the order of farads to thousands of farads. This is due to the following factors:

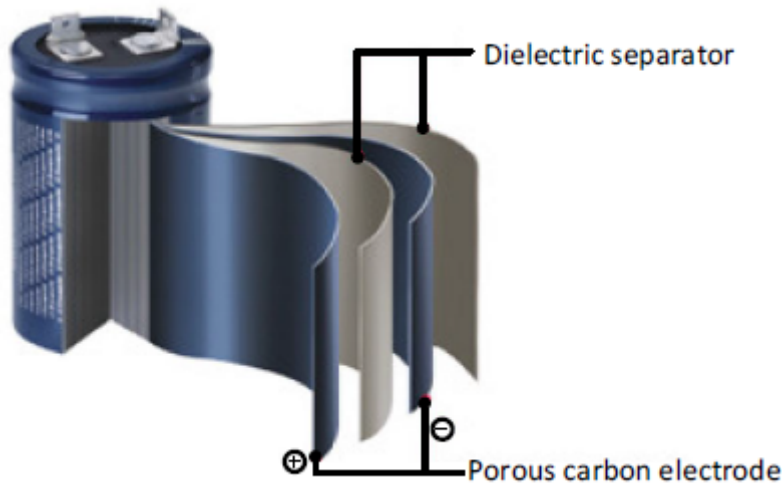


Figure 2.3: Multilayer cylindrical LSmtron supercapacitor

- (a) The huge surface area of the electrodes
- (b) The distance separating the opposite charges at the interfaces between the electrolyte and the electrodes is very small

Even though SCs have the advantages of providing a high equivalent surface area for electrodes, their parameters can be appraised using the same equations used for all other capacitors [57]. With the development of SC technology over last decade, SCs are now available ranging from fractional farads to a few tens of thousands of farads with power densities around 10,000 W/kg, energy densities around 170 Wh/L and ESR ranges from fractional m Ω to several m Ω [33, 56]. The maximum voltage across a single SC cell is limited to less than 5 V; this makes them different to normal capacitors, which can have ratings of up to several 1000 V DC.

According to the requirements of the application, SCs are connected in series to form an SC bank with higher voltage ratings [40, 42, 58]. This means the total capacitance of the SC bank decreases and the internal resistance increases. However, SCs normally show large deviations in their capacitance values, which can be as high as $\pm 20\%$ of their nominal capacitance value. Hence, the total voltage across the SC bank will not be equally distributed among the single SC cells connected in series, leading to over-voltage conditions appearing over one or more SC cells. This will result in individual cells being overcharged. Therefore, active or passive voltage balancing circuits are employed in SC banks to regulate the individual cell voltage. To improve the rated voltage of SCs, hybrid SCs have been developed by combining an anode of tantalum electrolytic capacitors with a cathode of electrochemical capacitors [59]. These hybrid SCs meet the requirements for larger capacitance while maintaining a high working voltage of about 100 V and a smaller internal resistance and size [42].

Figure 2.4 shows the internal resistance variation with depth of discharge of an electrochemical battery versus a supercapacitor, based on a disposable 6 V lantern cell and an EDLC supercapacitor of value 3000 F. From Figure 2.4 it can be seen that the SC has a constant 3 m Ω ESR over the percentage discharge whereas the 6 V Energizer cell resistance increases up to 4 Ω with percentage discharge. Hence, SC banks could be used to replace environmentally unfriendly electrochemical battery packs with a lower number of cycles. A comparison of the properties of energy storage devices is provided in Table 2.1.

Table 2.1: A comparison of energy storage technologies [60]

Item	Batteries	Supercaps	Capacitors
charge time	1-5 h	1-60 min	10^{-3} to 10^{-6} s
discharge time	0.3-3 h	0.1-30 min	10^{-3} to 10^{-6} s
energy density (Wh/kg)	20-100	1-20	< 0.1
power density (W/kg)	50-200	10,000	< 10,000
cycle time (cycles)	500-2000	50,000-1,000,000	> 10^6
charge/discharge efficiency	70 – 85%	near 100%	near 100%
Internal resistance or ESR	from 50 m Ω to few Ω (increases with DoD)	fractional m Ω to several m Ω (constant with DoD)	fractional Ω to several Ω

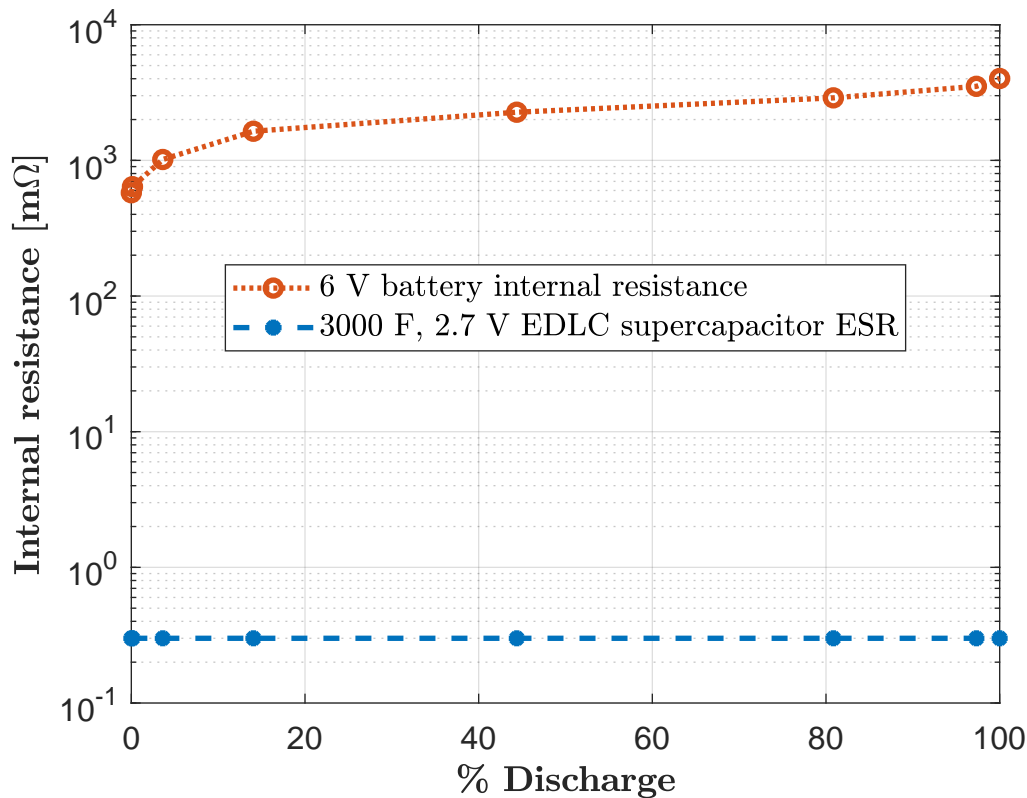


Figure 2.4: Variation of internal resistance of a 3000 F, 2.7 V EDLC supercapacitor and an Energizer 6 V battery with percentage discharge (internal resistance values for EDLC supercapacitor was obtained from SAMWHA data sheet and internal resistance for 6V battery data was collected from set of experiments done in the labs)

In the early developmental stages, supercapacitor companies aimed to develop these devices with low ESR to replace or supplement rechargeable battery packs, making use of their advantages including their higher operating temperature range, high power density (due to their low ESR), and extremely long life, in the order of 300,000 to 1,000,000 cycles. However, the energy density improvements for supercapacitor families over the last two decades have been lower than for rechargeable Li-ion battery chemistries, with two-to three-fold less energy density. Figure 2.5 provides a simplified view of an EDLC, with a comparison of some electrolytic capacitances with EDLCs where canister sizes are nearly similar even though SCs can store more energy than normal capacitors. This has encouraged the use of SCs in power electronic circuits.

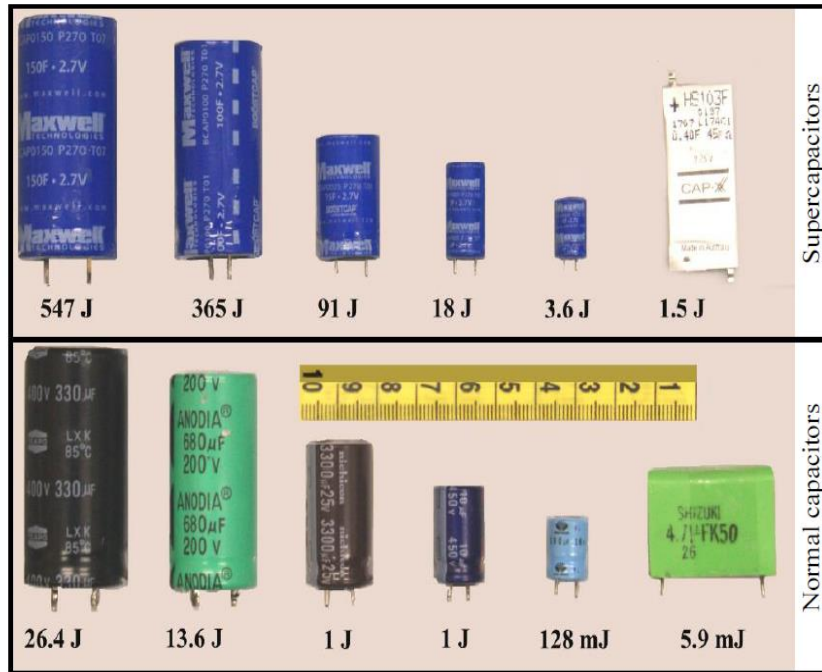


Figure 2.5: Comparison of electrolytic capacitors and supercapacitors

At this point, it is worth summarizing the differences between electrochemical battery cells and capacitors. In electrochemical batteries, charge is stored indirectly and is added to or withdrawn from the battery based on a Faradaic process. The charge transfer across the interface involves oxidation and reduction reactions. As explained previously, in electrochemical capacitors actual positive and negative electrostatic charges physically reside on a two-dimensional plate set. Therefore, the two processes can be distinguished as non-faradaic and faradaic in capacitors and batteries, respectively.

2.3 Comparison of Commercially Available Supercapacitors

During the last five to eight years, supercapacitor manufacturers in Asia have developed several more variations of these devices, giving us three different device families: (i) symmetrical EDLCs; (ii) hybrid types with one electrode based on lithium compounds such as lithium titanate; (iii) CAPAbatteries where pseudocapacitance properties of lithium compounds are mixed with activated carbon-based EDLCs. An interesting comparison of these advancements is provided in Figure 2.6, where the three types are shown in a similar canister size, with capacitances varying from 3000 F (in the symmetric EDLC) to a hybrid device of 7500 F and a giant 40,000 F CAPAbattery. A parameter comparison of these commercially available SC families is shown in Table 2.2.

When considering the newly introduced CAPAbattery-type SCs, it can be seen that they have improved energy density and capacitance as well as improved rated voltage. Despite the reduced cycle life and power density compared to mature families of symmetrical EDLCs, they offer much higher cycle life and power density than commonly used lead-acid batteries.



Figure 2.6: Three different supercapacitor families (Courtesy of Samwha Electric, Korea)

Table 2.2: Comparison of commercially available supercapacitors [33]

Parameter	EDLCs	Hybrid SCs	CAPAbatteries	Pb-acid	Li-ion
Energy density (Wh/l)	5 – 8	10 – 14	50 – 120	50 – 125	250 – 670
Power density (W/l)	8000	2500 – 4000	1600 – 3200	25 – 100	375 – 1750
Cycle Life (cycles)	1,000,000	40,000 – 50,000	15,000 – 20,000	500 – 2000	1000 – 1200
Rated voltage (V)	2.7	2.7	2.8	2.0	3.0 – 3.6
Capacitance (F)	1 – 3000	200 – 7500	1000 – 70000	NA	NA

Comparison of the performance characteristics of three different commercially available supercapacitor variations was carried out based on the following samples:

- (i) 3000 F, 2.7 V electrostatic double-layer supercapacitor (EDLC)
- (ii) 7500 F, 2.7 V supercapacitor of the pseudo-capacitive hybrid technology (Hybrid SC)
- (iii) 40000 F, 2.8 V supercapacitor of the battery-type hybrid technology (CAPAbattery)

Tests were carried out to assess the discharge voltage profiles, constant resistance discharge and constant current discharge. The results of these tests are given in Figures 2.7 and 2.8.

2.3.1 Constant resistance discharge

Figure 2.7 depicts the behaviour of EDLC, hybrid and CAPAbattery SCs when discharged using a constant resistance. Figure 2.7 shows that the discharge curve of an EDLC supercapacitor is similar to that of a normal electrolytic capacitor (i.e. during the discharge voltage and current undergo near-exponential decay). The discharge behaviour of SCs tends towards batteries as the SC technologies move from EDLCs to hybrid SCs and CAPAbatteries. This highlights the improvement in the energy density of supercapacitor technologies. From a voltage value of 2 V to the rated 2.7 V, the CAPAbattery can be approximated as a constant voltage source. The same applies to the hybrid SC from about 1.6 V to the rated 2.8 V.

2.3.2 Constant current discharge

In describing electrochemical batteries, charge or discharge current is often expressed as the *C-rate* normalized against battery capacity, which is very different from one battery to another.

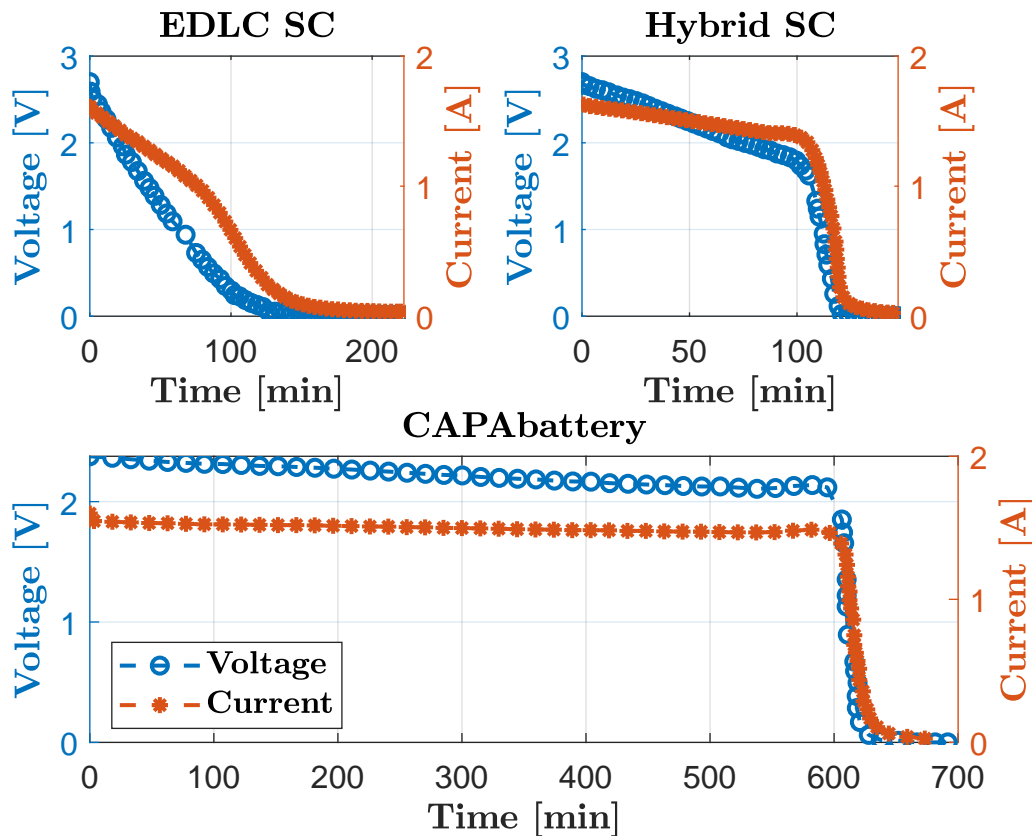


Figure 2.7: Discharge curves for different SC technologies - Under constant resistance (Devices tested were 3000 F , 2.7 V ELDC SC, 7000 F, 2.7 V Hybrid SC and 40000 F, 2.8 V CAPAbattery respectively)

The *C-rate* is a measure of the rate at which a battery is charged or discharged relative to its maximum capacity. A 1C rate means that the discharge or charge current will discharge or charge the battery in 1 hour as discussed in Chapter 1.

Based on the graphs in Figure 2.7 it is easy to see that both the hybrid SC and the CAPAbattery discharge curves are closer to the case of rechargeable batteries, without showing an exponential or a near-exponential curve. Therefore it was decided to observe the behaviour of both SCs when they were discharged at different C-rates.

C-rate calculation for Hybrid and CAPAbattery supercapacitors

The flat part of the discharge curves for hybrid and CAPAbattery SCs is a useful region for energy back-up. In this part of the curve, the SC voltage experiences minor changes per unit time during supercapacitor discharging. Both hybrid and CAPAbattery SCs act as a voltage source at this stage of discharge. This is the part used for the C-rate calculations. The SC voltage in this area averaged 2.2 V and 2.3 V for the = CAPAbattery and the hybrid SC respectively. Given this performance, the following method, as shown in Table 2.3, was used to calculate the C-rate for both cases. These calculated currents may differ from measured values, which can be attributed to the fact that the capacitance of a supercapacitor does not stay constant throughout the discharge process.

Table 2.3: C-rate calculation for supercapacitors

Parameter	Hybrid SC	CAPAbattery SC
Capacitance [F]	7500	40000
Mid-point voltage (from Figure 2.7) [V]	2.3	2.2
Energy = $0.5CV^2$ [J]	19838	96800
Capacity = $\frac{\text{Energy}}{3600 \cdot \text{Voltage}}$ [Ah]	2.4	12.2
1C rate [A]	2.4	12.2

Hence, it was estimated that the 7,500 F hybrid device could be considered as a 2.4 Ah battery and the 40,000 F CAPAbattery could be considered as a 12.2 Ah battery. Based on this a set of constant current discharges at 1C was carried out for both samples. The results are presented in Figure 2.8(a), showing the respective voltage profiles at 1C rate.

As shown in Figure 2.8(b), the devices show similar behaviour to batteries with higher C-rates having less DoD than lower C-rates. Therefore, just as in a battery, a CAPAbattery SC makes more energy available when discharged at lower current values. In order to draw a constant current, TEXIO PXL-151A, a solid-state electronic load, was used during this experiment.

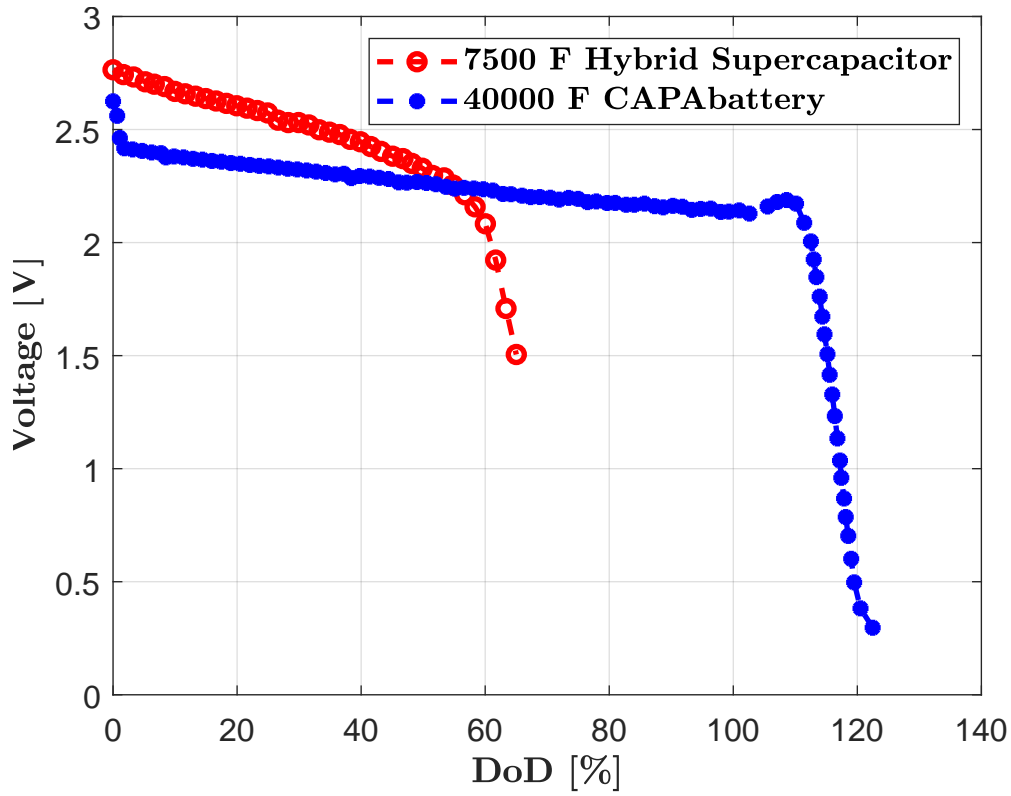
In all rechargeable battery chemistries, a well-known fact is the reduction of the cycle life with an increased depth of discharge. One unique useful property of supercapacitors is that their cycle life is relatively constant with the depth of discharge, resulting in a longer cycle life than batteries. Figure 2.9 shows the expected average cycles with DoD for batteries and SCs.

2.4 Traditional Applications of Supercapacitors

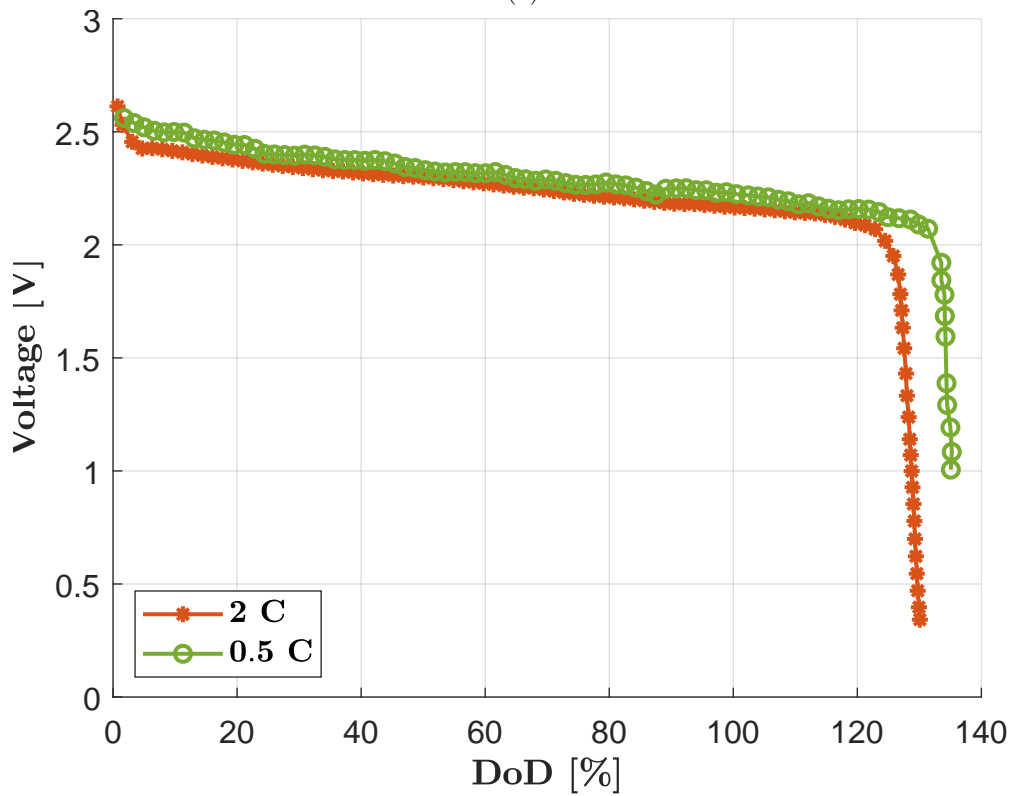
The continuous developments in SC technology have made supercapacitors available for a variety of applications. SCs are extensively used as power back-up for memory functions in a wide range of consumer products such as mobile phones, laptops and radio tuners. They are also used in pulsed applications to share the load and for providing peak power assistance to reduce the duty cycle on the battery to prolong battery life in products or devices using mechanical actuators, such as digital cameras.

Supercapacitors are used as an energy storage device for starter motors in modern vehicles, and emergency door opening systems in aircraft. Even though SCs are used as ESDs, they are not suitable to use as the primary energy source for automotive applications (in electric vehicles (EVs) and hybrid electric vehicles (HEVs)) because of the disadvantage of the low energy density of SCs. However, their advantages make them ideal for capturing and temporarily storing the energy from regenerative braking, and for providing short-duration peak power boosts allowing the primary battery to be downsized. Since SCs are connected in parallel with the battery pack in these applications, they can only be charged to the upper voltage level of the battery and can only be discharged to lower level of the battery, leaving considerable unused energy in the SC.

Supercapacitors are also used to provide fast-acting, short-term power back-up for uninterrupted power supply (UPS) applications. By combining a supercapacitor with a battery-based UPS system, the life of the battery pack can be extended, because batteries provide energy only during long-term interruptions and short-term interruptions are handled by the SC bank in the system. Reducing the peak loads on the battery pack permits the use of smaller batteries.



(a)



(b)

Figure 2.8: Constant current discharge curve for hybrid and CAPAbattery SCs: (a) Discharge curve for hybrid and CAPAbattery SCs at 1 C; (b) Discharge curves for 40,000 F CAPAbattery at different C-rates

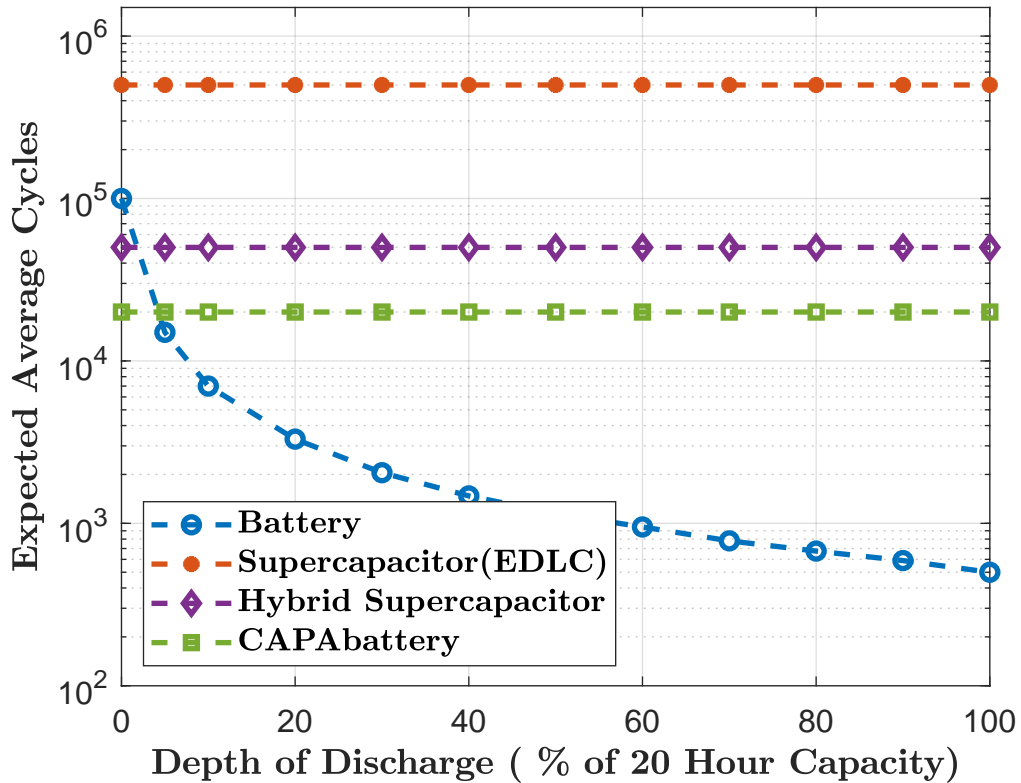


Figure 2.9: Variation of Average life cycle for batteries and SCs with Depth of Discharge [33]

The myriad of traditional applications that use SCs can be summarized as follows:

- (a) Battery-less UPS systems for short autonomy applications [61]
- (b) Automotive applications including the ECO Start/Stop function
- (c) Electric buses, aircraft and other transportation applications
- (d) Utility voltage stabilizer systems
- (e) Portable devices

2.5 Non-Traditional Applications of Supercapacitors: SCA Techniques from an Application viewpoint

Based on over a decade of a major research projects at the University of Waikato (UOW), the Power Electronic research team has shown that supercapacitors can be used in non-traditional applications such as;

- (i) High-efficiency and extra-low-frequency DC-DC converters
- (ii) High-performance surge protector circuits
- (iii) Temperature modification apparatus
- (iv) High-performance inverters

These circuits are currently known as supercapacitor assisted (SCA) circuits. This section provides a summary of these techniques from an application view point. More details about these early achievements are available in [62].

2.5.1 Supercapacitor assisted low drop-out (SCALDO) regulator

To achieve a DC-DC conversion, three commonly used traditional approaches are linear, inductor-based switch modes and switched capacitor types. Inductor-based switch-modes are complex high-frequency switching circuits. This raises the issue of RFI/EMI, which demands more complex overall circuits, but with high efficiency. In cases where high efficiency and lower noise are demanded by a load, designers combine low drop-out (LDO) linear regulators with a switch-mode converter, which is a costly and complex solution. Switched capacitor converters are also high frequency, low current capability converters, which frequently require additional voltage regulators for precise DC output.

In general, linear converters offer high-quality DC output with low noise and high current slew rate capability, but with the clear disadvantage of lower efficiency when the input to output voltage difference is higher. These circuits have minimum components and consume smaller amount of PCB real estate.

In LDOs, a very small voltage difference between the input voltage V_{in} and the regulated output voltage V_O is maintained to achieve an approximate efficiency of $\eta \approx V_O/V_{in}$. However, in LDOs the main power loss is due to series pass elements (such as a bipolar junction transistor (BJT), a metal oxide field-effect transistor (MOSFET) or their combinations).

If a lossless voltage dropper element can be inserted into the path of the series pass element, power loss in the series pass element can be minimized. This simple concept has given rise to the unique DC-DC converter topology known as the supercapacitor assisted low dropout (SCALDO) regulator which was patented in 2011 [63]. In this technique a very large capacitor is inserted in the series path of the regulator as depicted in Figure 2.10, and allows the load current to develop an incremental voltage, Δv , across the capacitor based on the relationship: $\Delta v = \frac{I_L \Delta t}{C}$ where I_L is the load current, Δt is the time duration and C is the capacitance of the capacitor. If C is very large (an SC) the voltage developed in the capacitor during Δt will be very small and will take a long time to block the circuit (due to the capacitor becoming fully charged).

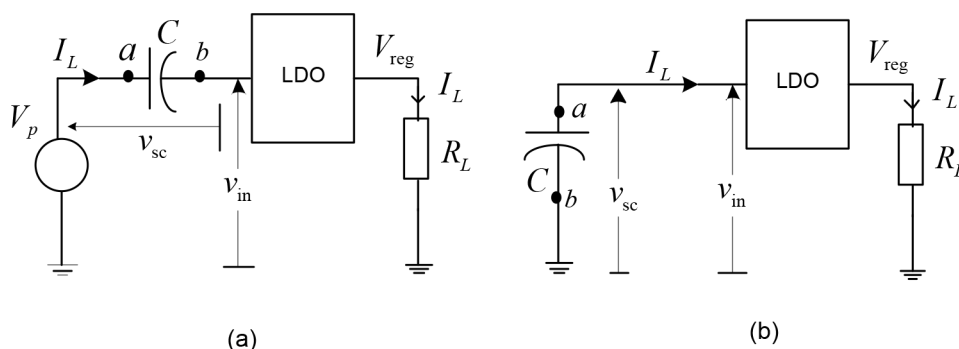


Figure 2.10: SCALDO converter: (a) SC bank charging while minimizing series dissipation; (b) Releasing stored energy in the SC bank [52]

Based on this principle, SCs can cyclically store and release energy. Figure 2.10(a) depicts the charging phase where the SC is charged from the unregulated DC voltage source, until the input voltage of LDO (V_{in}) reaches the minimum allowable voltage for regulation. Then the SC is connected parallel with the input of the LDO while disconnecting the unregulated DC source

as shown in Figure 2.10(b), to release the stored energy in the SC. This means the end-to-end efficiency (ETEE) of a linear regulator based on an LDO can be improved by a multiplication factor. The efficiency improvement factor for the SCALDO technique is indicated by:

$$\text{efficiency improvement factor} = \frac{\text{ETEE of SCALDO regulator}}{\text{ETEE of related linear regulator}}$$

where for the two cases of 5 – 3.33 V and 12 – 5 V, this factor is 1.33 and 2 respectively. The SCALDO converter, which is not a variation of switched capacitor converters [64], [60], has other useful characteristics such as:

- (i) DC UPS capability (by over-sizing the SC)
- (ii) Low noise and high slew rate output capability (due to load being directly fed by the low dropout regulator)
- (iii) Extra low-frequency operation eliminating the RFI/EMI issues typical of high frequency switching DC-DC converters

Table 2.4 compares typical DC-DC converter techniques with the supercapacitor assisted low drop-out (SCALDO) regulator technique. More details of the SCALDO converter are available in the literature [19], [60], [65], [64], [66].

Table 2.4: Comparison of DC-DC converter techniques [52]

Feature	Linear regulators	Charge pump converters	Switched-mode power supplies	SCALDO
Design complexity	Low	Moderate	Moderate to High	Moderate
Efficiency	Low to Moderate	Moderate to High	High	High
Noise	Lowest	Low	Low to Moderate	Low
Magnetic parts	No	No	Yes	No
Thermal management	Poor to Moderate	Good	Best	Best
Output current capability	Low	Moderate	High	Moderate to High
Cost	Low	Moderate	Moderate to High	Moderate to High
Limitations	Cannot Step up	V_{IN}/V_{out} ratio	Layout considerations	Number of switches

2.5.2 Supercapacitor assisted surge absorber (SCASA)

A simple RC circuit, with a 1Ω resistor and a $1\mu\text{F}$ capacitor, will have a very short time constant of $1\mu\text{s}$ where it will achieve its steady state after about $5\mu\text{s}$. However, if the capacitor is replaced with a supercapacitor of 1 F the time constant will change to 1 second, which will be almost three orders of magnitude longer than the duration of a typical transient surge voltage induced on a 230 V, 50 Hz or 120 V, 60 Hz power line. The basic theory for an RC charging loop indicates that when the capacitor starts charging, most energy is wasted in the resistive element, which keeps reducing as the capacitor acquires charge. The supercapacitor assisted surge absorber (SCASA) is based on this simple principle.

Figure 2.11 shows the basis of the patented SCASA concept, with a few microsecond of transient over-voltage of several thousand volts applied to a large time-constant RC circuit, where the supercapacitor has a very low DC voltage rating (usually less than 5 V). In this case,

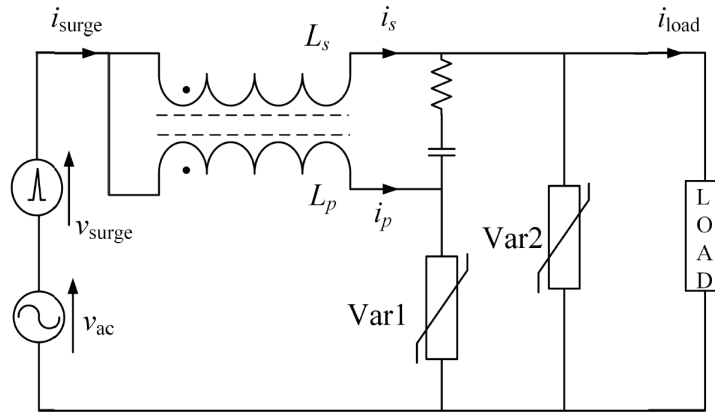


Figure 2.11: The simplified version of SCASA [67]

it is possible to theoretically show that if the high voltage surge lasts only a few tens of μs (microseconds), the energy in the transient voltage source is dissipated in the resistor, while achieving a minimum voltage on the supercapacitor, which is within the DC voltage limit of the device. References [67–69] give details on how this RC circuit situation allows supercapacitors to be used in surge absorption circuits.

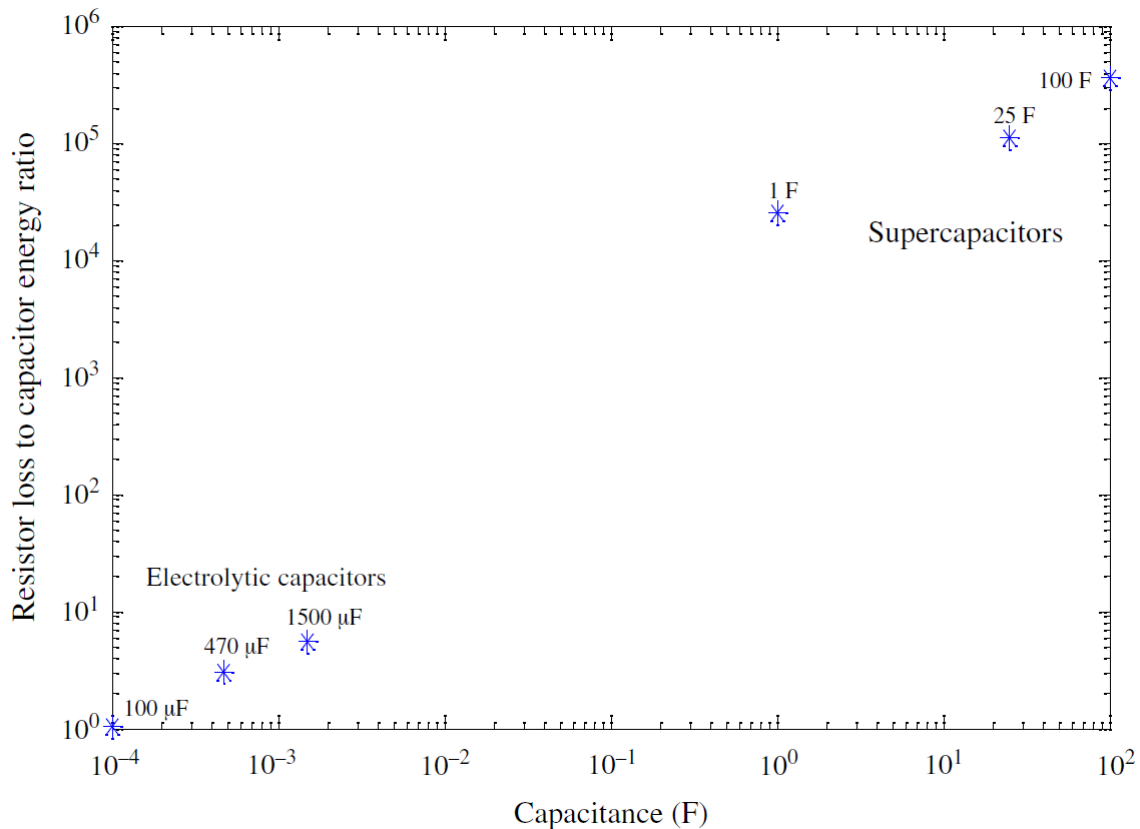


Figure 2.12: Comparison of energy lost and stored for electrolytic capacitors and SCs subjected to a 6 kV, 50 μs pulse [70]

Therefore, most commercial supercapacitors are capable of withstanding short-duration, high-voltage transient surges, the SCASA technique is based on the case of a normal capacitor in RC charging loop is replaced with 1 to 10 F supercapacitor. Figure 2.12(b), shows

$\left(\frac{\text{Energy loss in } R}{\text{Energy absorbed by } C} \right)$ for different values of C for devices from μF order to farad order. This shows that SCs can easily be used to divert surge energy into the loop resistance R . However, with the DC voltage rating of supercapacitors being only a few volts, and their impedance at line frequency also being quite low, they cannot be used directly across the line and neutral of the power line. To solve these issues a unique circuit configuration (SCASA), as shown in Figure 2.11, was developed.

In the SCASA technique, the RC circuit is configured in such a way that it uses the resistive element to absorb a significant part of the surge energy superimposed on the AC mains waveform, using the supercapacitor as an assistive circuit element to circulate the surge energy. One challenge in the practical SCASA circuit is to keep the terminals of the symmetrical supercapacitor within the maximum DC voltage rating. The coupled magnetic element, in essence, assists in the process of absorbing surge energy, and a commercial application circuit of SCASA is shown in Figure 2.11. More details are available in [70].

2.5.3 Supercapacitor assisted temperature modification apparatus (SCATMA)

In domestic hot water supply systems and central heating systems, whether they are gas or electrical, the hot water unit is usually placed in a central location and small diameter pipes carry hot water from the central unit to individual faucets. Though fast-acting gas heater systems are becoming popular, wasting processed water and heat energy due to the cold water being stored in the pipes between the central gas unit and the individual faucet is unavoidable in domestic situations. The delay in hot water coming out of a faucet is mainly due to the length of the pipes connecting the faucet to the hot water unit. In general, this delay could be in the range of 0.5 to 1 minute, with about 0.5 litre to over 1 litre of processed water wasted every time. In New Zealand, with a population of approximately 4.5 million, more than 15 million litres of treated water are wasted annually due to this problem. There are several commercially used techniques to overcome this problem, but none of them have been widely accepted by the building industry due to excessive cost and other issues [71, 72].

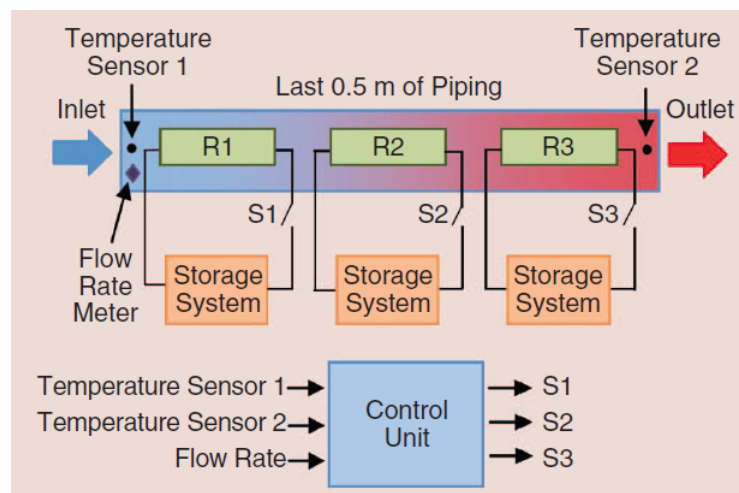


Figure 2.13: The implementation block diagram of the SCATMA technique [62]

To achieve an average temperature rise of nearly 20°C in the water within 5 to 10 seconds, with average water flow rates varying from 4 – 10 litres/min, the power required in a heating element (placed in the last half-metre of plumbing before the faucet) will be in the range shown in Table 2.5. In general, such power requirements are not permitted from a 230 V, 50 Hz, 10 A distribution circuit in a residential building. Another issue is that AC powered heating elements cannot be placed next to a water faucet due to safety regulations.

Table 2.5: Essential specifications for fast-heating solutions based on energy storage [29]

Parameter	Specification
Total maximum Temperature rise	20° C
Average water flow rate	6 L/min
Estimated time to receive central hot water from the gas heater	20 s
Total energy requirement (with losses neglected)	47 Wh
Power capability of heating element	8.4 kW
Maximum voltage allowed (based on AS/NZS 60950.1:2003)	60 V DC or 42.4 V _{peak}

The supercapacitor assisted temperature modification apparatus (SCATMA) is a novel patented technique, developed at the University of Waikato, to overcome the delay in the delivery of hot water at water faucets. This system [71, 72] delivers a power level varying from 10 to 20 kW from a pre-charged supercapacitor bank of around 100 F to 200 F, with a safe DC voltage of approximately 30 V. Figure 2.13 shows the block diagram. The system was originally built using 16 elements of 3000 F devices with a 2.7 V rating. In the early version, due to the cost of the supercapacitors, the research team had to use a supercapacitor-battery hybrid. However after 2016, with similar can size devices having capacitance values from 7,500 F to 70,000 F, the battery hybridization was no longer mandatory, giving the long life advantage of SC banks for a fit-and-forget system. Another key element in the success of this technique was the unique fast charger for supercapacitor modules.

2.5.4 Supercapacitor assisted high density inverter (SCADHI)

This research aims to increase inverter efficiency. There are several losses in inverters such as, including (a) switching loss; (b) magnetic loss; (c) the fundamental losses in capacitor charging and discharging; (d) loss due to ripples at the inverter input; and (e) losses due to the harmonics at the inverter output.

In this research, inverter efficiency will be increased by reducing the fundamental loss in capacitor charging. Supercapacitors will be used as they have lower ESR and have less energy dissipation during charging and discharging compared to electrolytic capacitors. In the basic RC circuit, the energy stored in the capacitor ($0.5CV^2$) is equal to the energy dissipated in the loop resistance. If an additional resistance is inserted as a useful resistive load (inverter) in the loop, while the source internal resistance, loop resistance and capacitor internal resistance waste energy, the resistive load (inverter) uses the waste energy and leads to improved charging efficiency [73]. This concept is shown in Figure 2.14 and a similar idea was indirectly used in the SCALDO technique to increase the efficiency of linear regulators.

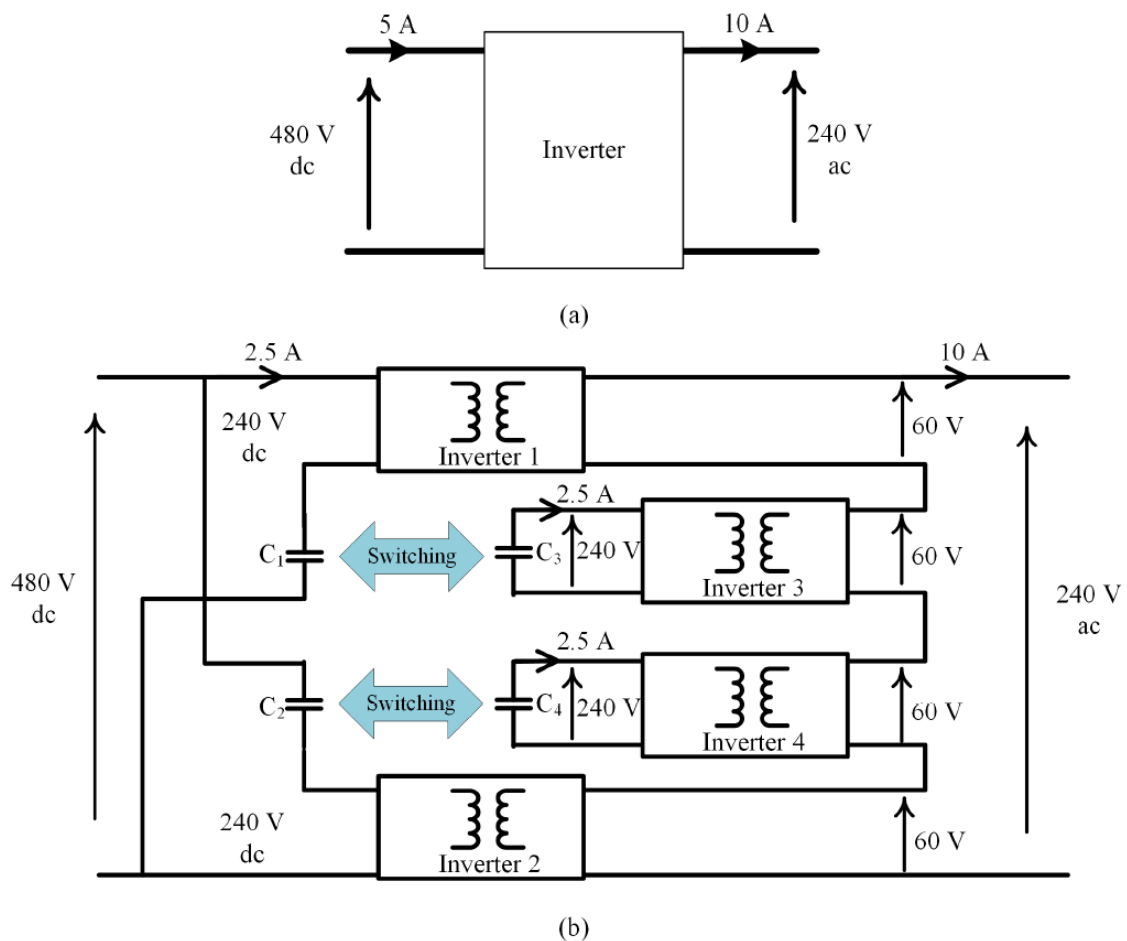


Figure 2.14: The simplified concept of the SCADHI technique: (a) overall inverter block; (b) block diagram of SCADHI [62]

2.5.5 Supercapacitor assisted LED (SCALED) lighting converter

The SCALED technique is another simple SCA technique, which is the main subject of this thesis, and is discussed in the next chapter.

2.6 Supercapacitor models and equivalent circuits

Depending on the application, different types of equivalent circuits with various complexities can be used. Figure 2.15(a) shows the simplest version of a series resistance and a capacitance in series assuming a constant capacitance (independent of the voltage) and constant ESR [46]. However, experimental behaviour and measurements indicate that this is only a very first approximation, which ignores leakage. Figure 2.15(b) represents the first-order model of a supercapacitor [43–45]. This model comprises four basic elements: R_S - ESR; R_P - parallel resistance (leakage resistance); C - capacitance; L - series inductance. R_S causes energy loss during capacitor charging and discharging, and R_P simulates energy loss due to capacitor self-discharge. Since R_P is always much greater than R_S , R_P is neglected in high-power applications. L results from the physical construction of the capacitor and is usually a very small value, which can be ignored in constant-current charging/discharging applications.

Generalized Loss Circumvention Concept Applied to RC Charging Circuit Leading to SCA Techniques

Traditionally, the charging of a capacitor is achieved either by a voltage or a current source. The main difference between charging a capacitor and supplying a resistive load is that the resistive load draws a constant current depending on the voltage supplied. As a result, the resistive load consumes continuous power.

However, in the case of a capacitor, the voltage of the capacitor depends on its state of charge. Therefore, it is possible to consider a capacitor as a variable voltage source with series resistance. The varying voltage is the capacitor voltage and the series resistance is the ESR of the capacitor. Charging a capacitor using a voltage source is not an efficient process as charging an electrochemical battery. This chapter will discuss the losses in a simple RC charging circuit and ways to improve the efficiency of the capacitor charging loop.

3.1 Analysis of a modified RC charging loop and the supercapacitor assisted loss management concept (SCALOM)

Considering a simple RC circuit with a total loop resistance of $1\ \Omega$ and an ideal capacitance of $1\ \mu\text{F}$, this circuit will have a time constant of $1\ \mu\text{s}$ and if the capacitor starts with zero voltage, it will acquire an energy content of $\frac{CV^2}{2}$, within about 5 time constants, or $5\ \mu\text{s}$, while the resistor dissipates the same amount of energy. This makes the circuit operation only 50% efficient unless the heat dissipated in the resistor is usefully applied.

3.1.1 Capacitor charging behaviour of an RC circuit leading to the loss circumvention concept (LCC)

Figure 3.1(a) represents a typical RC charging loop in which a capacitor is directly charged from a constant DC voltage source, V_s , starting from 0 V. In this case, the energy stored in the capacitor in terms of the maximum charge accumulated by the capacitor (Q) and the DC source voltage is given by:

$$E_C = \frac{CV_s^2}{2} = \frac{QV_s}{2} \quad (3.1)$$

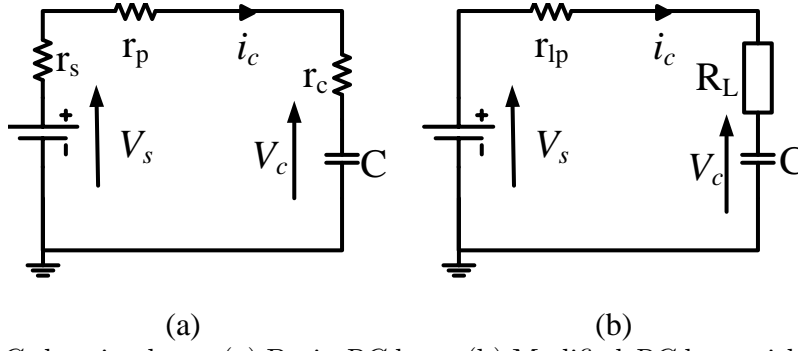


Figure 3.1: RC charging loop: (a) Basic RC loop; (b) Modified RC loop with loss circumvention concept (LCC)

The loop current for the circuit shown in Figure 3.1(a), i_C can be written as:

$$i_C = \frac{V_s}{r_p + r_c + r_s} \exp\left[\frac{-t}{C(r_p + r_c + r_s)}\right] \quad (3.2)$$

where r_p is the path resistance, r_c is the equivalent series resistance (ESR) of the capacitor and r_s is the internal resistance of the DC voltage source.

Therefore, the total loss in the charging process is

$$E_{\text{Loss}} = \int_0^t i_C^2 (r_p + r_c + r_s) dt = \frac{CV_s^2}{2} = \frac{QV_s}{2} \quad (3.3)$$

Thus, it is obvious that the total loss in charging the capacitor is also equal to the energy stored in the capacitor, irrespective of the total loop resistance given by $r_p + r_c + r_s$.

The efficiency of the charging loop shown in Figure 3.1(a) can be written as:

$$\eta = \frac{E_C}{E_C + E_{\text{Loss}}} \quad (3.4)$$

By using Eq. 3.1, 3.3 and 3.4, it can be seen that the efficiency of capacitor charging loop has dropped down to 50% because an energy content of $\frac{CV_s^2}{2}$ is wasted in the parasitic resistance of the loop.

The energy loss in each resistive elements in the loop can be derived as:

$$E_{sL} = \left(\frac{r_s}{r_p + r_c + r_s}\right) E_{\text{Loss}} \quad (3.5)$$

$$E_{pL} = \left(\frac{r_p}{r_p + r_c + r_s}\right) E_{\text{Loss}} \quad (3.6)$$

$$E_{cL} = \left(\frac{r_c}{r_p + r_c + r_s}\right) E_{\text{Loss}} \quad (3.7)$$

By examining equations 3.5, 3.6 and 3.7, it can be observed that inserting a useful load into the loop can divert some part of the energy loss into the load, which will usefully consume that energy. This idea of inserting a useful resistance into the loop motivated the development of the LCC for RC charging loops.

3.1.2 Capacitor charging behaviour of a modified RC loop

As mentioned before, Figure 3.1(b) indicates a special case where a “useful ” resistive load R_L (such as a heater) is inserted into the charging loop where $r_{lp} = r_p + r_c + r_s$.

In this situation, the total loss incurred in charging the capacitor from 0 to V_s is given by:

$$E_{r_{lp}} = \left(\frac{r_{lp}}{r_{lp} + R_L} \right) E_{Loss} \quad (3.8)$$

and the energy used by useful load can be written as:

$$E_{R_L} = \left(\frac{R_L}{r_{lp} + R_L} \right) E_{Loss} \quad (3.9)$$

In this case, with the resistive load consuming energy in a useful manner, the efficiency of the capacitor charging circuit in Fig. 3.1 (b) is given by Eq. 3.10. Therefore, by inserting a useful load into the charging loop it is possible to reduce the losses in the RC charging loop making the process more efficient.

$$\eta = \frac{E_C + E_{R_L}}{E_C + E_{R_L} + E_{r_{lp}}} > 50\% \quad (3.10)$$

From this analysis, it can be seen that by diverting part of the energy wasted into the load connected it is possible to increase the charging efficiency of the capacitor by more than 50%. As the next step in the LCC, the variation in efficiency (η) with an over-rated DC voltage source and a pre-charged capacitor was examined. A detailed analysis of this is given below.

Analysis of RC loop with over-rated DC voltage source and pre-charged capacitor

Initially, the behaviour of a simple RC circuit with an over-rated DC source and pre-charged capacitor, as shown in Figure 3.2, was analysed.

The DC voltage source is over-rated by a factor of m in relation to the rated DC voltage of the capacitor, V_W , and the capacitor carries a pre-charge voltage of kV_W where $m \geq 1$ and $0 \leq k < 1$.

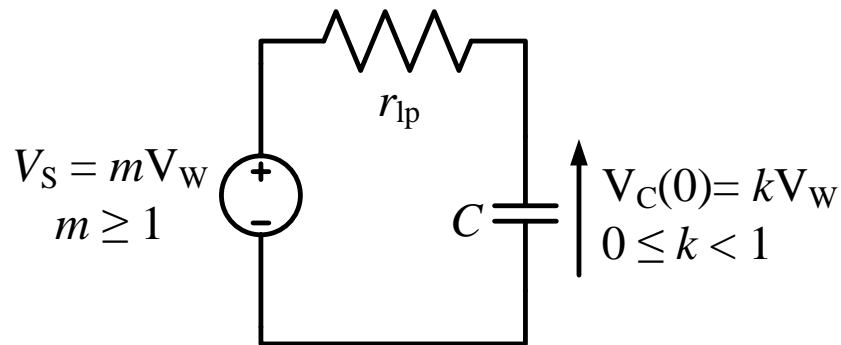


Figure 3.2: RC circuit with pre-charged capacitor and over-rated DC voltage source

When the capacitor is charged from kV_W to V_W , using a DC voltage source of voltage mV_W , the loop current i is given by:

$$i = \frac{(m-k)V_W}{r_{lp}} \exp\left[\frac{-t}{Cr_{lp}}\right] \quad (3.11)$$

where r_{lp} is the parasitic resistance of the loop.

The instantaneous voltage of the capacitor is,

$$V_C(t) = (m-k)V_W \left(1 - \exp\left[\frac{-t}{Cr_{lp}}\right]\right) \quad (3.12)$$

Therefore, the time t_1 taken for the capacitor to reach its rated voltage V_W can be written as:

$$\begin{aligned} V_W(1-k) &= (m-k)V_W \left(1 - \exp\left[\frac{-t_1}{Cr_{lp}}\right]\right) \\ 1-k &= (m-k) \left(1 - \exp\left[\frac{-t_1}{Cr_{lp}}\right]\right) \\ t_1 &= -Cr_{lp} \cdot \ln\left(\frac{m-1}{m-k}\right) \end{aligned} \quad (3.13)$$

Energy stored in the capacitor when it is charging from kV_W to V_W can be expressed using the following equation:

$$E_C = E_C(\text{final}) - E_C(\text{initial}) = \frac{1}{2} \cdot CV_W^2(1-k^2) \quad (3.14)$$

Energy dissipated in the parasitic resistance can be written as:

$$E_{\text{Loss}} = \int_0^{t_1} i^2 r_{lp} dt \quad (3.15)$$

Using equations 3.11, 3.13 and 3.15 the total loss in the loop is derived as:

$$E_{\text{Loss}} = E_{r_{lp}} = \frac{(1-k)V_W^2 C}{2} [2m-1-k] \quad (3.16)$$

Thus the efficiency of the charging loop will be:

$$\eta = \frac{E_C}{E_C + E_{r_{lp}}} = \frac{1+k}{2m} \quad (3.17)$$

According to Eq. 3.17, it is obvious that the charging efficiency of the RC charging loop can be varied by varying the over-rated factor m and the pre-charged factor k .

In the limit $k \rightarrow 0$ (no initial charge in the capacitor) with $m \rightarrow 1$ (no power supply overrated factor) efficiency $\eta \rightarrow \frac{1}{2}$, yielding the standard textbook result. Eq. 3.17 shows that this efficiency is enhanced if the capacitor carries a percentage (i.e., is never allowed to fully discharge during a cycle), thus avoiding the large energy losses that accrue when current is high. To minimize charging time, the over-rated factor must be set to $m > 1$, but this implies higher current and

reduced efficiency since $\eta \sim \frac{1}{m}$. These (k, m) energy trends are depicted in Figure 3.3. Optimum efficiency is achieved when $(k, m) \rightarrow (1; 1)$.

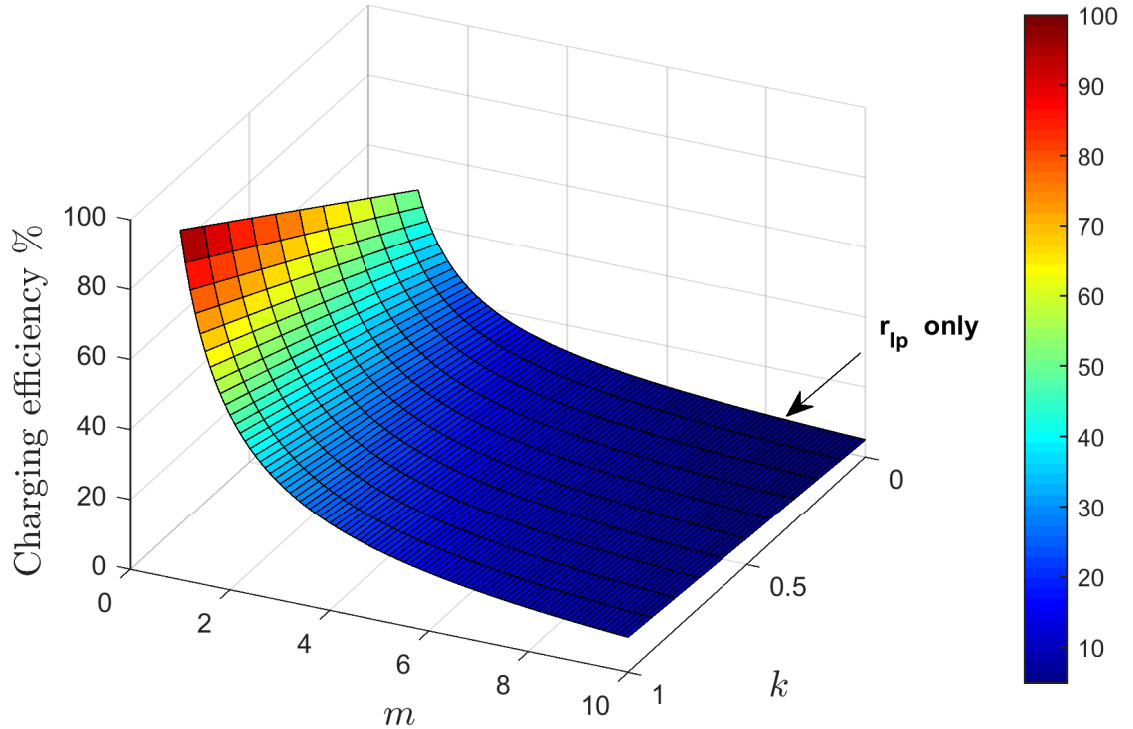


Figure 3.3: Variation of charging efficiency with over-rated factor m and pre-charged factor k

Analysis of RC loop with over-rated DC voltage source and pre-charged capacitor

Paradoxically, it is possible to improve the overall efficiency by inserting a “useful” load R_L into the charging loop. This analysis will consider the RC loop shown in Figure 3.4.

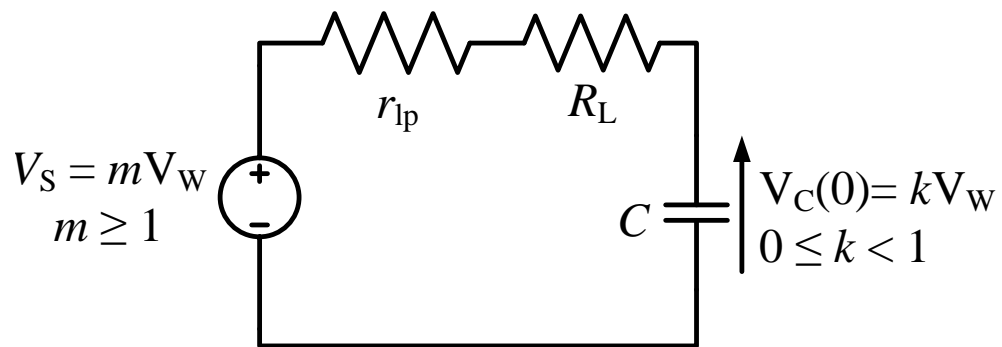


Figure 3.4: Modified case of RC circuit with pre-charged capacitor and over-rated DC voltage source

As mentioned at the beginning of subsection 3.1.2, the charging efficiency of the circuit will improve. This is because the energy consumed by R_L does useful work, while energy consumed by the parasitic circuit resistance r_{lp} is lost immediately.

If $\frac{R_L}{r_{lp}} = P$, Eq. 3.13 (time taken for the capacitor to charge to its rated voltage V_W) will be modified as follows:

$$t_1 = -C(P + 1)r_{lp} \cdot \ln\left(\frac{m - 1}{m - k}\right) \quad (3.18)$$

Hence, the energy dissipated in the resistive elements ($R_L + r_{lp}$) will be:

$$E_{R_L+r_{lp}} = \frac{(1-k)(2m-k-1)V_W^2 C}{2} \quad (3.19)$$

The energy used by R_L can be derived by using Eq. 3.9 as:

$$E_{R_L} = \frac{P(1-k)(2m-k-1)V_W^2 C}{2(P+1)} \quad (3.20)$$

The energy dissipated in the parasitic resistance (r_{lp}) of the loop can be found using Eq. 3.8 as:

$$E_{r_{lp}} = \frac{(1-k)(2m-k-1)V_W^2 C}{2(P+1)} \quad (3.21)$$

The total energy supplied by the DC voltage source E_S is

$$E_{r_S} = E_C + E_{R_L+r_{lp}} = V_W^2 C(1-k)m \quad (3.22)$$

Thus, using equations 3.14, 3.20, 3.21 and 3.22, Eq. 3.17 can be modified as:

$$\eta = \frac{E_C + E_{R_L}}{E_S} = \frac{1}{1+P} \left(P + \frac{1+k}{2m} \right) \quad (3.23)$$

where P is the R_L to r_{lp} ratio and $P \geq 0$.

When $P \rightarrow 0$, Eq. 3.23 collapses to Eq. 3.17. For $P=1$ and $P=9$ the following relationships were obtained respectively.

$$\eta(P=1) = \frac{1+k+2m}{4m}$$

$$\eta(P=9) = \frac{1+k+18m}{20m}$$

These trends are illustrated in Figure 3.5 in the middle and upper meshes.

As can be seen in Figures 3.5 and 3.6, the overall efficiency can be increased by increasing the useful load resistance. According to Eq. 3.23, the efficiency of the loop does not depend on the value of the capacitor (C) used in the loop. Therefore, it is feasible to extend the same LCC into a supercapacitor charging loop.

By replacing the $1\mu\text{F}$ capacitor with a supercapacitor (SC) of 1 F with a typical DC voltage rating of 2.7 V, with a DC power source of 10 V, it is possible to extend the LCC discussed above into supercapacitor-based RC charging circuits. In such cases, charging the capacitor with a higher DC voltage source is applicable because now the rated voltage of the SC is 2.7 V and the source voltage is 10 V.

The RC circuit will have a longer time constant of 1 second. If the capacitor is able to charge up to 10 V from an initial condition of zero voltage, it will take more than 5 seconds to reach the DC power supply rail voltage. However, for the safety of the supercapacitor, the SC should be disconnected from the loop before it reaches 2.7 V. An important practical consideration for

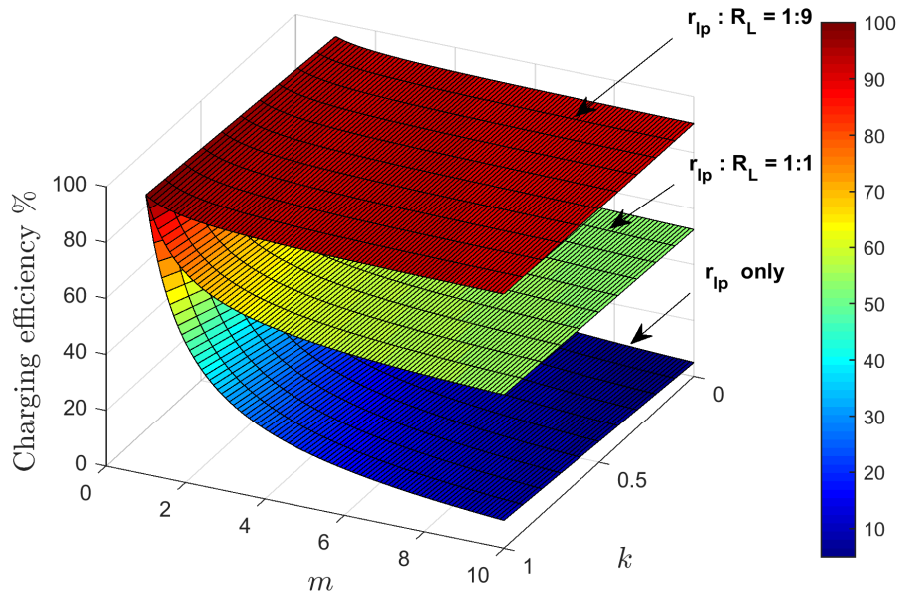


Figure 3.5: Graphical representation of circuit behaviour in terms of efficiency versus m (over-rated or over-voltage factor) and k (pre-charged factor)

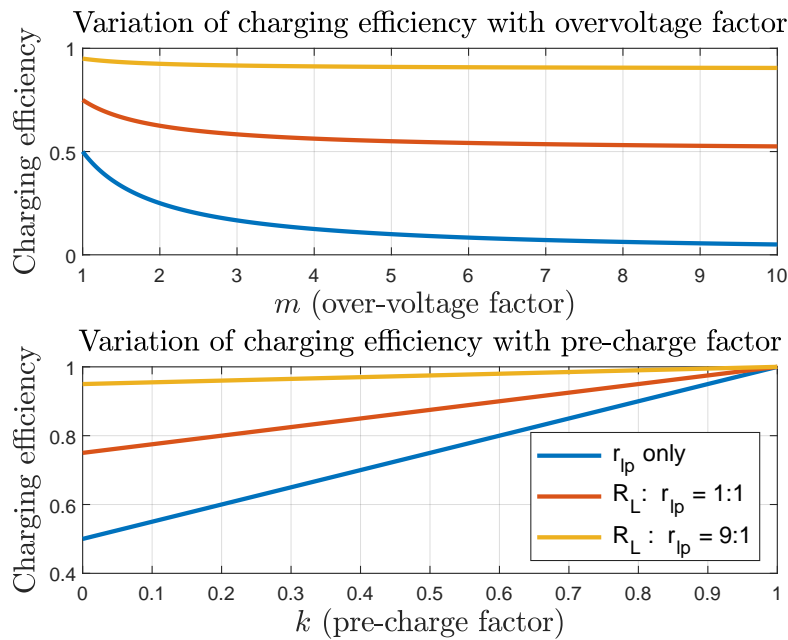


Figure 3.6: Variation of charging efficiency

a circuit designer is that since the circuit is a very low-speed version, with a time constant of 1 second, it is easy to insert and operate a switch to stop the capacitor over-charging.

In summary, by replacing the capacitor in an RC loop with a supercapacitor and inserting a useful load into the loop, the power electronics research team at the University of Waikato devised a new concept known as Supercapacitor Assisted Loss Management (SCALOM) [74]. This SCALOM concept opens up a whole new world of SC-based circuit topologies with high efficiency, based on an extension of the simple RC loop.

3.2 Applications of the SCALOM concept

3.2.1 Supercapacitor assisted low drop-out (SCALDO) regulator

The SCALDO regulator was the first patented technique based on the SCALOM concept. Here, a loaded low-dropout (LDO) in place of the R_L , with a supercapacitor replacing the normal capacitor, helps in two essential ways: (i) usefully utilizing resistive losses to power the LDO and its load while charging the supercapacitor; and (ii) slowing down the capacitor charging, to delay blocking of the circuit due to capacitor charging. If the capacitor's ESR is very small (which is the case with a supercapacitor) the supercapacitor acts as a lossless voltage dropper, recovering and storing the wasted energy in the series path of the LDO. Therefore, the end-to-end efficiency of the LDO is improved by a factor greater than 1, as discussed in subsection 2.5.1.

The SCALDO technique [60, 65, 75] is a modified case of a linear regulator based on a low drop-out regulator, where a pre-charged supercapacitor is in series with the LDO. The larger the value of the supercapacitor, the longer is the time taken to reach the limit. Once the ultimate limit is reached, a set of low-speed switches places the capacitor in discharge mode to reuse the stored energy, while maintaining the capacitor's charge balance. In SCALDO the supercapacitor in charging mode acts as a simple lossless dropper in the series path, while voltage regulation is based on a series power transistor-based linear regulator.

3.2.2 Supercapacitor assisted surge absorber (SCASA) technique

Referring to Figure 3.2, by considering the resistor as a useful-load, a unique surge absorber topology was also developed [76, 77]. The summary presented, based on Figure 3.5, indicates that when the capacitor starts charging, initially most energy is wasted in the resistive element, which keeps reducing as the capacitor acquires charge. Therefore, in an RC circuit with a 1Ω resistor and a $1\mu\text{F}$ capacitor, replacing the capacitor with a supercapacitor of 1 F will generate a time constant of 1 second, and the circuit will settle to steady-state after 5 seconds. However, the duration of a typical transient surge voltage induced on the an AC power line is around $100\ \mu\text{s}$ or less.

Thus, if an IEEE C62.4X standard compliance surge is applied to a large time constant RC circuit, where the supercapacitor has a very low DC voltage rating of several volts only (usually less than 5 V), the voltage developed in the SC will be in the order of mV and most of the surge energy will be dissipated in the path resistance and ESR of the SC. References [67–69] give details on how this RC circuit situation allows supercapacitors to be used in surge absorption circuits.

In the SCASA technique, the RC circuit is configured in such a way that it uses the resistive element to absorb a significant part of the surge energy superimposed on the AC mains waveform, using the supercapacitor as an assistive circuit element to circulate the surge energy. One challenge in a practical SCASA circuit is to keep the terminals of the symmetrical supercapacitor within the maximum DC voltage rating. The coupled magnetic element, in essence, assists in this process.

3.2.3 Supercapacitor assisted temperature modification apparatus (SCATMA) technique to provide rapid hot-water at domestic water faucets

SCATMA uses a pre-charged supercapacitor bank to deliver a high-power boost within a short-time period to the pipe directing flowing water, to overcome the delay in hot water delivery. This is achieved through a buried coil in the final 0.5 m of the pipe to a kitchen sink or a bathroom washbasin tap. The SCATMA concept is also based on simple a RC loop where a capacitance is represented by the pre-charged supercapacitor bank and R_L is the heating element. Since the resistance of the heating element is much larger than the ESR of the SC bank, the effect of the ESR can be neglected and most of the energy will be dissipated in the heating element.

3.2.4 Supercapacitor assisted high density inverter (SCAHDl)

SCAHDl is another application of the SCALOM concept that is under development. In 2014, inspired by the Google Little Box Challenge, the research team embarked on a new project to extend the SCALOM concept to solar inverters. In this case, loaded inverters are adopted as the useful load R_L in the supercapacitor charging circuit, which increases the end-to-end efficiency as explained in section 3.1.2. A large capacity inverter can be divided into an even number of identical inverters, with n identical inverters: this concept may help to reduce ESR losses in the input DC bus capacitors and ohmic and other losses in high-frequency transformers in the inverter stages [62].

3.3 Supercapacitor assisted loss circumvention concept leading to supercapacitor assisted LED (SCALED) lighting converter

There is a worldwide interest in DC-microgrids with renewable energy sources. LED lighting is one of the key areas in which to harness the benefits of DC-microgrid concepts. The supercapacitor assisted LED lighting (SCALED) converter [73, 78–83] is an extension of the SCALOM concept, based on the extending RC concepts into the DC-microgrid-based LED lighting area.

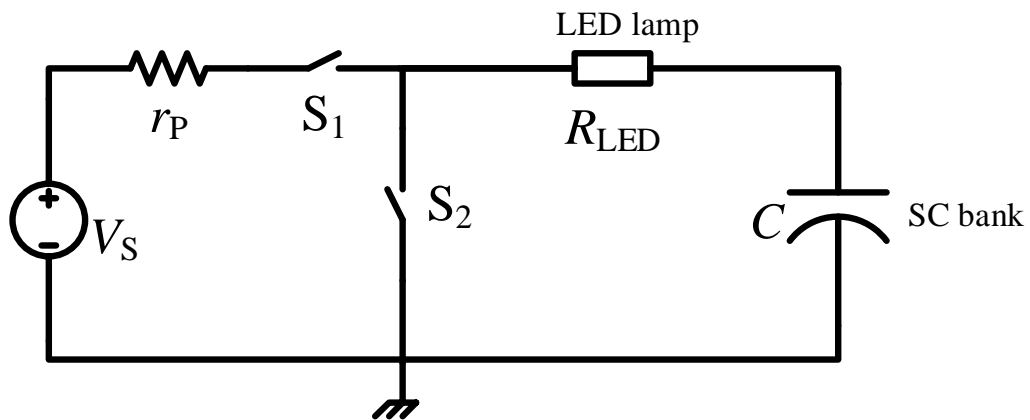


Figure 3.7: Modified RC charging loop with LED lamp

Figure 3.7 depicts a case where an RC charging loop is modified with a useful load of LED lamps. If these LED lamps operate on DC, they act as the useful resistive load of R_L in Figure 3.4, which is “usefully consuming ” energy while charging the capacitor. If the equivalent DC

resistance of the LED lamp, R_{LED} , is very much higher than the parasitic resistances of the loop represented by r_{P} in Figure 3.7, and the capacitor C is an adequately sized supercapacitor bank, this represents the simplified basis of the new SCALED technique.

In the SCALED converter, a PV module with an open-circuit voltage V_{OC} higher than the nominal voltage of the LED lamp and SC bank is used as the source, instead of a DC voltage source. If an empty SC bank is used in the circuit, initially the LED lamp will be subject to higher voltages than its operating voltage. Therefore, a pre-charged SC bank is used in the circuit. Thus, the SC bank not only acts as an energy storage device but also as a lossless voltage dropper in SCALED.

The switch S_1 is used to prevent overcharging the SC bank. In a practical situation, where the SC bank is to acquire energy and re-use it to power the LED later, the switches S_1 and S_2 should be operated in such a way that neither the LED lamp nor the SC bank are exposed to any unsafe higher DC voltages. Since the charging time for the SC bank is large according to the relationship $V_{\text{SC}}(t) - V_{\text{SC}}(0) = \frac{I_{\text{L}}t}{C_{\text{SC}}}$, it is quite easy to operate the two switches (switches operate at low frequency). When the SC bank reaches the higher limit, the excess energy within the bank should be released into the LED lamp load.

The SCALED converter uses the SCALOM concept with over-rated voltage source, pre-charged capacitor and useful load. Since $\frac{R_{\text{LED}}}{r_{\text{P}}}$ is large, the efficiency of the SCALED converter is high ($\approx 90\%$ to 94%) and is operating in the top plane of Figure 3.5.

3.4 Chapter Summary

This chapter has discussed the LCC applied to an RC charging loop, how it can be extended to supercapacitors, and the applications of the supercapacitor assisted loss management concept.

The next chapter will provide operational details of LED lamps.

Operational Details of commercial LED lamps

Lighting accounts for nearly 20% of average residential electricity use in the world [84]. According to a 2019 statistical report on world energy published by BP, the total energy consumption of the world in 2018 was 161,249 TWh [85]. The total energy consumption of New Zealand in 2018 was 252 TWh which is only 0.16% of global energy consumption [85]. However, 38.8 TWh of the total energy consumption in New Zealand (15%) was electricity [86]. In 2017, residential customers consumed 32% of the electricity produced in New Zealand. In accordance with the report on “Electricity in New Zealand” prepared by the Electricity Authority, 13% of household electricity usage is used for lighting [86]. Therefore, it is important to develop energy-saving luminaires as a part of an energy sustainability strategy.

Due to discoveries and advancements in new materials and lighting technologies, new generations of energy-efficient lighting devices have been developed over the past few decades. Even though, there are various types of lamps available on the market, they differ in their operating principle, materials used, and importantly their energy efficiency. Different types of luminaires are being used in many day-to-day applications, such as, outdoor lighting, indoor lighting, specialized lighting, and etc. However, this thesis addresses only indoor lighting.

Because of the rapid developments in materials and processing technologies, conventional lamps are disappearing and being replaced by newly developed solid-state lamps [87–89]. These lamps provide high efficiency and better quality than conventional lamps [89,90]. Figure 4.1 presents the typical varieties of LED lamps and their applications. All these newly developed lighting devices are considered to be promising technologies in the energy-efficient lamp family [89]. This chapter provides a comprehensive account of energy-efficient lighting devices. However, particular attention is given to solid-state lighting devices, since they have attracted the most interest and are the most promising for DC microgrid applications.

4.1 Comparison of lighting technologies

4.1.1 Incandescent lamps

These are the “standard ” light bulbs that were introduced for residential applications more than 140 years ago by Thomas Edison. These are also known as “filament lamps”. These luminaires can be considered one of the most mature lighting technologies in the world. They have the lowest initial cost and provide good colour rendering [84]. However, they have the shortest life

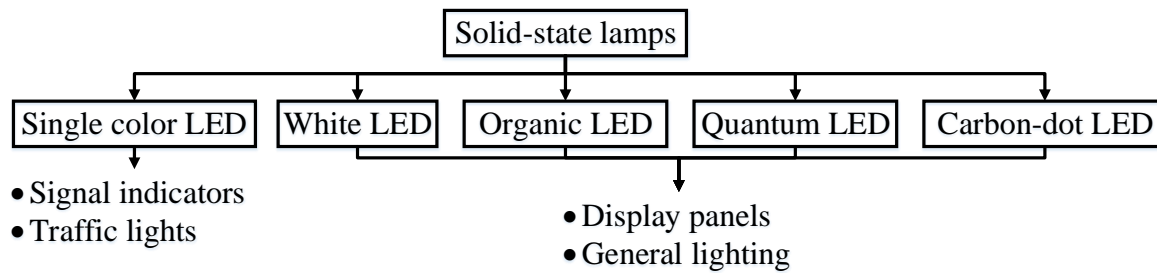


Figure 4.1: Types of solid-state lightings and their applications

span and use significantly more energy than other lighting technologies to produce the same lumen rating or light output. Incandescent bulbs are manufactured in a wide range of sizes, light outputs and voltage ratings ranging from 1.5 V to about 300 V. They do not require any external regulating circuitry and work equally with AC and DC voltages. Thus, they became widely used in both residential and commercial buildings. Also, they are used for portable lighting applications such as car headlamps, flash-lights and decorative lighting systems.

These lamps produce light by heating the metal (Tungsten) filament inside the lamp's glass globe. Therefore, more than 90% of the energy used by the lamp is dissipated as heat while less than 10% produces the light output. According to a report by "Star Energy", incandescent lamps are the most commonly found bulbs in American homes [84].

4.1.2 Halogen lamps

Halogen lamps are somewhat more efficient than incandescent lamps but operate at a higher lamp temperature. These lamps also have a tungsten filament like traditional incandescent bulbs. The main difference between incandescent and halogen lamps is that halogen lamps are filled with halogen gas. When halogen bulbs are powered, tungsten from the filament is evaporated into the halogen gas to provide the illumination. Later, the halogen gas carries the evaporated tungsten particles back to the filament [91]. Thus they consume less energy than incandescent lamps. The high operating temperatures can present a safety concern in some fixtures, such as torchiere fixtures which consume as much as 500 W [84]. Halogens are often used for recessed, and accent, and floodlighting.

4.1.3 Fluorescent lamps (FL)

It has been more than 110 years since the first mercury vapour lamp was introduced to the world by Hewitt [89]. The development of efficient, long-lasting electrodes and suitable fluorescent phosphor materials to convert invisible ultraviolet light into visible light made these lamps a commercial reality in the 1940s. Since then these lamps have been used in commercial buildings and households as low-cost, energy-saving light sources. They are a good alternative to inefficient incandescent lamps. Fluorescent lamps represent a significant advancement in technology since they consume 2–5 times less energy and last 8–10 times longer than incandescent lamps [88, 89, 91, 92]. However, lighting technologies have continued to develop to create more efficient lighting and minimize environmental hazard issues.

Compact Fluorescent lamps (CFL)

These are among the most popular fluorescent lamps. CFLs have been used for residential buildings for about 30 years, with recent advances increasing their popularity due to reduction in price and a desire to be more energy efficient [84]. They are an energy-efficient choice that is readily available in the home lighting market. These lamps use gases and phosphor inside the lamp to create light. CFLs last longer and use less power than incandescent and halogen lamps to provide the same amount of light. They operate at a low temperature and come in ‘warm’ and ‘cool’ colours. Because CFLs contain a small amount of mercury, they need to be properly disposed of or ideally recycled at the end of their life span. These lamps’ energy consumption is about $\frac{1}{3}$ that of comparable halogen bulbs’ consumption [91].

4.1.4 LED lamps

The rapid development of semiconductor technology has enabled the design of LED bulbs with lower energy consumption than the other available lighting technologies. LEDs have an extremely long life span, are energy efficient and available in a variety of colours. Continuous development in this technology has enabled the improvement of LED lamps and their use in new applications. Coloured LEDs are now commonly used commercially in exit signs and traffic signals, which can significantly reduce maintenance costs [89]. While LED technology is being explored for common residential use, technical and cost barriers remain. More details on this lighting technology will be provided in the next section.

A comparison of energy savings and consumptions for common lighting techniques is provided in Figure 4.2. In comparison to conventional incandescent lamps the energy consumption of LED lamps is less than 20%, giving an energy saving of more than 80%. A detailed comparison of incandescent, fluorescent and LED lighting technologies is provided in Table 4.1. Compared with compact fluorescent (CFL) or incandescent lamps, LED lamps have a longer life span, making them more reliable than other lighting technologies.

Table 4.1: Comparison of different lighting technologies

Parameter	Incandescent	CFL	Halogen	LED
Initial cost	Low	Medium to Low	Medium	Medium to High
Energy consumption	High	Low	High	Low
Operating temperature	High	Low	High	Low
Colour rendering ability	High	Medium to High	High	Low to Medium
Average rated lifetime [hrs]	750 – 1500	6000 – 10000	2000 – 4000	up to 100,000
Efficacy [lumen/W]	10 – 20	50 – 70	16 – 29	80 – 100+
Colour rendering index (CRI)	100	80 – 90	100	65 – 90
Color temperature [K]	2400 – 2900	2700 – 6500	2850 – 3200	2700 – 6500

Colour rendering index(CRI): This is a qualitative measure of the ability of a light source to reveal the colour of an object in comparison with an ideal or natural light source (or standard reference light source). The CRI scale is from 0 to 100, with a value of 100 indicating excellent colour rendering. Typically sunlight and most incandescent lamps have a CRI of 100.

Colour temperature: This is a way to compare the colour of the light emitted from different types of lamps. Colour temperature is measured in Kelvin (K) on a scale from 1,000 to 10,000. Colours with temperatures over 5000 K are called cool colours (slightly blue), while

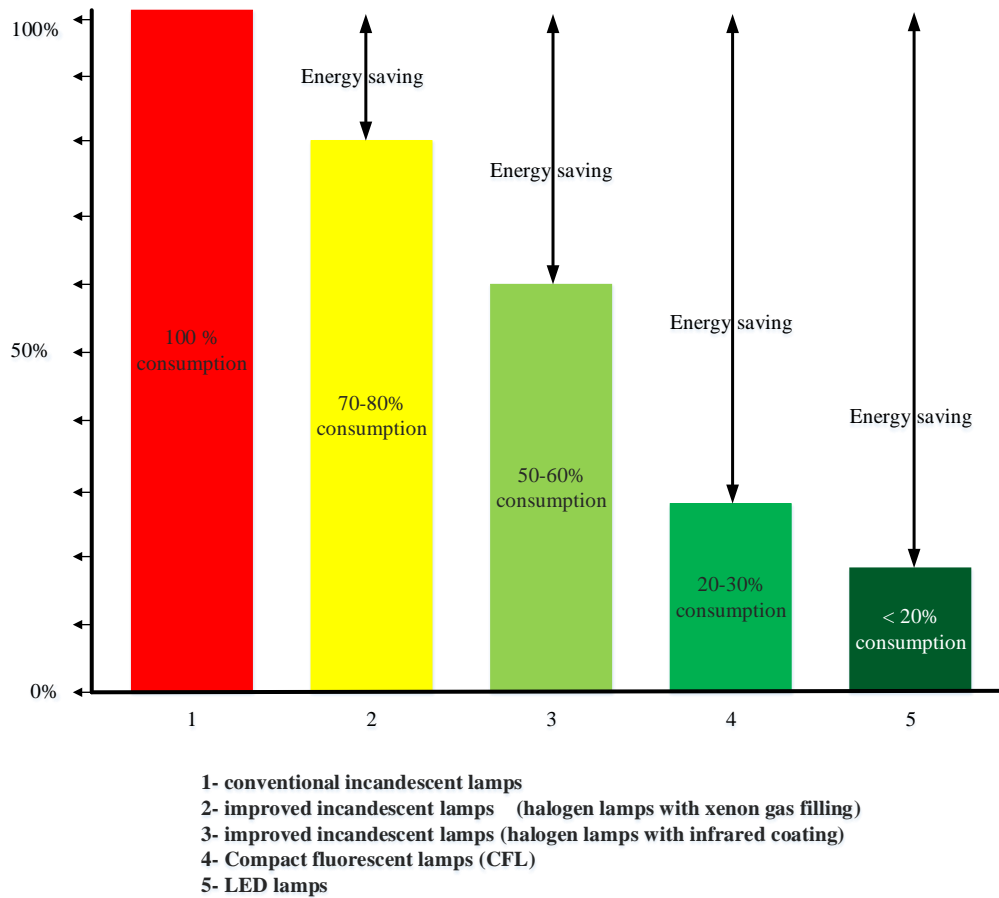


Figure 4.2: Energy saving vs consumption for common lighting technologies (Drawn from the data available from the European Commission 2009)

colour temperatures in the range of 2700 K to 3000 K are known as warm (slightly orange) colours. For example, incandescent lamps give warm colour temperatures, while some fluorescent lamps and sunlight emit cool colour temperatures. Typically, lamps with 2000 K to 6500 K colour temperatures are used for commercial and residential lighting applications.

Efficacy: This provides a measure of how much light output (in lumens) is delivered from a lamp per watt.

4.2 LED luminaires

LEDs have been around for many decades but were restricted to indication lamps (red in colour) and not used initially for general lighting. However, LED lamps has now become the newest and one of the fastest-developing energy-efficient lighting technologies in the category of general lighting. An LED lamp is a solid-state light-emitting source comprised of a substrate base, a $p - n$ junction diode and a protective glass or plastic enclosure, which emits light through a phenomenon known as electro-luminescence [93]. Solid-state lighting means a semiconductor converts electricity to light without producing heat, usually within a small area of about 1 mm^2 or less.

The structure of a single LED is much different from that of a regular semiconductor single diode. Single colour light will be emitted from the LED when its $p-n$ junction is forward biased. Typically, the $p-n$ junction is covered by a transparent epoxy resin hemisphere, shaped in such a way that the photons emitted by the junction are reflected away from the surrounding substrate base and are focused through the top of the LED. The structure of an LED device is shown in Figure 4.3.

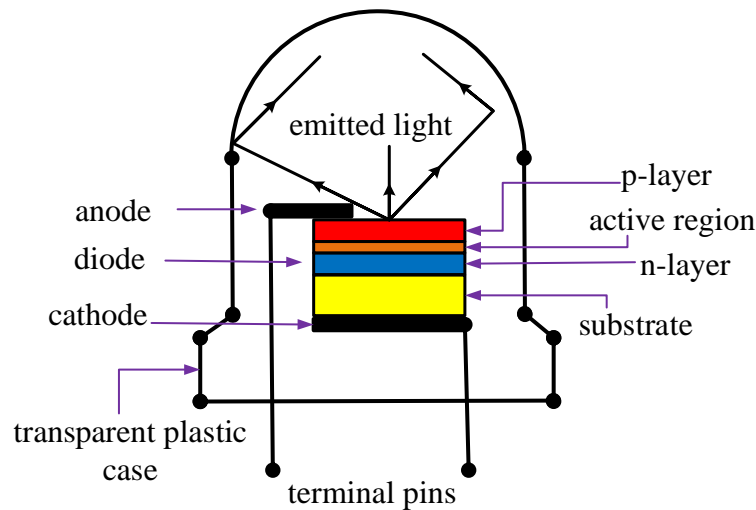


Figure 4.3: Simple structure of an LED device

In an LED lamp, there are multiple LEDs, and the light generated by each LED is projected in one direction, which creates the need to use diffusers or reflectors [87, 88, 92]. As most LED lamps are specified to last around 50,000 hours versus 1000 hours for incandescent and 8000 hours for CFLs, low maintenance costs are involved for the replacement of lamps in large facilities. LEDs also give instant brightness without needing to warm up like conventional high-power lamps. In addition, they are more efficient, with very low energy consumption as shown in Figure 4.2. Further, a reduction in CO₂ emissions by changing to LED alternatives is also a key driving factor for government environmental agencies. For example, a single 100 W incandescent bulb that is on for 4 hours in a day produces 63 kg of carbon per year. Switching to a 12 W LED lamp, which has the equivalent light output to a 100 W incandescent, result in the emission of only 3 kg of carbon per year [94]. According to the data available for 2012, USA saved about 675 million of annual energy costs by installing LED lamps [92].

The savings achievable by switching from incandescent lamps to energy-efficient lighting technology are given in Table 4.2. This illustrates the value of the latest LED bulbs compared with CFLs and incandescent bulbs in terms of overall energy saving and cost-effectiveness.

There are two categories of LED lamps commercially available categorized by their operating voltage as:

- (a) Line voltage ($230 V_{ac}$) operable LED lamps
- (b) Low voltage LED lamps

Table 4.2: Cost comparison between different lighting technologies (Note: cost of electricity and bulbs vary, and bulb replacement cost is not considered in this comparison)

Parameter	Incandescent	CFL	LED
Wattage (equiv. 60 W incandescent) [W]	60	18	10
Cost per bulb [NZD]	1	10	11
Electricity per year [kWh/yr] (5 hour operation time per day, 10 bulbs per household)	1095	329	183
Cost of electricity per year (at 0.2 per kWh) [NZD]	219	65.80	36.50
Cost for 10 bulbs [NZD]	10	100	110
Savings to household by switching to from incandescent [NZD]	0	63.20	82.50
Energy saving per year [kWh/yr]	0	≈ 153	≈ 183

4.2.1 Line voltage operable LED lamps

This type of LED lamp is the most commonly used in both commercial and residential buildings. These lamps can be directly connected to the AC mains. Line voltage operable LED lamps contain a power converter (AC/DC), a driver IC for the LEDs, a heat sink for thermal management and optics to optimize the light quality. Since these lamps are intended to be factor-compatible with current incandescent and CFL bulbs, they contain an AC/DC converter circuit so they can operate from standard bulb “sockets”. The construction of a typical residential LED lamp is shown in Figure 4.4.

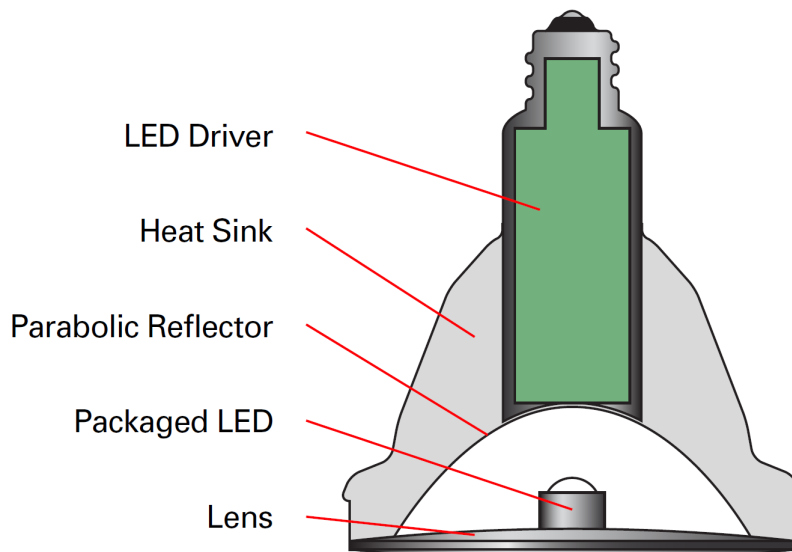


Figure 4.4: Typical residential LED lamp construction [94]

Since these lamps are directly connected to AC mains (e.g. 120/230 V AC) they can be damaged by lightning-induced surges and transient load switching (originating outside the bulb) can create voltage spikes or ring waves that can stress and damage the electronic components and can ultimately destroy the LED lamp [94]. Therefore, it is crucial to use a transient voltage protection circuit within the bulb.

Figure 4.5 provides an overview of the various components and systems within the power and control circuits inside an LED lighting assembly. As depicted in Figure 4.5, an AC fuse is used in series with the line to protect against short circuit and overload conditions. Either isolated or non-isolated topologies can be used as power converters. A transient voltage suppression

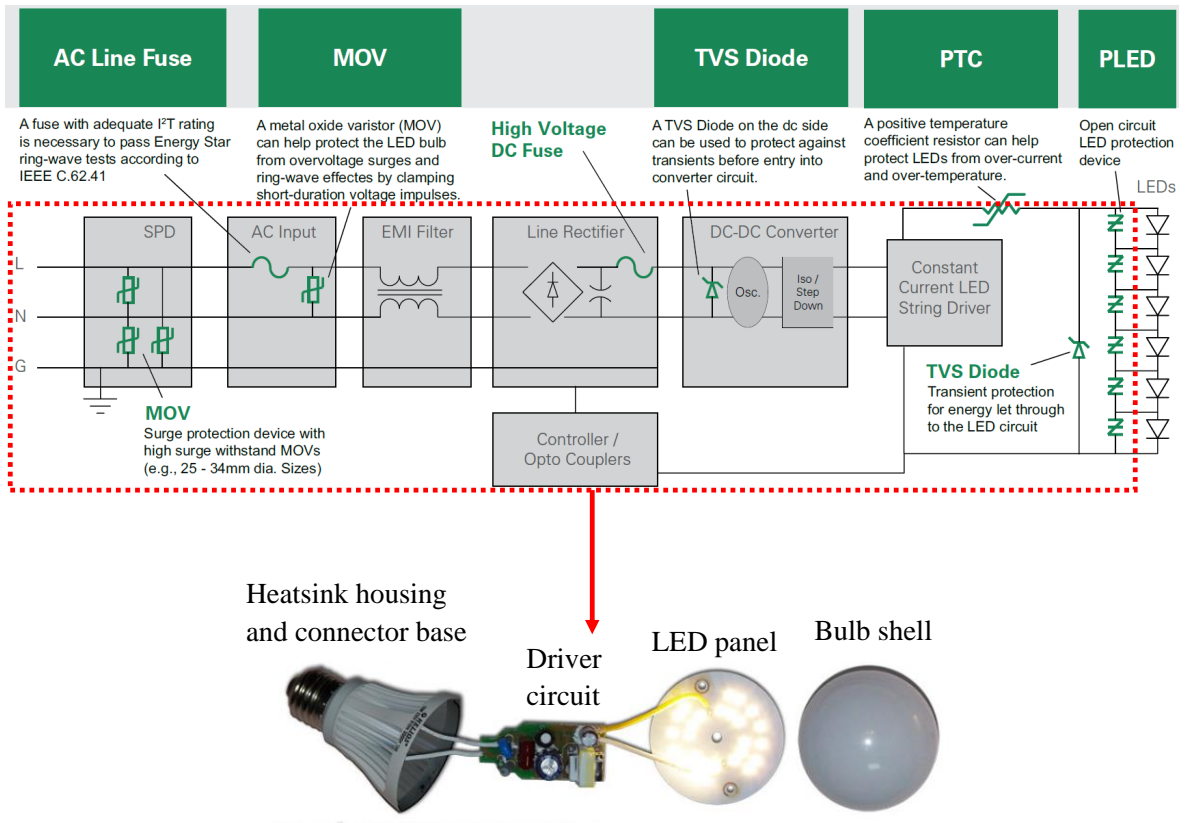


Figure 4.5: Generalized line voltage operable LED luminaire driver circuit with transient and surge protection devices [94]

(TVS) diode (which is transient rated for few hundred times for few milli-seconds, compared to its continuously rated DC current in the reverse direction) is used on the DC side as the transient protection circuitry. In the case of non-isolated LED drivers, which are more prominent in many retrofit lamps and low power applications, the LED array itself can be damaged by the surge energy as there is no transformer isolation between the AC input and the LEDs on the DC side [94]. Isolated LED drivers are more robust since the transformer in the DC-DC converter stage provides some degree of isolation and surge protection [94]. Nevertheless, surge protection is still required to limit higher surge events, especially in outdoor lamp and luminaire environments, because in the case of high energy surge events, such as those caused by nearby lightning strikes, there can be a flash-over from the primary to the secondary side of the transformer. A metal oxide varistor (MOV) across the AC line, as shown in Figure 4.5, is used in the lamp to protect against lighting-related transients.

Line operable LED light bulbs are available in different base types. The typical plug (E27) and pin (B22) are two common kinds of LED bulb bases. Many common household fixtures have pins, also known as Edison screw E, bases. There are several kinds of screw-in bases for LED light bulbs, which are categorized as Candelabra and Intermediate. It is important to choose a base type appropriate to the intended application.

4.2.2 Low voltage LED luminaires

Tungsten-halogen and standard incandescent have been the lamps of choice in low voltage lighting systems. They typically operate from 12 – 24 V DC or AC, using step-down transformers [90]. This transformer is usually located within the fixture. However, it may also be remotely mounted, depending on the application. These luminaires are used in many retail and consumer lighting applications. Common applications include residential and commercial decorative/display lighting, task lighting, and retail product highlighting [88,90,95]. Other special applications include swimming pool, fountain illumination, and landscape/garden lighting. However, low efficiency, heat generation and halogen capsule handling issues are among the disadvantages of using tungsten-halogen and incandescent lamps in low voltage lighting applications.

Low voltage LED lamps are a more energy-efficient and better solution to replace low voltage tungsten-halogen and incandescent lamps in some applications, because these low voltage LED luminaires are designed to retrofit to the same base connector (MR16) used for tungsten-halogen and incandescent bulbs. Therefore, upgrading them to new LED lamps presents no issues.

The internal circuitry of a low voltage LED lamp is shown in Figure 4.6. The LED array needs DC power for the operation. Hence, an appropriate circuit such as an LED driver, is required to convert AC voltage to DC voltage as depicted in Figure 4.6. Therefore, LED drivers are essential components of LED lamps. These drivers can be put inside the luminaire, which is called a built-in type (or integral) or be put outside, which is called an independent type (or remote). According to different applications, different types of LED drivers need to be applied; for example, an outdoor driver for a street light, an indoor point driver for a down-light, and an indoor linear driver for a panel light. It should be noted here that different LED lamp manufacturers use various LED driver circuits to drive a multi-die LED array. These low voltage LED lamps also include protection circuits, as in line voltage operable LED lamps. These low voltage lamps also come in different wattages and colour temperatures.

4.3 Practical operational region of low voltage LED luminaires

A set of experiments were carried out to investigate the practical behaviour of low voltage LED lamps. In order to identify the key operational conditions for LED lamps, three brands of commercially available LED lamp were tested in the laboratory using a variable power supply. Variations in luminance, current drawn, and power consumption with the voltage across the lamp were recorded for three brands of commercially available LED lamps. To measure the illuminance, an EXTECH HD450 light meter was used. The LED lamps were only tested up to 30 V DC because high power consumption and high voltage can reduce the lifetime of LED lamps. Figure 4.7 depicts the test set-up used for the experiment. The experiment was carried out in a dark room in order to get more accurate measurements of the illuminance.

4.3.1 Current-voltage characteristics

Figure 4.8 shows the $I - V$ characteristics curve, in which there is an approximately constant current region after initially drawing high current. This current is limited by the driver circuit, which avoids damage to the bulb due to excess power dissipation.

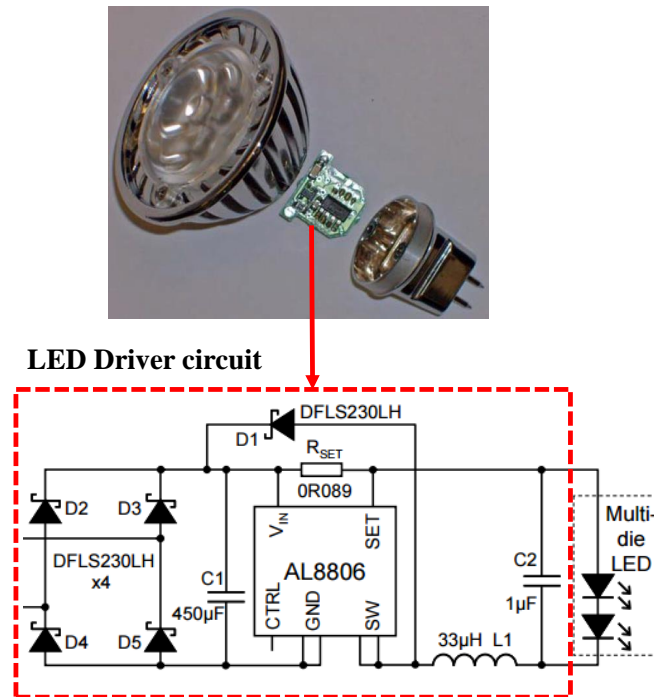


Figure 4.6: Typical low voltage operable LED luminaire internal circuitry [90]

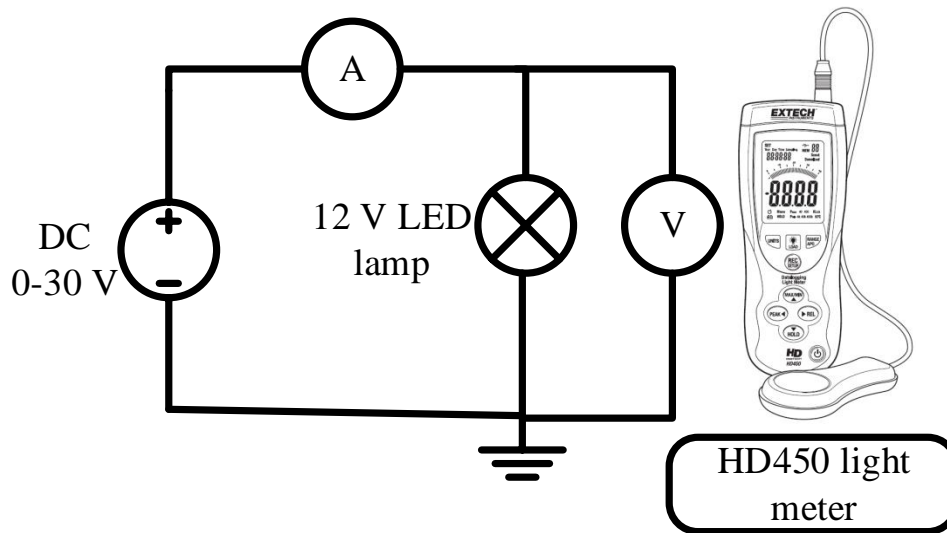


Figure 4.7: Test set-up used for the experiment

As per Figure 4.8, LED lamps draw more current when the voltage across the LED lamp is reduced. With the exception of one LED lamp, all other LED lamps drew the highest current around 5 V. This maximum current depends on the wattage rating of the LED lamp and the driver circuit. For example, for the TCP 4 W and Philips 5.5 W lamps, the highest current was 1.9 A and 1.6 A respectively. This confirms that each manufacturer uses different LED drivers inside their LED lamps. Figure 4.8 shows that, each brand has a different voltage, which the lamp starts to draw current. From these current-voltage characteristics, it can be observed that basically, an LED lamp does not act as a constant resistive load.

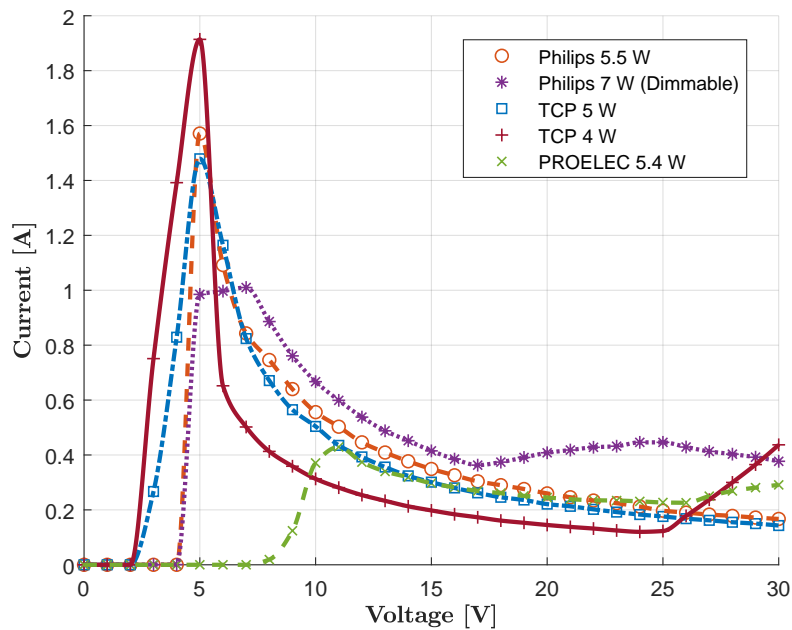


Figure 4.8: Current-voltage characteristics for 5 commercially available LED lamps

4.3.2 Luminance-voltage characteristics

Figure 4.9 shows the luminance vs the voltage curve, in which there is a constant brightness region. As the applied voltage increases, the lamp brightness increases proportionally until it reaches a certain voltage and then settles down to a constant brightness, regardless of any further increase in voltage. For the Philips 7 W dimmable LED lamp there were two different constant brightness regions as depicted in Figure 4.9. One region is from 8 – 17 V and other region starts at 25 V. Both the TCP 5 W and Philips 5.5 W LED lamp showed constant brightness in the 9 – 30 V voltage region. However, the design process of supercapacitor assisted LED (SCALED) converter only considered the 9 – 20 V region because higher voltages can reduce the lifetime of an LED lamp.

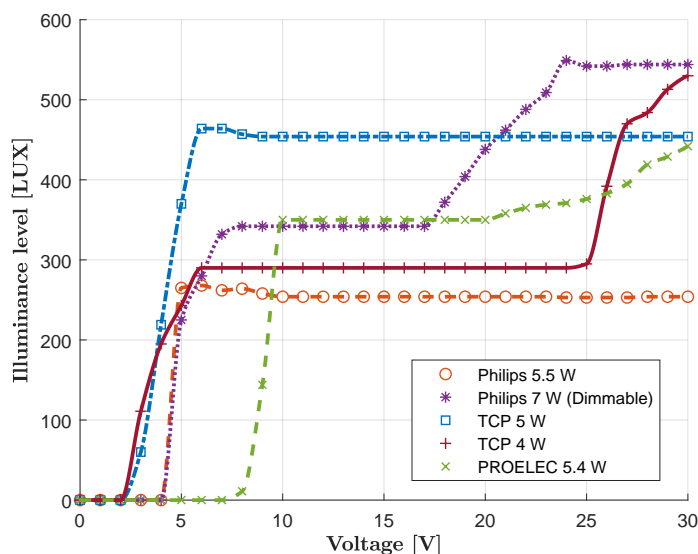


Figure 4.9: Variation of illuminance with voltage for 5 commercially available LED lamps

4.3.3 Power-voltage characteristics

Power dissipation in the tested LED lamps was calculated using the current-voltage measurements recorded during the experiment. The power-voltage characteristics for each lamp are shown in Figure 4.10. The graph indicates that every LED lamp dissipated approximately constant power in the constant brightness region. Therefore, instead of considering an LED lamp as a constant resistive device it is possible to consider it as a constant power device for a specific region of voltage.

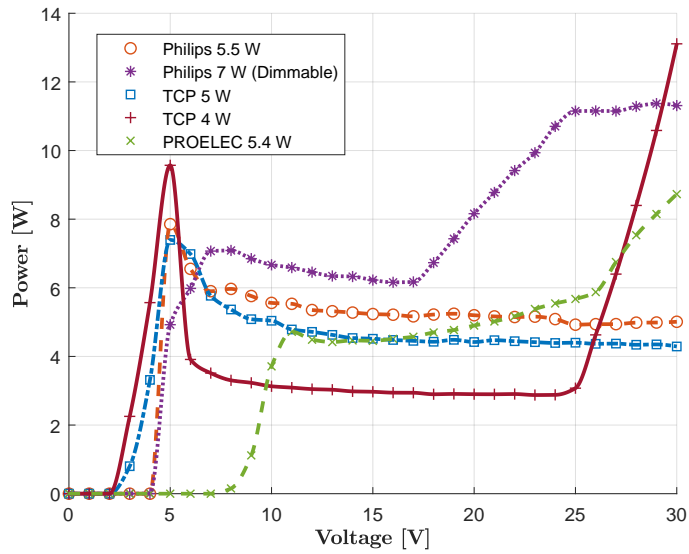


Figure 4.10: Power-voltage characteristics for 5 commercially available LED lamps

Figure 4.11 shows the DC voltage reverse capability for the Philips 5.5 W LED lamp. All five lamps were tested for DC reverse voltage capability. However, since Philips 5.5 W LED lamps were used in the development of SCALED, this capability in the Philips brand is shown here. From Figure 4.11 it can be seen that some LED lamps can operate with either positive or negative DC voltages without compromising the brightness. The test results are based on our own laboratory measurements since this data is not provided by the lamp manufacturers.

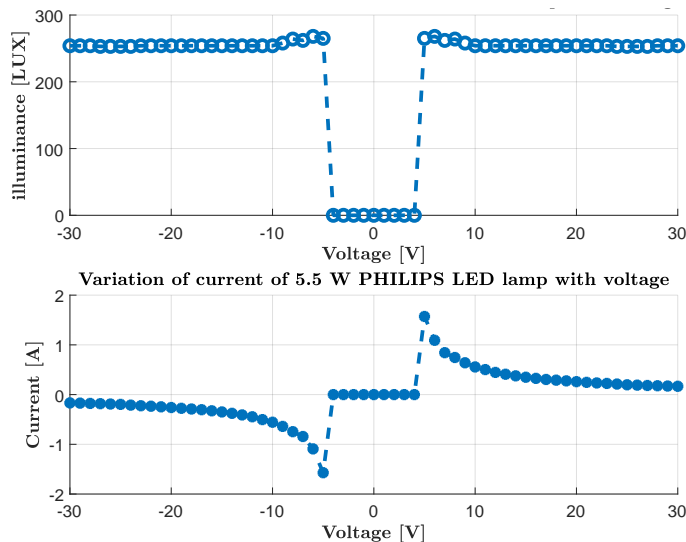


Figure 4.11: DC voltage reversal capability of Philips 5:5 W LED lamps

In summary, commercially available 12 V LED lamps have of the following desirable features:

- (i) ability to operate with positive or negative DC voltages
- (ii) ability to operate over a wide range of AC/DC voltages without compromising brightness
- (iii) ability to operate as a constant power load in the constant brightness region

These three features were used in developing a SCALED technique useful in DC-microgrid environments. Figure 4.11 depicts the voltage reversal capability of the Phillips 5.5 W LED lamp, which was also used to reduce the switch counts while developing the SCALED converter.

4.4 Chapter Summary

This chapter has provided an overview of commercially available lighting technologies, state of art of the LED lamps and practical operational details of the low voltage LED lamps that were used in developing the supercapacitor assisted LED (SCALED) converter.

The next chapter introduces the fundamentals of the supercapacitor assisted LED (SCALED) technique, generalised SCALED theory, implementation details for the SCALED converter and the application of SCALED in a Ports of Auckland DC microgrid container.

Supercapacitor assisted LED lighting (SCALED) converter for DC-microgrids

There is a global interest in DC-microgrids with the proliferation of renewable energy sources. Good evidence for this is the IEEE Power Electronics Society launching a biennial series of IEEE International Conference on DC Microgrids (ICDCM). With the third of the series very successfully held in Matsue Prefecture, Japan in May 2019, there is a rapidly growing interest in DC-powered products on a worldwide basis. LED lighting is a key area to for harnessing the benefits of DC-microgrid concepts, and one in which it is possible to extend the SCALOM theory [96,97], which is applicable to SCA techniques developed at University of Waikato.

In a DC-microgrid environment with a renewable energy supply, DC-powered appliances eliminate the need for an inverter, so they achieve a higher-end to end efficiency (E_{TEE}). However, this situation does not let us directly power the appliances that are configured to work from a 230 V 50 Hz or a 120 V 60 Hz AC source. In such a situation an energy storage system (ESS) is essential. Continuous advances in supercapacitor technologies have produced supercapacitors that can be used in electronic and electrical systems to overcome short-term fluctuations in the energy supply. Therefore, supercapacitor (SC) banks could be used to replace the environmentally unfriendly electrochemical battery packs currently used in the DC-microgrid environment as short-term or medium-term ESSs.

5.1 Basic concept

The supercapacitor assisted LED lighting (SCALED) converter uses the supercapacitor assisted loss management (SCALOM) concept discussed in Chapter 3. Here, 12 V DC operable LED lamps serve as the “useful load” in the RC loop, consuming the energy while charging the supercapacitor. If the DC equivalent resistance of LED lamps (R_{LED}) is much higher than the parasitic resistance of the loop (r_P) in Figure 5.1, most of the energy wasted in the RC charging loop is used by the LED lamps. Figure 5.1(a) depicts the case of a nominal 24 V DC voltage source, switch and LED lamp working in series, charging an SC bank operating with a DC voltage range of 8 V to 16 V. Figure 5.1(b) shows the voltage across the SC bank and LED lamp assuming that $R_{LED} \gg r_P$. The switch (S_1) should be operated in such a way that both LED lamp and SC bank are not exposed to any voltage higher than the maximum limit of the operational voltage regions. When the SC bank reaches the upper limit, the excess energy within the bank is released to the load by closing the switch S_2 , to maintain the charge balance

within the capacitor. By using an adequately rated SC bank (approximately twice as large as the DC voltage capability of the LED bank) with an LED lamp, the SCALED technique helps to significantly reduce losses in the RC loop.

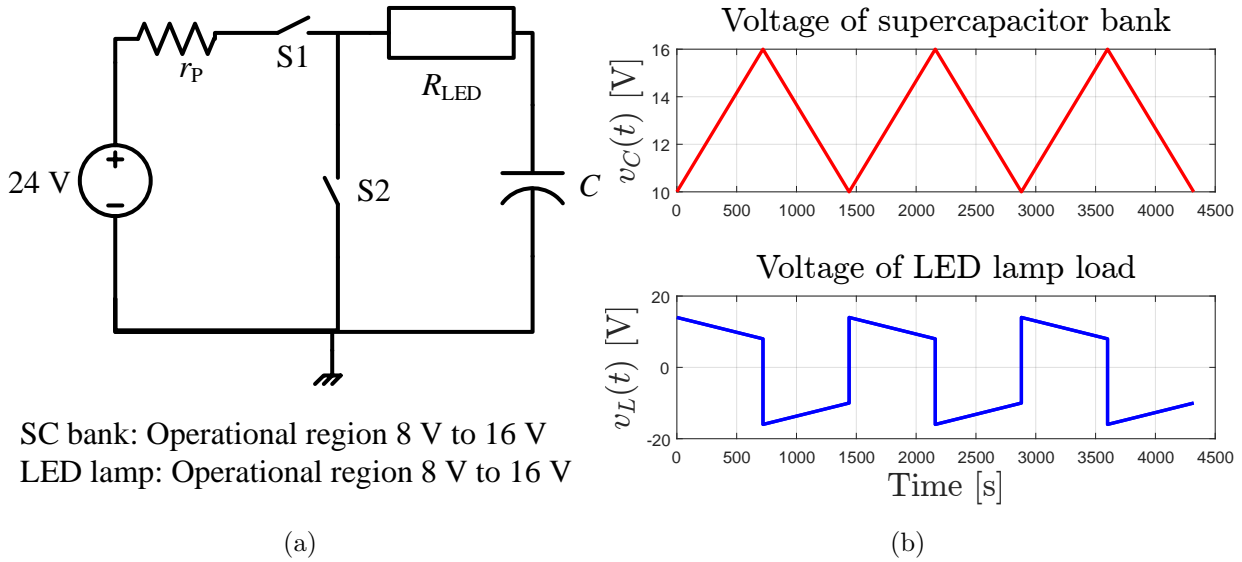


Figure 5.1: Concept of proposed SCALED converter: (a) Modified RC charging loop with LED lamp; (b) Voltage waveforms for SC bank and LED lamp load

5.2 Design considerations

In order to conserve energy, minimum conversion stages from DC to AC, AC to DC and DC to DC must take place. When considering existing solar-powered LED lighting systems there are several conversion stages, each of which will lead to the reduction of the overall efficiency. The end-to-end efficiency of a system will be the product of the efficiency of each conversion stage. Hence, by reducing the number of conversion stages it is possible to improve the efficiency of the system.

Typically, existing solar-powered LED lighting systems consist of three conversion stages as shown in Figure 5.2. DC voltage generated by the solar panel is converted into higher DC voltage using a DC-DC converter. Using a DC-AC converter (solar inverter) the output of the DC-DC converter is converted into AC, which will power the LED lighting system. An LED lamp consists of a LED driver circuit, containing an AC-DC converter (rectifier), which will convert the AC supplied by the solar inverter to DC to drive the internal LED array.

Since these 12 V LED lamps can also be powered directly from a 12 V DC supply also, the focus of this thesis was to implement a Supercapacitor Assisted LED (SCALED) lighting system for DC-microgrids, which can operate directly from solar panels as shown in Figure 5.3.

During the design of the SCALED converter, an operational voltage region (from 9 V to 20 V) with constant brightness, as shown for a Philips 5.5 W LED lamp, was considered. A mathematical model for the Philips 5.5 W LED lamp was fitted via `cftool` in the curve-fit toolbox in MATLAB as shown in Figure 5.4. General model for current-voltage characteristics for a LED lamp with 95% confidence bounds is;

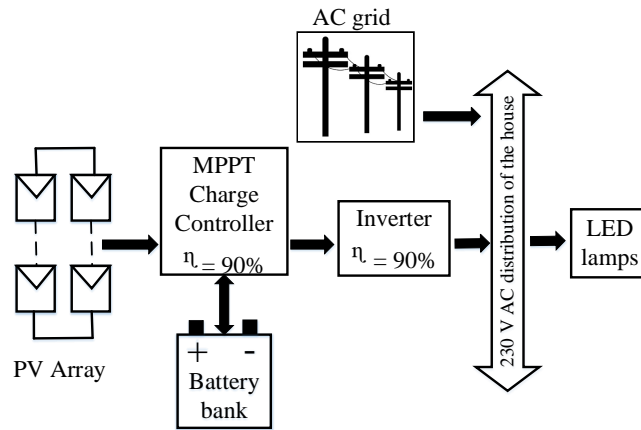


Figure 5.2: Existing solar-powered LED lighting systems

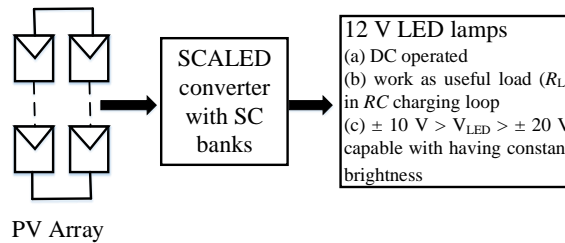


Figure 5.3: Proposed concept of SCALED converter for solar-powered DC microgrids: Simplified block diagram

$$I_{\text{LED}} = 0.4145 * e^{-1.355V_{\text{LED}}} + 0.7208 * e^{-0.2552V_{\text{LED}}} + 0.4365 * e^{-0.03946V_{\text{LED}}}$$

with sum of squares due to error (SSE) of 0.0009457, R-square of 0.9997, adjusted R-square of 0.9996 and root mean squared error (RMSE) of 0.006876.

This model was used for the simulation of the SCALED converter in the later stages of this research.

The current-voltage characteristic curve of a solar cell or a panel shows a unique behaviour, starting with a nearly constant current source changing over to a voltage source with an approximately constant array resistance. This characteristic made the combination of a PV panel with a supercapacitor bank and LED lamp more challenging when developing the SCALED topology. Initially, a prototype circuit to test the concept discussed in Section 5.1 was designed and built. This circuit was designed to power two LED lamps (i.e. 11 W).

5.2.1 SCALED converter: Proof-of-concept

Three important properties of 12 V LED lamps are the ability to operate: (a) with positive or negative DC voltages; (b) over a wide range of AC/DC voltages without compromising brightness; and (c) as a constant power load in the constant brightness region. These properties were used during the design phase of the SCALED converter.

As depicted in Figure 5.5, once switch S_1 is closed the PV panel will charge the SC bank C while powering the LED lamp. When the SC bank C, has charged until V_{LED} reaches to

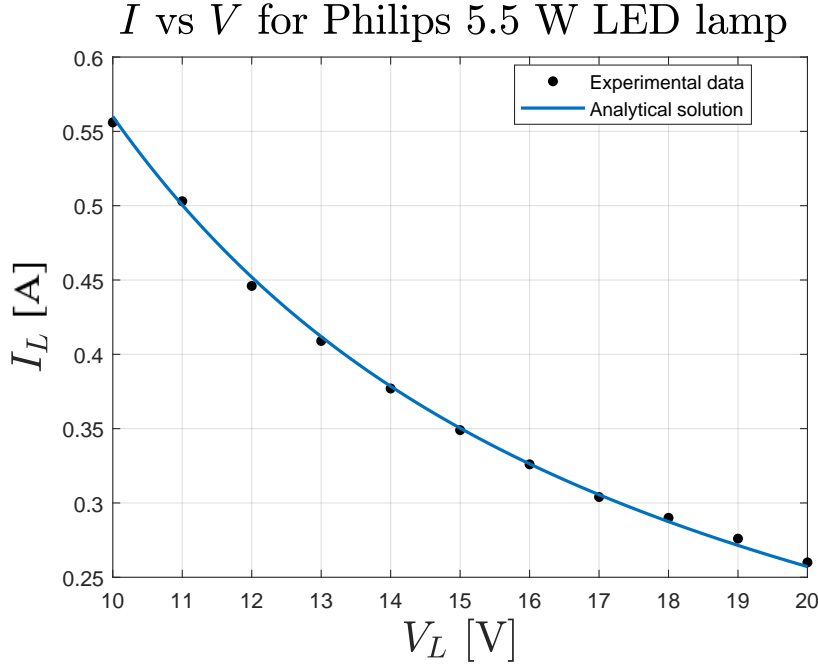


Figure 5.4: Current-voltage characteristics for Philips 5.5 W LED lamp in the constant brightness region

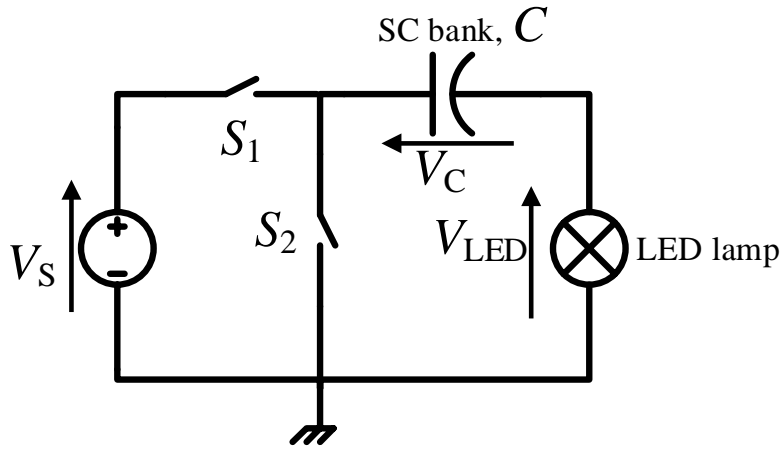


Figure 5.5: Basic SCALED converter (proof of concept)

V_{LED}^{\min} it will switch to the discharging phase by closing S_2 and opening S_1 . Then, C will be discharged to the LED lamp until V_C drops to V_{LED}^{\min} . This cycle repeats to keep the circuit working continuously. During the initial proof of concept V_{LED}^{\max} was set as 14 V and V_{LED}^{\min} was set as 10 V.

The initial circuit was designed to operate in the following voltage ranges;

1. Operational voltage range of LED lamp: $10 \text{ V} \geq V_{LED} \geq 14 \text{ V}$
2. Operational voltage range of SC bank: $10 \text{ V} \geq V_C \geq 14 \text{ V}$
3. Input voltage range: $21 \text{ V} \geq V_S \geq 24 \text{ V}$

A digital controller to monitor the voltage of the LED lamps and control the switches was implemented using a peripheral interface controller (PIC) micro-controller. This circuit was

built and tested using a laboratory power supply, as a proof-of-concept. Table 5.1 shows a summary of the components used for this design.

Table 5.1: Summary of Components used for basic SCALED converter

Parameter	Specification
Supercapacitor	Twelve 100 F/2.7 V MAXwell supercaps in series (15 mΩ ESR each, Max. leakage current of 0.260 mA)
Switches	PVN012 photovoltaic relay (ON resistance of 100 mΩ, 3 ms ON time delay)
Micro-controller	PIC16F684
LED lamp	12 V, 5.5 W, Philips LED lamps

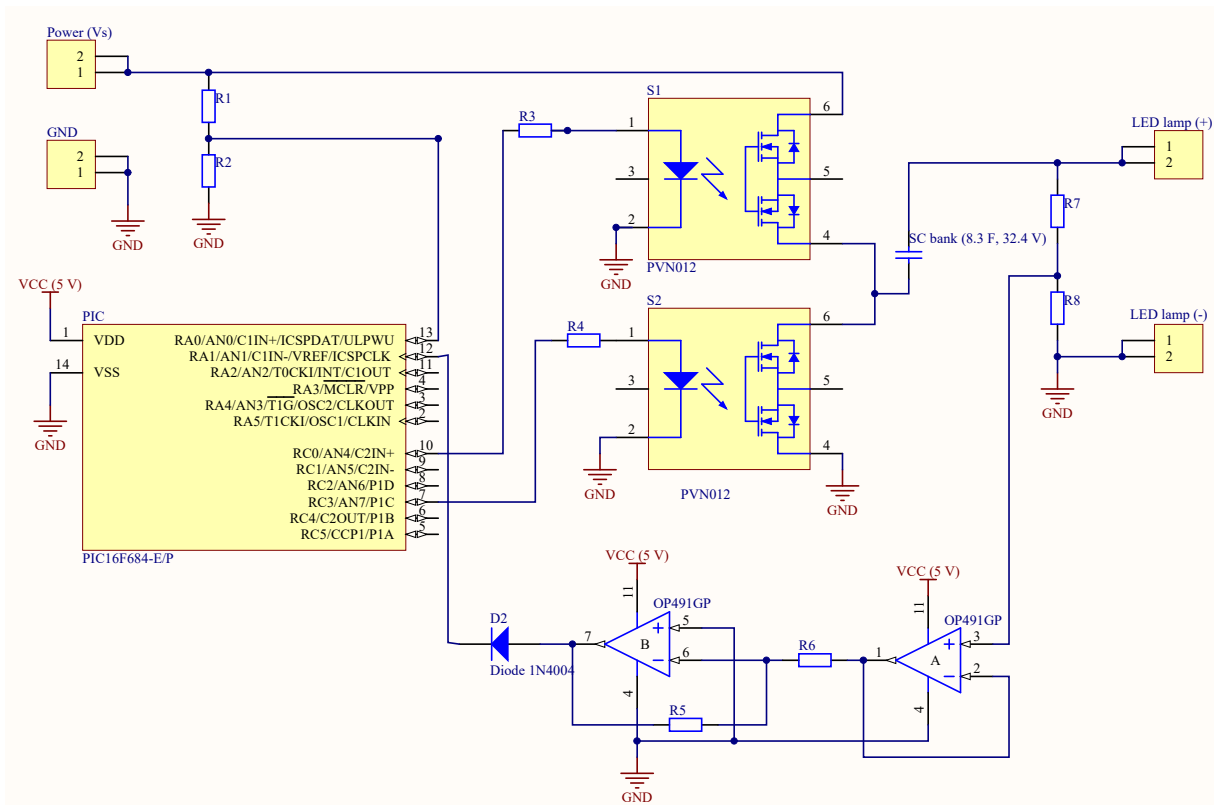
Figure 5.6(a) provides a schematic diagram of the circuit used for proof-of-concept based on a PIC processor as the controller, and Figure 5.6(b) shows the oscilloscope waveforms of the circuit implemented (results obtained for 22 V input voltage only is shown here). When considering the current trace, during the charging phase of the SC bank, the current is positive (at this stage current is drawn from the power supply) and during the discharging phase, the current is negative (at this stage the SC bank is discharged to the LED lamp and the LED is working with a voltage reversal).

In the first few proof-of-concept prototypes, minimizing losses in the control circuit was not considered, because the main target during this stage was to prove that the basic concept used to design the SCALED converter was valid. With the initial prototype working as expected, the applicability of the SCALOM concept for LED lighting was verified. However, since loss minimization was not considered in the initial stage of the SCALED design, it was decided to calculate the overall efficiency of the circuit to check the loss percentage in this prototype. The formula shown in Eq. 5.1 was used to calculate the overall efficiency of the circuit.

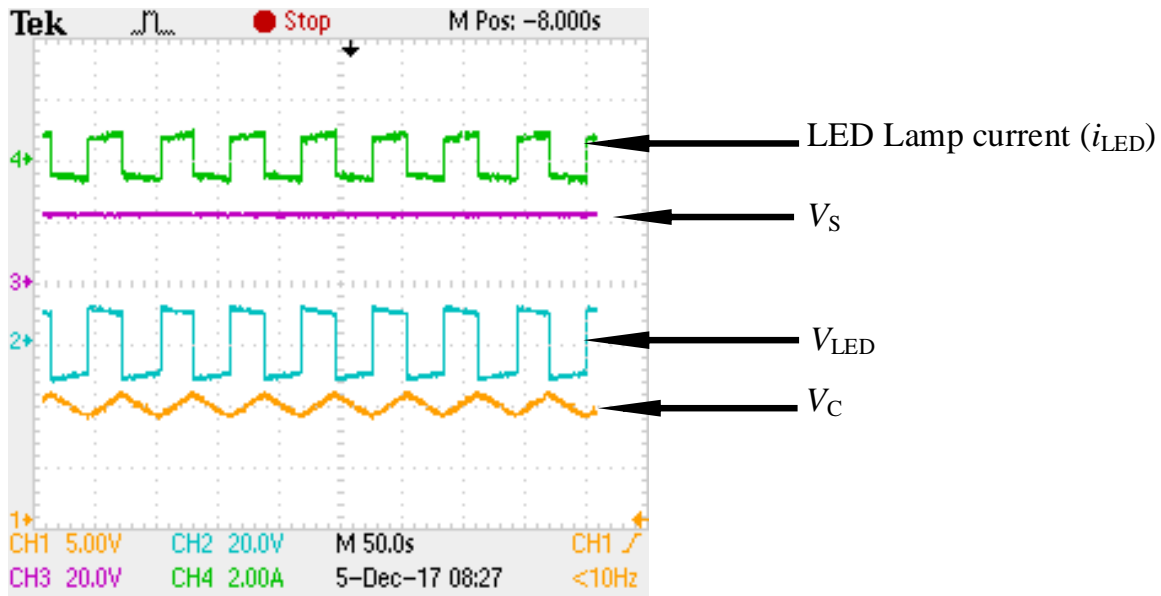
$$\eta = \frac{P_{\text{out}}}{P_{\text{in}}} = \frac{\overline{V_{\text{LED}}} \cdot \overline{i_{\text{LED}}}}{\overline{V_{\text{S}}} \cdot \overline{i_{\text{S}}}} \quad (5.1)$$

where the over-bar denotes average over time. Even without minimizing the loss in the control circuit it was possible to achieve $\approx 89\%$ overall efficiency for this prototype. Therefore, it was verified that a SCALED converter can be used to minimize losses in DC-microgrid based lighting application. It is important to consider here that the complete LED pack was considered as “useful-load”, and the power consumption of the converters inside the selected commercial LED lamp were regarded as part of the LED load.

Also, during the testing of the converter, the switching frequency was found to be well below 100 Hz. Therefore, the SCALED converter would not have any RFI/EMI issues. However, this frequency can be varied by changing the LED lamp load (i.e. increasing or decreasing the number of LED lamps used) and the size of the SC bank (i.e. the capacitance of the SC bank) used. During testing of this early prototype, the brightness of the LED lamp was also recorded and is shown in Figure 5.7. The brightness of the LED lamp was approximately constant during the operation of the SCALED converter.



(a)



(b)

Figure 5.6: Proof of concept: (a) Schematic diagram of basic SCALED converter; (b) Oscilloscope waveforms of the basic SCALED converter at input of 22 V

Modified SCALED converter

In this basic SCALED topology, during the discharging phase of the SC bank, the PV panel is disengaged from the converter and won't supply energy until the SC bank voltage reaches V_{LED}^{min} .

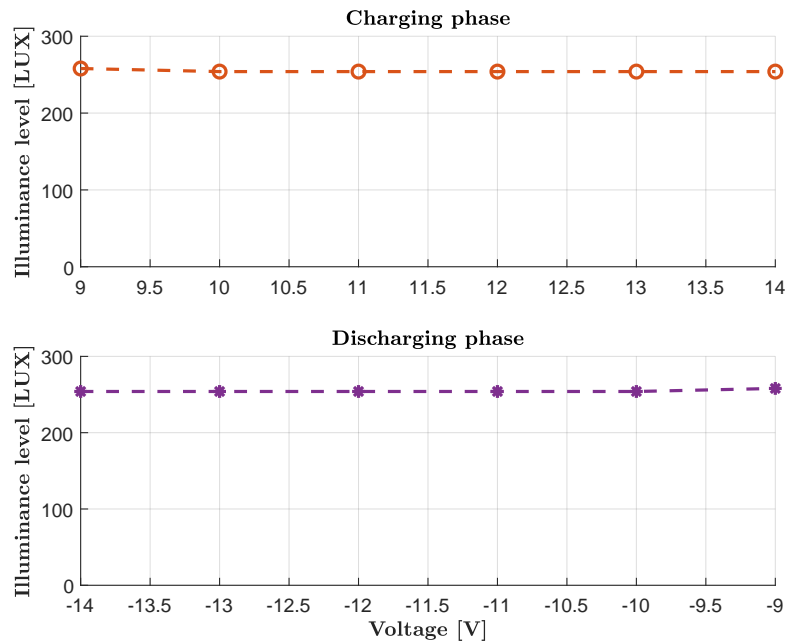


Figure 5.7: Brightness of the Philips 5.5 W LED lamp during SCALED operation

Therefore, during the discharging phase, the power generated from the PV panel will be wasted. In a practically useful implementation, a large LED lighting load (12 V, 24 V, 48 V or over 100 V DC cases) can be first divided into two halves, and one of these can be connected in series with a partly charged SC module, which is nominally around the DC rated voltage of the LED lamp bank. The other half is expected to operate from a fully charged identical SC module.

Hence, the basic SCALED converter was modified by dividing the LED lamp load into halves and using two individual SC banks with each LED lamp load. In order to use SC banks as practical energy storage devices in an overall system, with charge balance over each cycle, the concept shown in Figure 5.8 was developed.

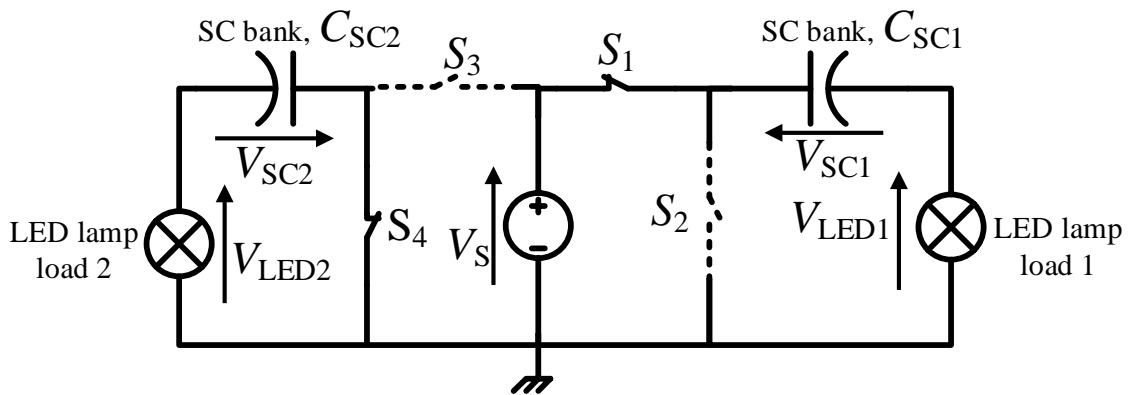


Figure 5.8: Basic SCALED converter (proof of concept)

At any given time it is possible to look at the right or left side of the circuit as a replica of the circuit in Figure 5.5, where we have added S_2 and S_4 to discharge excess energy into the same LED lamps, acting as useful lighting loads. Since commercial LED lamps can operate with

a negative DC voltage, S_2 and S_4 to maintain the charge balance of the respective SC banks, by alternatively switching S_1 and S_3 as a pair. A controller is required to maintain the sequence of switching accordingly. As explained in Section 5.1, in this topology the resistive losses in the well-known text-book case of an RC circuit fed by a voltage source are mostly absorbed into the LED lamp banks, for higher efficiency. One major advantage of this technique is that it does not require switching of the polarity of the SC bank during discharge as the LED lamps can operate with either positive or negative polarity voltage.

We can now consider the charging phase of the SC bank, C_{SC1} . After charging for a period of t seconds, the instantaneous voltage across the SC bank is given by

$$V_{SC1} = V_{SC1}(0) + \frac{I_{LED1}t}{C_{SC1}} \quad (5.2)$$

where I_{LED1} is the average LED lamp current, and $V_{SC1}(0)$ is the initial voltage of the capacitor.

The PV panel voltage V_S , is the sum of the SC bank voltage and LED lamp voltage,

$$V_S = V_{SC1}(t) + V_{LED1}(t) \quad (5.3)$$

The SC bank charges until the voltage across LED lamp load 1 reaches V_{LED1}^{\min} while the voltage across the C_{SC1} reaches $V_S - V_{LED1}^{\min}$ at the end of the charging time (t_{ch}). However, during the discharging phase in order to discharge this SC bank until the voltage across the LED lamp reaches V_{LED1}^{\min} , the criterion $V_S - V_{LED1}^{\min} > V_{LED1}^{\min}$ must be satisfied. This creates the condition,

$$V_S > 2V_{LED1}^{\min} \quad (5.4)$$

However, to avoid any potential damage to the LED due to over-voltage during the SC discharging phase, the final voltage of the SC bank at the end of the charging phase (i.e. $V_S - V_{LED1}^{\min}$) should not exceed the maximum voltage limit of the LED lamp load, V_{LED1}^{\max} . Hence, this creates another condition,

$$\begin{aligned} V_S - V_{LED1}^{\min} &\leq V_{LED1}^{\max} \\ V_S &\leq V_{LED1}^{\min} + V_{LED1}^{\max} \end{aligned} \quad (5.5)$$

In order to maintain the charge balance of the SC bank, the same amount of charge stored during the charging phase should be delivered back to the LED lamp load 1 during the discharging phase. Therefore, considering the charge balance of the supercapacitor during the charge-discharge cycle ($Q_{ch} = Q_{dch}$) it is possible to derive the following relationship,

$$I_{LED1}t_{ch} = I_{LED1}t_{dch} \quad (5.6)$$

where t_{ch} and t_{dch} are charge and discharge time respectively. These times will be dependent on the number of LED lamps used. This provides,

$$t_{\text{ch}} = t_{\text{dch}} \quad (5.7)$$

It is assumed that the both LED lamp loads are identical under all conditions (i.e. $V_{\text{LED1}}^{\text{max}} = V_{\text{LED2}}^{\text{max}}$, $V_{\text{LED1}}^{\text{min}} = V_{\text{LED2}}^{\text{min}}$ and $I_{\text{LED1}} = I_{\text{LED2}}$). Hence, when SC bank C_{SC1} changes to the discharging phase, SC bank C_{SC2} changes to the charging phase [in other words $t_{\text{ch(SC1)}} = t_{\text{dch(SC2)}}$]. Therefore, the same equation set (from Eq. 5.2 to 5.7) discussed earlier is also valid for LED lamp load 2.

5.2.2 Design of a prototype SCALED system

All the above-discussed conditions and factors were used during the design process of the final SCALED converter. In the basic SCALED converter, PVN102 photovoltaic relays with maximum current limitation of 4 A were used as the switches. It was decided to replace them with power MOSFETs in the modified SCALED converter to scale up the converter.

The maximum LED load the converter should supply in this case was 22 W (4 x 5.5 W LED lamps). The average current drawn by an LED lamp when its voltage decreased from 20 V to 10 V was 0.336 A. The minimum autonomy time (i.e. how long supercapacitor banks can supply energy to LED lamps in case of sudden power loss from solar input) for full load condition was 15 minutes. Hence by manipulating Eq.5.3, the capacitance value of the SC bank that should be used with the converter was derived as;

$$C = \frac{0.336 * 4 * 15 * 60}{20 - 10} = 121 \text{ F} \quad (5.8)$$

Therefore, to increase the autonomy time of the topology, SC banks were also upgraded to 166 F 50.4 V SC modules. As a further improvement to topology, initial charging of the SC bank was also included in the actual SCALED design as shown in Figure 5.9. The final converter incorporated three configurations:

1. initial charging phase of SC1 and SC2
2. charging phase of SC2 (or discharging phase of SC1)
3. discharging phase of SC2 (or charging phase of SC1)

During the start-up phase (initial phase) of the converter, SC banks 1 and 2 will charge up to 20 V and 12 V respectively by directly connecting a PV module to the SC banks and disconnecting the two LED lamp banks as shown in Figure 5.9(b). Once both SC banks are charged up to the required voltage levels, the converter commences normal operation in which one SC bank charges to 20 V through the LED lamps while the other SC bank discharges to the other LED lamps.

When the first SC bank is charged to 20 V, it will switch to the discharging phase, while the other bank now switches to the charging phase and the cycle repeats. Due to the ability of LED lamps to operate within a wide range of positive or negative voltages around the nominal value without loss of brightness, this technique can cope with large fluctuations in solar irradiance.

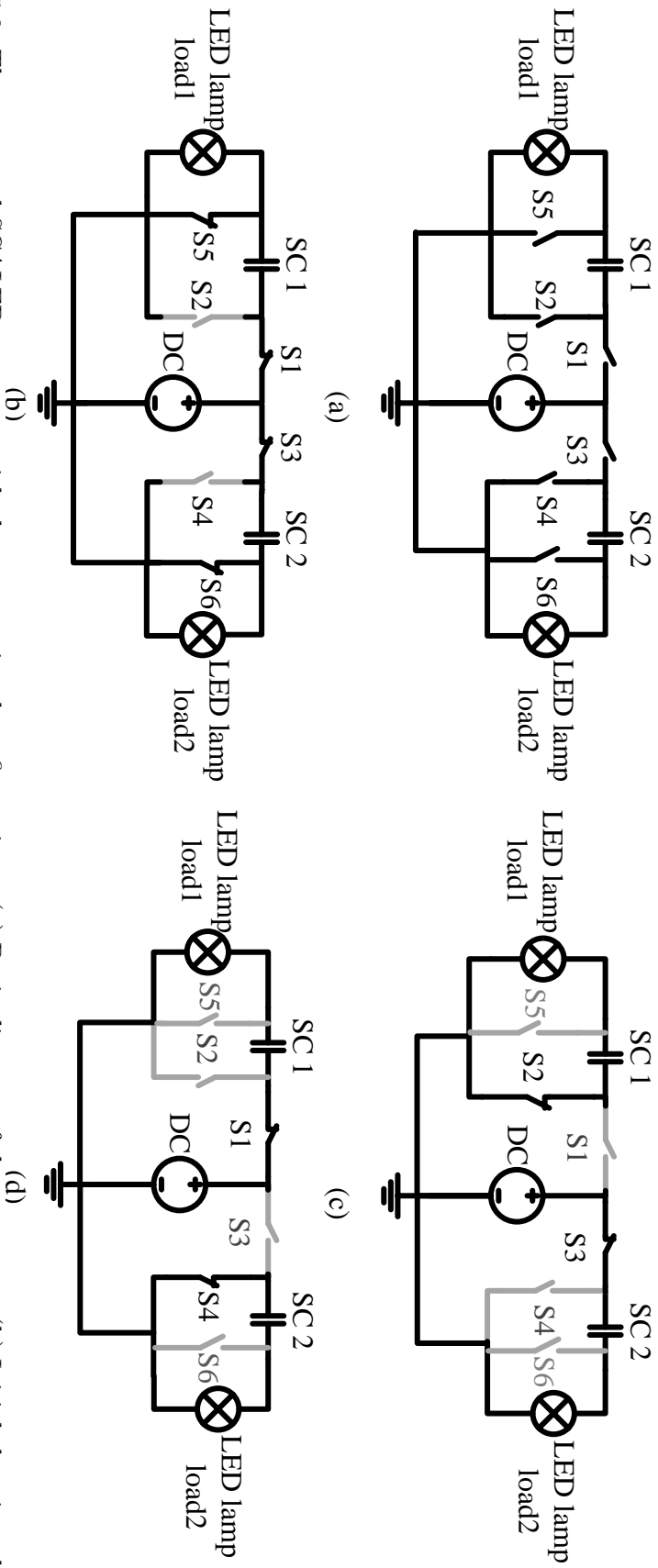


Figure 5.9: The proposed SCALED converter with three operational configurations: (a) Basic diagram of the converter; (b) Initial charging phase for SC1 and SC2; (c) SC1 discharging, SC2 charging phase; (d) SC1 charging, SC2 discharging phase.

In addition, SC banks are able to provide power to LED lamp loads during low irradiance levels to provide a short-term (in the order of minutes) DC-uninterruptible power supply (DC-UPS) capability. In this converter, switches S2 and S4 help to preserve the charge balance of respective SC banks by alternately switching S1 and S3 as a pair. In order to maintain the switching sequence shown in Table 5.2, using a controller is essential.

Table 5.2: Switching arrangement of proposed SCALED converter

Mode	S1	S2	S3	S4	S5	S6
Initial charging phase	On	Off	On	Off	On	On
SC2 charging and SC1 discharging	Off	On	On	Off	Off	Off
SC2 discharging and SC1 charging	On	Off	Off	On	Off	Off

5.2.3 Initial charging phase of the supercapacitor banks

Duration of the initial charging phase (start-up time) depends on the irradiance level available at the time of charging. During this phase of the SCALED converter, two supercapacitor banks will be directly connected to the PV panel. Now, the PV panel operates in the constant current region and with the irradiance level short-circuit current of the panel changes as shown in Figure 5.10.

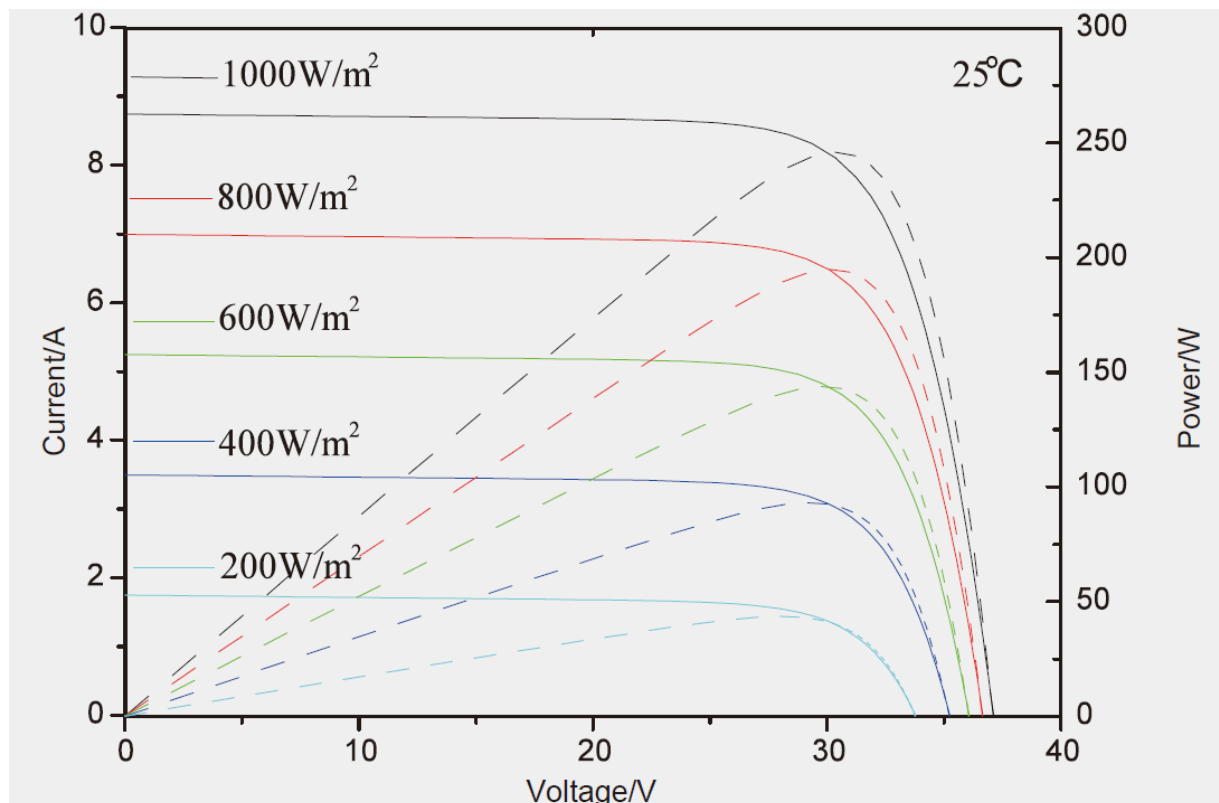


Figure 5.10: *CSUN250 – 60P* PV panel characteristics curves [103]

Initial charging phase of the converter is depicted in Figure 5.11. Start-up time of the SCALED converter can be calculated as follows.

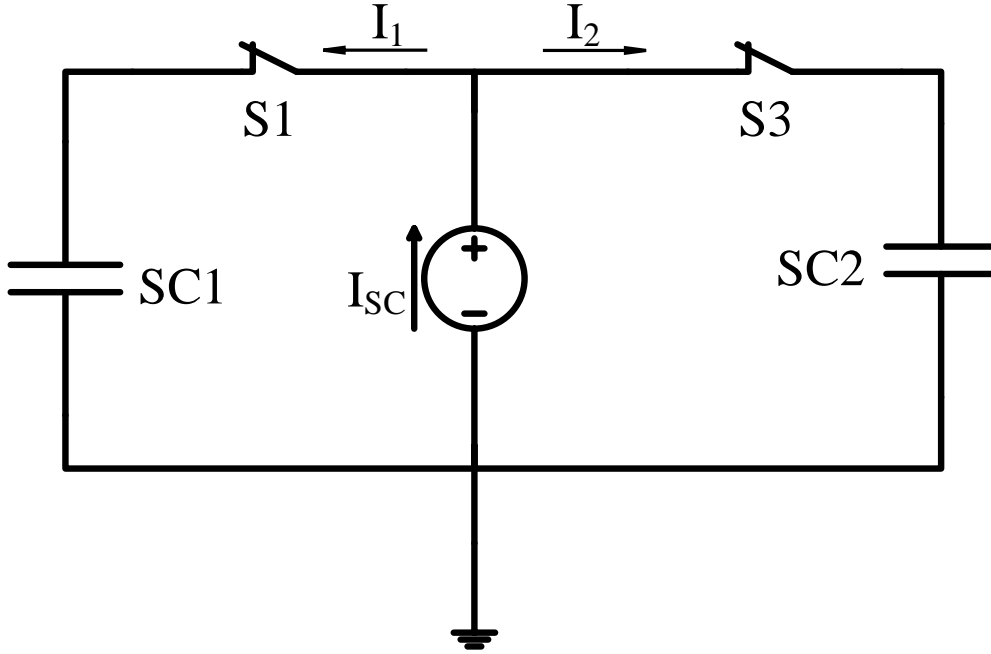


Figure 5.11: Initial charging phase of the SCALED converter

Since both sides of the SCALED converter is identical (i.e. $SC1=SC2=C$, $R_{S1} = R_{S2} = R_{SW}$ and initial voltage of the both supercapacitor banks is zero),

$$I_1 = I_2 = \frac{I_{SC}}{2} \quad (5.9)$$

Therefore, it is possible to derive an expression for both supercapacitor banks to charged to 12 V as,

$$t_1 = \frac{C \times 12}{0.5I_{SC}} \quad (5.10)$$

where C is the capacitance and I_{SC} is the short circuit current of the panel at a given irradiance level.

After supercapacitor bank 2 (SC2) charges to 12 V, the switch S3 will open and now total current I_{SC} will follow through supercapacitor bank SC1 until it charges to 20 V. Time taken for supercapacitor bank 1 to charge to 20 V can be found as;

$$t_2 = \frac{C \times (20 - 12)}{I_{SC}} \quad (5.11)$$

Therefore, the total duration of initial charging phase can be written as;

$$T = t_1 + t_2 = \frac{C \times 12}{0.5I_{SC}} + \frac{C \times (20 - 12)}{I_{SC}} \quad (5.12)$$

The total energy loss occurs during this phase can be written as,

$$E = 2 \times (0.5I_{SC})^2 R_{SW} \times t_1 + (I_{SC})^2 R_{SW} \times t_2 \quad (5.13)$$

where R_{SW} is the resistance of the switches.

During the experiment carried out in Port of Auckland (POAL) DC-microgrid site this energy loss was found to be 0.62 Wh for day 1,2 and 2.9 Wh for day 3.

Since MOSFETs were used as the switches, a control circuit was used to provide the required gate voltages (V_G) to the switches. P-channel MOSFETs were used as S1 and S2 where N-channel MOSFETs were used as all the other switches shown in Figure 5.9. The main reason for using P-channel MOSFETs as S1 and S2 is that high side switching of N-channel MOSFETs is difficult, as shown in Figure 5.12(a). The solar panel used for the SCALED converter had an output voltage that varied between 30 V and 36 V. Hence, if an N-channel MOSFET is used as S1 (or S2), the voltage required as the gate voltage (V_G) is greater than the solar panel output voltage (V_{solar}) which is not feasible. Therefore, it was decided to use P-channel MOSFETs as S1 and S2. In the case of driving a P-channel MOSFET in the high side, the gate voltage (V_G) should be less than source voltage (V_S) of the MOSFET, in the case of a SCALED topology which is at the same potential as the solar panel output as depicted in Figure 5.12(b).

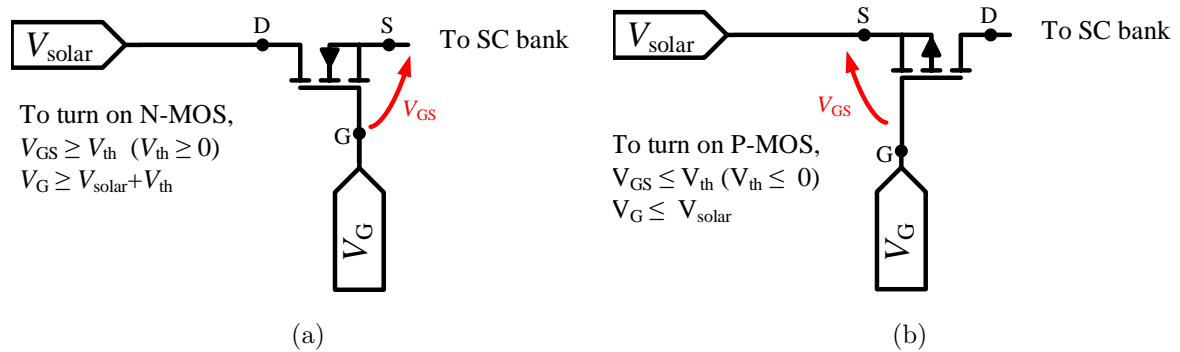


Figure 5.12: High side switching of a MOSFET (V_{th} : Gate threshold Voltage, V_{GS} : Gate-Source voltage and V_{solar} : solar panel output voltage): (a) the case of N-channel MOSFET; (b) the case of P-channel MOSFET

Most of the commercially available P-channel MOSFETs have ± 20 V as the maximum allowable gate-to-source voltage, V_{GSS} , with drain and source short-circuited. The P-channel MOSFET used in the SCALED converter had a V_{GSS} of ± 20 V. Hence, it was necessary to use MOSFET drivers that could supply at least 20 V as the gate voltage, which was not cost-effective. Therefore, the circuit shown in Figure 5.13 was used to drive the P-channel MOSFET. In this arrangement, an N-channel MOSFET was used as Q_1 . When Q_1 is ON, the resistor R_2 is connected to ground potential creating a voltage divider, which provides the gate voltage to the P-channel MOSFET. When Q_1 is OFF, the gate of the P-channel MOSFET (G_1) is at the same potential as V_{solar} because $R_{DS(OFF)} \gg R_1$ and most of the voltage drop is across the $R_2, R_{DS(OFF)}$ combination. The same value resistors were used as R_1 and R_2 , so that during the ON state gate, G_1 always receive half of the solar voltage. This approach avoided the gate-to-source voltage exceeding its maximum allowable limit.

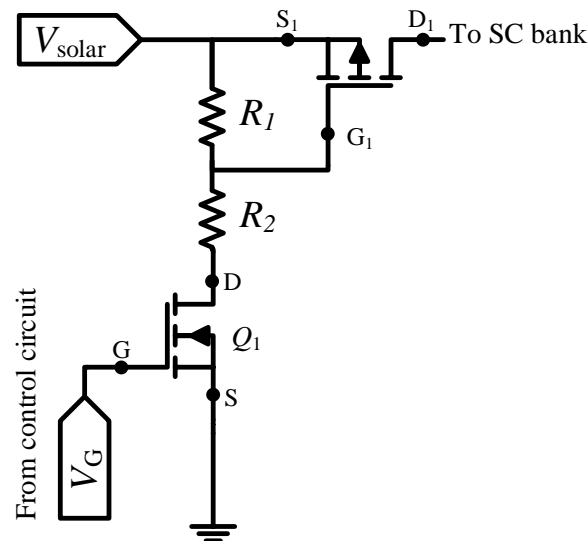
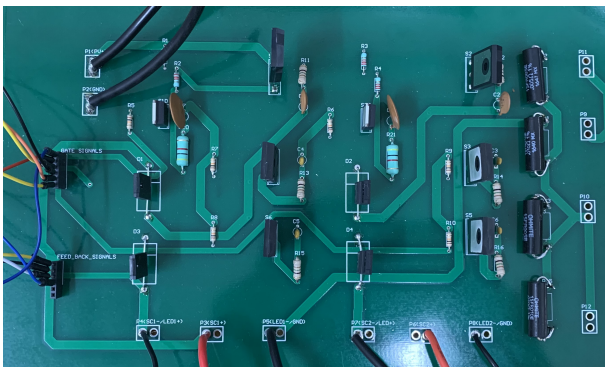
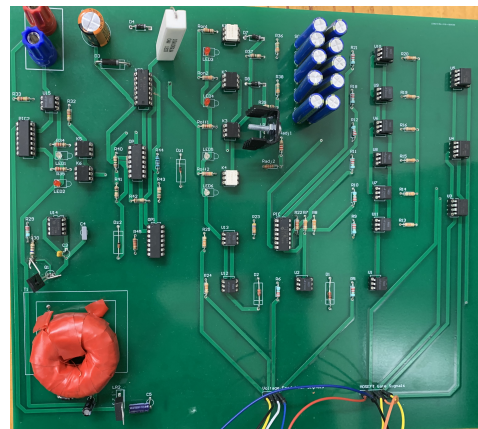


Figure 5.13: P-channel MOSFET driver circuit

The schematics and PCB layouts of this prototype, designed using Altium Designer, are available in Appendix A.1 and A.2. A compact prototype version of the SCALED converter is depicted in Figure 5.14.



(a)



(b)

Figure 5.14: A compact version of SCALED converter: (a) Power stage circuit board; (b) Control circuit board

The main purpose of the controller was to control the switching sequence of the SCALED converter, and a PIC16F684 micro-controller from Microchip Technologies was used to maintain the appropriate switching sequence. The S1, S2, S3, S4, S5 and S6 switches were controlled through the RC0, RC1, RC2, RC3, RC4 and RC5 port pins of the micro-controller respectively. The voltage across the LED banks was monitored through the RA0 and RA1 port pins. The voltage levels at these pins were converted to digital format using an inbuilt 10-bit Analogue to Digital converter (ADC) in the PIC, which operated at a 4 MHz oscillation frequency. Then the results were compared with the reference value (digital value of V_{LED}^{min}) and the transition between the SC charging and discharging phase was carried out accordingly. The micro-controller

firmware (shown in Appendix A.3) was developed to drive the switches based on an algorithm shown in the flow-chart in Figure 5.15.

5.2.4 Power supply design for SCALED controller

In the early iterations of the SCALED converter, batteries were used to power the control circuit rather than the solar panel. With the aim of avoiding extra power sources in the circuit and making a self-powered system, it was decided to implement an auxiliary power supply for the SCALED controller. Since the controller circuit operated using 5 V, it was necessary to step down the PV output voltage ($\approx 30 - 33$ V) without decreasing the overall efficiency, of the system as well as minimising the heating issues of the overall circuit. Therefore, a power supply unit (which can be operated using a PV panel) for the control circuit was also implemented using the supercapacitor assisted low dropout regulator (SCALDO) concept [52, 60, 65, 75].

Analogue supercapacitor assisted low-drop out (SCALDO) regulator design

Most of the components used in the SCALED controller can be safely operated using a 10 V supply. Therefore, it was decided to design a 10 V linear regulator. However, if a typical regulator is used to get 10 V, the efficiency of the conversion will be very low (around 30%). Hence, in order to step down the solar panel voltage to 10 V, it was decided to use the SCALDO regulator technique, [52, 60, 65, 75] which provides moderate to high-efficiency levels. Due to RFI/EMI issues in switched-mode converters, it was decided not to use inductor-based switched-mode converters for this application.

In a SCALDO regulator, a supercapacitor is placed in series with the input of the LDO. When the supercapacitor is charged to V_{sc}^{max} , it will disconnect from the supply and is connected in parallel with the input of the regulator, to release the energy stored in it. The SCALDO converter has two different configurations depending on the supply voltage, V_P and the minimum allowable input voltage of the regulator, V_{in}^{min} , as [60];

- (a) $V_P > 2V_{in}^{min}$: Series to parallel SC array
- (b) $V_P < 2V_{in}^{min}$: Parallel to series SC array

In this context since the solar panel voltage, V_{SP} is greater than twice the minimum allowable input voltage of the LDO, V_{in}^{min} , the number of supercapacitors (n) needed for the regulator was calculated using the following formula [52].

$$n < \frac{V_{SP} - V_{in}^{min}}{V_{in}^{min}} = \frac{30 - 13}{13} = 1.308 \quad (5.14)$$

The voltage across the supercapacitor at the end of charging is,

$$V_{sc}^{max} = \frac{V_{solar} - V_{in}^{min}}{n} = \frac{30 - 13}{1} = 17 \text{ V} \quad (5.15)$$

However, commercially available single supercapacitors are rated at 2.7 V and thus cannot be used in this application. As a solution 10 single capacitors with 7 F, 2.7 V capacity were connected in series to achieve the required voltage level. The circuit diagram of the implemented SCALDO regulator is shown in Figure 5.16.

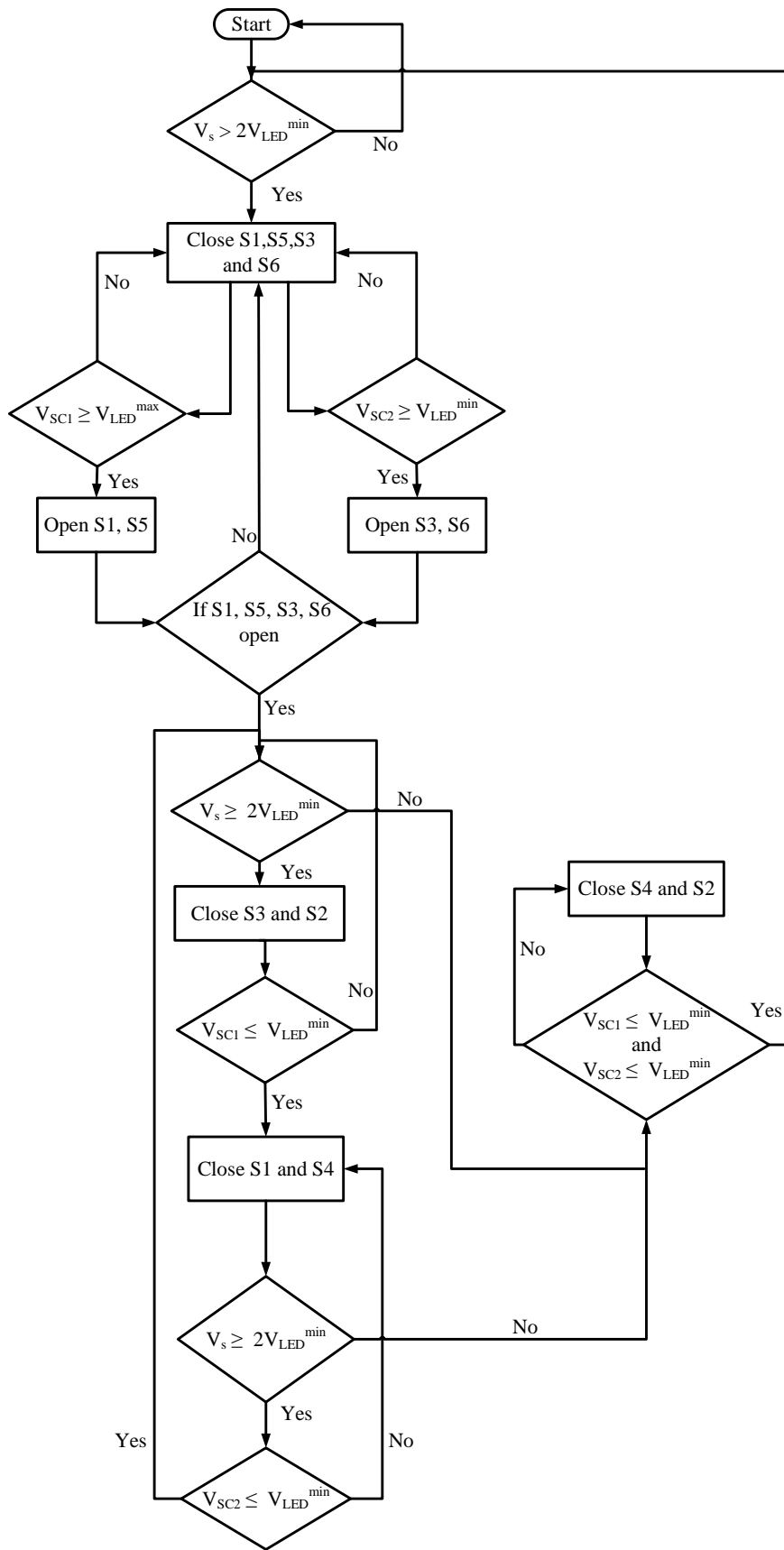


Figure 5.15: The flow-chart of the PIC algorithm

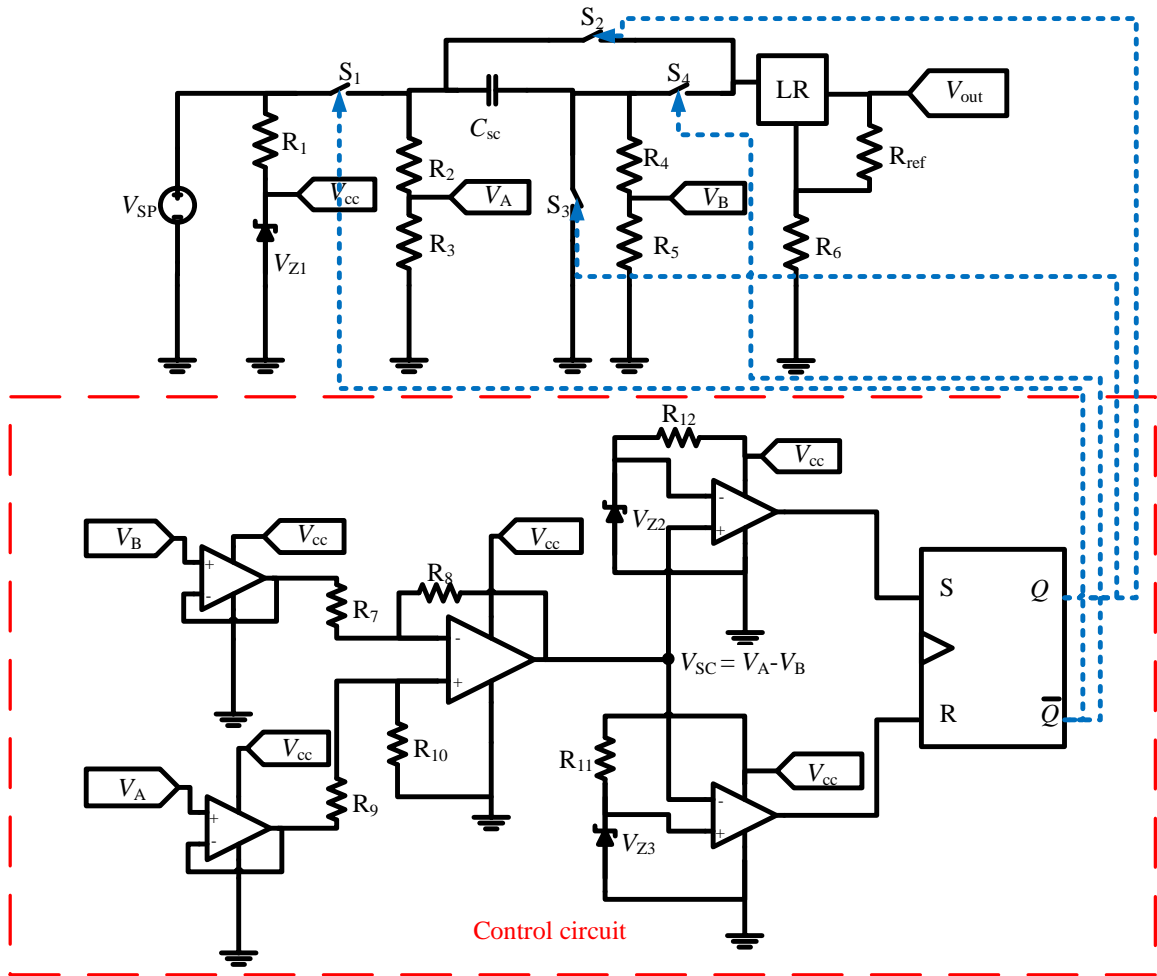


Figure 5.16: Circuit diagram of 10 V SCALDO regulator

In order to control the transition between charging and discharging of the supercapacitor in the SCALDO regulator, a control circuit shown in Figure 5.16 was used. The voltage across the capacitor is compared with two pre-defined voltage levels using two OPAMP comparator circuits. The outputs of the comparators are used as the inputs (R and S) of the SR flip-flop. The outputs of Q and \bar{Q} are used to control S_2, S_3 pair and S_1, S_4 pair respectively. The SR flip-flop was constructed using two NOR gates. The control sequence of this circuit is given in Table 5.3. The output of the SCALDO regulator was used to supply the MOS drivers and 5 V isolated supply.

Table 5.3: Control sequence of SCALDO regulator

Case	S	R	Q	\bar{Q}	S1	S1	S3	S4	Comment
$V_{sc} > V_{Z3}$ and $V_{sc} < V_{Z2}$	0	1	0	1	On	Off	Off	On	Charging phase C_{SC}
$V_{sc} < V_{Z3}$ and $V_{sc} < V_{Z2}$	0	0	0	1	On	Off	Off	On	No change (charging phase)
$V_{sc} < V_{Z3}$ and $V_{sc} > V_{Z2}$	1	0	1	0	Off	On	On	Off	Discharging phase C_{SC}
$V_{sc} > V_{Z3}$ and $V_{sc} < V_{Z2}$	0	0	1	0	Off	On	On	Off	No change (discharging phase)

Transformer isolated 5 V power supply design

All the switching signals given to the switches in the SCALED converter are controlled using a PIC micro-controller which normally operates using a 5 V supply. Since the SCALDO regulator was designed to provide 10 V, it was necessary to implement a 5 V supply for PIC micro-controller. However, it is common practice to have isolation between power stage and the low voltage control circuits for safety and reliability improvements. This is done to prevent unwanted currents flowing between two parts while still enabling signal and power transfer. Also, isolation is used in a wide variety of applications to protect human operators and low-voltage circuitry from high voltages, to improve noise immunity, and to handle ground potential differences between communicating subsystems [98]. There are several isolation techniques available, such as optical (optoisolators) and electromagnetic (transformers). However, in this case the need was to design an DC-DC converter that could step down 10 V to 5 V and provide electrical isolation between the power and control stages. Therefore, a simple transformer was used as the isolator.

Using the transformer a simple 5 V supply as shown in Figure 5.17 was implemented. A 1 : 1 toroidal transformer was used. The SCALDO output was connected to one end of the primary winding and an NPN bipolar junction transistor (BJT) was connected across the other end and ground as shown in Figure 5.17. This power transistor was switched ON and OFF using a 555 timer circuit at a frequency of 26 kHz so that the transformer always received an AC signal. At the secondary winding a simple diode-based rectifier circuit was used to convert the voltage from AC to DC. Then using a linear regulator, the DC output was stepped down to 5 V.

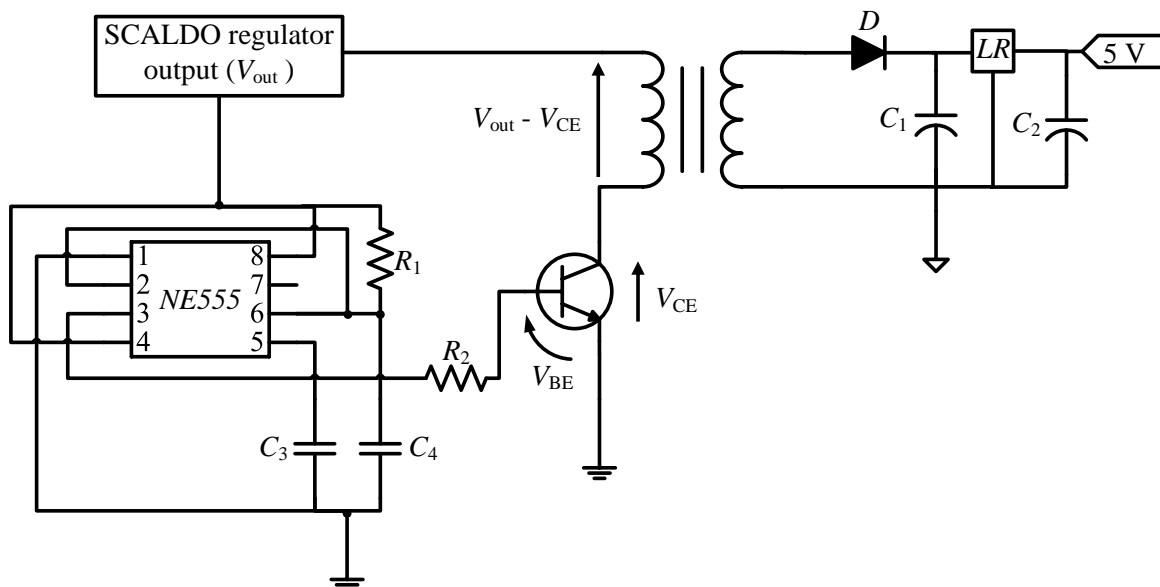


Figure 5.17: Circuit diagram of 5 V isolated power supply

When selecting the transformer core, the following key parameters were taken into account;

1. switching frequency
2. operating flux density
3. suitable core material for adequately low core losses

4. operating temperature

Core size is selected based on the power handling capability of the core. The size of the core can be minimized by using a high operational frequency. Operating temperature rise is caused by core losses and copper losses in the transformer. Core losses include both hysteresis and eddy current losses. Hysteresis loss is a function of core flux swing (magnetization and demagnetization of the core) and operating frequency [99]. However, hysteresis loss is independent of input voltage and load current. The eddy current loss is a function of the volts per turns applied to the winding and the duty cycle.

Since toroids are the more efficient and most economical solution, as they do not require a bobbin or any assembly accessories, it was decided to use a toroidal core for the SCALED prototype. For all the following calculations, Magnetics Inc's (Pittsburgh, PA) transformer design guide and data sheets were used as the reference.

The power handling capability of a transformer can be determined by its $W_a A_c$ product, where W_a is the available core window area in cm^2 and A_c is the core effective cross-sectional area in cm^2 . For a square wave [100]:

$$V = 4BA_c N f \times 10^{-8} \quad (5.16)$$

where V is the rms voltage [V], B is flux density [G], A_c is core effective cross-sectional area [cm^2], N is the number of turns and f is the operating frequency [Hz]. The use of window area by the winding is called the winding factor, K . This can be derived using the wire area A_w [cm^2] as follows,

$$K = \frac{NA_w}{W_a} \quad (5.17)$$

where A_w can be written in terms of the current capacity of the wire C_w and the input current I as,

$$A_w = C_w I \quad (5.18)$$

By combining Eq. 5.16, Eq. 5.17 and Eq. 5.18, the $W_a A_c$ product can be calculated as;

$$W_a A_c = \frac{VIC_w N \times 10^8}{4NBfK} = \frac{P_{in} C_w \times 10^8}{4BfK} \quad (5.19)$$

where $P_{in} = VI$ is the input power. For a square wave excitation and toroidal cores, $C_w = 5.07 \times 10^{-3} \text{ cm}^2/\text{A}$ and $k = 0.4$.

As marked in Figure 5.18, at an operating frequency of 26 kHz, F material has the highest flux density. However, core losses in F material increase with temperature above 30 °C [101]. Therefore it was decided to use P material to minimize the core losses and has a flux density of 1600 G at 26 kHz.

Using Eq. 5.19 $W_a A_c$ product was calculated as follows;

$$W_a A_c = \frac{1 \times 5.07 \times 10^{-3} \times 10^8}{4 \times 1600 \times 26 \times 10^3 \times 0.4} = 7.62 \times 10^{-3} \text{ cm}^4 \quad (5.20)$$

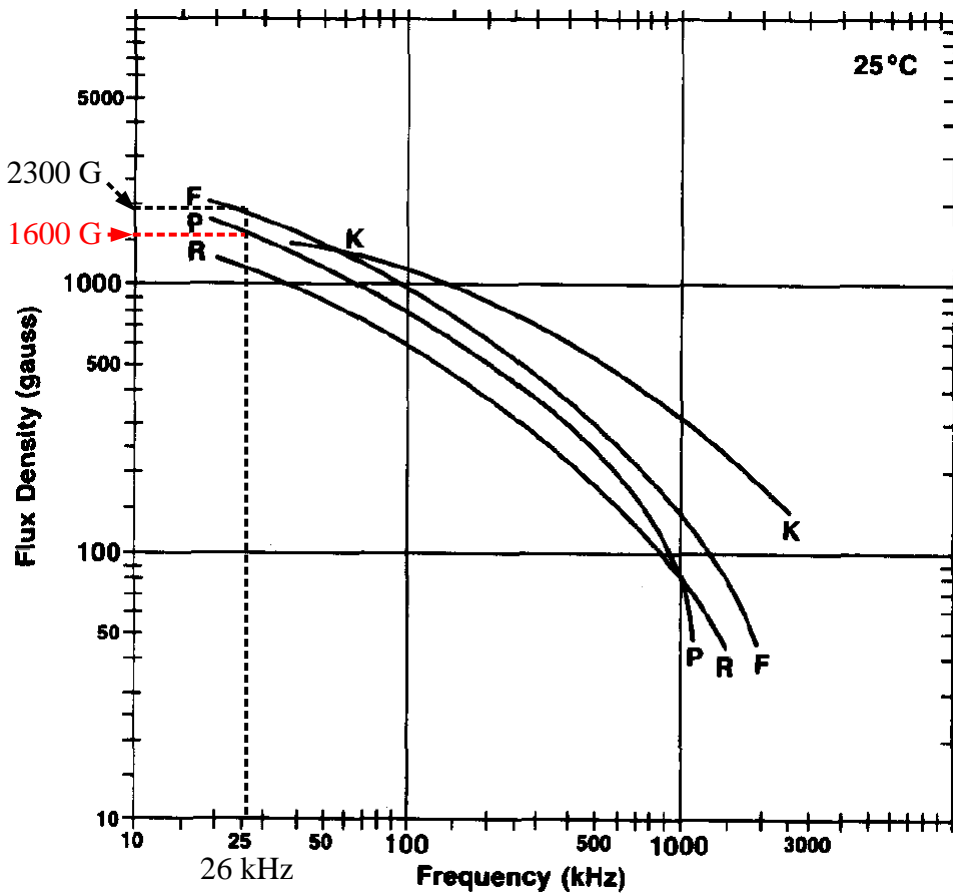


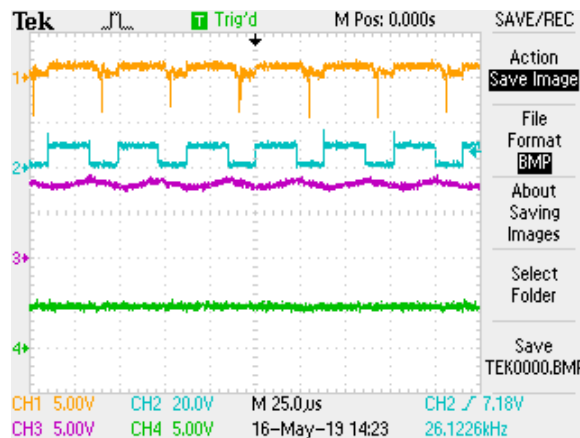
Figure 5.18: Maximum usable flux density variation for F, P, R, and K ferrite materials with frequency for a constant core loss of 100 mW/cm^3 [101]

From Magnetics Inc's Ferrite core catalogue [102], a toroid core 40705TC with an area product of 8×10^{-3} was selected. From the core data, A_c was extracted as $11.03 \times 10^{-2} \text{ cm}^2$. Then using Eq. 5.16, the primary and secondary number of turns were calculated as;

$$N_P = \frac{10 \times 10^8}{4 \times \sqrt{2} \times 1600 \times 11.03 \times 10^{-2} \times 26 \times 10^3} \approx 40 \quad (5.21)$$

Since a 1:1 transformer was used, the number of turns in the secondary, N_S , was also 40. The transformer was wound in the lab and tested in the circuit given in Figure 5.17. The results are depicted in Figure 5.19.

During the initial charging phase of the SC banks, the SCALED system operates in the constant current region of the PV characteristic curve; solar panel output current remains constant across a range of low voltages. This results in a power cut to the control circuit, as the PV voltage is not high enough to trigger the controller switching logic that will ultimately terminate the operation of SCALED. To avoid this, a 40 V buffer capacitor was used to provide power to the controller during this stage.



CH1 – V_{BE} of switching transistor

CH2 – Timer circuit output

CH3 – transformer output

CH4 – regulated 5 V output

Figure 5.19: 5 V transformer isolated power supply test results at a load current of 100 mA

5.3 Remedy for MOSFET body diode effect in SCALED converter

Figure 5.20 illustrates the power stage of the SCALED converter where MOSFETs were used as the switches. During the discharging phase of C_{SC1} (Q_1 , Q_5 OFF and Q_2 ON), the body-diode in Q_5 creates a parasitic path potentially creating a short circuit of the SC bank C_{SC1} . Therefore, this avoids supplying the LED lamp load1 which interrupts the normal operation of the SCALED converter as well as damaging Q_5 . This situation is shown in Figure 5.20(a). This scenario occurs due to point 4 (positive terminal of C_{SC1}) being connected to the ground when Q_2 is in its ON-state so that the voltage at point 5 (negative terminal of C_{SC1}) is low enough to forward bias the body-diode of Q_5 .

A similar sequence of events happens during the discharging phase of the SC bank C_{SC2} (Q_3 , Q_6 OFF and Q_4 ON), as shown in Figure 5.20(b). In here, the body diode of Q_6 creates the parasitic path for C_{SC2} to discharge without supplying the LED lamp load 2. Here, the voltage at point 3 (negative terminal of C_{SC2}) is low enough to forward bias the body diode of Q_6 because when Q_4 is in its ON-state, the point 2 (positive terminal of C_{SC2}) is now connected to the ground.

5.3.1 Possible solutions and limitations

Instead of using a single N-channel MOSFET for Q_5 and Q_6 can use two N-channel MOSFETs can be used back to back as shown in Figure 5.21(a) and (b), either common source or drain. Also, it is possible to use a diode connected to either drain or source to block the current path of the body diode as in Figure 5.21(c). However, since high power MOSFETs are used as switches, using another MOSFET is not cost-effective. Therefore, it was decided to use the simplest configuration shown in Figure 5.21(c) for Q_5 and Q_6 two N-channel MOSFETs.

The initial performance test for this circuit was carried out using a bench power supply as the voltage source. The main purpose of this experiment was to observe and verify the behaviour of the circuit with a controlled current and voltage source before powering it using the PV panel outputs. The equipment and devices used during the testing are listed below.

1. 30 V, 3 A dual output bench power supply (in place of PV panel)
2. Two identical 166 F, 50.4 V supercapacitor banks

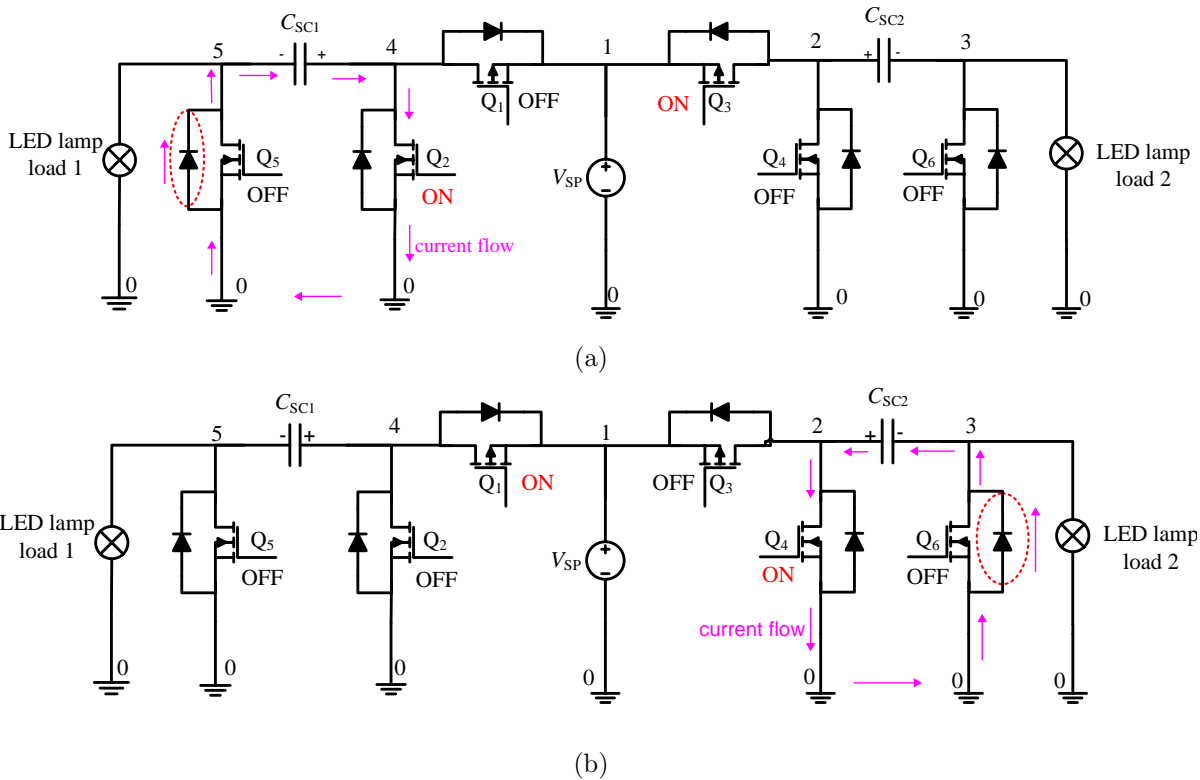


Figure 5.20: MOSFET body diode effect on SCALED converter: (a) Q_5 body-diode can form a current when Q_2 is in the ON-state in C_{SC1} discharging phase; (b) Q_6 body-diode can form a current when Q_4 is in the ON-state in C_{SC2} discharging phase

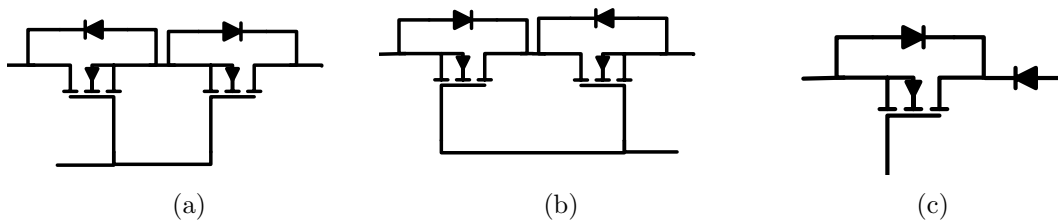


Figure 5.21: N-channel MOSFET blocking the body-diode effect: (a) common source configuration ; (b) common drain configuration; and (c) diode connected at the drain (or source)

3. Two identical 22 W (4 x 5.5 W) LED lamp banks
4. Digital multimeters to measure voltages

The initial performance evaluation was carried out by measuring the current on each side, the input current, the source voltage and the voltage across each LED and the SC banks. Since the testing covered a long period of time, a large number of measurements needed to be recorded. Therefore, the best option was to arrange an automatic recording system. However, the isolated four-channel oscilloscope that was commonly used for these kinds of multiple measurements had a restriction in its time scale, which prevented the whole cycle of switching being captured. Therefore, the only option was to record the reading manually using digital multimeters. During the initial charging phase, measurements were not recorded.

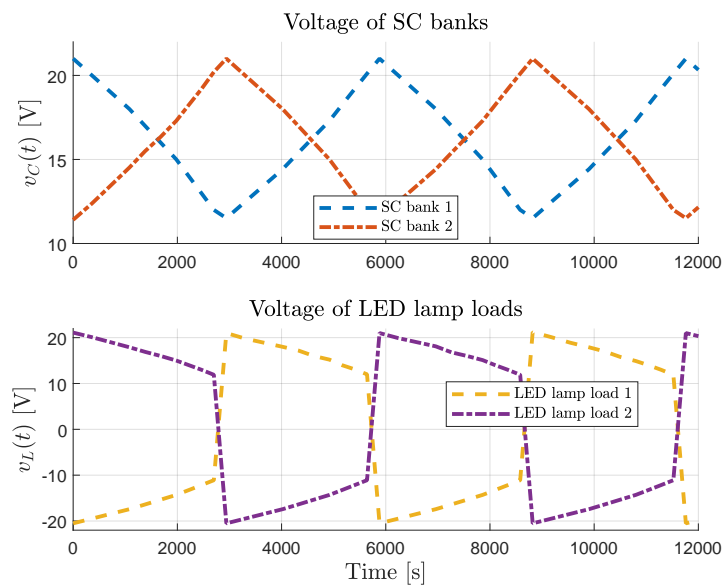
The laboratory test was carried out for two cases as follows;

- (a) Case 1: Two LED lamps (11 W) in each side

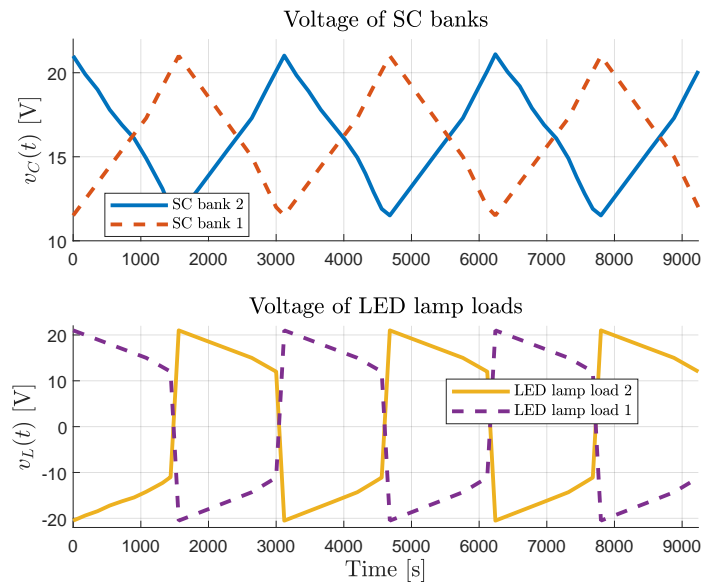
(b) Case 2: Four LED lamps (22 W) in each side

For case 1, the voltage readings were recorded every 10 minutes, while for case 2, voltage and current readings were recorded every 5 minutes to observe the performance of the SCALED circuit. For case 1, measurements were only taken for four changeovers, which took approximately 3 hours. It was possible to take readings for nearly six changeovers for case 2, which only took around 2.5 hours. For each these cases, the supply voltage was kept at 33 V.

Test results for the circuit are shown in Figure 5.22. The initial test showed that the changeover was happening as expected. There was a smooth transition between the main source and the SC banks, maintaining the operating voltage range of the LEDs with expected brightness.



(a)



(b)

Figure 5.22: Laboratory test results of modified SCALED converter: (a) With 11 W LED lamp load; (b) With 22 W LED load

The end-to-end efficiency (ETEE) of the SCALED converter when operating using a laboratory power supply was calculated using Eq. 5.22. It was possible to achieve higher ETEE of $\approx 94\%$ for both cases.

$$\eta = \frac{P_{\text{out}}}{P_{\text{in}}} = \frac{\overline{V_{\text{LED1}}} \cdot \overline{i_{\text{LED1}}} + \overline{V_{\text{LED2}}} \cdot \overline{i_{\text{LED2}}}}{\overline{V_s} \cdot \overline{i_s}} \quad (5.22)$$

where the over-bar denotes average over time.

After initial laboratory tests, the converter was tested using a PV panel installed at the University of Waikato to identify its behaviour with irradiance and temperature variations. The energy source is not a constant voltage source such as a lab power supply. During the experiment, a 22 W LED lamp load was used on both sides of the converter. The test was conducted on a sunny day from 1200 to 1500 h. Digital multimeters were used to record both voltages and currents. All the data were recorded manually every 5 minutes. Figure 5.23(a) shows the behaviour of the converter. With variations in irradiance and temperature, both the PV panel output voltage and the current change. Therefore, as can be seen in Figure 5.23(a), during the charging phase of the SC banks the respective LED bank voltage won't change as it did with the constant voltage source case shown in Figure 5.22(b). However, this does not affect the normal operation of the converter, because all these factors were considered during the design process.

Figure 5.23(b) shows the irradiance variance throughout the day. Irradiance data was recorded manually using irradiance meter TM-206. This meter measures the amount of solar power (in watts) striking 1 m² of the earth's surface. The meter used has an accuracy of $\pm 5\%$ with an operating range between 5 °C and 40 °C. Measurements were taken on the same rooftop where the solar panels were installed. Since the panels were installed facing north at an angle of 38° to get the most energy from the sun as it travelled from east to west, irradiance is also measured using a solar power meter at the same angle facing north to obtain the most accurate radiation data possible. These recorded data were compared with the data from National Institute of Water and Atmospheric Research (NIWA) database as shown in Figure 5.23(b). During a sunny day, since the sky is clear, with no cloud to cause shading of the solar panels, measured and NIWA data follow almost identical curves as shown in Figure 5.23(b).

It can be observed from the results that even though irradiance varies, the converter operated as expected. The ETEE of the circuit for this test was also calculated using Eq. 5.22. In this case, it was possible to achieve an efficiency of $\approx 94\%$. Hence, by using appropriate SC banks the converter was able to overcome the intermittent nature of the solar power while achieving high-efficiency values.

5.4 Application of SCALED in POAL DC-Microgrid container

The SCALED converter was developed with a pilot grant from Ports of Auckland Ltd (POAL). This converter was installed in an experimental shipping container used as an office cubicle in the jetty area which was illuminated by commercially available 12 V LED lamps. Figure 5.24 depicts the simplified block diagram of the overall system installed in a POAL DC-micro grid container. A summary of components used for the implementation is given in Table 5.4.

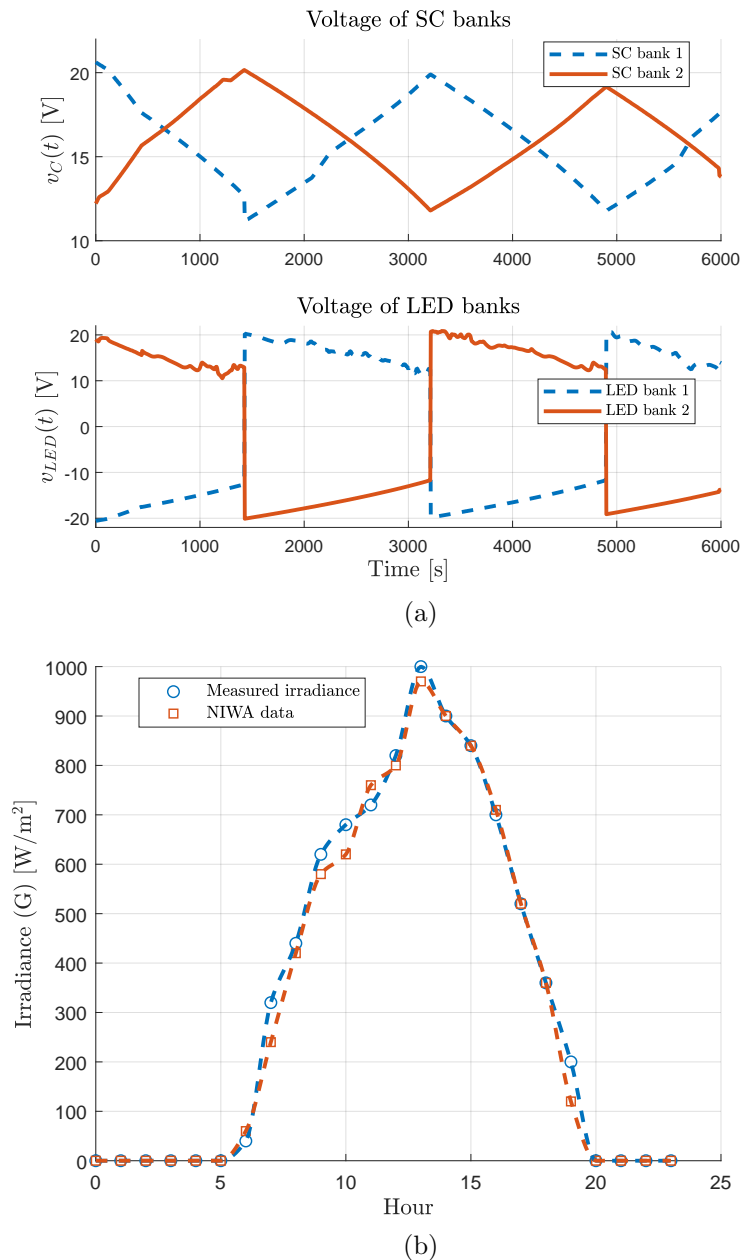


Figure 5.23: Operational behaviour of SCALED converter with PV panel connection: (a) Supercapacitor and LED bank voltages vs time; (b) Variation of irradiance throughout the day in University of Waikato

5.4.1 Field results of SCALED converter

Field testing of the full version of the SCALED system was carried by using a *CSUN250 – 60P* PV panel [103] as the energy source, which was installed in the rooftop of the DC-microgrid container at POAL site. Field testing was carried out for three days continuously to observe the behaviour of the topology in the long run. The open-circuit of the PV panel was 37.3 V, SC banks were charged to 20 V and discharged to 12 V to avoid the unnecessary higher voltage across LED lamp loads during the charging phase of SC banks. A GL240 data logger was used to acquire the experimental data at the POAL site. Operational behaviour of SCALED converter for three different days with average irradiance levels of 730 Wm^{-2} , 643 Wm^{-2} and

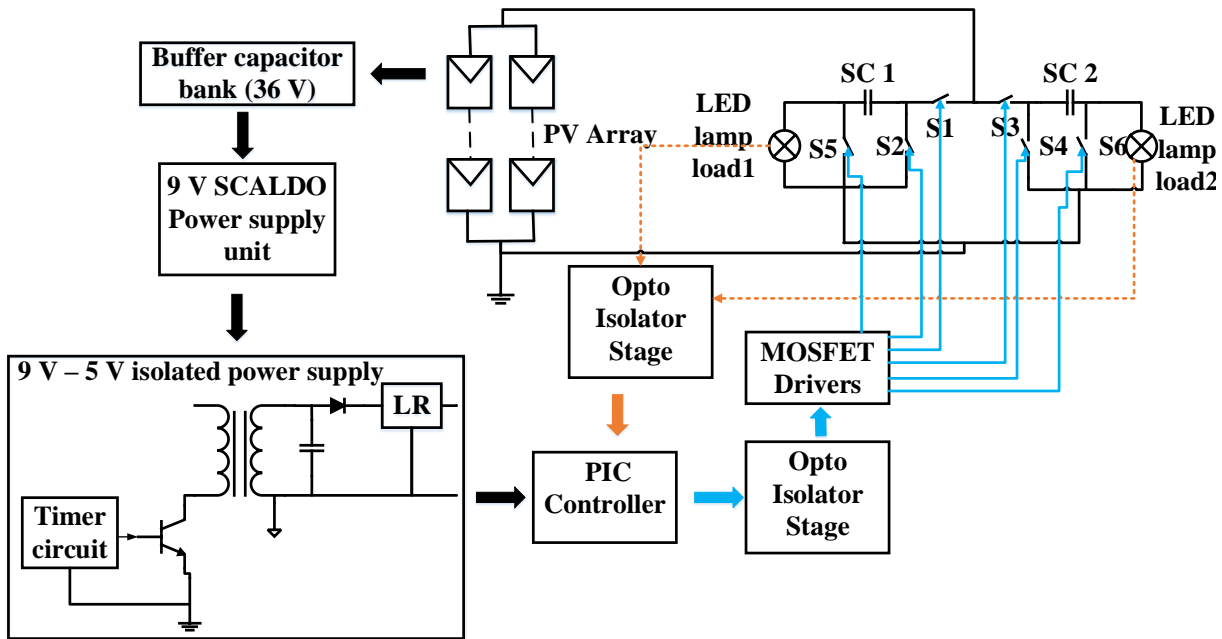


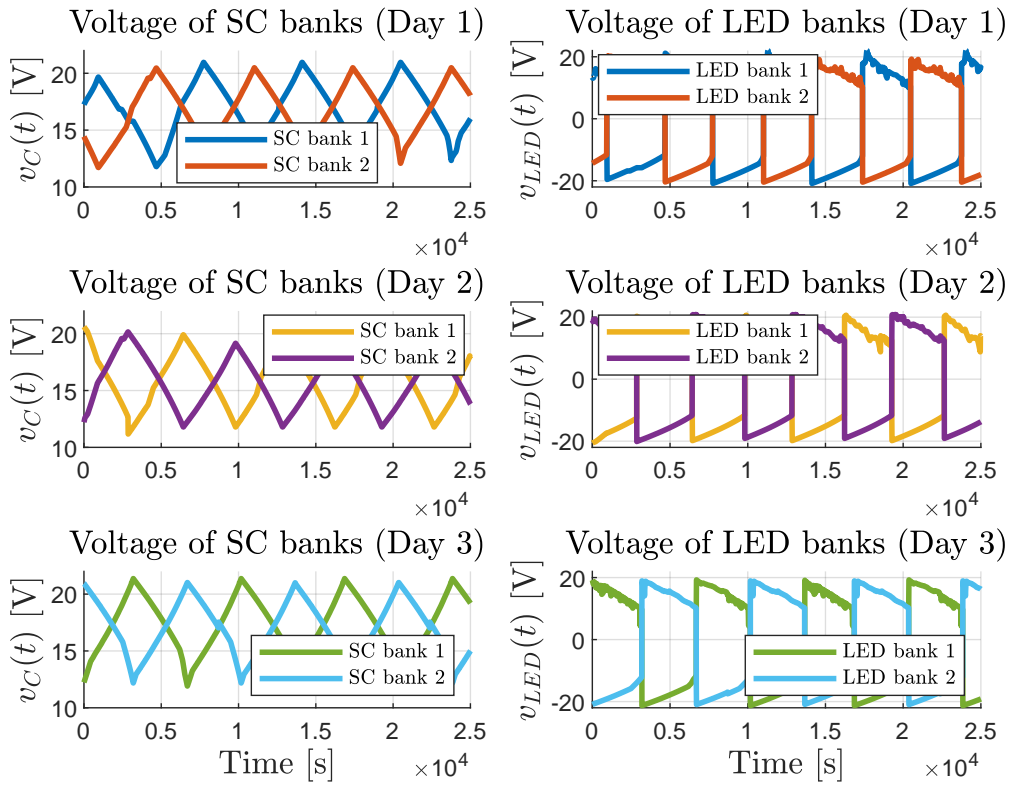
Figure 5.24: Simplified block diagram of implemented SCALED converter

Table 5.4: Summary of components used for SCALED converter

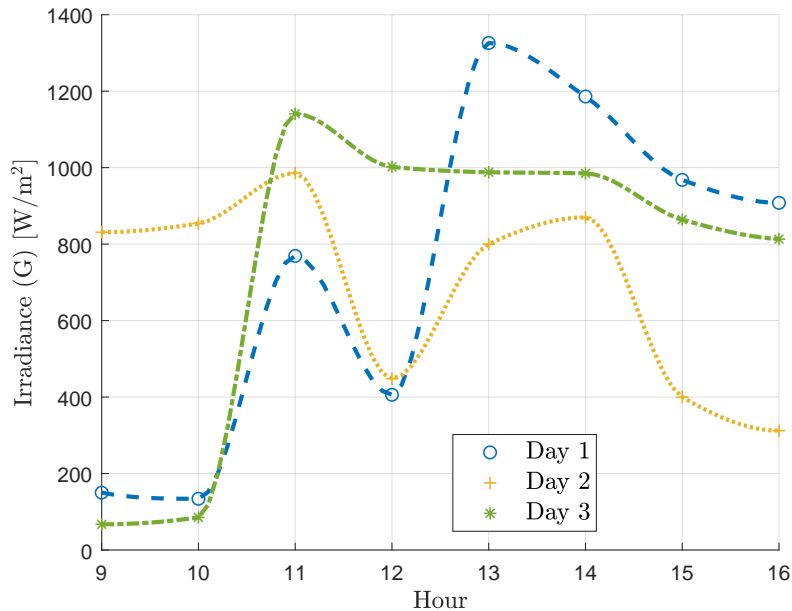
Component	Specification
Supercapacitors	Two 166 F, 51.3 V LSMtron supercapacitor module, 10 Nos of 10 F, 3 V single cell supercapacitors
Switches	PMOS - IRF4905, IXTH20P50P NMOS - IRFB7434 and IRFP4332 PVN102 photovoltaic relay
LED lamps	12 V, 5.5 W PHILIPS LED lamps
Micro-controller	PIC16F684
MOSFET driver	IRS4427
Opto-isolator	4N25
Timer IC	LM555
Regulators	LM338, LM7805
Transformer	1 : 1 toroidal transformer (custom design)

744 Wm^{-2} is shown in Figure 5.25. Figure 5.25(a) shows the voltage across two SC banks and two LED banks. 11 W LED lamp loads (2 LED lamps) were used on both sides of the converter. Irradiance variations throughout the day (from 0900 to 1600 h) were recorded using an irradiance meter and are shown in Fig. 5.25(b).

The ETEE of the overall system was calculated using Eq. 5.22, which was discussed earlier in this chapter. Using this proposed system, it is possible to achieve higher ETEE levels, in the range of 90% to 94%. It is important to highlight here that the above range of efficiencies were achieved without using any MPPT controllers, since the impedance matching required in MPPT is not practicable in this case, due to the SC banks being used for temporary energy storage. Figure 5.25, shows that this configuration is capable of buffering against irradiance fluctuations. This is because LED lamps can be operated across a wide range of positive and negative voltages without degrading the brightness, with the SC banks acting as energy buffers to smooth out irradiance fluctuations. In addition, this technique provides short-term DC-UPS capability in case of a sudden power loss. During testing, it was established that the switching



(a)



(b)

Figure 5.25: Operational behaviour of SCALED converter installed in POAL DC microgrid container: (a) Supercapacitor and LED bank voltages vs time for SCALED converter; (b) Variation of irradiance throughout the day in POAL site

frequency of the converter was well below 1 Hz for small loads. This frequency increases with the size of the LED lamp load. Results obtained from this testing are summarized in Table 5.5.

Table 5.5: Summary of experimental results of SCALED converter

Parameter	Specification
Operating voltage range of SC banks (LED bank)	20 – 12 V
Switching losses (for one cycle)	254 mW
E _{TEE}	90% ~ 94 %
Switching frequency	0.15×10^{-3} Hz
Switching period	≈ 2 hours
Autonomy time (depends on the lamp load)	15 to 30 minutes

The SCALED converter is applicable for large LED lighting loads such as 24 V, 48 V or over 100 V cases. Fluctuations in solar irradiance can be effectively accommodated by appropriate sizing of the SC banks.

5.5 Loss estimation of SCALED implementation

Minimizing the loss in a circuit is very import to increase the overall efficiency. By using supercapacitors as an energy storage device as well as the lossless droppers in the series path and reusing the energy stored in the supercapacitors, combined with commercially available LED lamps, the SCALED converter can be designed with high end-to-end efficiencies. Though the use of supercapacitors combined with LED lamps in the SCALED technique is simple enough to appreciate, it has several implementation issues. Some of the main loss contributors and implementation issues are:

1. ESR and leakage current losses in the supercapacitors
2. Losses due to switches
3. Losses of the parasitics in the circuit
4. Control circuit energy consumption

It is important to note that, minimizing losses requires both a substantial amount of design and construction effort. A poor circuit layout can undo an excellent design, and vice versa.

5.5.1 Equivalent series resistance (ESR) and leakage current losses in the supercapacitors

In this technique, SC banks are charged and discharged at the DC current equal to the LED lamp load current. Therefore, there will be an ohmic loss in the SC banks due to the DC ESR of the supercapacitors. However, the DC ESR is in the range of less than 100 m Ω [33,52] and these losses can be minimised. If the voltage drop across the supercapacitor ESR is high, this can push the voltage across the LED bank to drop below V_{LED}^{\min} causing the controller to switch between phases before the SC bank has charged or discharged to acceptable voltage levels. Therefore, selecting SC banks with very low ESR is important to achieve the desired operation of the circuit.

The SC banks used for this technique had an ESR of 5 m Ω , which will result in very much lower losses than typical MOSFET on-resistance, $R_{DS(on)}$ related loses. Therefore, the SC banks used in the topology were near-ideal voltage droppers with low ESR related losses.

Since modern supercapacitor families have very low leakage currents, in the range of 5 to 50 μA compared to their high charge/discharge currents, losses related to leakage currents can be neglected [33, 104]. At room temperature, the rule of thumb for leakage current in supercapacitors is 1 $\mu\text{A}/\text{F}$ [104].

5.5.2 Losses due to switches

Similar to supercapacitor ESR, the dissipation across $R_{\text{DS(on)}}$ of the MOSFETs also contributes to making the voltage drop across LED bank lower, potentially creating false triggering of controller and jeopardizing the normal operation of the SCALED. MOSFETs with 20 m Ω on-resistance were used as the switches in these prototypes.

Since the SCALED technique works in the range of mHz to Hz frequencies (this can change depending on the LED lamp load connected), dynamic losses are significantly low, without any RFI/EMI issues.

5.5.3 Losses of the parasitics in the circuit

In a PCB design, copper traces and the conducting materials of the components can have considerable resistance. According to Ref. [105], a 0.25 mm (10 mil) wide copper trace has a resistance/length of about 19 m Ω/cm (48 m Ω/inch). Similar to supercapacitor ESRs and switch on-resistances, dissipation across these resistances creates additional loss terms. In designing more compact PCBs with shorter PCB traces, the effect of these parasitics can be minimised. The data is shown Table. 5.6 shows four most commonly used copper weights and the resistivity at 25 $^{\circ}\text{C}$ and 100 $^{\circ}\text{C}$. During the PCB design, it was decided to use 2 oz Cu tracks (due to budget limitations) and maintain the voltage drop caused by these parasitics at a very low level around ≤ 10 mV. Depending on this, the track width and length were calculated for each PCB track.

Table 5.6: Copper resistance versus copper weight [106]

Cu weight [oz.]	Thickness [mm]	m Ω /square at 25 $^{\circ}\text{C}$	m Ω /square at 100 $^{\circ}\text{C}$
0.5	0.02	1	1.3
1	0.04	0.5	0.65
2	0.07	0.25	0.36
4	0.13	0.13	0.18

5.5.4 Control circuit power consumption

In the SCALED design, a PIC micro-controller was used to drive the MOSFET switches. Typically, a current around 60 mA was consumed by the micro-controller and powered by a 5 V power supply. In order to build this 5 V power supply combination of SCALDO and switch-mode DC-DC converter techniques were used. The power consumption of the control circuit was around 2 – 3 W, which is fairly significant, but, due to the limited budget and time-frame of the research, a PIC micro-controller-based control circuit was the most economical solution available. However, in future SCALED designs, measures could be taken to maintain the control

circuit power consumption at a bare minimum. Therefore, in our present analysis, the power consumption of the control circuit was not considered.

In order to analyse and estimate the energy losses in SCALED converter due to switch resistance, ESR on SC banks and PCB parasitic during charging and discharging phases the following analysis was done. More details on this are provided in Chapter 6.

The total power loss at a given instance in the charging phase can be estimated using the LED lamp current i_{LED} as;

$$P_{\text{ch}} = i_{\text{LED}}^2 (r_{\text{C}} + r_{\text{DS(on)}} + r_{\text{P}}) \quad (5.23)$$

where r_{C} is the ESR of SC bank, $r_{\text{DS(on)}}$ is the on resistance of the switch and r_{P} is the parasitic path resistance.

The corresponding energy loss can be found as;

$$E_{\text{ch}} = \int_0^{t_{\text{ch}}} i_{\text{LED}}^2 (r_{\text{C}} + r_{\text{DS(on)}} + r_{\text{P}}) dt \quad (5.24)$$

The same Eq.5.24 can be used to estimate the energy loss in SC discharging phase.

The above equations were added to the MATLAB-based analytical solutions developed for the SCALED converter in Chapter 6 to compute the energy losses for 2 main phases in the SCALED cycle. The numerical integration was done by using **trapz(X, Y)** function in MATLAB, which computes the integral of X with respect to Y using a trapezoidal method. Table 5.7 shows the energy and power losses in two phases for LED lamp loads ranging from 5.5 to 22 W in steps of 5.5 W obtained using this analytical solution. The corresponding power losses can be calculated using the following equation.

$$\text{Power loss} = \frac{\text{Energy loss}}{\text{Phase time period}} \quad (5.25)$$

It should be noted that when one SC bank charges through an LED lamp load, other SC bank discharges to the remaining LED lamp load. Therefore, the total energy loss in SCALED during the charging phase of one SC bank is the sum of the losses in the charging and discharging loops.

Table 5.7: Theoretical estimation of power/energy losses for SCALED converter

Parameter	LED lamp load in one side [W]	5.5	11	16.5	22
	Number of lamps used in each side	1	2	3	4
	Phase time [s]	4474	2233	1486	1113
SC1 charging,	Energy loss [J] (Phase 1)	87	175	264	356
SC2 discharging	Power loss [mW] (Phase 1)	19	78	164	320
SC1 discharging,	Energy loss [J] (Phase 2)	87	175	264	356
SC2 charging	Power loss [mW] (Phase 2)	19	78	164	320
Total resistive power loss in one cycle [mW]		38	156	328	640

Table 5.7 shows the estimation of the resistive power dissipation of the individual phases of SCALED design due to supercapacitor ESR, the on-resistance of switches and the parasitics of PCB traces. The total resistive loss in one cycle was estimated by using the power losses

in individual phases. It should be noted here, charging of SC bank from 12 V to 21 V and discharging back to 12 V was considered as one cycle.

5.6 SCALED loss measurement

The total power loss in the SCALED converter for one cycle was calculated by using the measured voltages and currents. A MATLAB code was used to calculate the resistive loss from the measured data. In this case, power loss in the control circuit board was neglected. During the estimations, only the power loss in the supercapacitors, switches and parasitics were taken into account. However, when field testing was performed at the POAL site, the overall system was connected to the PV panels using wires that introduced additional losses into the overall circuit. Therefore, the discrepancy between the two traces in Figure 5.26 is mainly accounted by the power losses in the connectors. Furthermore, the resistance of the wires used to connect LED lamps was also a loss element during the field testing.

Table 5.8: Measured power losses for SCALED converter

LED lamp load in one side [W]	5.5	11	16.5	22
Number of lamps used in each side	1	2	3	4
Total power loss for one cycle [mW]	102	254	497	916

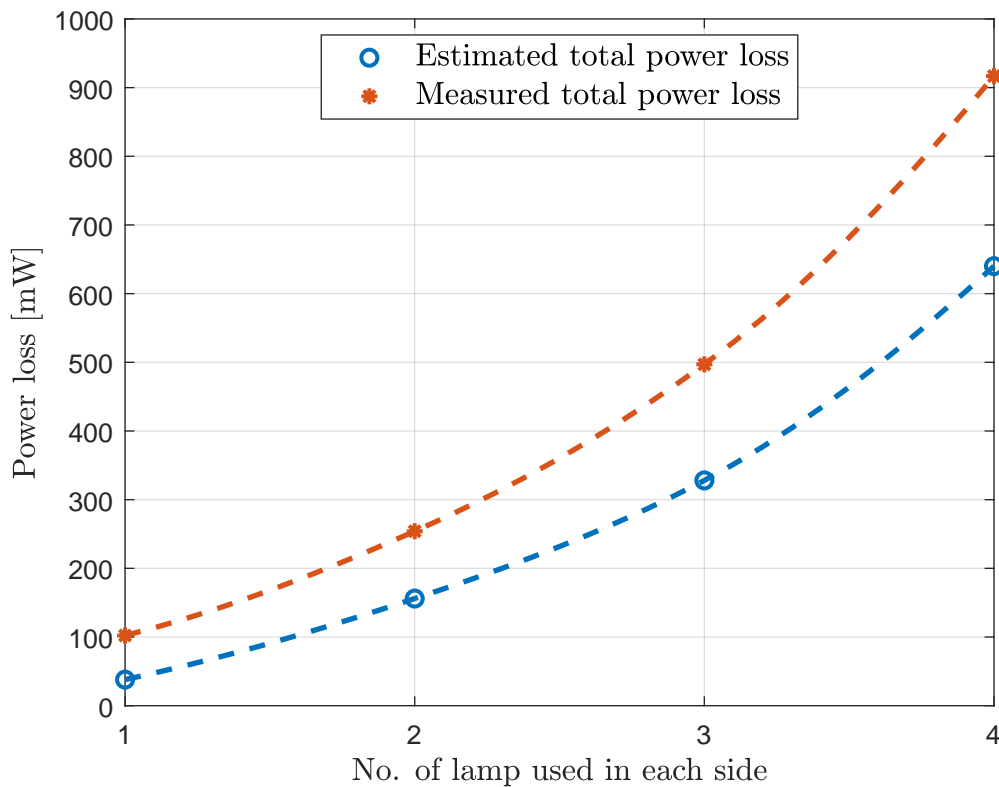


Figure 5.26: Comparison of measured and estimated power losses of the SCALED prototype

It can be observed that when the number of lamps increases, the power loss increases. Within the limited time and budget, this design was performed to keep the losses to a bare minimum

level while achieving the expected operation and efficiency. However, in future, with further improvement to the circuit, it will be possible to reduce these losses further.

5.7 Efficiency comparison

Figure 5.27 compares the two possibilities for demonstrating the efficiency advantage of the SCALED converter. If a battery pack is replaced by a pre-charged SC bank, for efficiency we have the case of the lower graph in Figure 5.27, whereas by inserting an LED lamp load into the loop while charging the SC bank it is possible to achieve a significant efficiency gain, as demonstrated in Chapter 3 and the upper graph in Figure 5.27. This is because SC banks are charged with a series LED lamp load (acting as the useful R_L load in RC charging loop), using most of the “wasted” energy in the RC charging loop. Also, in this technique, the SC banks are not fully discharged and the PV panel always charges a pre-charged capacitor, which also leads to higher efficiency.

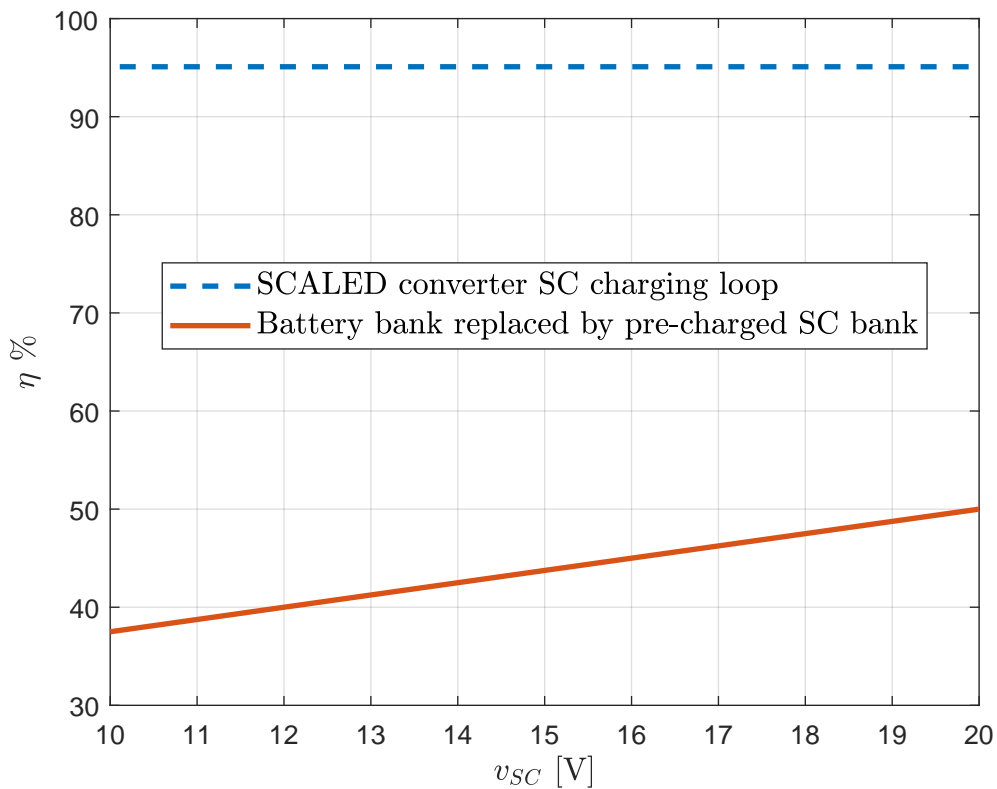


Figure 5.27: Comparison of charging efficiency between direct SC bank replacing battery pack and SCALED converter

This comparison showed that the proposed SCALED converter can achieve higher efficiency levels than direct replacement of a battery bank with a supercapacitor bank.

5.8 SCALED Advantages

By combining the unique properties of commercially available LED lamps with supercapacitor banks, a novel loss-circumventing SCALED converter for DC lighting in buildings was developed. In summary, the main features and advantages of this novel converter are:

- Higher ETEE with SC banks acting as lossless droppers
- No high-frequency DC-DC converters required thus eliminating RFI/EMI issues
- Short term DC-UPS capability for irradiance fluctuations, by over-sizing the SC banks, thus eliminating the need for battery banks

Compared with the high-frequency switching converters coupled with a complex processor algorithm to achieve MPPT in a battery-based system to achieve an ETEE of around 90% [39,107–113], the SCALED technique is able to achieve efficiencies in the range of 90% to 94%, while maintaining the switching frequency in an extra-low range, from a few Hz to fractional Hz.

5.9 Chapter Summary

The design and experimental details of a SCALED converter that can be used in DC microgrid environments are given in this chapter. According to the efficiency calculation done using the experimental data taken from prototypes, the SCALED technique is capable of achieving high end-to-end efficiency in the range of 90% to 94%, which is significantly higher than corresponding efficiencies in battery-based systems.

The next chapter presents the essential theory of supercapacitor energy circulation in a SCALED converter, with analytical and simulation results and discusses the reasons why existing maximum power point tracking techniques are not applicable for supercapacitors.

Theoretical foundation, analysis and simulation of the SCALED converter

This chapter presents an analysis of the charging and discharging phases of the SCALED circuit under the more realistic assumption that the solar panels operate in the non-constant current region, modelled as a constant DC voltage source with a series internal resistance.

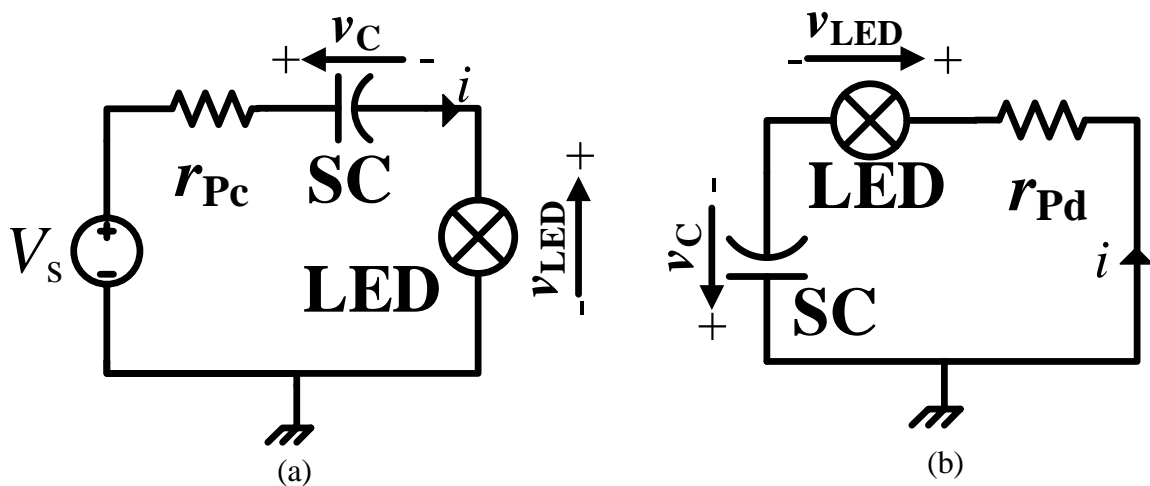


Figure 6.1: Basic configurations of the SCALED converter: (a) SC charging phase; (b) SC discharging phase

This converter has two main configurations as shown in Fig. 6.1, and is based on the fact that LED lamps are capable of operating with both positive and negative rails. Analysis of the charging phase and the discharging phase of the SCALED converter is presented below.

6.1 Analysis of the charging phase of a SCALED converter

The simplified version of the SCALED charging phase is depicted in Figure 6.1(a). The parasitic resistance r_{Pc} , includes the internal resistance of the supply source, the ESR of the capacitor and the path resistance. The analysis of the charging loop was performed for two cases: zero and non-zero r_{Pc} .

6.1.1 Case A: Neglecting parasitic resistance r_{PC}

In this case, the supply was considered as an ideal constant voltage source with voltage V_S and the path resistance and the ESR of the capacitor were ignored. Since the power consumption of the LED lamp load P_0 is approximately constant over the constant brightness region (as discussed in Chapter 4 and 5), the voltage across the LED lamp is:

$$v_{LED} = \frac{P_0}{i} \quad (6.1)$$

where the second equality follows from Kirchoff's voltage law (KVL) as;

$$v_{LED} = V_S - v_C \quad (6.2)$$

and the loop current of the circuit given by:

$$i = C \cdot \frac{dv_C}{dt} \quad (6.3)$$

Using equations 6.1, 6.2 and 6.3 the general expression for the charging phase can be obtained as:

$$(V_S - v_C) \frac{dv_C}{dt} = \frac{P_0}{C} \quad (6.4)$$

Since Eq. 6.4 is a non-linear differential equation the we derived both analytical solutions and numerical solutions for capacitor voltage v_C . The Euler method was used to derive the numerical solution. Integrating Eq. 6.4:

$$\int_0^{v_C(t)} (V_S - v_C) dv_C = \int_0^t \frac{P_0}{C} dt \quad (6.5)$$

leads to

$$\left(V_S - \frac{v_C(t)}{2}\right) \cdot v_C(t) = \frac{P_0}{C} t + K \quad (6.6)$$

a quadratic equation in $v_C(t)$ with the solution,

$$v_C(t) = V_S - \sqrt{V_S^2 - \frac{2 \cdot P_0}{C} t - 2K} \quad (6.7)$$

to satisfy the initial conditions with the condition that

$$V_S^2 \geq 2 \cdot \left(\frac{P_0}{C} t + K\right) \quad (6.8)$$

Here K is a constant whose value can be found by substituting the initial conditions into equation 6.6. It was found that the charging time for the capacitor to reach the supply voltage V_S was:

$$t_{\text{charging}} = \frac{C}{2 \cdot P_0} (V_S - v_C(0))^2 \quad (6.9)$$

6.1.2 Case B: Including parasitic resistance r_{Pc}

In this case, a practical voltage source having finite internal resistance r_S was considered as the supply source to the SCALED circuit. When the effect of parasitic resistance is accounted for, Eq. 6.4 is modified as:

$$\left(V_S - v_C - r_{Pc} \cdot C \frac{dv_C}{dt} \right) \frac{dv_C}{dt} = \frac{P_0}{C} \quad (6.10)$$

Solving Eq. 6.10 for $\frac{dv_C}{dt}$, we obtain a differential equation that can be evaluated using the Euler method:

$$\frac{dv_C}{dt} = \frac{(V_S - v_C) - \sqrt{(V_S - v_C)^2 - 4 \cdot r_{Pc} \cdot P_0}}{2 \cdot r_{Pc} \cdot C} \quad (6.11)$$

6.2 Analysis of the discharging phase of a SCALED converter

During the discharging phase of the SCALED topology the pre-charged supercapacitor bank is discharged to the LED lamp load. The simplified version of the SCALED discharging phase is depicted in Figure 6.1(b). The parasitic resistance r_{Pd} , includes both path resistance and the ESR of the capacitor.

Case C: Neglecting the effect of parasitic resistance r_{Pd}

To simplify the analysis the effect of the parasitic resistance r_{Pd} is neglected. Applying Ohm's law to Figure 6.1(b), we can derive an expression for capacitor voltage v_C in terms of capacitance C and power of the LED lamp load P_0 as follows:

$$v_C \frac{dv_C}{dt} = -\frac{P_0}{C} \quad (6.12)$$

which integrates to:

$$\frac{v_C(t)^2}{2} = -\frac{P_0}{C}t + K' \quad (6.13)$$

where the value of K' can be found by substituting initial conditions. Hence

$$v_C(t) = \sqrt{2K' - \frac{2 \cdot P_0}{C}t} \quad (6.14)$$

with the condition

$$K' \geq \frac{P_0}{C}t \quad (6.15)$$

By using Eq. 6.15 and substituting the initial conditions in Eq. 6.13 the time taken to fully discharge the capacitor is:

$$t_{\text{discharging}} = \frac{C}{2 \cdot P_0} v_C(0)^2 \quad (6.16)$$

Case D: Including parasitic resistance r_{Pd}

When the effect of parasitic resistance is taken into account, Eq. 6.12 becomes:

$$\left(v_C + C \frac{dv_C}{dt} \right) \frac{dv_C}{dt} = -\frac{P_0}{C} \quad (6.17)$$

which can be rewritten as:

$$\frac{dv_C}{dt} = \frac{-v_C + \sqrt{v_C^2 - 4r_{Pd}P_0}}{2r_{Pd}C} \quad (6.18)$$

and solved numerically.

Euler numerical integration of equations 6.7,6.9,6.11, 6.14, 6.16 and 6.18 was carried out using MATLAB. Table 6.1 shows the component values and initial conditions used for these simulations. Simulation results are depicted in Figures 6.2 and 6.3. All the MATLAB script files used for these analyses are provided in Appendix B.

Table 6.1: Component data used for MATLAB simulations

Parameter	Value
Capacitor	166 F, 51.3V
LED lamp	12 V, 5.5 W
Parasitic resistance r_{Pc} (for charging)	0 Ω to 2 Ω
Parasitic resistance r_{Pd} (for discharging)	0 Ω to 2 Ω
Initial voltage of SC bank $v_C(0)$ (for charging)	12 V
Initial voltage of SC bank $v_C(0)$ (for discharging)	20 V
Supply voltage V_S	32 V DC

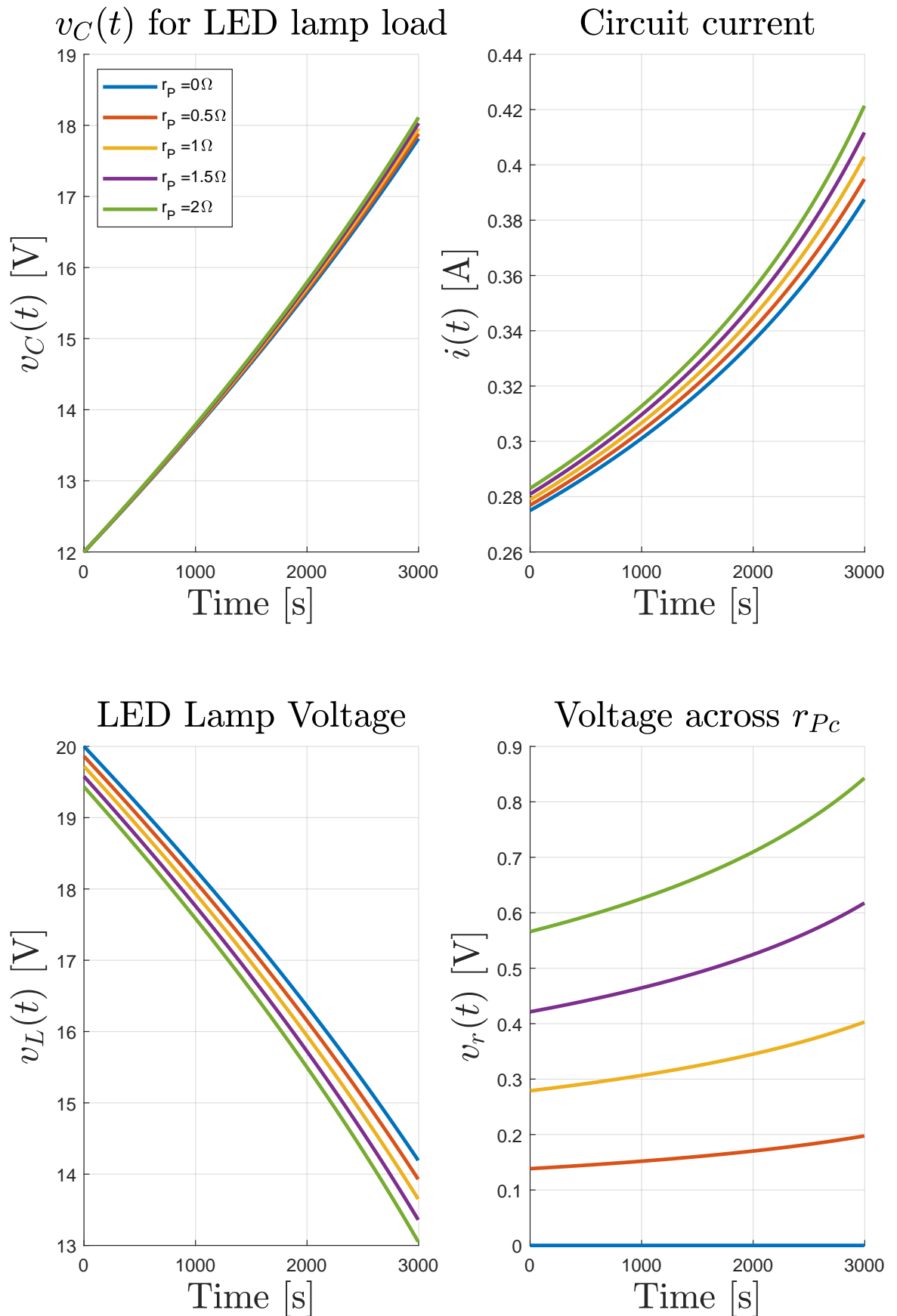


Figure 6.2: Simulation results for the charging phase of a SCALED converter

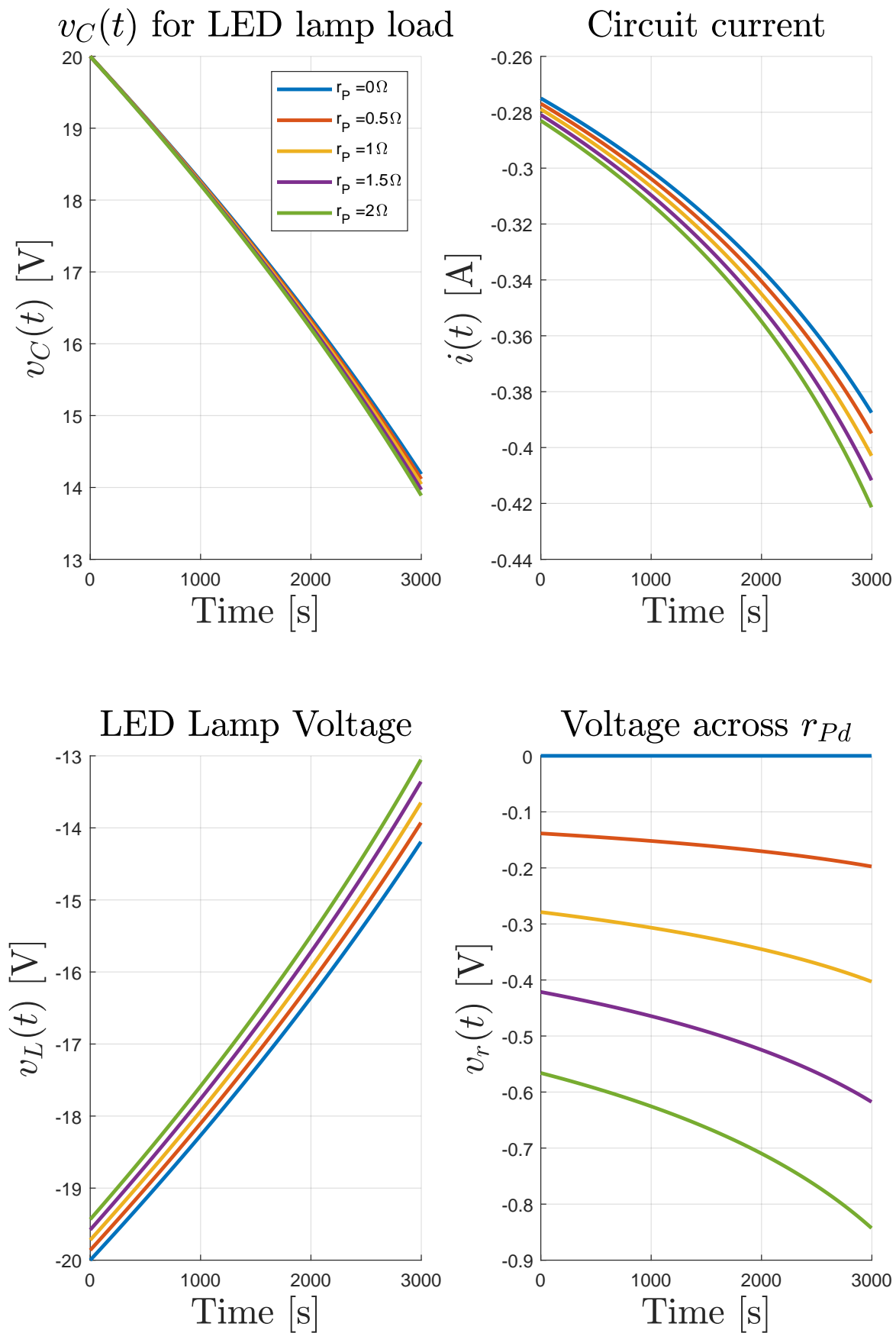


Figure 6.3: Simulation results for the discharging phase of a SCALED converter

6.3 Simulation of SCALED converter

After analysing the charging and discharging phases separately, the switching sequences of the SCALED converter discussed in Chapter 5 were used in MATLAB code (in Appendix B.7) for full simulation of the converter. The LTSpice simulation package was also used to verify the MATLAB and experimental results. The Spice Netlist for the circuit shown in Figure 6.4 was used during Spice simulations. More details about Netlisting are available in Appendix B.11. In the Spice simulation, a model for the PV panel was created using its characteristic equations as discussed in Chapter 1. LTSpice simulation data was imported to MATLAB and plotted in MATLAB.

Simulation results for the SCALED converter obtained from MATLAB and Spice are presented in Figure 6.5 respectively and later compared with the experimental results.

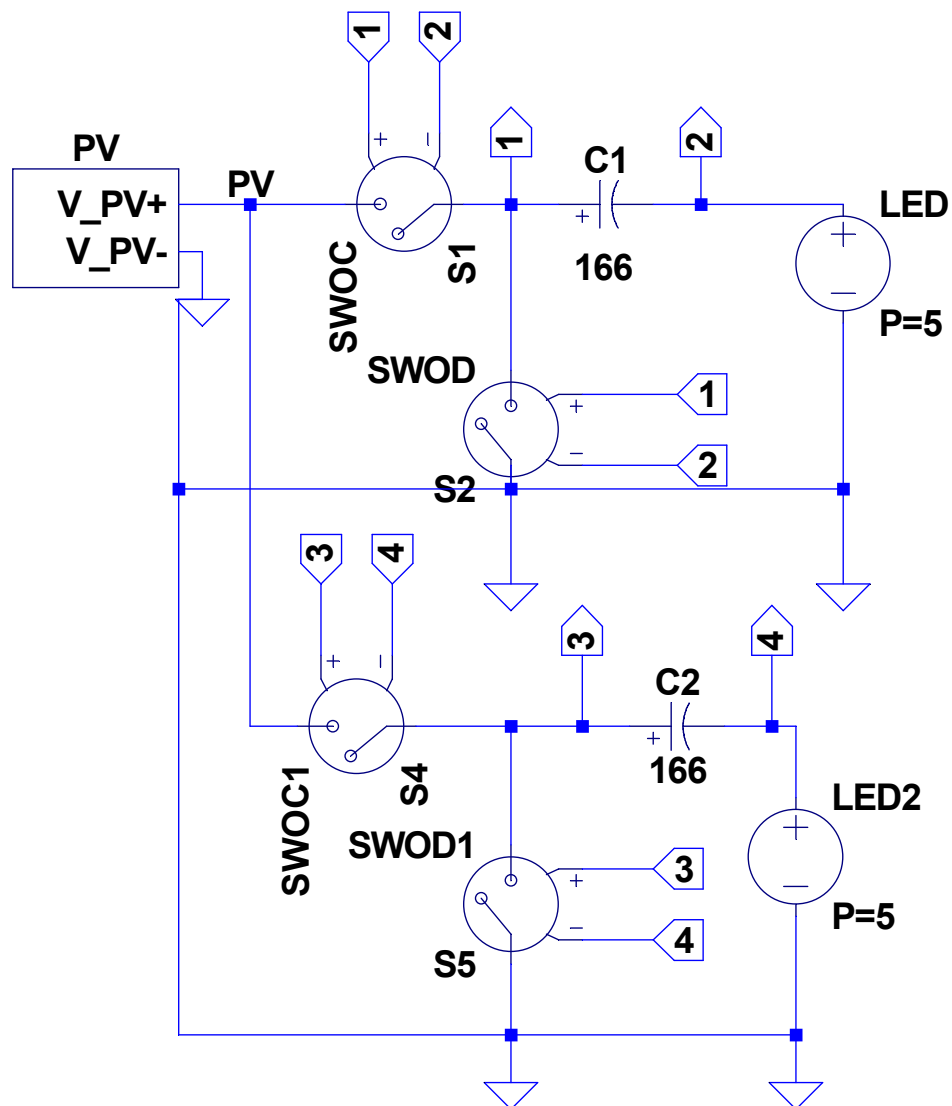


Figure 6.4: LTSpice model of SCALED converter used for simulation

By comparing the simulation results in Figure 6.5 with the experimental results in Chapter 5, it can be seen that both experimental and simulation results matched well with each other.

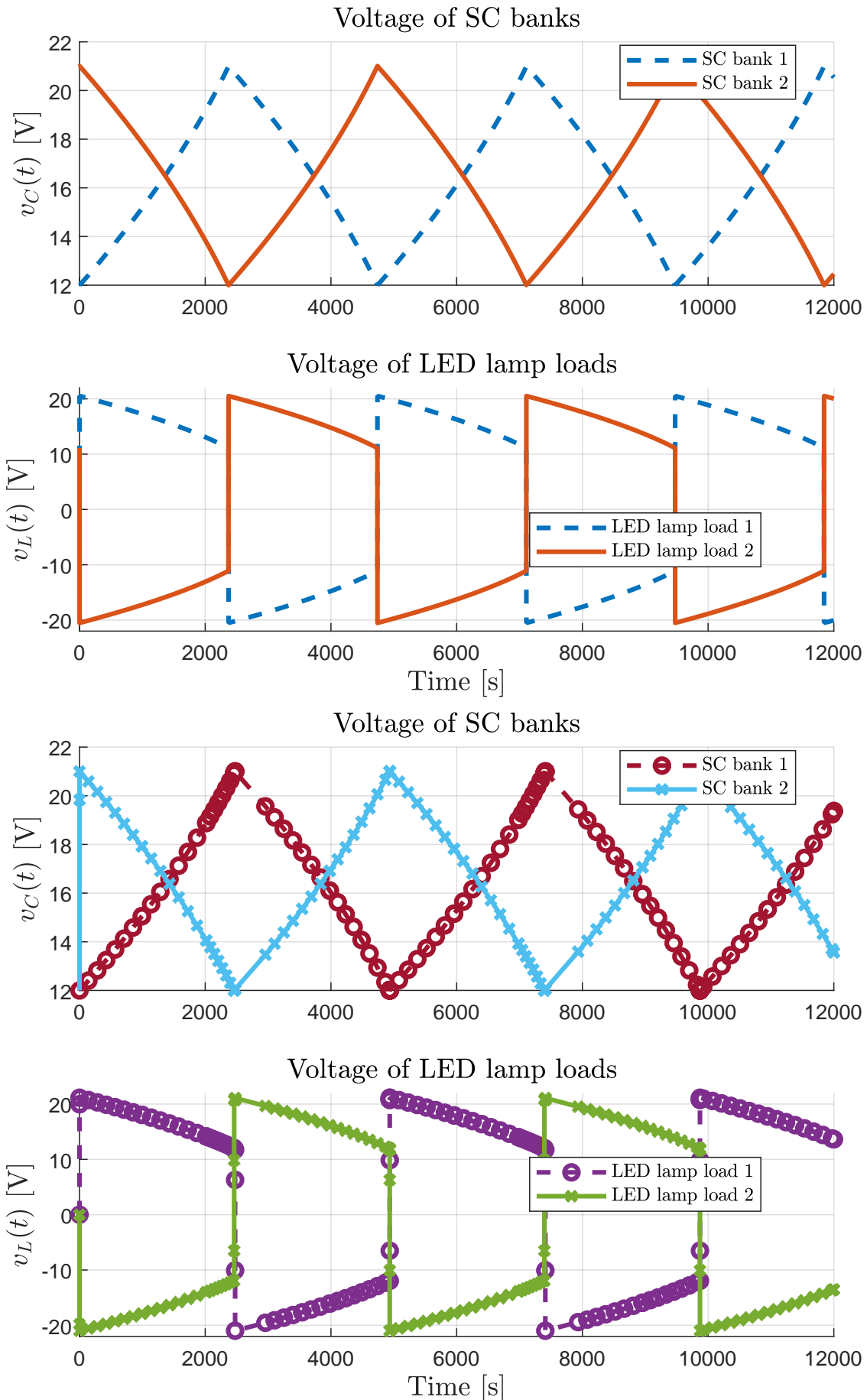


Figure 6.5: Simulation results for SCALED converter: (a) MATLAB simulation results; (b) Spice simulation results

6.4 Feasibility of replacing a battery pack with supercapacitors

The fluctuating nature of solar energy necessitates the use of suitable energy storage systems in solar-powered DC microgrids. Compared to typical battery banks, supercapacitors offer a longer cycle life, eliminating the need to replace them regularly. However, compared to a typical maximum power point tracking (MPPT) controller, where the battery bank and resistive load fed by a switch-mode DC-DC converter allows impedance matching for maximum power transfer, a supercapacitor bank's significantly large capacitive load does not permit the typical impedance matching for maximum power transfer. This section discusses this scenario.

6.4.1 Input impedance of switch mode DC-DC converters

A switch mode DC-DC converter, regardless of its topology, presents a negative incremental input impedance. A typical DC-DC converter as shown Figure 6.6 works to maintain a constant output voltage V_o , at an output power of P_o . For an ideal switch-mode DC-DC converter with 100% efficiency, the following valuable relationships can be easily established [114].

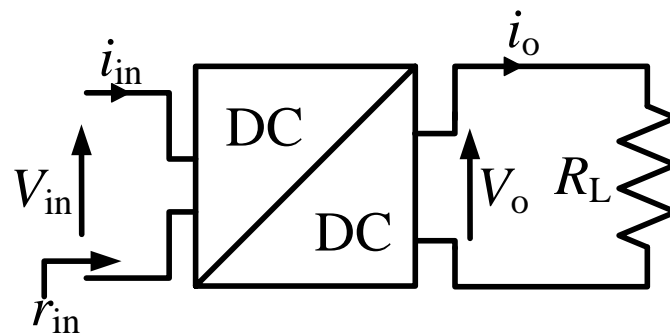


Figure 6.6: Block diagram of loaded switched mode DC-DC converter

The converter in continuous conduction mode (CCM) acts as a DC transformer with a turns ratio of n , which leads to the useful relationship

$$r_{in} = \frac{V_{in}}{i_{in}} = n^2 R_L \quad (6.19)$$

where R_L is the load resistance ($R_L = \frac{V_o}{i_o}$).

In accordance with Eq. 6.19 and Table 6.2 it is apparent that the input impedance of a switched mode DC-DC converter is a function of the duty cycle of the converter. Hence by varying D it is possible to vary the effective input impedance of the converter. This approach is used in MPPT controllers to match the PV array resistance with the load resistance. Figure 6.7 depicts the variation of input resistance with duty cycle ratio for the above converter types.

Table 6.2: Transformation coefficient n for switched mode converter (D is the duty ratio of the converter)

Converter Type	Transformation coefficient (n)
Buck converter	$1/D$
Boost converter	$1 - D$
Buck-boost converter	$(1 - D)/D$

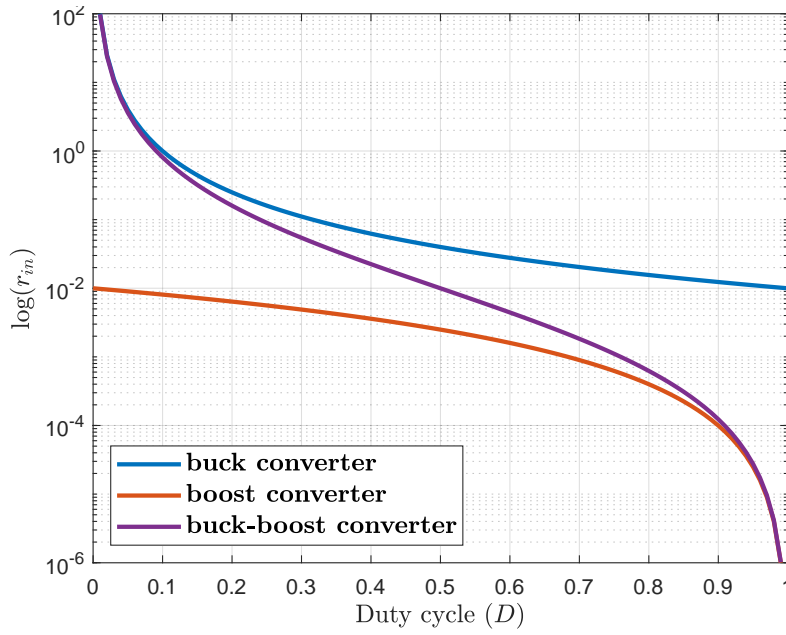


Figure 6.7: Variation of input resistance r_{in} of an ideal switching converter under CCM with duty cycle D

Battery connected to the output of the buck converter

With the aim of further exploring the variation in the input resistance of a switch mode DC-DC converter, the following analysis was carried out with both battery pack and capacitor bank connected at the output of the converter separately. For this analysis a buck converter was used as the DC-DC converter. This section analyses the situation shown in Figure 6.8, where a resistive load buffered by a battery pack is connected to the output of a buck converter.

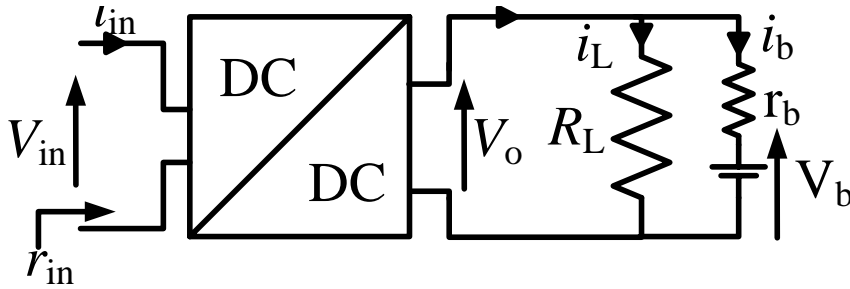


Figure 6.8: Buck converter with resistive load is buffered by a battery bank

By considering Figure 6.8, the Thevenin resistance of the combined battery and load is,

$$R_0 = \frac{R_L r_b}{R_L + r_b} \quad (6.20)$$

with r_b being the internal resistance of the battery. Therefore r_{in} can be modified as,

$$r_{in} = \frac{R_0}{D^2} = \frac{R_L r_b}{D^2 (R_L + r_b)} \quad (6.21)$$

showing that, r_{in} varies from $\infty \rightarrow R_0$ as D goes from 0 to 1. With variations in irradiance and temperature, the maximum power point (MPP) of the PV panel also changes. Hence, by varying

the duty cycle it is possible to match the load impedance with the PV module impedance to extract maximum power.

Capacitor connected to the output of the buck converter

With recent advances such as hybrid supercapacitors and CAPAbatteries offering higher energy densities, battery packs may be easily replaced by the higher life cycle-based supercapacitor banks, with the secondary advantage of a constant equivalent series reistance (ESR) irrespective of the depth of discharge. However, if a battery bank is replaced solely by a SC bank, existing maximum power point tracking (MPPT) schemes are not adaptable since the load becomes predominantly capacitive, compared to the case of a battery bank and resistive load which allows simple impedance matching based on the effective resistive load seen by the solar panel. The following analysis provides a summary of the two cases; parallel and series connection of the capacitor as depicted in Figure 6.9.

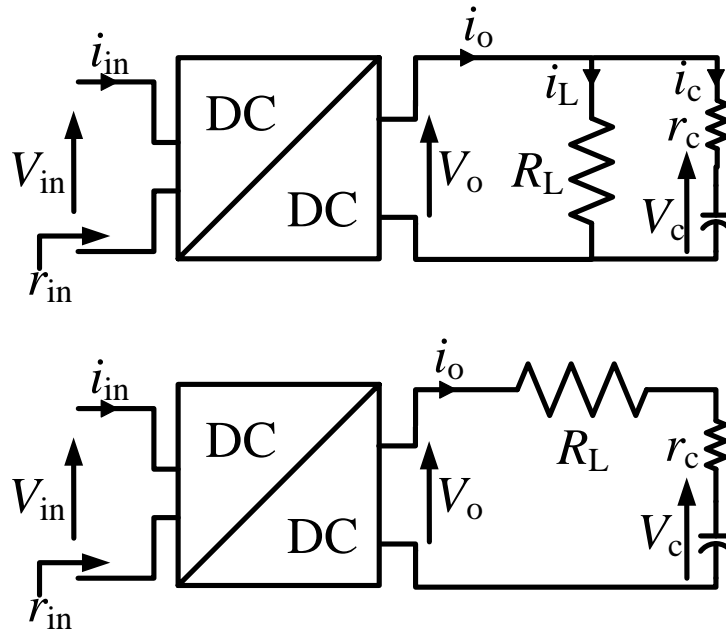


Figure 6.9: Buck converter with a capacitor at the output: (a) Parallel connection; (b) Series connection

(A) Parallel connection of the capacitor:

Considering Figure 6.9(a), where the load is buffered with a SC bank.

Using Ohm's law the output current i_0 can be derived as:

$$i_0 = i_c + i_L = \frac{V_0}{R_L r_c} \left(r_c + R_L e^{\frac{-t}{\tau}} \right) \quad (6.22)$$

where C is the capacitance and r_c is the ESR of the capacitor. The capacitor is assumed to start with zero initial voltage.

Using Eq. 6.22, the general expression for output resistance R_0 can be obtained as:

$$R_0 = \frac{R_L r_c}{r_c + R_L e^{\frac{-t}{\tau}}} \quad (6.23)$$

Accordingly, r_{in} of the buck converter will be:

$$r_{\text{in}} = \frac{R_L r_c}{D^2 \left(r_c + R_L e^{\frac{-t}{r_c C}} \right)} \quad (6.24)$$

From Eq. (6.24) it can be seen that, when $t = 0$ (initially) r_{in} of the DC-DC converter is $\frac{R_L r_c}{D^2 (R_L + r_c)}$, and as $t \rightarrow \infty$ input impedance r_{in} approaches R_L/D^2 .

(B) Series connection of the capacitor:

Considering Figure 6.9(b), i_0 can be derived as:

$$i_0 = \frac{V_0}{R_L + r_c} \exp(-t/(r_c + R_L)C) \quad (6.25)$$

We can therefore estimate the input resistance of the DC-DC converter r_{in} to be:

$$r_{\text{in}} = \frac{V_0}{D^2 i_0} = \frac{(R_L + r_c) \exp(t/(r_c + R_L)C)}{D^2} \quad (6.26)$$

When considering Eq. 6.26, it is clear that in the case of series connection, input impedance r_{in} varies from $(R_L + r_c)$ to ∞ as t goes from $0 \rightarrow \infty$.

Figure 6.10 illustrates the behaviour of the input impedance of the buck converter when an SC bank is used as the sole energy storage device (ESD) for both parallel and series connection.

The impedance of a PV panel varies significantly with the irradiance (G) and temperature (T). Since G and T are continuously varying in real-world conditions, the panel resistance is also changing continuously. Therefore, in order to transfer maximum power, the impedance of the connected load should also be varied continuously. When a battery bank is connected as the ESD in a PV system, this is achieved by continuously varying the duty ratio D of the DC-DC converter according to Eq. 6.21. In the case of a battery bank, the input impedance of the DC-DC converter is a function of the duty ratio D only.

Compared to the case of a battery bank resulting in an input resistance given by Eq. 6.21, a supercapacitor bank makes the input resistance of the converter dependent on the state of charge of the SC bank, which is also related to the time constant of the output circuit. This makes it extremely difficult to adapt existing MPPT schemes into SC-based ESD systems. This is clear from Eqs. 6.24 to 6.26.

If a capacitor with an initial charge (or initial voltage V_{Cin}) was used in the case of series connection, Eq.6.25 can restated as:

$$i_0 = \frac{V_0 - V_{\text{Cin}}}{R_L + r_c} \exp(-t/(r_c + R_L)C) \quad (6.27)$$

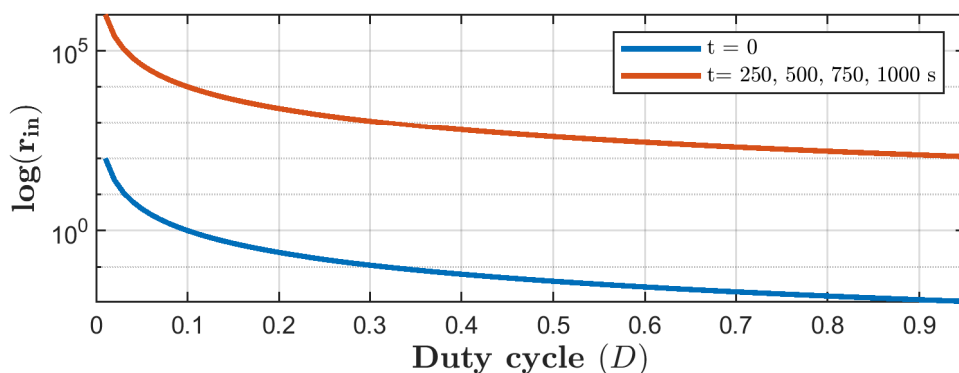
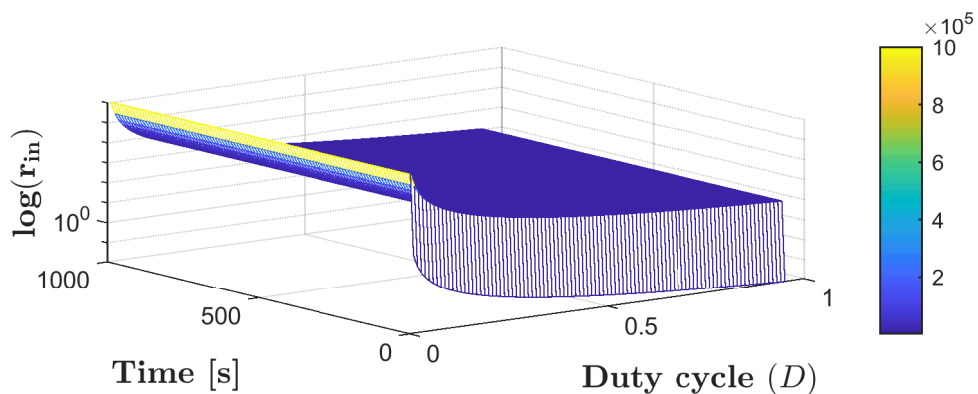
Defining $k = \frac{V_{\text{Cin}}}{V_0}$ where $0 \leq k \leq 1$, Eq. 6.27 becomes:

$$i_0 = \frac{V_0(1 - k)}{R_L + r_c} \exp(-t/(r_c + R_L)C) \quad (6.28)$$

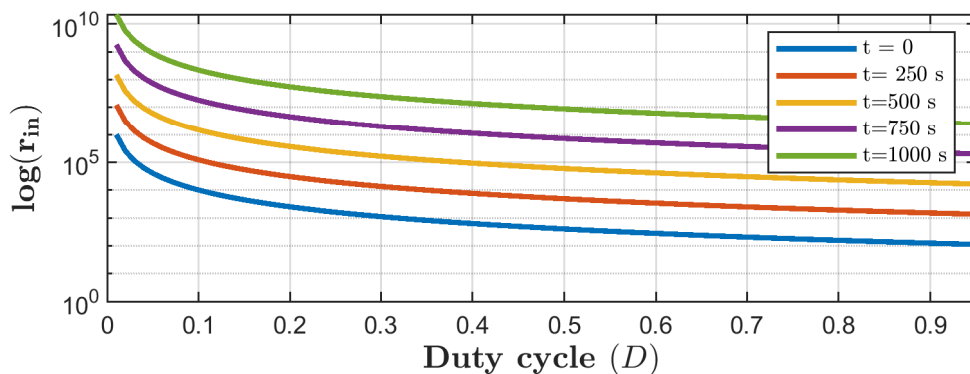
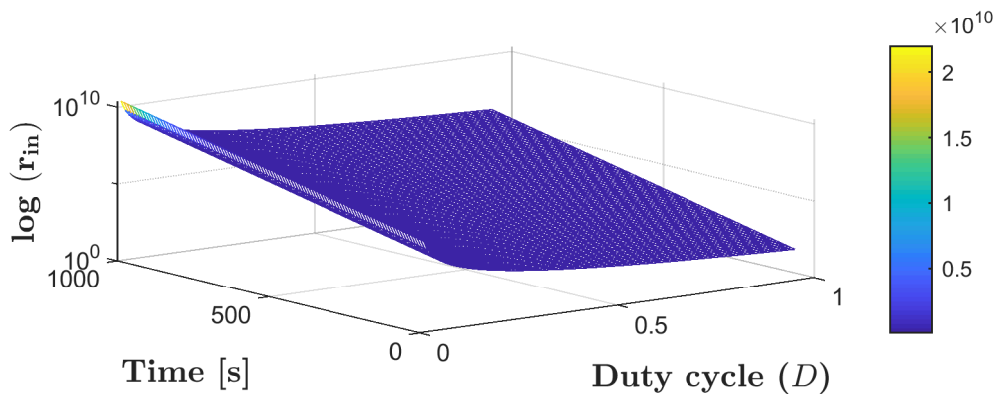
So, input impedance r_{in} can be rewritten as:

$$r_{\text{in}} = \frac{(R_L + r_c) \exp(t/(r_c + R_L)C)}{(1 - k)D^2} \quad (6.29)$$

Figure 6.11 depicts the variation of r_{in} of the buck converter considering Eq. 6.29, where $V_0 = 24$ V, $R_L = 100 \Omega$, $r_C = 0.01 \Omega$, $C = 1$ F and $V_{\text{Cin}} = 9$ V. Figure 6.11 also shows that, the input impedance of the converter also changes with the state of charge of the capacitor, making difficult to match the PV panel impedance with the r_{in} of the converter.



(a)



(b)

Figure 6.10: Variation of r_{in} for a buck converter with a capacitor at the output: (a) Parallel connection of capacitor; (b) Series connection of capacitor ($C = 1 \text{ F}$, $R_L = 100 \text{ } \Omega$, $r_c = 0.01 \text{ } \Omega$)

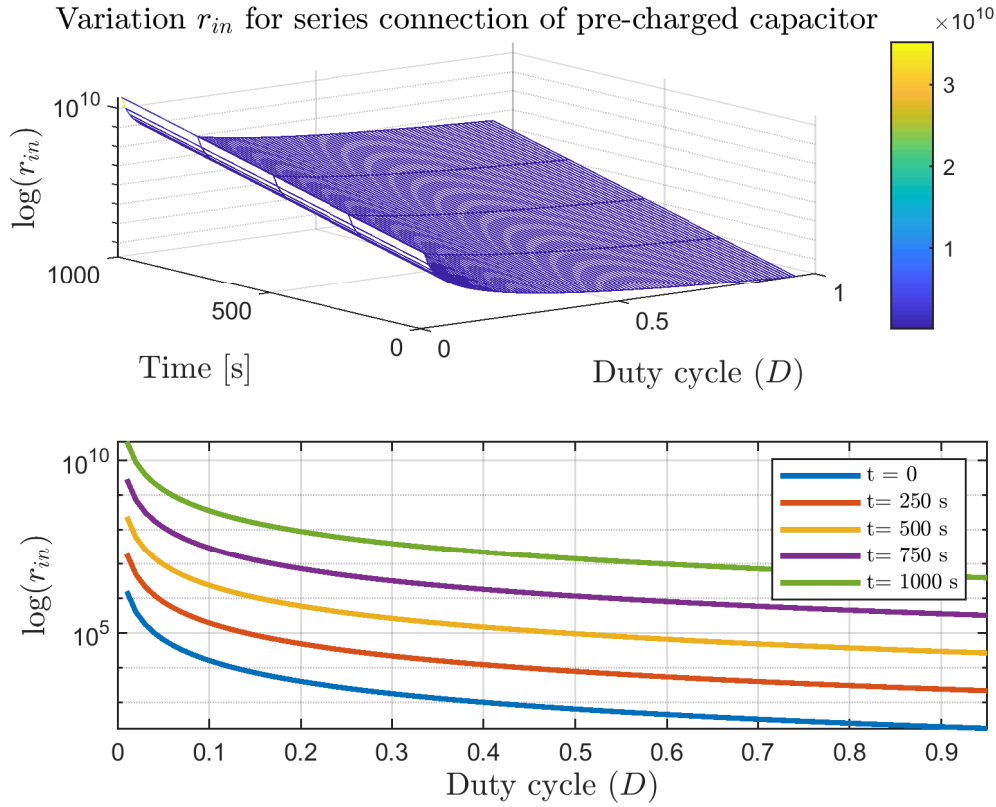


Figure 6.11: Series connection of pre-charged capacitor

Input Impedance of buck converter with SCALED converter connected at the output

The proposed SCALED converter will connect to the PV panel only during the charging phase of either SC1 or SC2. Throughout the discharging of SC's there is no connection with the PV panel. Therefore, it is possible to consider the case of series connection of the capacitor as shown in Figure 6.9 (b) where the capacitor is a supercapacitor and the load is an LED lamp bank. Since LED lamps operate as a constant power load in the range of 9 to 20 V, they cannot be treated as a load having a constant resistance. Eq. 6.29 will not provide acceptable values for r_{in} of the buck converter. For that reason the following analysis was carried out to determine the input impedance.

Since the power consumption of the LED lamp load P_0 is constant over the constant brightness region as discussed in Chapter 4, the voltage across the LED lamp load v_{LED} is:

$$v_{LED} = \frac{P_0}{i_0} \quad (6.30)$$

and the loop current of the circuit is given by:

$$i_0 = C \frac{dv_C}{dt} \quad (6.31)$$

Using Eq. 6.30 and Eq. 6.31 the general expression for the charging phase can be obtained as:

$$\left(V_0 - V_C(t) - r_c C \frac{dv_C}{dt} \right) \frac{dv_C}{dt} = \frac{P_0}{C} \quad (6.32)$$

Solving Eq. 6.32 for $\frac{dv_C}{dt}$, a differential equation was derived which can be evaluated numerically,

$$\frac{dv_C}{dt} = \frac{(V_0 - V_C(t)) - \sqrt{(V_0 - V_C(t))^2 - 4r_c P_0}}{2r_c C} \quad (6.33)$$

By using Eq. 6.30 and 6.31 the input impedance of the buck converter is obtained as:

$$r_{in} = \frac{2r_c V_0}{D^2 \left((V_0 - V_C(t)) - \sqrt{(V_0 - V_C(t))^2 - 4r_c P_0} \right)} \quad (6.34)$$

Euler numerical integration of Eq. 6.31, 6.33 and 6.34 was carried out using MATLAB. Table 6.3 shows the component values and initial conditions used for the simulations. Simulation results are depicted in Figure 6.12.

Table 6.3: Component data used for MATLAB simulations

Parameter	Value
Supercapacitor bank	166 F, 51.3V
LED lamp	12 V, 5 W
Parasitic resistance r_c (for charging)	0.1 Ω
Initial voltage of SC bank $V_C(0)$ (for charging)	9 V
Output voltage of Buck converter V_0	24 V DC

It is obvious from the results shown in Figure 6.12 and Eq. 6.26 that standard MPPT charge controllers cannot be used with the proposed SCALED converter. This is because the SC bank in a SCALED converter acts as a nearly ideal capacitor and the LED lamp load acts as a nearly constant power load. This will cause difficulty in achieving impedance matching between the PV module and load. The variation of current and impedance of the LED lamps with voltage in the range of 9 – 20 V is shown in Figure 6.13.

From Figure 6.13, we can see that the current drawn by the lamp increase with the reduction of the voltage across the LED lamp. LED lamp characteristics emphasize that, at the start of the charging phase of SC banks, the SCALED converter requires higher current than at the end which means that the buck converter sees a load with negative incremental impedance. Hence the behavioural characteristics of the SCALED converter directly depends on the characteristics of the LED lamp load connected.

Table 6.4 summarizes the input impedance of a DC-DC converter for each case discussed in this section. It is obvious that existing MPPT techniques are not adaptable to situations where an SC bank is used solely as the energy storage device for a PV system because capacitors store energy in their electrostatic fields, while in a battery, electrochemical reaction is related to the back electromotive force (EMF).

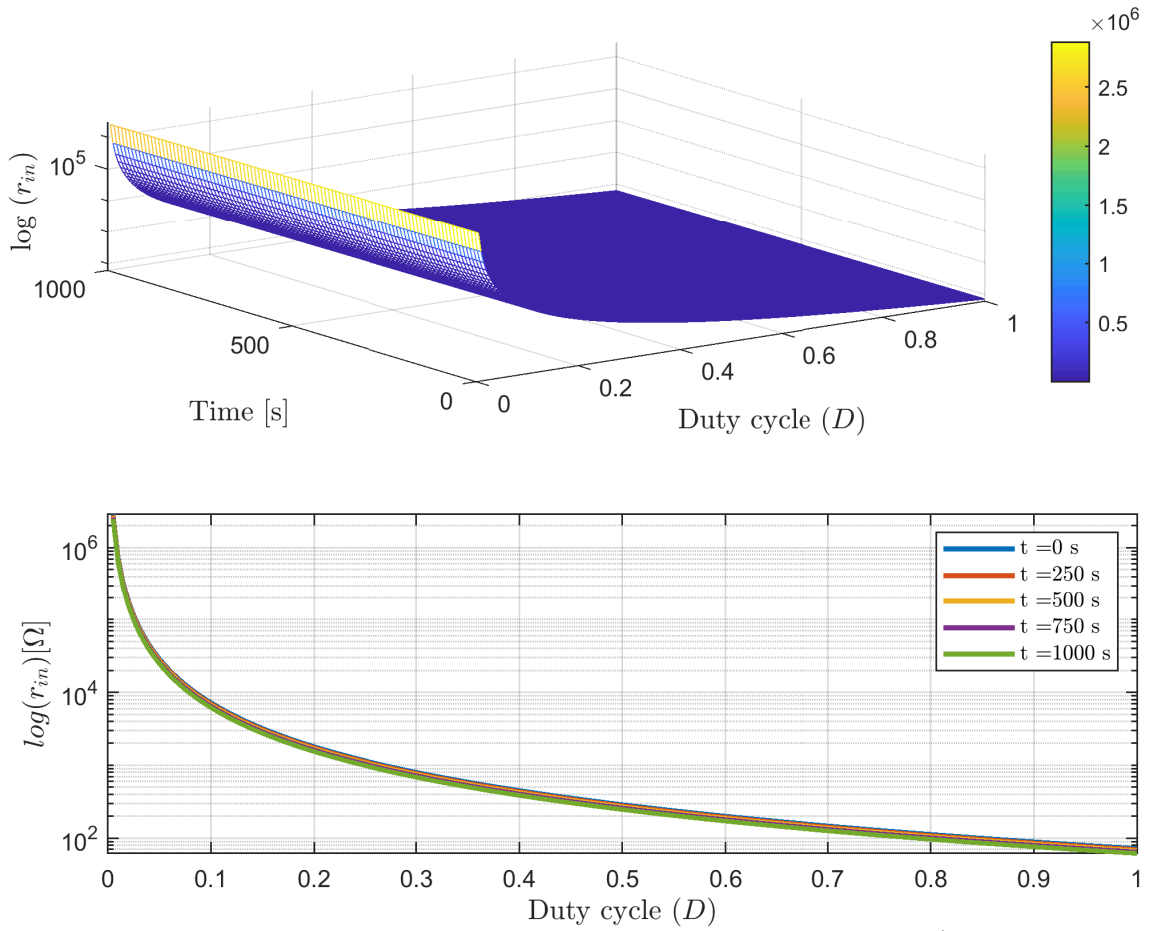


Figure 6.12: Variation in r_{in} for buck converter with SCALED converter (for different duty cycles)

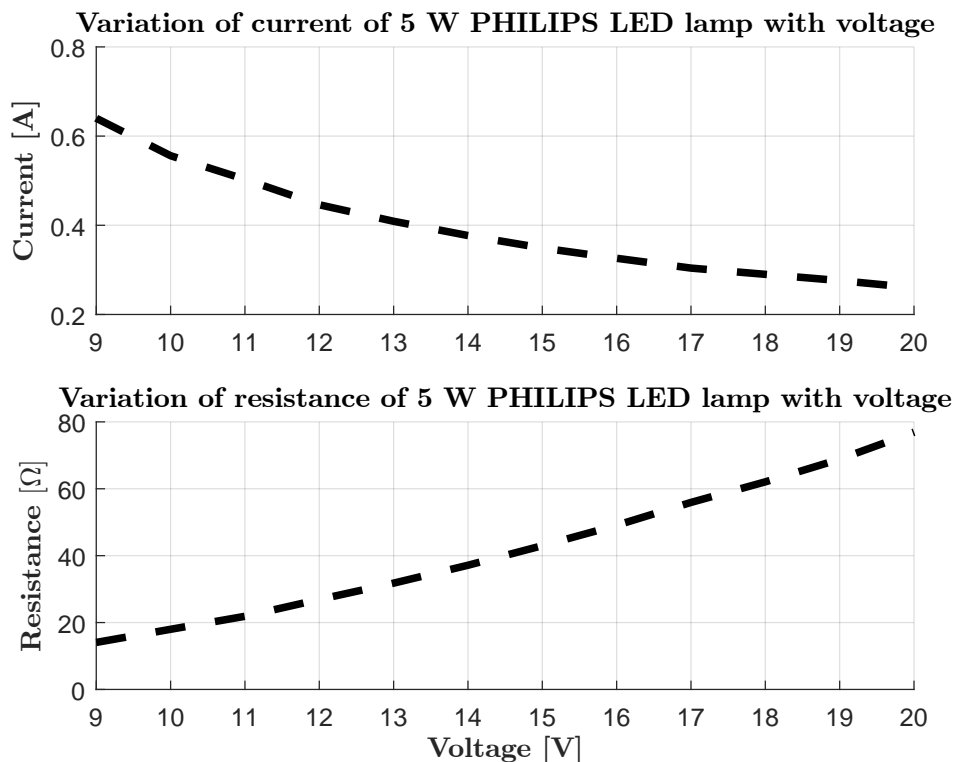


Figure 6.13: 5 W LED PHILIPS lamp characteristics

Table 6.4: Input impedance of switch mode DC-DC converter

Configuration	r_{in}
Battery connected to the output	$n^2 \frac{R_L r_b}{(R_L + r_b)}$
Parallel connection of the empty capacitor	$\frac{n^2 R_L r_c}{r_c + R_L \exp(-t/r_c C)}$
Series connection of the empty capacitor	$n^2 (R_L + r_c) \exp(t/(r_c + R_L)C)$
Series connection of the pre-charged capacitor	$\frac{n^2 (R_L + r_c) \exp(t/(r_c + R_L)C)}{(1-k)}$
with SCALED converter	$\frac{2 r_c V_0 n^2}{(V_0 - V_C(t)) - \sqrt{(V_0 - V_C(t))^2 - 4 r_c P_0}}$

6.5 SCALED converter with battery bank and MPPT charge controller

As discussed in the previous section, it is not possible to connect this proposed topology directly to existing MPPT charge controllers due to the fact that an SC bank in the converter behaves as a nearly ideal capacitor and LED lamps have non-linear voltage-current characteristics. Thus the MPPT charge controller does not see a constant resistive load at its output. Hence, it is not possible to match the r_{in} of the MPPT charge controller with the PV panel resistance by changing the duty cycle D of the DC-DC converter in the MPPT charge controller.

Therefore, it was decided to analyse the behaviour of input resistance, r_{in} , of a DC-DC converter when this novel system is connected to converter, as shown in Figure 6.14. In this format, the SCALED circuit is connected in parallel with a rechargeable battery pack. For this analysis, the buck converter was considered as the DC-DC converter. However, this analysis can also be adapted to other converters.

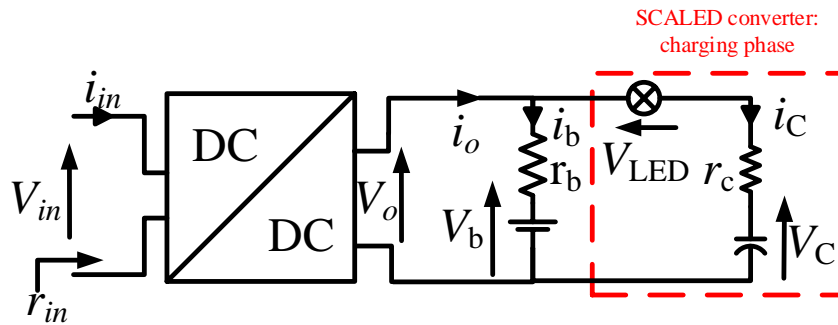


Figure 6.14: Buck converter with SCALED circuit buffered by a battery

By considering Figure 6.14 and using KCL, the total loop current i_0 can be written as:

$$i_0 = i_b + i_C = \frac{V_0 - V_b}{r_b} + C \frac{dv_C}{dt} \quad (6.35)$$

where V_0 , V_b and r_b are the DC-DC converter output voltage, battery bank voltage and internal resistance of the battery respectively.

Using KVL, it is possible to derive an equation for V_0 in terms of the LED lamp voltage V_{LED} , SC bank voltage V_C , ESR of the SC bank r_c and capacitor current i_C as;

$$V_0 = V_{\text{LED}} + i_C r_c + V_C(t) \quad (6.36)$$

Since an LED lamp consumes constant power in its constant brightness region Eq. 6.36 can be modified as:

$$\frac{P_0}{C} = \frac{dv_C}{dt} \left(V_0 - r_c C \frac{dv_C}{dt} + V_C(t) \right) \quad (6.37)$$

By solving Eq. 6.37 for $\frac{dv_C}{dt}$, it is possible to derive Eq.6.33. By substituting Eq.6.33 into Eq. 6.35, the total loop current can be rephrased as;

$$i_0 = \frac{V_0 - V_b}{r_b} + \frac{(V_0 - V_C(t)) - \sqrt{(V_0 - V_C(t))^2 - 4r_c P_0}}{2r_c} \quad (6.38)$$

Therefore, r_{in} of the buck converter can be written as;

$$r_{\text{in}} = \frac{V_0}{D^2 i_0} = \frac{2V_0 r_b r_c}{D^2 \left[2(V_0 - V_b)r_c + r_b \left((V_0 - V_C(t)) - \sqrt{(V_0 - V_C(t))^2 - 4r_c P_0} \right) \right]} \quad (6.39)$$

Euler numerical integration of Eq. 6.39 was carried out using MATLAB and the variation of r_{in} of the buck converter was plotted against time t and the duty cycle D as shown in Figure 6.15.

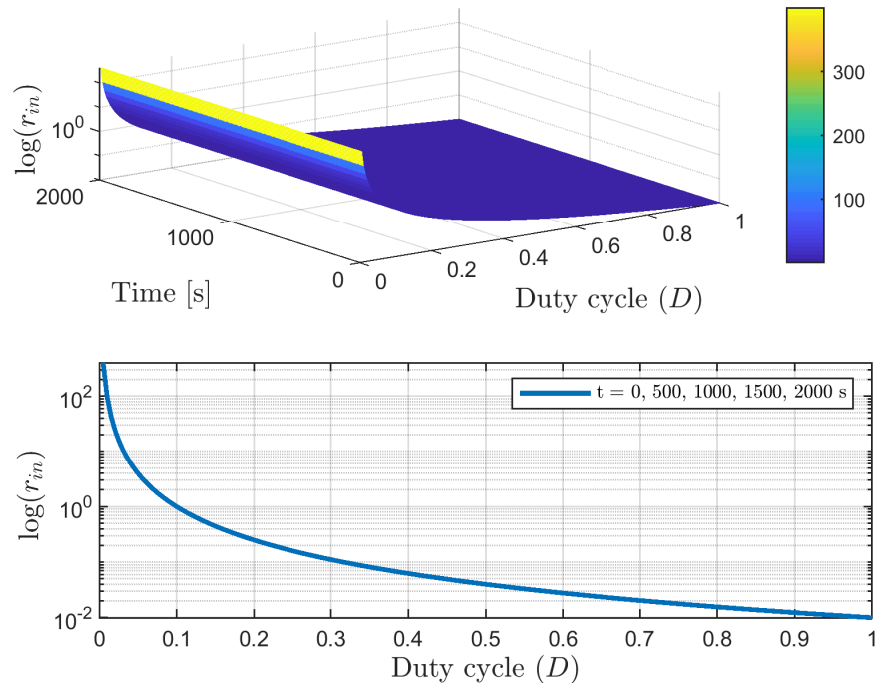


Figure 6.15: Variation of r_{in} for buck converter with SCALED circuit buffered by a battery pack

Previously, when the SCALED converter was directly connected to the buck converter, r_{in} varied from 10^6 to 100Ω when D changed from 0 to 1 (can be seen in Figure 6.12). However, with the new modification, the r_{in} of the converter varies from 100 to $10^{-2} \Omega$ when D changes

from 0 to 1, irrespective of the variation in time, t as depicted in the lower graph of Figure 6.15. Hence, it is possible to use existing MPPT controllers because now the impedance seen by the MPPT controller unit mostly depends on the internal resistance of the battery pack. This impedance can be matched with the PV panel impedance easily in order to extract maximum power from the panel.

6.6 Matlab Simulink simulation of SCALED converter with battery bank and MPPT controller

In order to verify the scenario discussed in section 6.5, a MATLAB Simulink model for the overall circuit (including PV panels, MPPT controller, battery bank and SCALED converter) was created and run. This model is shown in Appendix B.8. The simulation was done by feeding the real world irradiance and temperature measurements of University of Waikato site to PV panel model in Simulink. This data was collected from the National Institute of Water and Atmospheric Research (NIWA) New Zealand database.

The CSUN250-60P PV panel model with $I_{SC} = 8.81$ A, $V_{OC} = 37.3$ V, $I_{MPP} = 8.36$ A, $V_{MPP} = 29.9$ V, $P_{MPP} = 250$ W, 24 V, 300 Ah Li-ion battery model and 24 V buck converter model was used for this simulation. Two PV panels in parallel were used during the simulations to match the site conditions. The Perturb and Observe (P&O) technique was used as the MPPT method and a MATLAB script file was developed, which is shown in Appendix B.9. A model for the SCALED converter also developed in the Simulink environment and the controller script file is shown in Appendix B.10. Since a 24 V buck converter and battery bank was used, the changeover voltages of the SCALED converter was updated to 9 V and 16 V.

This model was simulated for all four seasons (Summer, Autumn, Winter and Spring). However, the results obtained for only one season are depicted in Figures 6.16, 6.17 and 6.18. Figures 6.16 and 6.17 indicate that the SCALED converter is operating properly even though it is now connected with an MPPT controller. This is because the SCALED converter is buffered with a battery bank and the input resistance of the MPPT controller mostly relies upon the internal resistance of the battery pack as discussed in section 6.5.

The 4th and 5th graphs in Figure 6.18, enable verification that the PV panel operates at its maximum power point (MPP) irrespective of the irradiance variations shown in the first graph in the same figure. Further, the power output from two combined PV panels was calculated for the same irradiance variation and compared with the results obtained from the simulation to verify that the panels were operating at their MPP. These values are provided in Table 6.5 and Figure 6.19, showing the difference between estimated and measured power.

It can be concluded that by combining a battery bank with a SCALED converter, it is possible to extract the maximum power from the PV panels. Since SC banks are used in SCALED converter, the battery bank can be downsized and the cycle life of the battery bank increased because SC banks acts as short-term energy storage units. Another advantage of hybridizing a battery bank with this novel converter is the ability to operate the overall system even at night.

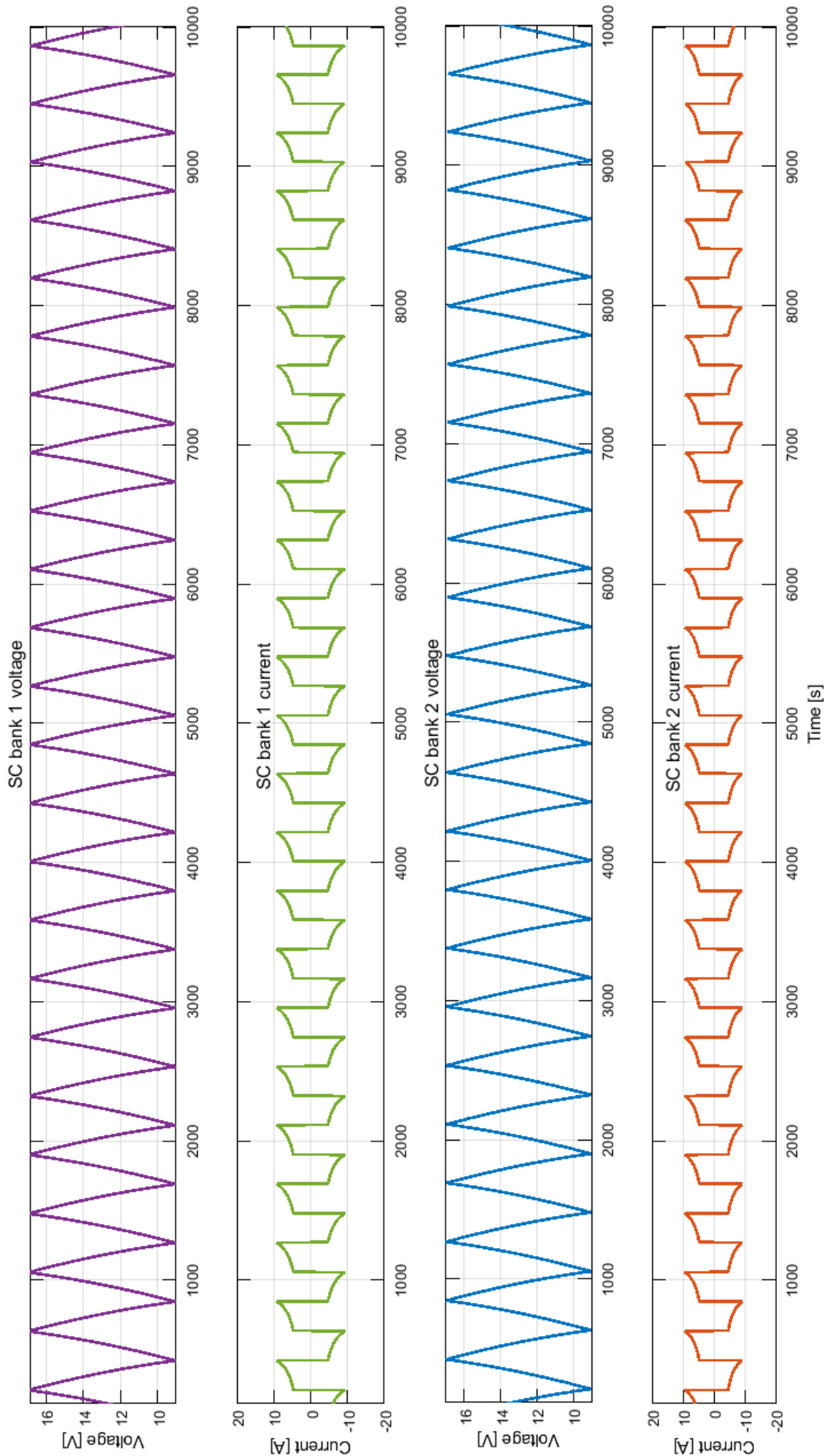


Figure 6.16: Variation of voltages and currents of two SC banks (MATLAB Simulink results of SCALED converter with battery bank and MPPT controller)

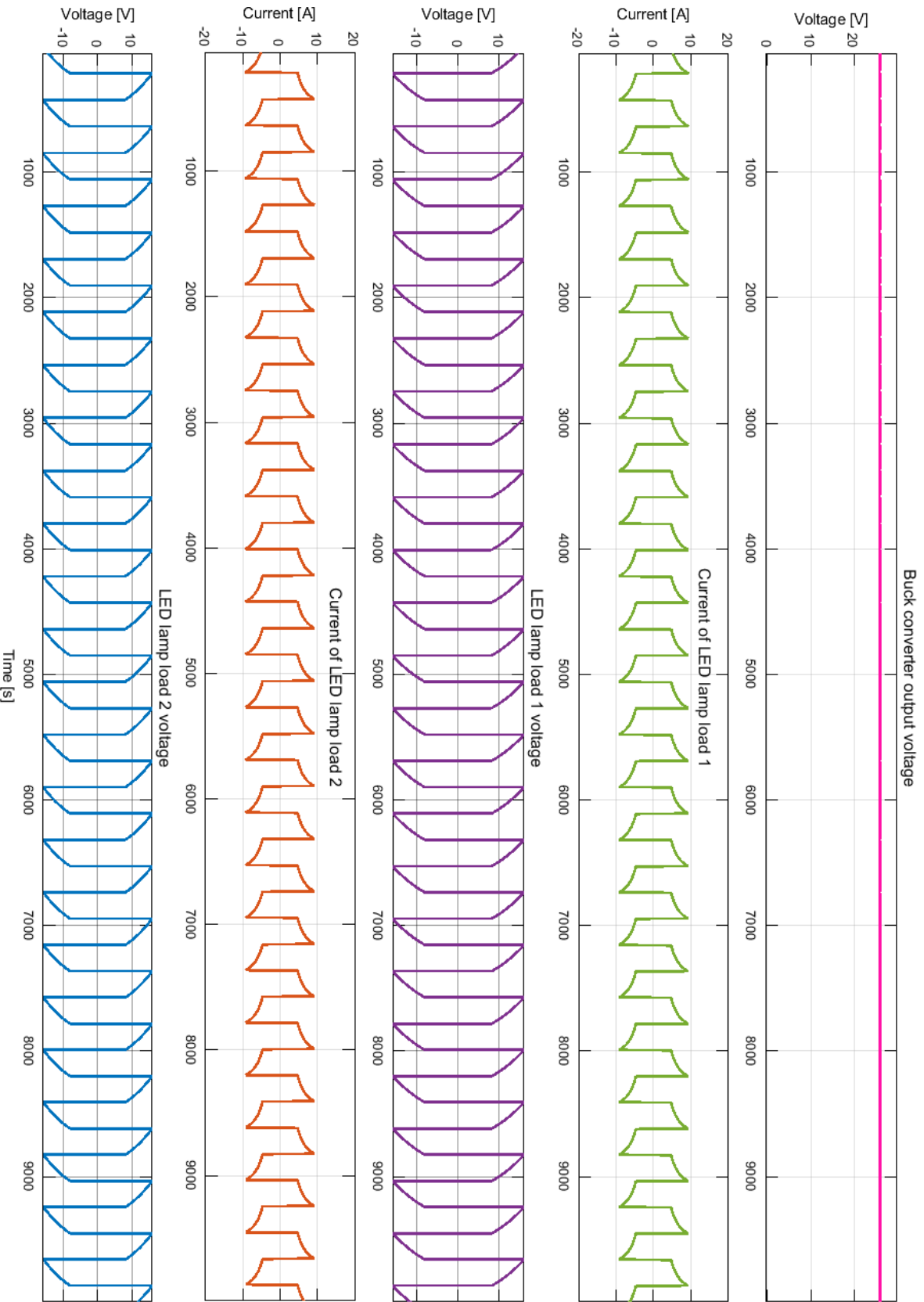


Figure 6.17: Variation of voltages and currents of two LED lamp banks (MATLAB Simulink results of SCALED converter with battery bank and MPPT controller)

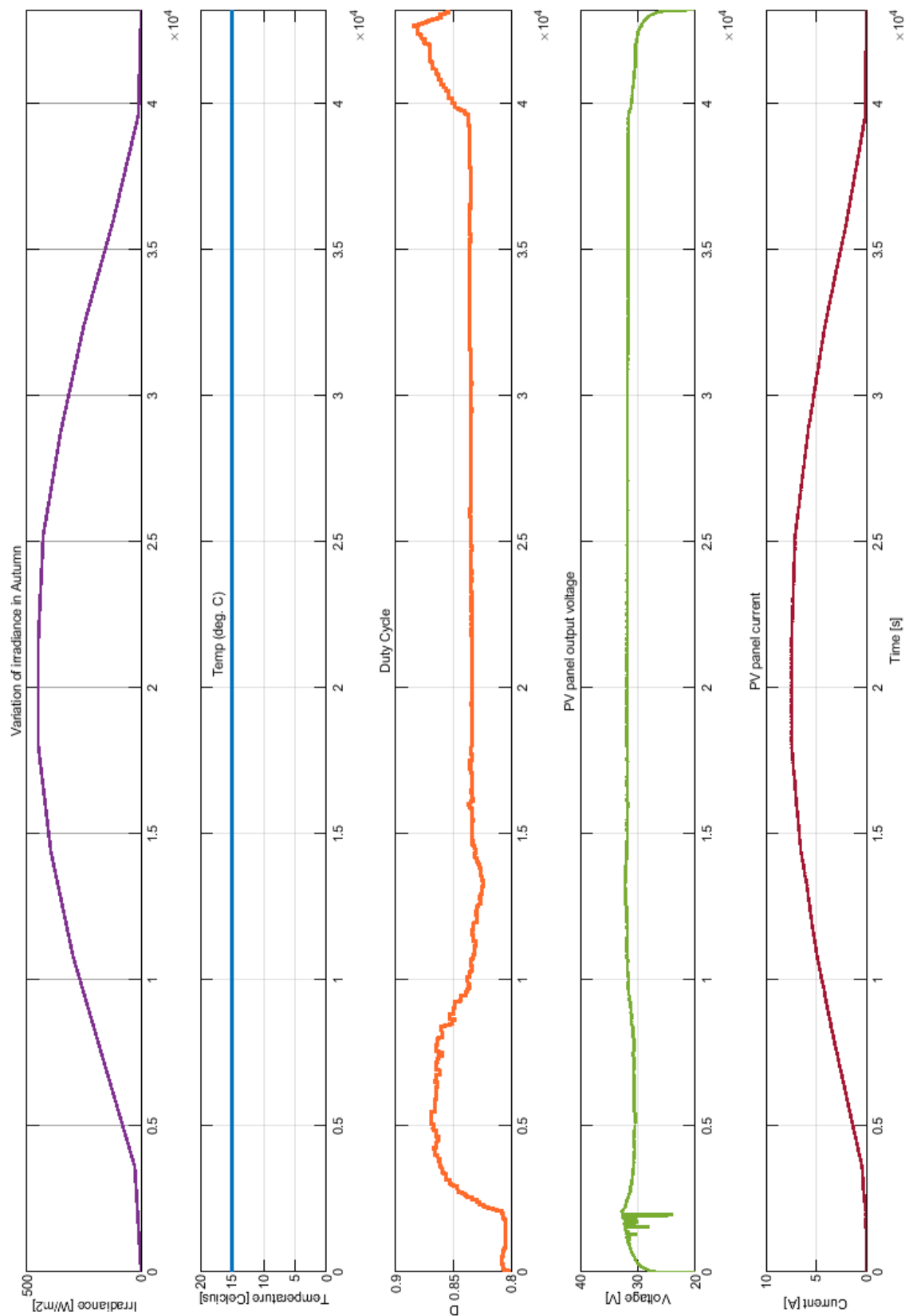


Figure 6.18: Behaviour of the PV panel (MATLAB Simulink results of SCALED converter with battery bank and MPPT controller)

Table 6.5: Comparison between estimated and measured MPP power of PV panels

Irradiance [Wm^{-2}]	Estimated power [W]	Measured power (simulation) [W]
0	0	0
137.5	69.77	67.6
343.4	176.61	172.1
490.6	253.64	247.8
542.5	280.75	274.0
500.7	258.35	253.1
393.4	202.53	199.6
216.3	108.15	107.8
43.21	18.93	19.6
0	0	0

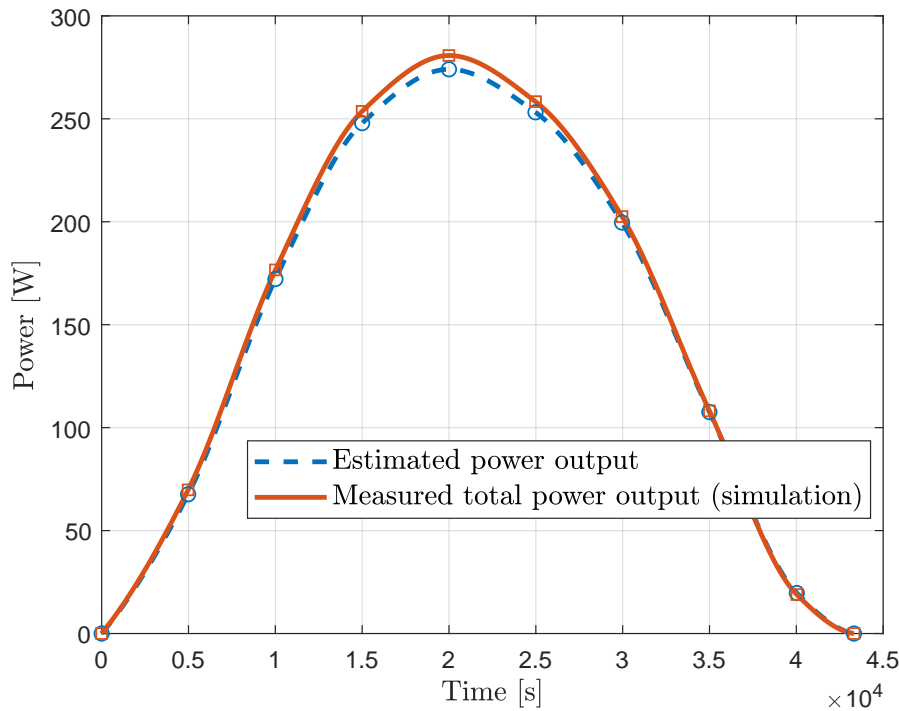


Figure 6.19: Comparison of estimated and measured output power levels of PV panels

6.7 Chapter Summary

The performance and associated waveforms of the individual phases (charging and discharging) of the SCALED converter were accurately predicted by the analytical solution and the LTSpice simulations. Analytical results were obtained using MATLAB simulations. The theoretical analysis clearly showed that standard maximum power point tracking controllers cannot be used with the SCALED converter, since the SC banks in the converter act as almost ideal capacitors and the LED lamp load acts as a constant power load. However, using analytical solutions and MATLAB Simulink simulations it was verified that by hybridising the SCALED converter with a battery pack it is possible to use existing maximum power point tracking controllers.

The next chapter will discuss the extended applications of the SCALED concept, which will be applicable in DC microgrids.

Extended application of SCALED concept

The newly proposed SCALED converter was based on the supercapacitor assisted loss management (SCALOM) concept of a simple RC charging loop discussed in Chapter 3. In the SCALED circuit, 12 V, a bank of 5 W LED lamps were adapted as the useful load in a modified RC charging loop as discussed in Chapter 5. This topology was used in a PV-based DC microgrid to increase the energy efficiency of a PV-based indoor lighting system. The SC banks used in the circuit even provide power to the LED lamp loads in the case of solar fluctuations (short-term DC UPS) and this converter has the ability to cater for fluctuations in solar energy.

This novel concept is not only applicable to 12 V indoor LED lamps but can also be extended to power 24 V, 48 V or over 100 V LED lamps and flood lights (outdoor lamps). Since most of white goods are internally DC operated, this concept can also be used to power miscellaneous items in a DC microgrid. Figure 7.1, shows that this concept can be used for low power loads, outdoor lighting, cooling and non-cooling loads. This can be achieved by appropriately selecting the supercapacitor (SC) banks and using a proper switching arrangement depending on the operating conditions of the selected equipment. The size of SC banks to be used with each of these devices will not be same as in a SCALED converter, but will still be able to use the same concept. The sizing of SC banks mainly depends on the ratings and operating region of lamps or white goods. This chapter will provide a summary of some of these extended applications, which are already underdevelopment as undergraduate projects at the University of Waikato (UOW).

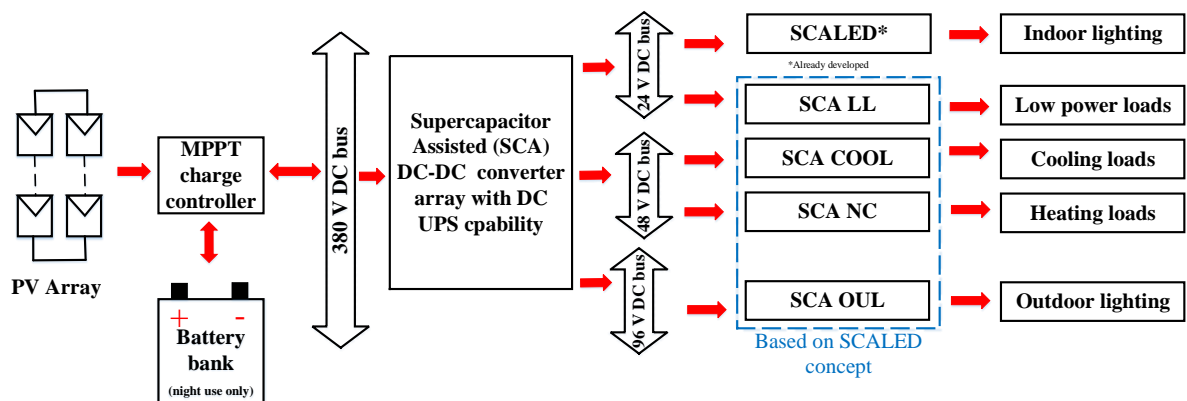


Figure 7.1: Extension of SCALED concept to other applications

7.1 24 V LED luminaires

As the first step, it was decided to test a Philips 24 V, 15 W DC-operated LED lamp to find the current voltage and illuminance voltage characteristics of the lamp. The current and illuminance readings were recorded while changing the voltage applied to the lamp. The results are depicted in Figure 7.2. As shown in Figure 7.2, a 24 V LED lamp has a constant brightness over a range of voltages around the nominal 24 V. The constant brightness region for this specific lamp is from 20 V to 30 V. During testing it was found that this lamp did not operate when negative DC voltages were supplied. This is because these lamps are DC voltage rated and do not contain an AC/DC converter. The input DC voltage is applied to the series LED array through an LED driver. In fact the input voltage rail is directly connected to the series LED array through a transistor sub-circuit without even using a driver circuit. Since this is outside the scope of this thesis, it is not discussed in detail.

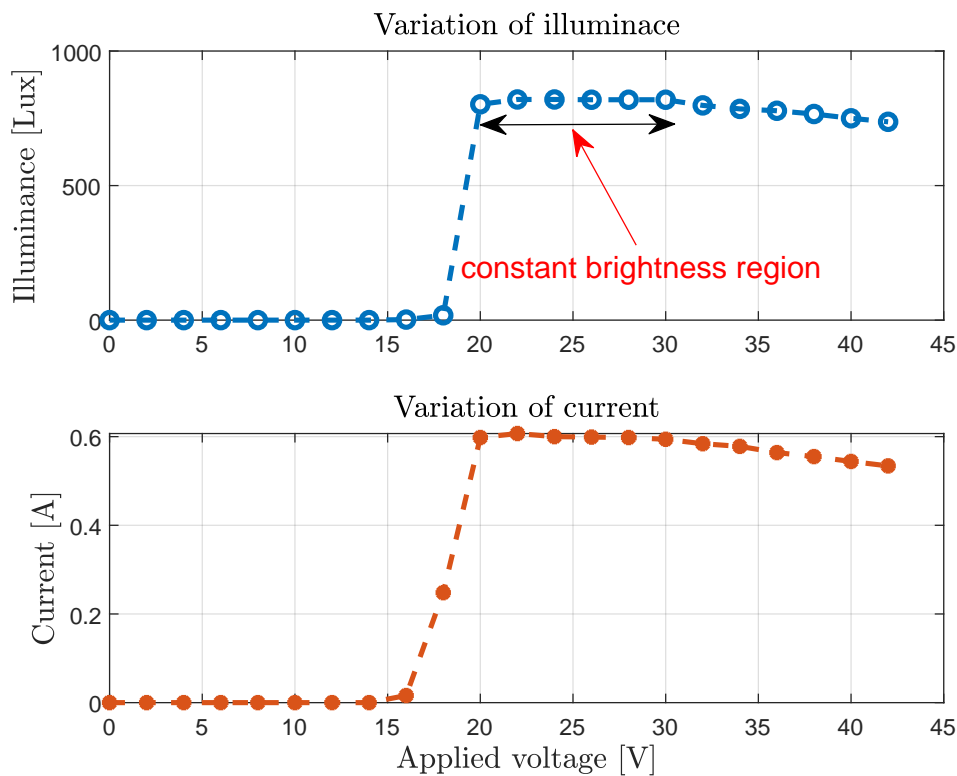


Figure 7.2: Variation of brightness and current of a 24 V PHILIPS with applied voltage

The test results indicated that the SCALED concept could also be extended to 24 V LED lighting systems. However, since these LED lamps cannot be operated using negative DC voltages, it is necessary to either use a bridge rectifier with the LED lamp load or increase the number of switches used in the circuit. Instead of increasing the number of switches used, it is preferable to use a bridge rectifier circuit, or alternatively, AC-rated LED lamps can be used because those lamps already contain an AC/DC converter. With minor modification to the SCALED converter and proper sizing of the SC banks to be used, this new SCALED concept can be directly and easily extended to high power and voltage rated LED lamps.

7.2 Flood lights

In order to verify that the SCALED concept could be extended to flood lamps, a sample of 110 V and 200 V DC rated lights were tested separately. For these tests we used a variable AC (variac) power supply and a diode bridge to get the required DC voltage levels. During the testing the variation in illuminance level with the applied voltage was recorded and is depicted in Figure 7.3. When testing 110 V flood lamp, it was not possible to record the lamp brightness values for the voltages from 116 V to 119 V, due to sudden spikes occurs in the LED current. This situation causes the variac to jump from 115 V to 120 V. It can be seen from the top graph in Figure 7.3 that the 110 V flood lamp has approximately constant brightness regions in three different voltage ranges:

1. Region 1: from 105 V to 108 V
2. Region 2: from 110 V to 115 V
3. Region 3: from 118 V to 120 V

However, since these three regions have different brightness levels an operating voltage range can be selected depending on the brightness requirement. Therefore, the SCALED concept can easily be applied to 110 V flood lamp. However, although this seems easy, completely new design aspects will need to be considered during hardware design because 110 V rated flood lamps have three constant brightness regions. This application may need to use different switching arrangements to the one used in the SCALED converter.

Conversely, when considering the lower graph in Figure 7.3, the 200 V flood lamp has only one constant brightness region. Therefore, the SCALED concept can be directly applied to 200 V flood lamps by adequately sizing the SC banks and selecting switches with appropriate ratings.

Accordingly, this section establishes that this novel technique is not only valid for 12 V indoor lighting, but also can be extended to outdoor lighting applications and the indoor lamps with various voltage and power ratings.

7.3 Extension of the SCALED concept into white goods

With the aim of investigating the feasibility of extending the SCALED concept to white goods, several experiments were carried out on a DC-powered refrigerator. A DC-powered compressor based 50 L, 50 W rated fridge was used for the preliminary tests. According to the SunnyTech manufacturer's user instruction manual this fridge will run on either 12 V or 24 V DC [115]. Experiments were conducted to get an understanding of the voltage, temperature and current characteristics of this fridge. It was found that the DC compressor of the refrigerator started operating in a range of voltages around 12 V and 24 V as shown in Figure 7.4. In the 12 V range the compressor would start at voltages from 11 V to 17 V, and in the 24 V range the compressor would start from 23 V up to 30 V.

After finding the two operating regions an experiment was conducted to estimate how long the compressor would stay on and how long it would stay off on average. The experimental data

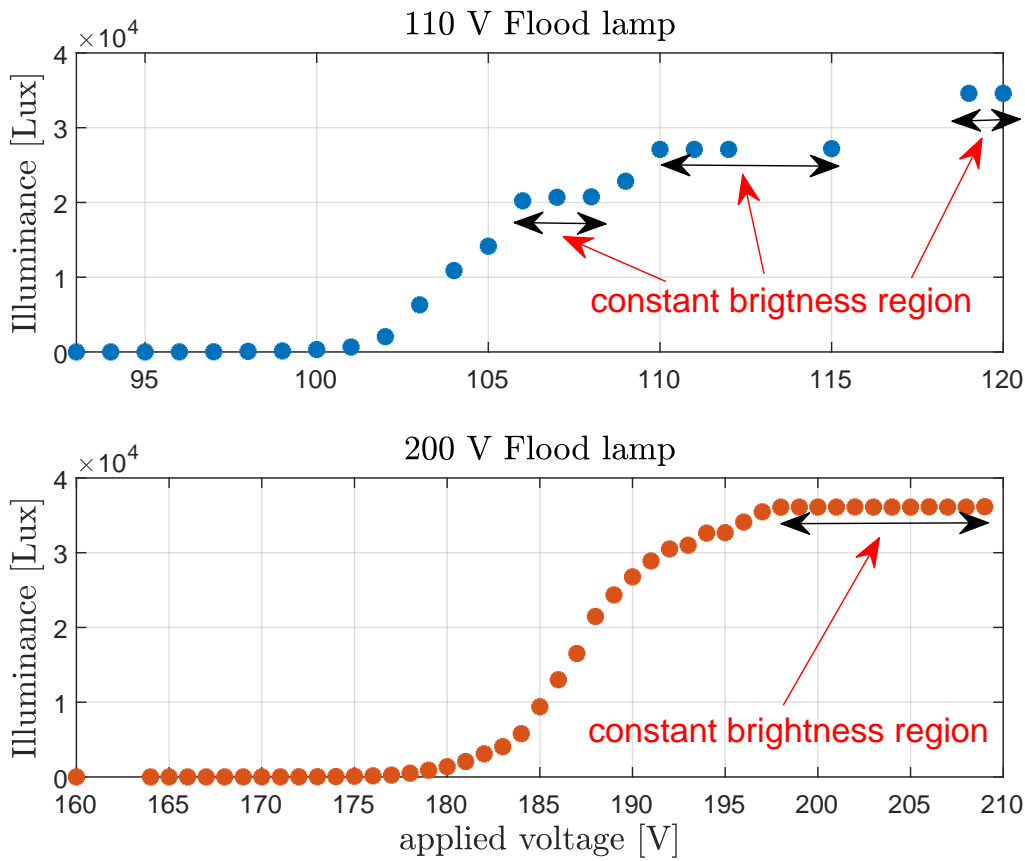


Figure 7.3: Variation of brightness in flood lamps with applied voltage

showed that on average, the compressor will be on for 5 minutes and off for 19 minutes. The collected data can be used for sizing the required supercapacitor banks.

Since this fridge is operating in a range of voltages between 12 V and 24 V, it is possible to use the same concept used in the SCALED converter. Depending on the PV array voltage, the operating voltage range of the refrigerator can be determined. Therefore, a new circuit as depicted in Figure 7.5 is under development at the University of Waikato to power this DC refrigerator using solar power. The two SC banks will connect in series with the DC fridge during charging to achieve high efficiency, and they will be connected in parallel with the fridge and supply power to the refrigerator in an event of sudden solar fluctuations. Since the SC banks will be in parallel with the refrigerator they should not be charged beyond the operating voltage ranges of the fridge.

As an example, if the PV array is considered as a 28 V constant voltage source and the SC banks are already charged to 11 V before beginning operation, the SC banks can only be charged up to 17 V. At this point the load voltage will have 11 V which is still in the range of operating voltages. Once both the supercapacitor banks are charged the refrigerator is directly connected to the power source until the PV panel output is goes below the minimum required level for running the refrigerator. In an event of a solar fluctuation, where the PV array output is not sufficient to power the fridge, then either one or both of the charged SC banks can be connected in parallel with the load to power the refrigerator. Therefore, it is necessary to use properly

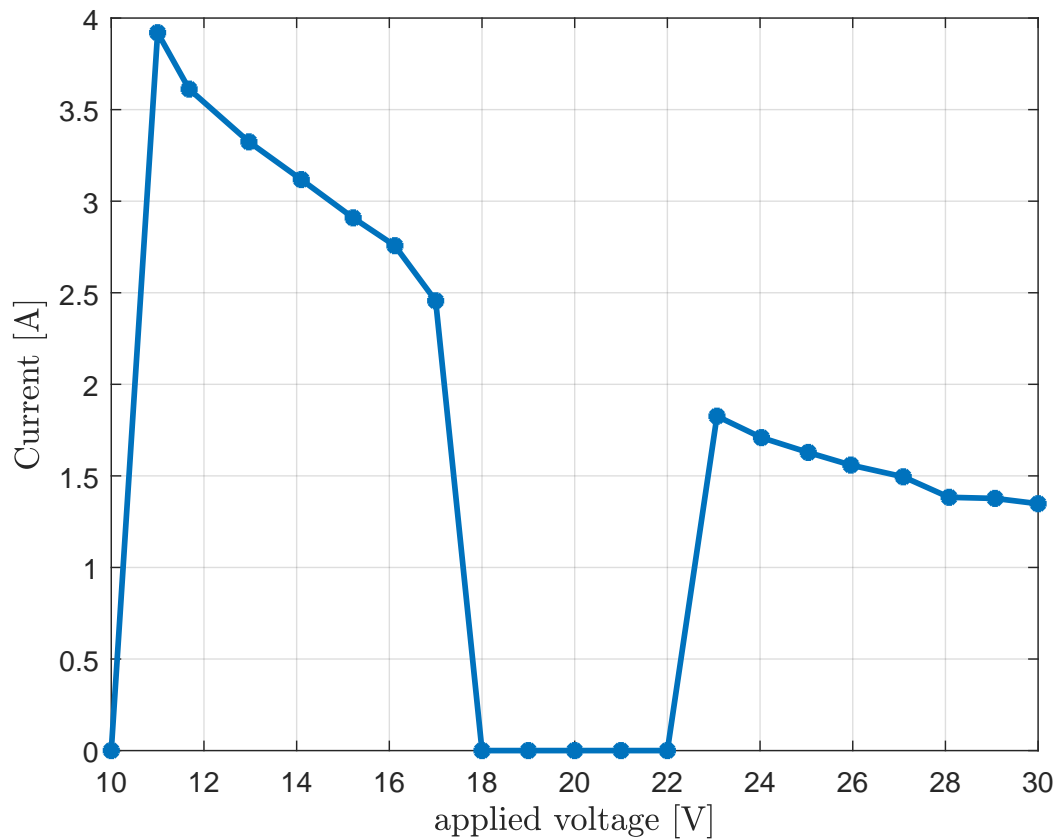


Figure 7.4: Current voltage characteristics of the compressor

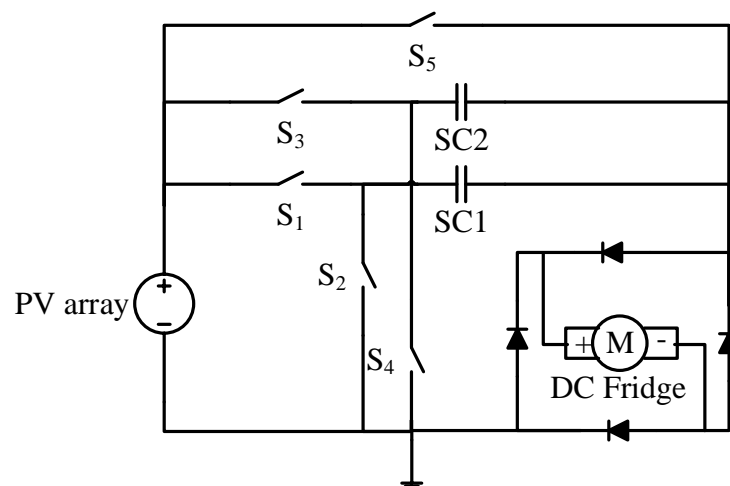


Figure 7.5: Basic circuit designed based on SCALED concept to power up DC refrigerator

sized SC banks, which can power the load during fluctuations. However, since this fridge only works on positive DC voltages and during the SC discharging phase provides negative voltage, a bridge rectifier is used to achieve operating regions with positive and negative supplies, so the refrigerator can operate on both positive and negative voltages. This reduces the number of switches that are required. However, it adds an unwanted voltage drop and power loss in the circuit. These results indicate that this novel hypothesis can be extended to any DC-powered load.

In summary, with the use of this approach for any DC powered appliance available in a DC microgrid environment, it is desirable to achieve high energy efficiencies within the microgrid. Since all these are ongoing undergraduate projects and not related to the context of this thesis, only a basic idea of how to use the SCALED concept for the other DC-powered loads has been presented and discussed. More detail will be available in future publications by the power electronic research team at the University of Waikato.

7.4 Chapter Summary

This chapter has provided an overview of how the SCALED concept can be extended to 24 V LED luminaires, flood lamps and white goods.

Conclusions and Recommendation

8.1 Summary

The main focus of this thesis was to design a new energy conversion technique with high energy efficiency, for LED lighting systems in PV-based DC microgrids, incorporating supercapacitors that can be directly fed from a PV array and can be used to buffer short-term energy supply interruptions.

Among the many types of sustainable energy sources, solar energy remains the most popular choice because it is available almost anywhere in the world at no cost. Accordingly, in recent years, there has been growing interest in the use of DC electricity in homes, because modern domestic appliances operate using DC voltages and currents internally, despite being connected to an AC power supply. Hence, they comprise AC/DC converters followed by multiple DC-DC converters, which will ultimately result in a reduction of energy efficiency. By using the DC power generated from the PV array directly to power the electronic equipment, it is possible to achieve better energy efficiency and be less dependent on the AC grid. However, the use of solar energy as a power source raises the need for energy storage devices (ESDs) for reliable operation of the overall system, as described in Chapter 1.

As discussed in Chapter 2, traditionally supercapacitors (SCs) were looked at as simple ESDs with low energy and high power density compared to conventional rechargeable batteries. However, due to electric double layer construction and activated carbon electrodes, SCs now have very high capacitance, very low equivalent series resistance (ESR) and can be used as more than just an ESD. Therefore, the power electronic research group at the University of Waikato uses SCs for non-traditional SC applications including:

- as a capacitor which can be used to achieve large time constant circuits
- as a lossless dropper
- to improve the end-to-end efficiency of linear power-management circuits
- as a surge absorbing device
- as a farad order capacitor with very low ESR

As described in Chapter 3, when a fully discharged capacitor is charged using a voltage source of V pumping Q coulombs, the capacitor stores $(1/2)QV$ while dissipating the same amount of energy in the loop resistance. Therefore, the overall charging efficiency of the RC loop is 50%. This efficiency can be improved by using a “useful ” load as the R in the charging loop and inserting a pre-charged capacitor in the loop. By using this loss circumvention technique with

SCs, the research team devised a new loss management concept for SCs named SCALOM. The SCALED converter is also one of the major applications of the SCALOM concept [96].

This thesis has presented a novel topology, named SCALED, to achieve high energy efficiency in PV-based DC microgrid environment. The proposed SCALED converter includes two SC banks, which act as lossless droppers and short-term ESDs while buffering solar fluctuations. The new topology is more energy efficient, and can be used with any domestic appliance and lighting system. In this converter, the LED lamp bank is used as the “useful load ” in the SC charging path. Since LED lamps operate in a wide range of voltages around their nominal voltage it is possible to use a PV array directly to power an LED lighting system. It was possible to reduce the number of switches used in SCALED because LED lamps can be operated with both positive and negative voltages. The properties of the commercially available LED lamps, which were used in the SCALED converter, were discussed in Chapter 4. As described in Chapters 5 and 6, a detailed analytical study of the design was carried out using practical experiments and simulations in SPICE and MATLAB.

The extended applications of this technique for white goods, LED-based flood lights and 24 V LED lamps were discussed in Chapter 7.

8.2 Conclusions

In this research, it was found that commercially available 12 V LED lamps have the ability to:

- operate with positive or negative DC voltages
- operate over a wide range of AC/DC voltages around nominal voltage without compromising the brightness
- operate as a constant power load in the constant brightness region

These unique features of the LED lamps were combined with supercapacitor banks to develop the novel loss-circumventing SCALED converter for DC lighting in buildings.

The proof-of-concept prototype of this circuit was tested in the Ports of Auckland (POAL) dock yard site and was able to achieve efficiencies in the range of 90% to 94%, compared to the existing high frequency switching converters coupled with a complex processor algorithms to achieve maximum power point tracking (MPPT) in a battery-based system. The combination of supercapacitor and LED luminaires formed a large time-constant RC circuit. Therefore, it was possible to operate the switches in the extra-low frequency range from a few Hz to fractional Hz. Thus, there are no RFI/EMI issues associated with this proposed converter. In this technique the supercapacitor acts as an energy storage device as well as a lossless dropper, enabling direct connection of the PV array to the SCALED converter.

It was established that existing MPPT techniques cannot be used directly with this SC-based converter for theoretical reasons. With further analysis, it was found that existing MPPT techniques can be used for hybrid circuit versions of a rechargeable battery pack supplementing the SCALED converter. Since, the proposed technique already has an energy storage, it is feasible to down size the battery bank.

The main goal of this research was to design and develop a prototype version of a new energy-efficient converter based on supercapacitors to be used for DC lighting in a PV-based

DC microgrid. It can be concluded that, the present version of the SCALED converter achieved this goal and has the following features and advantages.

- high end-to-end efficiency with supercapacitor banks acting as lossless droppers
- short-term DC UPS capability for solar fluctuations, by over-sizing the SC banks
- ability to overcome RFI/EMI issues due to very low frequency switching

This new proposed SCALED technique will allow energy engineers to overcome the problems of energy efficiency in power electronic converters used in DC microgrid environments.

8.3 Recommendations and Future work

Based on the results of experimental and theoretical analysis of the SCALED approach, the following recommendations are suggested for future implementations. Minimising the losses associated with the design and making the design more compact, will give the SCALED technique more opportunity to be a successful candidate for modern PV-based DC microgrids.

More investigation needs to be done in the battery SCALED converter hybrid topology. Because of time limitations, only MATLAB Simulink simulations were performed on this hybrid topology. Therefore, practical implementation of the overall circuit and field tests need to be done in order to verify the battery SCALED hybrid circuit.

At the time this project was begun, CAPAbattery SCs with 10 to 15 times more energy density than symmetrical electric double layer capacitors (EDLC) were not commercially available. By the end of this project, CAPAbattery SCs were commercially available from manufacturers such as Samwha Capacitor Inc. [33]. Instead of activated carbon electrodes, they use a lithium titanium oxide (LTO) as the negative electrode and lithium transition metal oxide as the positive electrode to improve the energy density and achieve the characteristics of both Li-ion battery and supercapacitor. Table 8.1 compares the engineering specifications of these three devices with popular rechargeable battery chemistries such as lead-acid and Li-ion [33]. It can be seen that lead-acid batteries and CAPAbattery SCs have the same energy density.

Table 8.1: Comparison of engineering specifications of supercapacitor families compared with rechargeable batteries [33]

Parameter	EDLCs	Hybrid SCs	CAPAbatteries	Pb-acid	Li-ion
Energy density (Wh/L)	5 – 8	10 – 14	50 – 120	50 – 125	250 – 670
Power density (W/L)	8000	2500 – 4000	1600 – 3200	25 – 100	375 – 1750
Cycle life (cycles)	1000000	40000 – 50000	15000 – 20000	500 – 2000	1000 – 1200
Rated voltage (V)	2.7	2.7	2.7	2.0	3.0 – 3.6
Capacitance (F)	1 – 3000	200 – 7500	1000 – 70,000	NA	NA

Using the SC banks made from these CAPAbattery supercapacitors may possibly overcome the issue of using existing MPPT techniques with capacitors and thus minimize the use of

rechargeable battery banks for long-term energy requirements. Therefore, more investigation and research is required around the adoption of CAPAbatteries in SCALED converters.

More optimization should be done on the controller circuit to reduce the initial inefficiencies in the circuit. This would result in a lower energy consumption by the controller circuit and increase overall efficiency of the SCALED converter.

More investigation and research could be done to test the surge absorption capability of the overall circuit.

Schematic, PCB layouts and PIC codes of SCALED converter prototypes

A.1 Schematic and PCB Layout for SCALED Converter Power Stage

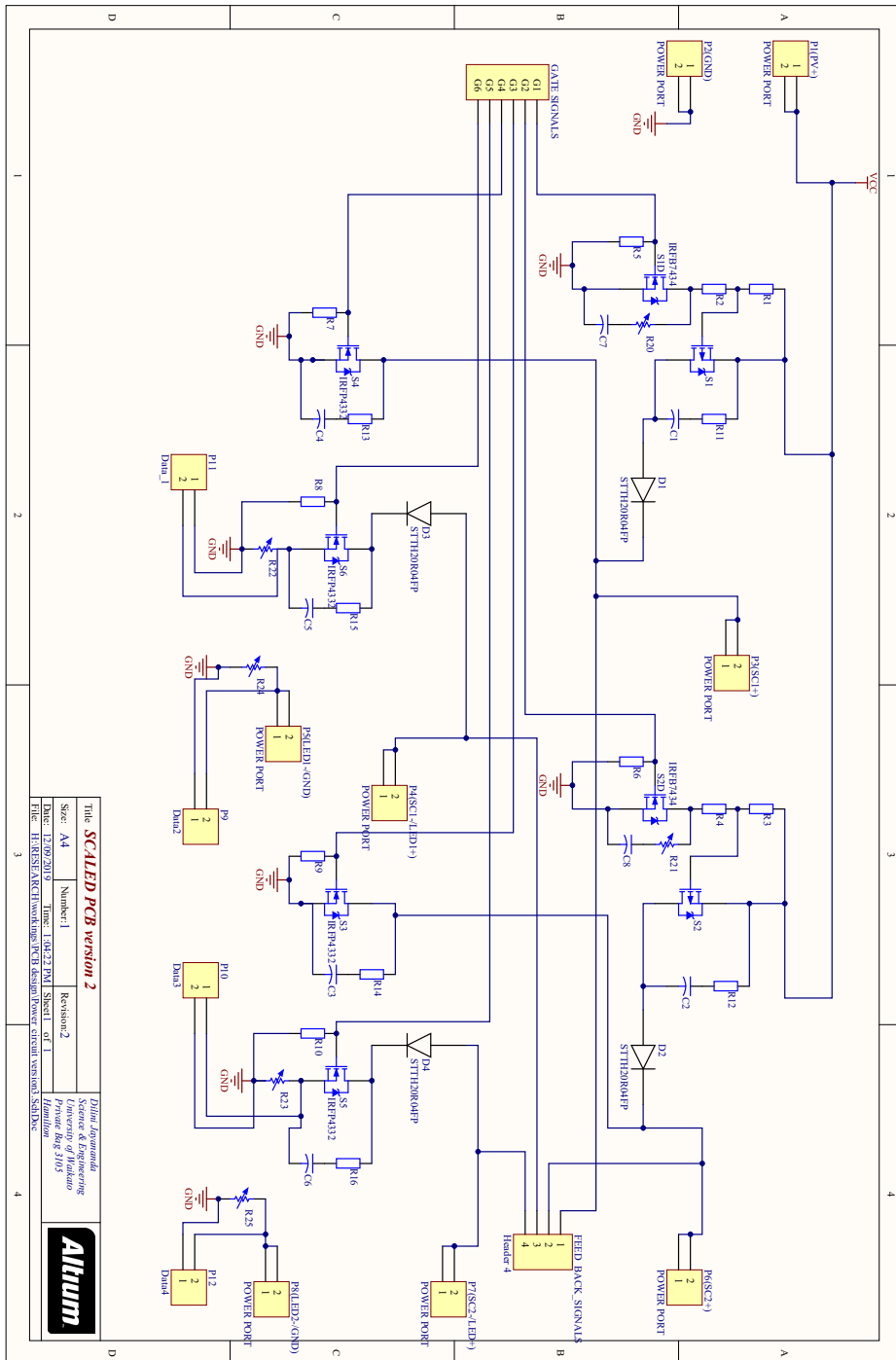


Figure A.1: Schematic for SCALED Power Stage

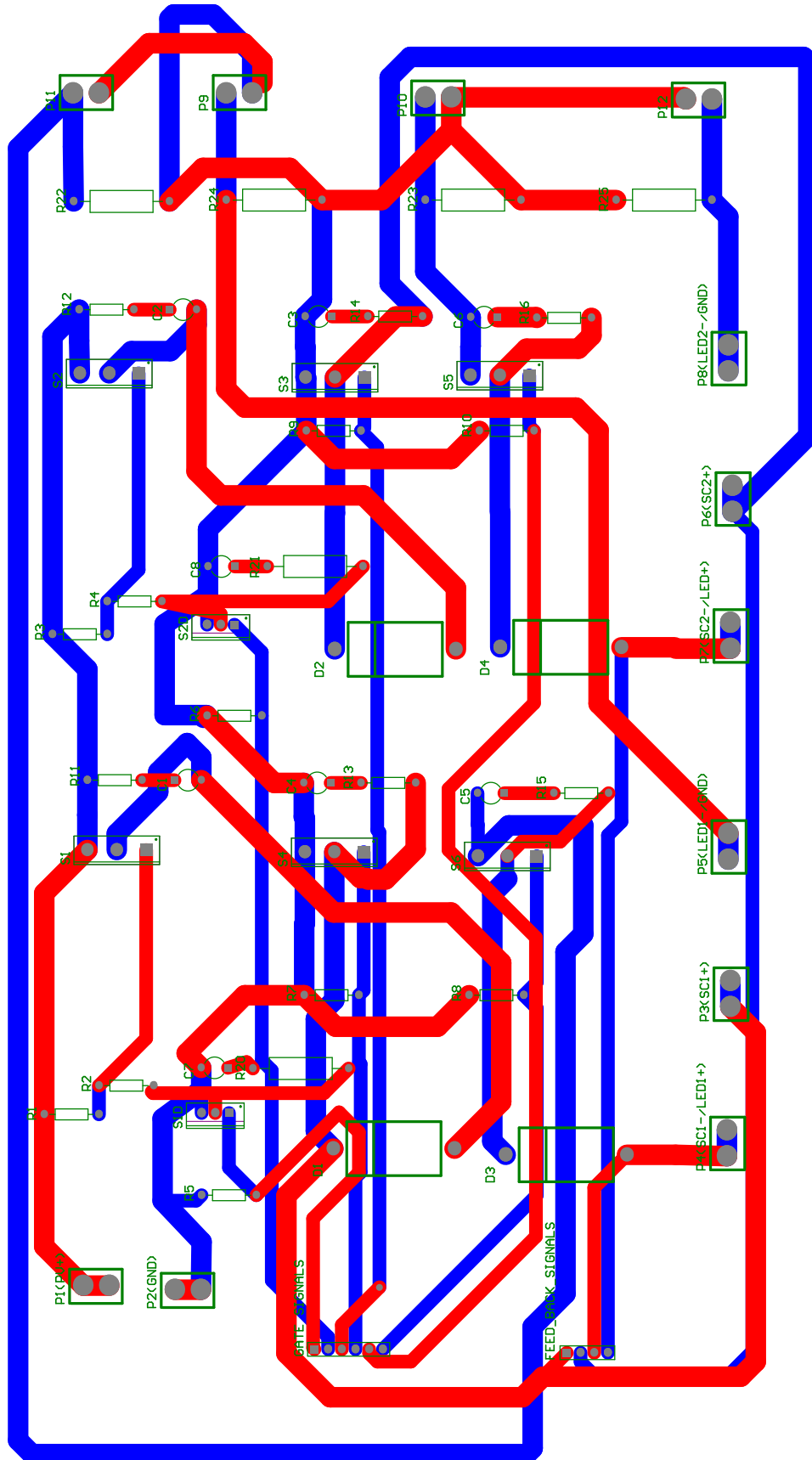


Figure A.2: PCB layout for SCALED Power Stage

A.2 Schematic and PCB Layout for SCALED Converter controller

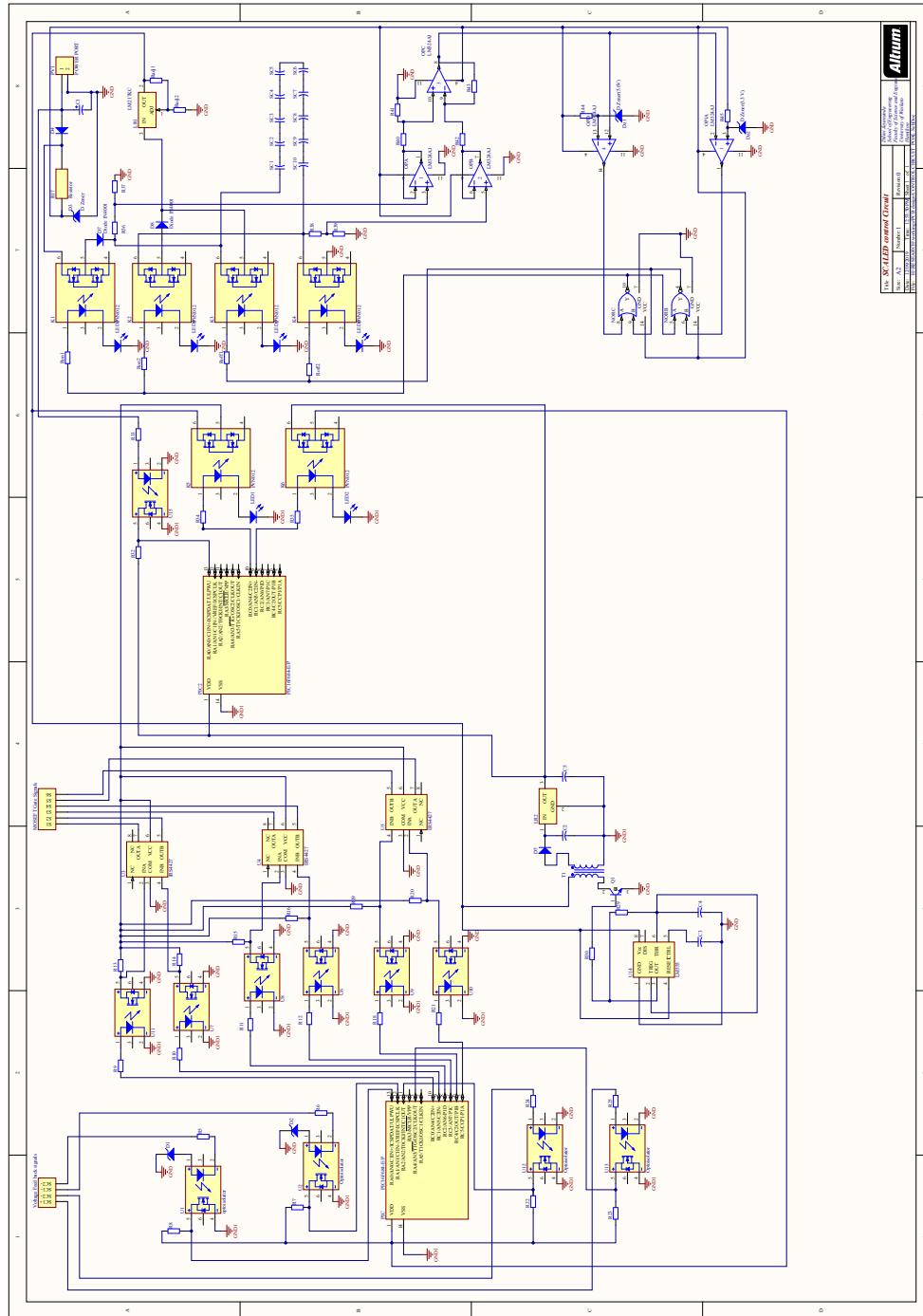


Figure A.3: Schematic for SCALED control circuit

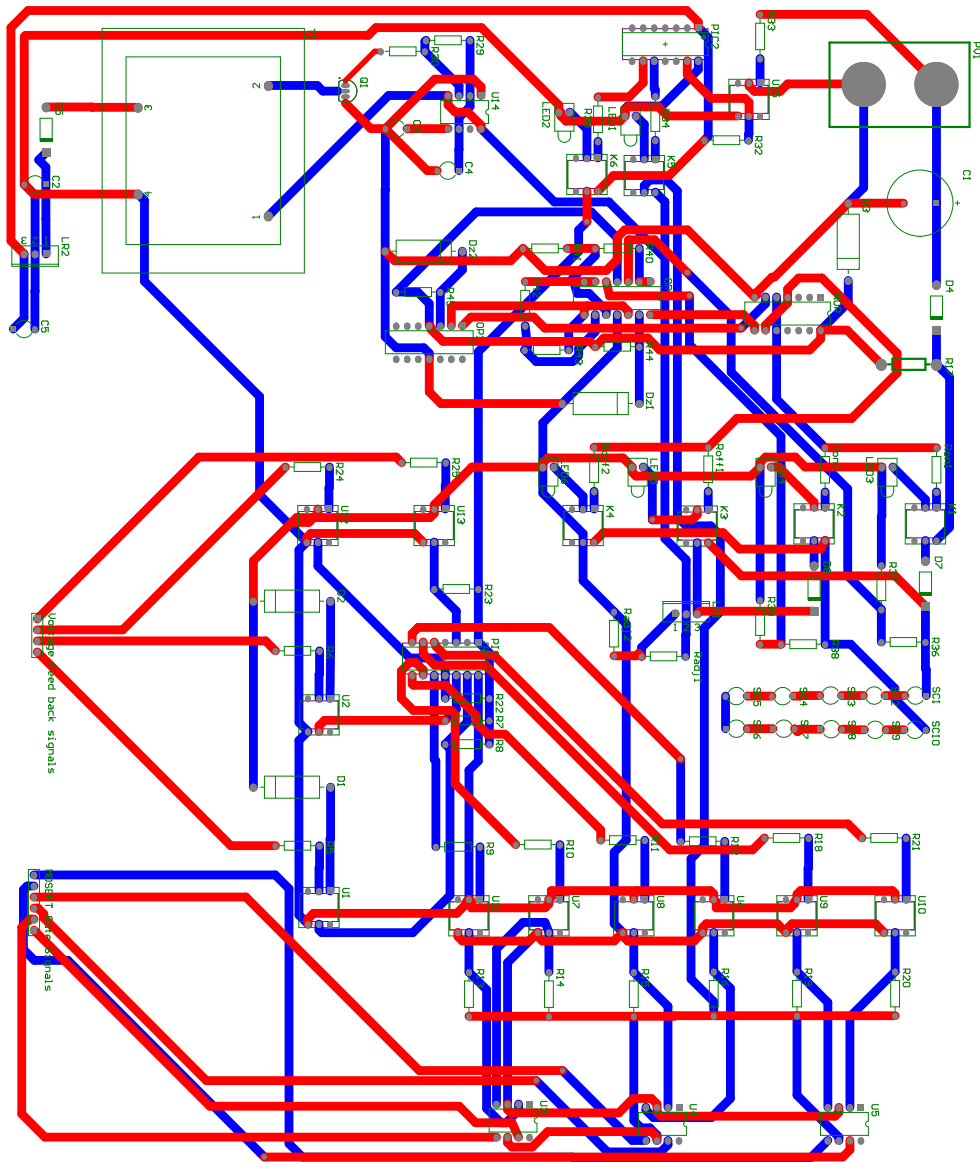


Figure A.4: PCB layout for SCALED control circuit


```

55         state2 = 0;
56         state3 = 1;
57         SC_charging2();
58         for (i=0;i<5000;i++);           // Switchover
59         delay
60     }
61 }
62 }
63
64 void change_sw_discharging2()
65 {
66
67     ADCON0 = 0b10000101;    //RA1(AN1) analogue input which take LED1
68     ADC_value =0;
69     GO_nDONE =1;
70     while (GO_nDONE);
71     ADC_value = (ADRESH << 8)+ADRESL;
72
73     if (L2_H <= ADC_value)
74     {
75         state1 = 0;
76         state2 = 1;
77         state3 = 1;
78         SC_charging1();
79         for (i=0;i<500;i++);           // Switchover
80         delay
81     }
82 }
83
84 void check()
85 {
86
87     ADCON0 = 0b10001101;    //RA4(AN3) analogue input which take SC1 voltage
88     ADC_value =0;
89     GO_nDONE =1;
90     while (GO_nDONE);
91     ADC_value = (ADRESH << 8)+ADRESL;
92
93     if (L2 >= ADC_value)
94     {
95         V1 = 1;
96         PORTC = 0b00011110;
97         for (i=0;i<500;i++);           // Switchover
98         delay
99     }
100
101     ADCON0 = 0b10001001;    //RA2(AN2) analogue input which take SC2 voltage
102     ADC_value =0;
103     GO_nDONE =1;
104     while (GO_nDONE);
105     ADC_value = (ADRESH << 8)+ADRESL;
106
107     if (L3 >= ADC_value)
108     {
109         V2 = 1;
110         PORTC = 0b00101101;

```

```

111             for(i=0;i<500;i++);           // Switchover
112                 delay
113             }
114
115             if( V1 == 1 && V2 == 1)
116             {
117                 PORTC = 0b00111111;
118                 state1 = 0;
119                 state2 = 1;
120                 state3 = 1;
121             }
122 }
123
124
125
126
127
128 void charging_phase()           // Charging SC bank 1 from the solar panel and
    discharging the SC bank 2 to LED2
129 {
130     while(state1 == 0)
131     {
132         SC_charging1();
133         for(i=0;i<500;i++);
134         change_sw_discharging1(); // Check the voltage across LED2
135         for(i=0;i<500;i++);       // Switchover delay
136     }
137 }
138 }
139
140
141
142
143
144 void discharging_phase() // Charging SC bank 2 from the solar panel and discharging the
    SC bank 1 to LED1
145 {
146     while (state2 == 0)
147     {
148
149         SC_charging2();
150         for(i=0;i<500;i++);
151         change_sw_discharging2(); // check the voltage across LED1
152         for(i=0;i<500;i++);       // Switchover delay
153     }
154 }
155
156 void initial_charging()
157 {
158
159     while(state3 == 0)
160     {
161         check(); // Check the capacitor voltages
162         for(i=0;i<500;i++);       // Switchover delay
163     }
164 }
165 }
166
167

```

```
168
169
170
171 void main()
172 {
173     // initialize the ADC
174
175     ANSEL = 0b00001111;           //Channel AN0:AN1 selected since
        we are using RA0:RA2 and RA4 as analogue input to ADC
176     ADCON1 = 0b00010000;         //bit 4:6 ADCS<2:0> = 001 which gives
        Fosc/8*
177     TRISC = 0b00000000;         // RC0:RC5 are the output from
        the PIC to drive the switches
178
179     //start process
180
181     state1 = 1;
182     state2 = 1;
183     state3 = 0;
184
185     //state1 = 0;
186     //state2 = 1;
187     //state3 = 1;
188
189     PORTC = 0b00111111;
190     for (i=0;i <1000;i++);
191
192
193     PORTC = 0b00001100;
194     initial_charging();
195
196
197     while(1)
198     {
199         initial_charging();
200         charging_phase();
201         discharging_phase();
202     }
203
204 }
```

A.4 PIC code for SCALED start-up circuit

```

1  #include <stdio.h>
2  #include <htc.h>
3  #include <pic16F684.h>
4  #include <stdlib.h>
5  #include <pic.h>
6  #define _XTAL_FREQ 4000000
7
8  //initial configurations
9  _CONFIG(FOSC_INTOSCIO & WDTE_OFF & PWRTE_OFF & MCLRE_OFF & CP_OFF & CPD_OFF & BOREN_OFF
    & IESO_OFF & FCMEN_OFF);
10
11 int ADC_value;
12 int state1;
13 int const L1 = 600;
14 int const L2 = 5;
15 int i;
16
17 void Switch_on(){
18
19 ADCON0 = 0b10000001; //RA0(AN0) analogue input which take input voltage
20     ADC_value =0;
21     GO_nDONE =1; // Enable ADC
22     while(GO_nDONE);
23     ADC_value = (ADRESH << 8)+ADRESL;
24
25 if(L2 >= ADC_value)
26     {
27
28         PORTC = 0b00000011; // switch on
29         for(i=0;i<500;i++); // Switchover delay
30
31     }
32
33 else if (L1 <= ADC_value){
34     PORTC = 0b00000000; // switch off
35 }
36 }
37
38 void main()
39 {
40     // initialize the ADC
41
42     ANSEL = 0b10001111; //Channel AN0:AN1 selected since we are using RA0:RA2
    and RA4 as analogue input to ADC
43     ADCON1 = 0b00010000; //bit 4:6 ADCS<2:0> = 001 which gives Fosc/8*
44     TRISC = 0b00001000; // RC0:RC2 are the output from the PIC to drive the
    switches
45
46     state1 = 1;
47
48     //start process
49     PORTC = 0B00000000;
50     while(1)
51     {
52         Switch_on();
53
54     }
55 }

```


MATLAB and Spice Simulation of SCALED converter

B.1 Curve fitting for LED characteristics

```

1 function CurvefittingForLEDCharac
2 %by ASR and Dilini
3 sheet = xlsread('LED Philips Resistance.xlsx');
4 [vL, iL] = deal(sheet(:,1), sheet(:,2));
5
6 % suppress zero data
7 z = find(iL==0);
8 vL(z) = [];
9 iL(z) = [];
10 % remove horizontal offset
11 o = 5;
12 vL = vL - o;
13 % Model 1: After suppressing zeros, removing horizontal offset
14 %
15 % General model (via cftool in curvefit toolbox):
16 %      f(x) = a*exp(-b*x) + c*exp(-d*x) + e*exp(-f*x)
17 % Coefficients (with 95% confidence bounds):
18 a =      0.4145;      % (0.2965, 0.5325)
19 b =      1.355;      % (0.9351, 1.775)
20 c =      0.7208;      % (0.6505, 0.7911)
21 d =      0.2552;      % (0.1878, 0.3227)
22 e =      0.4365;      % (0.3368, 0.5362)
23 f =      0.03946;     % (0.02934, 0.04957)
24
25 % Goodness of fit:
26 % SSE: 0.0009457
27 % R-square: 0.9997
28 % Adjusted R-square: 0.9996
29 % RMSE: 0.006876
30
31 % anonymous function for curve fit
32 iL_curvefit = @(x) a*exp(-b*x) + c*exp(-d*x) + e*exp(-f*x);
33
34 vL_x = linspace(0, 27, 1001);
35 iL_x = iL_curvefit(vL_x);
36
37 figure(2); clf
38 subplot(211);
39 plot(vL, iL, 'k', 'markersize',12); % Experimental data
40 hold on;
41 plot(vL_x, iL_x, 'linewidth',2); % fitted curve data
42 hold off;

```

```

43 grid on; zoom on;
44 xlim([0 27]);
45 ylabel('$I_L$ [V]', 'interp', 'latex', 'fontsize',20);
46 xlabel('$V_L - 4.5$ [V]', 'interp', 'latex', 'fontsize',20);
47 L = legend('Analytical solution','Experimental data');
48 set(L,'Location','best');
49 title('$I$ vs $V$ for LED lamp (offset suppressed)', 'interp', 'latex', 'fontsize',20);
50 subplot(212);
51 % include horizontal offset
52 plot(vL+o, iL, '.k', 'markersize',12); % experimental data
53 hold on;
54 plot(vL_x+o, iL_x, 'linewidth',2); % fitted curve data
55 hold off;
56 grid on; zoom on;
57 xlim([0 27+o]);
58 ylabel('$I_L$ [V]', 'interp', 'latex', 'fontsize',20);
59 xlabel('$V_L$ [V]', 'interp', 'latex', 'fontsize',20);
60 L = legend('Analytical solution','Experimental data');
61 set(L,'Location','best');
62 title('$I$ vs $V$ for LED lamp (with offset)', 'interp', 'latex', 'fontsize',20);
63
64 %% power and resistance plots for Philips LED lamp (using fitted curve)
65
66 P = iL_x.*vL_x; % power
67 R = vL_x./iL_x; % dc resistance
68 r = diff(vL_x)./diff(iL_x); % ac (small signal) resistance
69 r = [NaN r] ;
70
71 P1 = iL'.*vL'; % power
72 R1 = vL'./iL'; % dc resistance
73 r1 = diff(vL')./diff(iL'); % ac (small signal) resistance
74 r1 = [NaN r1] ;
75
76 %Plot Power
77 figure(1); clf;
78 subplot(311);
79 hold on
80 plot(vL_x+o, P, 'linewidth',2); %plot LED power (fitted curve)
81 plot(vL'+o, P1, '.k', 'markersize',12); %plot LED power (experimental data)
82 grid on; zoom on;
83 ylabel('$P$ [W]', 'interp', 'latex', 'fontsize',20);
84 title('$P$ vs $V_L$ for LED lamp (with offset)', 'interp', 'latex', 'fontsize',20);
85 L = legend('Analytical solution','Experimental data');
86 set(L,'Location','best');
87 xlim([0 27+o]);
88
89 %Plot DC resistnce
90 subplot(312);
91 hold on;
92 plot(vL_x+o, R, 'linewidth',2); %using fitted curve
93 plot(vL'+o, R1, '.k', 'markersize',12); %experimental data
94 grid on; zoom on;
95 ylabel('$R_L$ [$\Omega$]', 'interp', 'latex', 'fontsize',20);
96 title('dc resistance: $R_L = V_L/I_L$', 'interp', 'latex', 'fontsize',20);
97 L = legend('Analytical solution','Experimental data');
98 set(L,'Location','best');
99 xlim([0 27+o]);
100
101 %Plot ac resistance
102 subplot(313);

```

```
103 hold on;
104 plot(vL_x+o, r, 'linewidth',2); %using fitted curve
105 plot(vL'+o, r1, '.k', 'markersize',12); %experimental data
106 grid on; zoom on;
107 xlabel('$V_L$ (volts)', 'interp', 'latex', 'fontsize',20);
108 title('ac resistance: $r_L = dV_L/dI_L$', 'interp', 'latex', 'fontsize',20);
109 ylabel('$r_L$ [$\Omega$]', 'interp', 'latex', 'fontsize',20);
110 L = legend('Analytical solution','Experimental data');
111 set(L, 'Location', 'best');
112 xlim([0 27+o]);
113 end
```

B.2 MATLAB Script for Charging Loop of SCALED converter

```

1 function ODE_Sol
2
3 % Investigation of SCALED RC charging loop
4 % Dilini 12-02-2018
5 clear;
6 mV_s_max = 30; % maximum solar volatge (V)
7 C = 166; % capacitance (F)
8 P_0 = 5; % Power rating of the LED lamp (W)
9 t_max = C*(mV_s_max * mV_s_max-81)/(2*P_0);
10 t = linspace(0,3100, 10001);
11 P = NaN(size(t));
12 P_LED = NaN(size(t));
13 V_c = NaN(size(t)); %SC bank voltage
14 V_L = NaN(size(t)); % LED bank voltage
15 v_c = 9; V(1)=9; % initial voltage of the capacitor
16 dt = t(2) - t(1);
17 %% Analytical Solution
18 for j = 1: length(t)-1
19     V_c = mV_s_max - sqrt((mV_s_max - v_c)^2 - (2*P_0 * t/C));
20     i = P_0./(mV_s_max - V_c); % current following through the loop
21     P = V_c .* i ; % Power delivered to the capacitor
22     P_LED = (mV_s_max -V_c).* i; % Power of the LED lamp
23     V_L = (mV_s_max -V_c);
24 end
25
26 %% Numerical Solution
27 v_L (1) = mV_s_max - V(1);
28 i_L (1) = P_0./(mV_s_max - V(1));
29 % Euler integartion
30 for k = 1: length(t)-1
31     V(k+1) = V(k)+(P_0*dt)/(C*(mV_s_max -V(k)));
32     v_L(k+1) = mV_s_max - V(k+1);
33     i_L(k+1) = C* (V(k+1)-V(k))/dt;
34 end
35
36 %% Plot results
37
38 Y = 30 * ones(size(t));
39 figure('Color', 'w')
40 subplot(2,2,1)
41 title('$v_C(t)$ for LED lamp load','interp', 'latex', 'fontsize',20)
42 hold on
43 plot(t,V_c, 'color', 'b', 'LineWidth', 2)
44 plot(t,V, 'r:', 'LineWidth', 2)
45 ylabel('$v_C(t)$ [V]','interp', 'latex', 'fontsize',20);
46 L = legend('Analytical solution', 'Numerical solution');
47 set(L,'Location', 'SouthEast');
48 xlabel('Time [s]','interp', 'latex', 'fontsize',20);
49 xlim([0,3100]);
50 grid on; zoom on;
51
52 subplot(2,2,[3,4])
53 hold on;
54 plot(t,V_L, 'LineWidth',2)
55 plot(t,v_L, 'r:', 'LineWidth', 2)
56 ylabel('$V_{L}(t)$ [V]','interp', 'latex', 'fontsize',20);
57 L = legend('Analytical solution', 'Numerical solution');
58 xlabel('Time [s]','interp', 'latex', 'fontsize',20);

```

```
59 set(L,'Location','NorthEast');
60 title('Voltage across the LED lamp','interp','latex','fontsize',20);
61 xlim([0,3100]);
62 grid on; zoom on;
63
64 subplot(2,2,2)
65 hold on;
66 plot(t,i,'LineWidth',2)
67 plot(t,i_L,'r:','LineWidth',2)
68 ylabel('$i(t)$ [A]','interp','latex','fontsize',20);
69 title('Circuit current','interp','latex','fontsize',20);
70 L = legend('Analytical solution','Numerical solution');
71 set(L,'Location','SouthEast');
72 xlabel('Time [s]','interp','latex','fontsize',20);
73 xlim([0,3100]);
74 grid on; zoom on;
75 end
```

B.3 MATLAB Script for Charging Loop of SCALED converter with parasitic resistance

```

1 function ODESolparasitic
2
3 % Investigation of SCALED RC charging loop with parasitic resistance
4 % Dilini 13-02-2018
5 % for minus solution
6 clear;
7 V_s_max = 30;           % maximum solar volatge (V)
8 C = 166;               % capacitance (F)
9 P_0 = 5;               % Power rating of the LED lamp (W)
10 r_P = linspace(0,2,5); %parasitic resistance (ohm)
11 t_max = C*(V_s_max * V_s_max - 81)/(2*P_0);
12 t = linspace(0, 3000, 1001);
13 dt = t(2)-t(1);       % time step
14 v_c = NaN(size(t));
15 i = NaN(size(t));
16 v_c(1)= 9;            % initial voltage of the capacitor (V)
17
18 %% Numerical solution using Euler intergration method
19 for k = 1:length(r_P)
20     for j= 1:length(t)-1
21         if r_P(k) ==0
22             dv_c = (P_0*dt)/(C*(V_s_max -v_c(j)));
23         else
24             dv_c = dt * ((V_s_max - v_c(j))-sqrt((V_s_max -v_c(j))^2 -4*r_P(k) *P_0))/(2*
                C*r_P(k));
25         end
26         v_c(j+1) = v_c(j)+ dv_c;
27         if v_c(j+1) >= V_s_max
28             % delete last entry: (vc exceeds Vs!), then quit
29             v_c(j+1) = NaN;
30
31             break;
32         end
33         i(j) = C*dv_c/dt;
34         % suppress complex solutions (when vc >= Vs)
35         i(imag(i) ~= 0) = NaN;
36         v_c(imag(v_c) ~= 0) = NaN;
37     end
38     % compute power in LED (dissipation), parasitic resistance (dissipation) and
        capacitor (rate of energy storage)
39     p_C = v_c .* i;
40     v_r_P = r_P(k) .* i;
41     p_LED = (V_s_max - v_c - v_r_P).*i;
42     p_r_P = v_r_P .* i;
43     v_L = (V_s_max - v_c - v_r_P);
44
45     %% Polt the results
46     figure(1);hold on;
47     subplot(221);
48     title('$v_C(t)$ for LED lamp load','interp','latex','fontsize',20)
49     hold on
50     plot(t',v_c', 'LineWidth', 2)
51     ylabel('$v_C(t)$ [V]','interp','latex','fontsize',20);
52     xlabel('Time [s]','interp','latex','fontsize',20);
53     L = cell(length(r_P),1);
54     for r = 1: length(r_P)
55         L{r}=strcat('r_P = ', num2str(r_P(r)),'\Omega');

```

```
56     end
57     M = legend(L);
58     set(M, 'Location', 'NorthWest')
59     grid on; zoom on;
60
61     subplot(222)
62     hold on
63     plot(t, i, 'linewidth',2);
64     ylabel('$i(t)$ [A]', 'interp', 'latex', 'fontsize',20);
65     xlabel('Time [s]', 'interp', 'latex', 'fontsize',20);
66     grid on; zoom on;
67     title('Circuit current', 'interp', 'latex', 'fontsize',20);
68
69     subplot(223)
70     hold on
71     plot(t, v_L, 'linewidth',2);
72     ylabel('$v_{L}(t)$ [V]', 'interp', 'latex', 'fontsize',20);
73     xlabel('Time [s]', 'interp', 'latex', 'fontsize',20);
74     grid on; zoom on;
75     title('LED Lamp Voltage', 'interp', 'latex', 'fontsize',20);
76
77     subplot(224)
78     hold on
79     plot(t, v_r_P, 'linewidth',2);
80     ylabel('$v_{r}(t)$ [V]', 'interp', 'latex', 'fontsize',20);
81     xlabel('Time [s]', 'interp', 'latex', 'fontsize',20);
82     grid on; zoom on;
83     title('Voltage across $r_{P}$', 'interp', 'latex', 'fontsize',20);
84
85 end
86 end
```

B.4 MATLAB Script for Charging Loop of SCALED converter with parasitic resistance and solar panel

```

1 function ODESolSolar
2
3 % Investigation of SCALED RC charging loop with parasitic resistance and
4 % solar
5 % Dilini 14-02-2018
6 % varing solar voltage
7 clear;
8 V_s = linspace(30,36,5);           % solar volatge (V)
9 V_s = flip(V_s);
10 C = 166;                          % capacitance (F)
11 P_0 = 10;                          % Power rating of the LED lamp (W)
12 r_P = 1;                           % parasitic resistance (ohm)
13 t = linspace(0, 2000, 1001);
14 dt = t(2)-t(1);                   % time step
15 v_c = NaN(size(t));
16 i = NaN(size(t));
17 v_c(1)= 12;                        % initial voltage of the capacitor (V)
18 E_C(1) = 0.5*C*v_c(1)*v_c(1);     % initial energy in the capacitor (J)
19
20 %% Numerical solution using Euler intergration method
21 for k = 1:length(V_s)
22     for j= 1:length(t)-1
23         dv_c = dt*((V_s(k) - v_c(j))-sqrt((V_s(k) -v_c(j))^2 -4*r_P *P_0))/...
24             (2*C*r_P);
25         v_c(j+1) = v_c(j)+ dv_c;
26         if v_c(j+1) >= V_s
27             % delete last entry: (vc exceeds Vs!), then quit
28             v_c(j+1) = NaN;
29
30             break;
31         end
32         i(j) = C*dv_c/dt;
33         % suppress complex solutions (when vc >= Vs)
34         i(imag(i) ~= 0) = NaN;
35         v_c(imag(v_c) ~= 0) = NaN;
36     end
37     % compute power in parasitic resistance (dissipation) and energy stored
38     % in the capacitor
39     E_C1 = 0.5.*C.*v_c.*v_c - E_C(1);
40     v_r_P = r_P .*i;
41     p_r_P = v_r_P .* i;
42
43     %% Polt the results
44     fig1 = figure(1);hold on;
45     subplot(211);
46     title('$v_C(t)$ for LED lamp load with the effect of $r_P$'...
47         , 'interp', 'latex', 'fontsize', 20)
48     hold on;
49     plot(t', v_c', 'LineWidth', 2)
50     ylabel('$v_C(t)$ [V]', 'interp', 'latex', 'fontsize', 20);
51     L = cell(length(V_s),1);
52     for r = 1: length(V_s)
53         L{r}=strcat('V_S = ', num2str(V_s(r)));
54     end
55     M = legend(L);
56     set(M, 'Location', 'NorthWest')
57     grid on; zoom on;

```

```

58
59     subplot(212)
60     plot(t, i, 'linewidth',2);
61     ylabel('$i(t)$ [A]', 'interp', 'latex', 'fontsize',20);
62     xlabel('Time [s]', 'interp', 'latex', 'fontsize',20);
63     L = cell(length(V_s),1);
64     for r = 1: length(V_s)
65         L{r}=strcat('V_S = ', num2str(V_s(r)));
66     end
67     M = legend(L);
68     set(M, 'Location', 'NorthWest')
69     grid on; zoom on;
70     title('Circuit current', 'interp', 'latex', 'fontsize',20);
71
72     fig2 = figure(2);hold on;
73     plot(t', E_C1, 'linewidth',2);
74     ylabel('$\big(E_{C}-E_{C(initial)}\big)$ [J]', 'interp', 'latex', 'fontsize',20);
75     xlabel('Time [s]', 'interp', 'latex', 'fontsize',20);
76     grid on; zoom on;
77     L = cell(length(V_s),1);
78     for r = 1: length(V_s)
79         L{r}=strcat('V_S = ', num2str(V_s(r)));
80     end
81     M = legend(L);
82     set(M, 'Location', 'best')
83     title('Energy stored in the capacitor', 'interp', 'latex'...
84         , 'fontsize',20);
85
86     fig3 = figure(3);hold on;
87     plot(t', p_r_P, 'linewidth',2);
88     ylabel('$P(t)$ [W]', 'interp', 'latex', 'fontsize',20);
89     xlabel('Time [s]', 'interp', 'latex', 'fontsize',20);
90     grid on; zoom on;
91     title('Power dissipation in $r_P$', 'interp', 'latex', 'fontsize',20)
92     L = cell(length(V_s),1);
93     for r = 1: length(V_s)
94         L{r}=strcat('V_S = ', num2str(V_s(r)));
95     end
96     M = legend(L);
97     set(M, 'Location', 'best')
98
99 end
100 end

```

B.5 MATLAB Script for Discharging Loop of SCALED converter

```

1 %function ODE_Sol_Discharging
2 %% Investigation of SCALED C discharging loop
3 % Dilini 14-02-2018
4 clear;
5
6 C = 166; % capacitance
7 P_0 = 5; % Power rating of the LED lamp
8 V_c(1) = 14; v_c(1)=14; % initial voltage of the capacitor
9 tmax = C*(v_c(1)*v_c(1))/(2*P_0);
10 t = linspace(0,1900, 10001);
11 dt = t(2)-t(1); % time step
12 v_c = NaN(size(t)); % capacitor voltage
13 i = NaN(size(t)); % loop current
14
15 %%% Numerical solution using Euler intergration method
16
17 for k= 1:length(t)-1
18     dv_c = -dt * P_0/(C*v_c(k));
19     v_c(k+1) = v_c(k)+ dv_c;
20     if v_c(k+1) <= 0
21         % delete last entry: (vc exceeds Vs!), then quit
22         v_c(k+1) = NaN;
23
24         break;
25     end
26     i(k) = C*dv_c/dt;
27     % suppress complex solutions (when vc >= Vs)
28     %     i(imag(i) ~= 0) = NaN;
29     %     v_c(imag(v_c) ~= 0) = NaN;
30 end
31 % compute power in LED (dissipation), parasitic resistance (dissipation)
32 %and capacitor (rate of energy storage)
33 p_C = -v_c .* i;
34 p_LED = -(v_c).*i;
35 v_L = -v_c;
36
37 %% Analytical Solution
38 for k= 1:length(t)-1
39     V_c = sqrt(V_c(1)^2-2*P_0*t/C);
40     if V_c <= 0
41         % delete last entry: (vc exceeds Vs!), then quit
42         V_c = NaN;
43         break;
44     end
45
46     I = -P_0./ V_c; % current following through the loop
47     % suppress complex solutions (when vc >= Vs)
48     I(imag(I) ~= 0) = NaN;
49     V_c(imag(V_c) ~= 0) = NaN;
50     P = -V_c .* I; % Power delivered to the capacitor
51     P_LED = -V_c.* I; % Power of the LED lamp
52     V_L = -V_c;
53 end
54
55 %% Polt the results: Analytical and Numerical
56
57 fig1 = figure(1);
58 subplot(221);

```

```

59 plot(t',V_c','LineWidth',2);
60 hold on;
61 plot(t,v_c,'r','LineWidth',2);
62 ylabel('$v_C(t)$ [V]','interp','latex','fontsize',20);
63 title('$v_C(t)$ for LED lamp load','interp','latex','fontsize',20);
64 xlabel('Time [s]','interp','latex','fontsize',20);
65 grid on; zoom on;
66 L = legend('Analytical solution','Numerical solution');
67 set(L,'Location','NorthEast');
68 hold off;
69
70 subplot(222)
71 hold on;
72 plot(t',I','linewidth',2);
73 hold on;
74 plot(t',i','r','LineWidth',2);
75 ylabel('$i(t)$ [A]','interp','latex','fontsize',20);
76 xlabel('Time [s]','interp','latex','fontsize',20);
77 grid on; zoom on;
78 title('Circuit current','interp','latex','fontsize',20);
79 L = legend('Analytical solution','Numerical solution');
80 set(L,'Location','NorthEast');
81
82 subplot(2,2,[3,4])
83 hold on;
84 plot(t',V_L','linewidth',2);
85 hold on;
86 plot(t',v_L','r','LineWidth',2);
87 ylabel('$v_{L}(t)$ [V]','interp','latex','fontsize',20);
88 xlabel('Time [s]','interp','latex','fontsize',20);
89 grid on; zoom on;
90 title('LED lamp Voltage','interp','latex','fontsize',20);
91 L = legend('Analytical solution','Numerical solution');
92 set(L,'Location','NorthEast');
93
94 fig2 = figure(2);hold on;
95 subplot(211)
96 hold on
97 plot(t',P_LED','linewidth',2);
98 plot(t',p_LED','r','LineWidth',2);
99 ylabel('$P(t)$ [W]','interp','latex','fontsize',20);
100 grid on; zoom on;
101 ylim([0, 6]);
102 L = legend('Analytical solution','Numerical solution');
103 set(L,'Location','SouthEast');
104 title('LED Power','interp','latex','fontsize',20)
105
106 subplot(212)
107 hold on;
108 plot(t',P','linewidth',2);
109 plot(t',p_C','r','LineWidth',2);
110 ylabel('$P(t)$ [W]','interp','latex','fontsize',20);
111 xlabel('Time [s]','interp','latex','fontsize',20);
112 grid on; zoom on;
113 ylim([0, 6]);
114 title('Capacitor Power','interp','latex','fontsize',20)
115 L = legend('Analytical solution','Numerical solution');
116 set(L,'Location','SouthEast');

```

B.6 MATLAB Script for Discharging Loop of SCALED converter with parasitic resistance

```

1 %% Investigation of SCALED C discharging loop
2 % Dilini 14-02-2018
3 clear;
4 C = 166; % capacitance (F)
5 P_0 = 5; % Power rating of the LED lamp
6 t = linspace(0,1900, 1001);
7 r_P = linspace(0,0.5,5);
8 dt = t(2)-t(1); % time step
9 v_c = NaN(size(t));
10 i = NaN(size(t));
11 V_c(1) = 14; v_c(1)=14; % initial voltage of the capacitor
12
13 %%% Numerical solution using Euler intergration method
14
15 for k = 1:length(r_P)
16     for j= 1:length(t)-1
17         if r_P(k) == 0
18             dv_c = -dt * P_0/(C*v_c(j));
19         else
20             dv_c = dt * (-v_c(j)+sqrt(v_c(j)^2-4*r_P(k)*P_0))/(2*C*r_P(k));
21         end
22         v_c(j+1) = v_c(j)+ dv_c;
23         if v_c(j+1) <= 0
24             % delete last entry: (vc exceeds Vs!), then quit
25             v_c(j+1) = NaN;
26
27             break;
28         end
29         i(j) = C*dv_c/dt;
30         % suppress complex solutions (when vc >= Vs)
31         i(imag(i) ~= 0) = NaN;
32         v_c(imag(v_c) ~= 0) = NaN;
33     end
34     % compute power in LED (dissipation), parasitic resistance (dissipation)
35     %and capacitor (rate of energy storage)
36     p_C = -v_c .* i;
37     v_L = -(v_c+r_P(k).*i);
38     p_LED = v_L.*i;
39     p_r = r_P(k).*i.*i;
40     v_r_P = r_P(k).*i;
41     %%% Polt the results: Analytical and Numerical
42     fig1 = figure(1);
43     hold on;
44     subplot(221);
45     title('$v_C(t)$ for LED lamp load','interp','latex','fontsize',20)
46     hold on
47     plot(t',v_c','LineWidth',2);
48     ylabel('$v_C(t)$ [V]','interp','latex','fontsize',20);
49     xlabel('Time [s]','interp','latex','fontsize',20);
50     L = cell(length(r_P),1);
51     for r = 1: length(r_P)
52         L{r}=strcat('r_P = ', num2str(r_P(r)),'\Omega');
53     end
54     M = legend(L);
55     set(M,'Location','NorthEast')
56     grid on; zoom on;
57

```

```
58     subplot(222)
59     hold on
60     plot(t,'i','LineWidth',2);
61     ylabel('$i(t)$ [A]', 'interp', 'latex', 'fontsize',20);
62     xlabel('Time [s]', 'interp', 'latex', 'fontsize',20);
63     grid on; zoom on;
64     title('Circuit current', 'interp', 'latex', 'fontsize',20);
65
66     subplot(223)
67     hold on
68     plot(t, v_L, 'linewidth',2);
69     ylabel('$v_{L}(t)$ [V]', 'interp', 'latex', 'fontsize',20);
70     xlabel('Time [s]', 'interp', 'latex', 'fontsize',20);
71     grid on; zoom on;
72     title('LED Lamp Voltage', 'interp', 'latex', 'fontsize',20);
73
74     subplot(224)
75     hold on
76     plot(t, v_r_P, 'linewidth',2);
77     ylabel('$v_{r}(t)$ [V]', 'interp', 'latex', 'fontsize',20);
78     xlabel('Time [s]', 'interp', 'latex', 'fontsize',20);
79     grid on; zoom on;
80     title('Voltage across $r_{Pd}$', 'interp', 'latex', 'fontsize',20);
81 end
```

B.7 MATLAB Script for SCALED converter

```

1 % MATLAB simulation of SCALED Converter done by: Dilini Jayananda
2 dt = 1;
3 t=0:dt:12000;
4 i1 = NaN(size(t)); % LED bank1 current
5 v_L1 = NaN(size(t)); % LED bank1 voltage
6 v_c1 = NaN(size(t)); % Supercapacitor (SC) bank1 voltage
7 v_c1(1) = 12; % Initial voltage of SC bank1 voltage
8 i2 = NaN(size(t)); % LED bank2 current
9 v_L2 = NaN(size(t)); % LED bank2 voltage
10 v_c2 = NaN(size(t)); % SC bank 2 voltage
11 v_c2(1) = 21; % SC bank 2 initial voltage
12 V_s = 33; % operating voltage of solar panel
13 r_Pc = 1; % charging loop resistance
14 r_Pd = 1; % charging loop resistance
15 C= 166; % SC bank capacitance
16 P = 10; % LED power
17
18 if v_c1(1) == 9
19     state = 0;
20 else
21     state = 1;
22 end
23
24 for k=1: length(t)-1
25     if state == 0
26         dv_c1 = dt * ((V_s - v_c1(k)) - sqrt((V_s - v_c1(k))^2 - 4*r_Pc * P)) / (2*C*r_Pc);
27         v_c1(k+1) = dv_c1 + v_c1(k);
28         i1(k) = C*dv_c1/dt;
29         v_L1(k) = V_s - i1(k)*r_Pc - v_c1(k);
30
31         dv_c2 = dt * (-v_c2(k) + sqrt(v_c2(k)^2 - 4*r_Pd*P)) / (2*C*r_Pd);
32         v_c2(k+1) = dv_c2 + v_c2(k);
33         i2(k) = C*dv_c2/dt;
34         v_L2(k) = -(v_c2(k) + r_Pd.*i2(k));
35         a(k) = v_L1(k)*i1(k) + v_L2(k).*i2(k);
36         b(k) = V_s * (i1(k));
37         %suppress complex solutions (when vc >= Vs)
38         i1(imag(i1) ~= 0) = NaN;
39         v_c1(imag(v_c1) ~= 0) = NaN;
40         %suppress complex solutions (when vc <= 0)
41         i2(imag(i2) ~= 0) = NaN;
42         v_c2(imag(v_c2) ~= 0) = NaN;
43
44         if v_c2(k+1) <= 12 %v_L1(k) <= 9
45             state = 1;
46         end
47     end
48     if state == 1
49         dv_c1 = dt * (-v_c1(k) + sqrt(v_c1(k)^2 - 4*r_Pd*P)) / (2*C*r_Pd);
50         v_c1(k+1) = dv_c1 + v_c1(k);
51         i1(k) = C*dv_c1/dt;
52         v_L1(k) = -(v_c1(k) + r_Pd.*i1(k));
53
54         dv_c2 = dt * ((V_s - v_c2(k)) - sqrt((V_s - v_c2(k))^2 - 4*r_Pc * P)) / (2*C*r_Pc);
55         v_c2(k+1) = dv_c2 + v_c2(k);
56         i2(k) = C*dv_c2/dt;
57         v_L2(k) = V_s - i2(k)*r_Pc - v_c2(k);
58         a(k) = v_L1(k)*i1(k) + v_L2(k).*i2(k);

```

```

59     b(k) = V_s * (i2(k));
60
61     % suppress complex solutions (when vc >= Vs)
62     i2(imag(i2) ~= 0) = NaN;
63     v_c2(imag(v_c2) ~= 0) = NaN;
64     %suppress complex solutions (when vc <= 0)
65     i1(imag(i1) ~= 0) = NaN;
66     v_c1(imag(v_c1) ~= 0) = NaN;
67
68     if v_c1(k+1)<= 12
69         state =0;
70     end
71 end
72 end
73 % For plot the results
74 fig6 = figure(6);
75 hold on;
76 subplot(211)
77 hold on;
78 plot(t,v_c1,'—','color','#0072BD','LineWidth',2);
79 plot(t,v_c2,'-','color','#D95319','LineWidth',2);
80 ylabel('$v_C(t)$ [V]','interp','latex','fontsize',12);
81 title('Voltage of SC banks','interp','latex','fontsize',12)
82 M = legend('SC bank 1','SC bank 2');
83 set(M,'Location','best','Interpreter','latex');
84 ylim([12 22]); xlim([0 12000]);
85 grid on; zoom on;
86
87 subplot(212)
88 hold on;
89 plot(t,v_L1,'—','color','#0072BD','LineWidth',2);
90 plot(t,v_L2,'-','color','#D95319','LineWidth',2);
91 ylabel('$v_L(t)$ [V]','interp','latex','fontsize',12);
92 title('Voltage of LED lamp loads','interp','latex','fontsize',12)
93 M = legend('LED lamp load 1','LED lamp load 2');
94 set(M,'Location','best','Interpreter','latex');
95 ylim([-22 22]); xlim([0 12000]);
96 xlabel('Time [s]','interp','latex','fontsize',12);
97 grid on; zoom on;
98 hold off;

```

B.8 Simulink model of SCALED converter with battery bank and MPPT controller

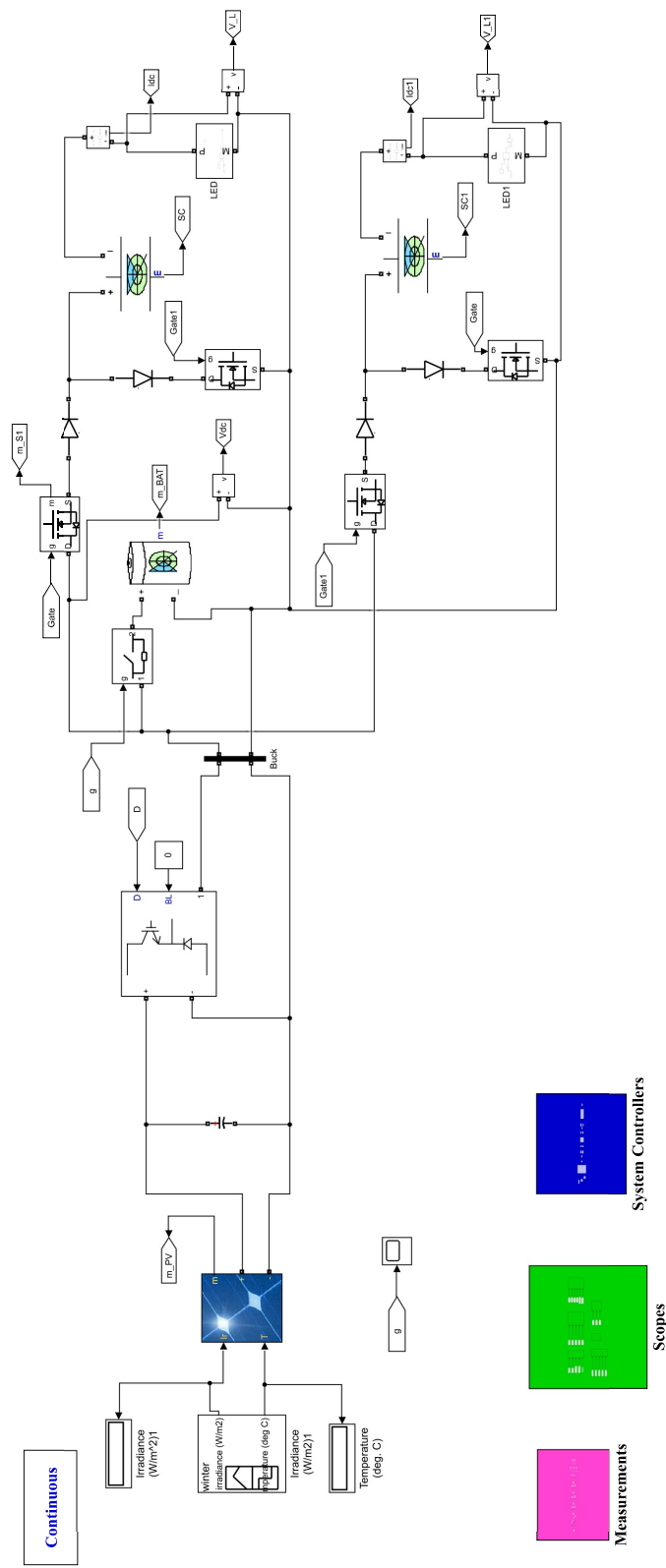


Figure B.1: Simulink model of SCALED converter with battery bank and MPPT controller

B.9 MATLAB Script for MPPT controller in Simulink model

```

1 function D = PandO(Param, Vpv, Ipv)
2
3 % Param input:
4 Dinit = Param(1); %Initial value for D output
5 Dmax = Param(2); %Maximum value for D
6 Dmin = Param(3); %Minimum value for D
7 deltaD = Param(4); %Increment value used to increase/decrease the duty cycle D
8 % ( increasing D = decreasing Vref )
9 %initialize the internal values for voltage, duty cycle and power
10 persistent Vn Pn Dn;
11 dataType = 'double';
12 %initialize deltaD
13 if isempty(Vn)
14     Vn=0;
15     Pn=245;
16     Dn=Dinit;
17 end
18
19 % calculate the measured power
20 Ppv = Vpv*Ipv;
21
22 if (Ppv-Pn)~= 0
23     if (Ppv-Pn)>0
24         if (Vpv-Vn)>0
25             D = Dn-deltaD;
26         else
27             D = Dn+deltaD;
28         end
29     else
30         if (Vpv-Vn)>0
31             D = Dn+deltaD ;
32         else
33             D = Dn-deltaD;
34         end
35     end
36 else
37     D = Dn;
38 end
39 if D >= Dmax || D<= Dmin
40     D=Dn;
41 end
42 % update internal values
43 Dn = D;
44 Vn = Vpv;
45 Pn = Ppv;

```

B.10 MATLAB Script for SCALED controller in Simulink model

```
1 function [g,gn] = SW(V1,V2)
2
3 persistent V_SC1 V_SC2 d d1 eps ;
4
5 dataType = 'double';
6
7 if isempty(V_SC1)
8 V_SC1 = 17;
9 V_SC2 = 9 ;
10 d=1;
11 d1=-1;
12 eps = 0.01;
13 end
14
15 if (abs(V2) <= (V_SC2+eps)) && (abs(V2)>=(V_SC2-eps))
16     d = -1;
17     d1 = 1;
18 elseif (abs(V1) <= (V_SC2+eps)) && (abs(V1)>=(V_SC2-eps))
19     d = 1;
20     d1 = -1;
21 end
22
23 V_SC1 = 17;
24 V_SC2 = 9 ;
25 g= d;
26 gn = d1;
```

B.11 Spice Net list for SCALED converter

B.11.1 Voltage-controlled switch in LTSpice

Introduction

LTSpice incorporates a large number of excellent Field Effect Transistor (FET) models, but sometimes you need to simulate a simple switch that opens and closes at specific times or under certain conditions. This switch is a special kind of voltage-controlled resistor. This model was designed to minimize numerical problems. However, there are a few things to consider when configuring it. This document discusses how to use a simple voltage controlled switch in LTSpice according to your requirements.

Insert and configure a switch in LTSpice

It is better to use **SPICE netlist** in LTSpice rather than using the schematic. General form to use a voltage-controlled switch in netlist is given below.

General form:

S<name>< (+) switch node>< (-) switch node>< (+) controlling node>< (-) controlling node><model name>

Example:

S1 1 2 3 0 SWON

This means switch S1 is connected across node 1 and 2 where switching operation (switch's impedance between node 1 and 2) is controlled by the voltage across node 3 and 0. Model name of the switch is SWON. We have to define the model parameters to operate the switch according to our requirements.

Model form:

.MODEL <model name> SW [model parameters]

Model parameters are given in Table B.1. In here G_{MIN} is the minimum conductance used for any branch. Default value used for G_{MIN} in LTSpice is $1.0E-12 \Omega^{-1}$. the voltage controlled switch is deigned to trips at $(V_t - V_h)$ and $(V_h + V_t)$. This switch has three distinct modes of voltage control as depicts in Table B.2, depending on the value of V_h .

Example 01:

Lets consider circuit shown in Figure B.2 with a voltage having the characteristics shown in Figure B.3. Switch S1 should be turn on when $V_{12} \geq 4.5$ V and Switch S1 should turn off when $V_{12} \leq 3$ V. In this case $(V_h + V_t)$ have to use the turn on voltage (at which voltage we need to close the switch) and for $(V_t - V_h)$ have to turn off voltage (at which voltage we need to open the switch).

$$V_h + V_t = 4.5 \quad (B.1)$$

$$V_t - V_h = 3 \quad (B.2)$$

By solving eq: (1.20) and (B.2) we can derive the required values for V_h and V_t as 0.75 an 3.75 respectively. So we can define the switch model as:

S1 2 3 1 2 SWOC

.model SWOC SW($R_{on} = 50$ m $R_{off} = 10000$ G $V_t = 3.75$ $V_h = 0.75$)

Figure B.3 shows the voltage across resistor R1. As depicts in Figure B.4 switch closes when voltage across node 1 to 2 reaches 4.5 V and opens when voltage reaches to 3 V. Switch S1 is operating properly as we wanted.

Example 02:

Table B.1: Model parameters

Model parameter	Description	Default value	Unit
V_t	Threshold voltage	0.0	V
V_h	Hysteresis voltage	0.0	V
R_{on}	On resistance	1.0	Ω
R_{off}	Off resistance	$\frac{1}{G_{MIN}}$	Ω
L_{ser}	Series inductance	0.0	H
V_{ser}	Series voltage	0.0	V
I_{limit}	Current limit	Infinity	A

Table B.2: Three operating models of voltage controlled switch

Value of V_h	Mode
0.0	Switch is completely on or off if control voltage is above the threshold V_h
Positive	Switch shows hysteresis, controlled by a Schmitt trigger with trip points at $(V_t - V_h)$ and $(V_h + V_t)$
Negative	Smooth transition between R_{on} R_{off} . Transition occurs between the control voltages of $(V_t - V_h)$ and $(V_h + V_t)$

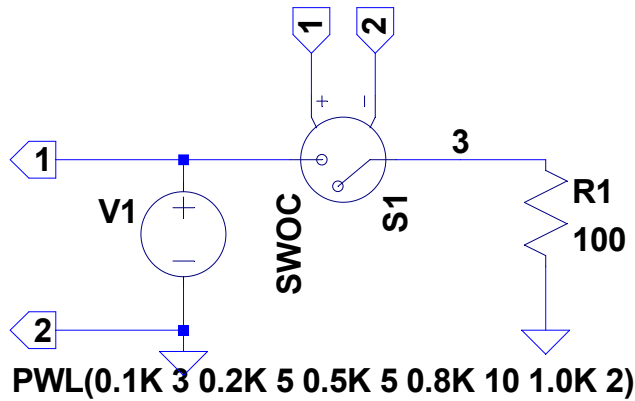


Figure B.2: Schematic diagram for example 1

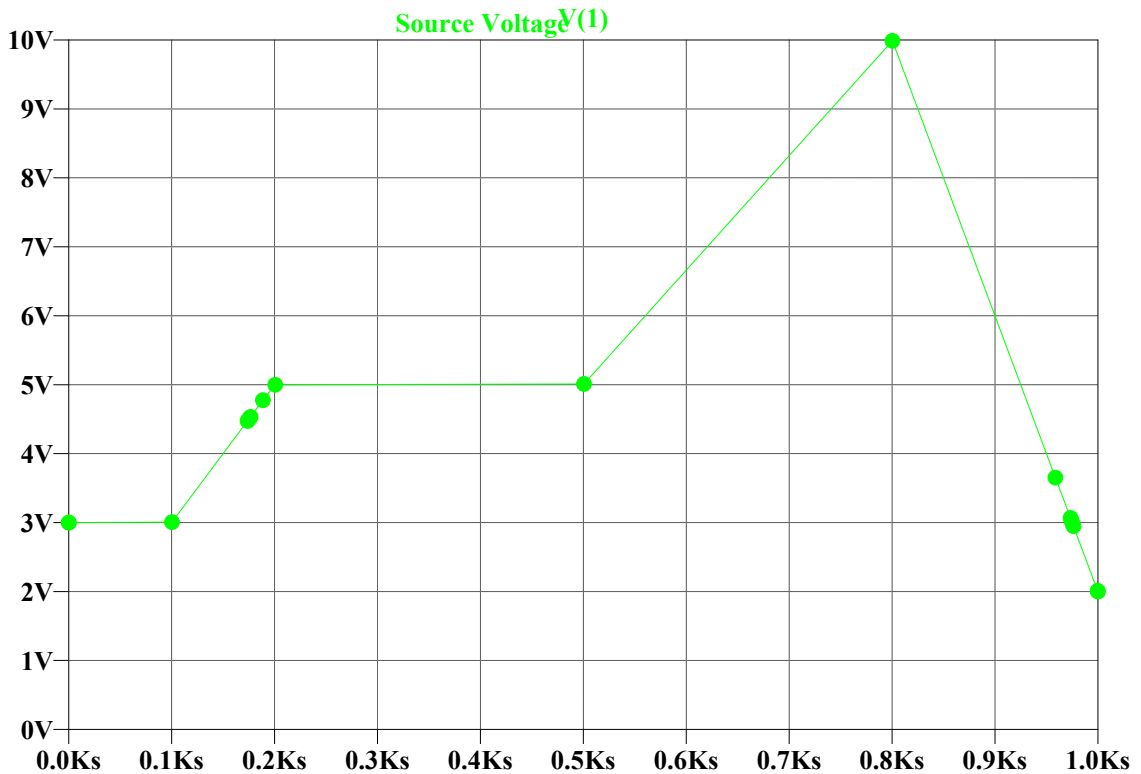


Figure B.3: Voltage source characteristics

Let's consider the circuit shown in Figure B.5. Lets assume capacitor C1 is initially charged to 21 V. When capacitor charge to 21 V it should discharge to the R1. Operating Voltage range of R1 should be between 12 V to 21 V. (i.e initially we want to close S2 and open S1).

In this example we are not able to consider the resistor voltage as our control voltage of the two switches because during the discharging phase of the capacitor voltage across the R1 will be negative. So we have to consider the voltage

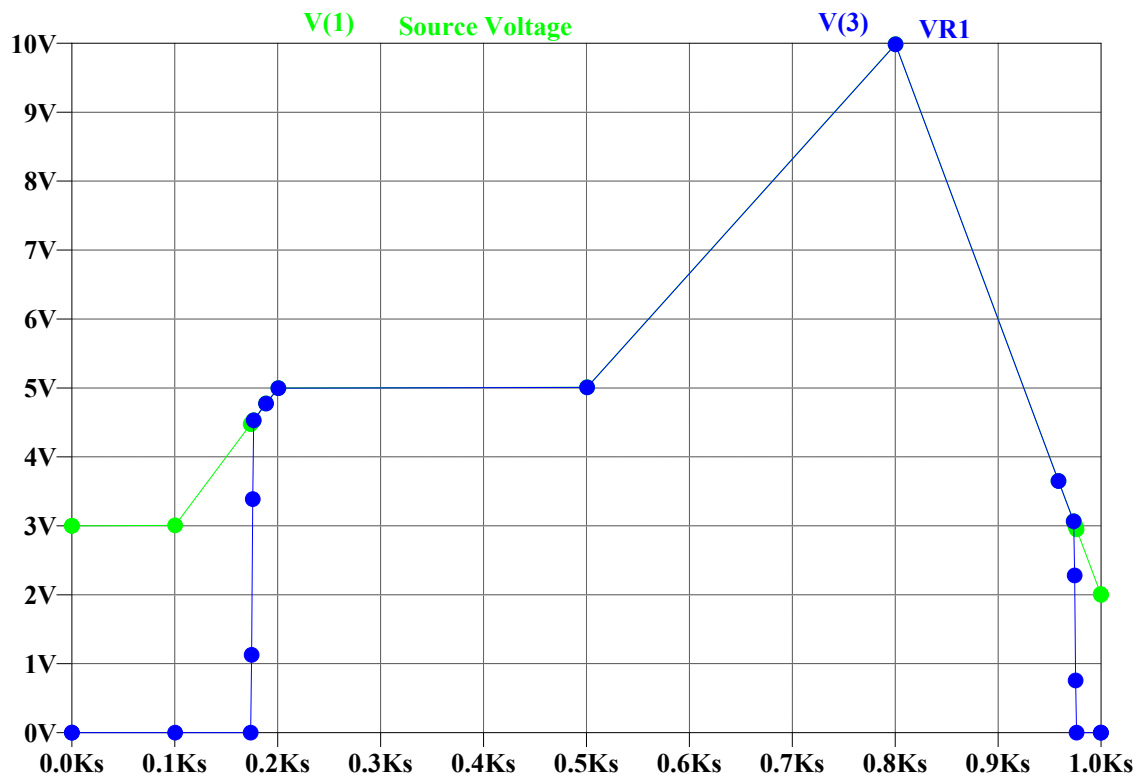


Figure B.4: Voltage across R1

across the capacitor C1.

$$V_h + V_t = 21 \quad (\text{B.3})$$

$$V_t - V_h = 12 \quad (\text{B.4})$$

By solving eq: (B.1) and (B.2) we can derive the required values for V_h and V_t as 4.5 and 16.5 respectively.

Since initially S1 should be open and S2 should be close we have to set $R_{on} = 10000 \text{ G}$ $R_{off} = 50 \text{ m}$ for S1 and $R_{on} = 50 \text{ m}$ $R_{off} = 10000 \text{ G}$ for S2.

LTSpice netlist for this problem is as below:

```
V1 1 0 33
C1 2 3 166 V=51.3 Rser=0.001 Lser=0 IC=12
R 3 0 20
S1 2 1 2 3 SWOC
S2 0 2 2 3 SWOD
.tran 0 12000 0 1 UIC
.model SWOC SW(Ron = 10000 G Roff = 50 m Vt = 16.5 Vh = 4.5)
.model SWOD SW(Ron = 50 m Roff = 10000 G Vt = 16.5 Vh = 4.5)
```

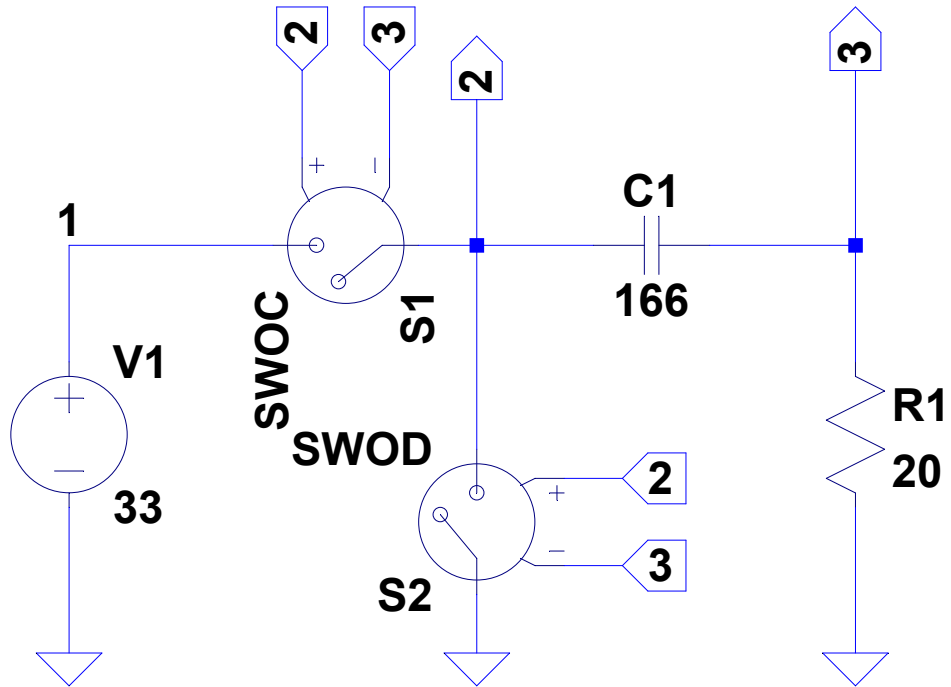


Figure B.5: Schematic diagram for example 2

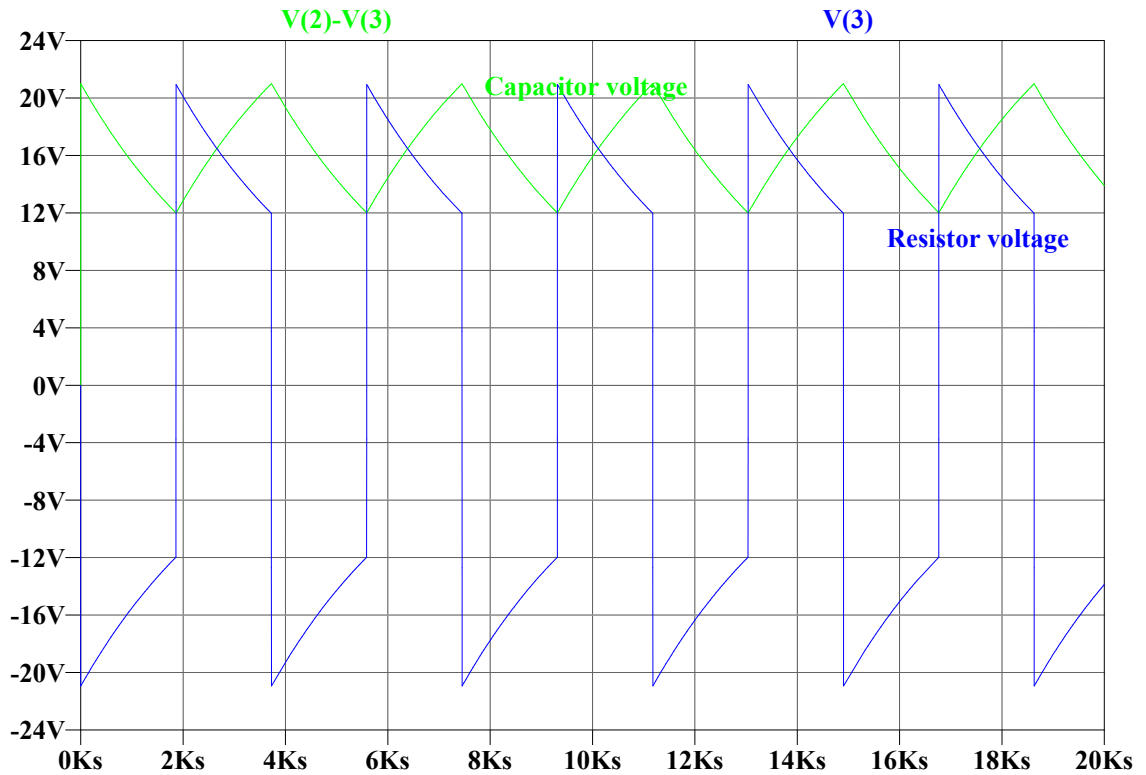


Figure B.6: Voltage waveforms for example 2

Numeric value conventions in LTSpice

Table B.3: Appropriate scale suffix

Scale	Symbol	Symbol
10^{-15}	F	femto
10^{-12}	P	pico
10^{-9}	N	nano
10^{-6}	U	micro
10^{-3}	m	milli
10^3	K	kilo
10^6	MEG	mega
10^9	G	giga
10^{12}	T	tera

B.11.2 Net list for SCALED converter with solar model

```
*H:\RESEARCH\workings\simulations\Solar Cell\LT spice\PV\newmodel.asc XPV PV 0 pv_sim2
C1 1 2 166 V=51.3 Rser=0.001 Lser=0 IC=12
B$LED 2 0 P=10
S1 1 PV 1 2 SWOC
S2 0 1 1 2 SWOD
S4 3 PV 3 4 SWOC1
S5 0 3 3 4 SWOD1
C2 3 4 166 V=51.3 Rser=0.001 Lser=0 IC = 21
B$LED1 4 0 P=10
I1 PV 0 1
*block symbol definitions
.subckt pv_sim2 V_PV+ V_PV-
XPV_Panel 3 V_PV+ V_PV- pv
I$G 0 3 Iph
.param TEMP 298
.param TR=273+25
.param DT = TEMP -TR
.param Isc = 8.78
.param G 1000
.param Iph = Isc* G/1000 + DT*3.4242M
.ends pv_sim2
.subckt pv G Vpv+ Vpv-
D _PV G Vpv- D_CELL
Rp G Vpv- Rp
Rs 2 G Rs
Epv Vpv+ Vpv- 2 Vpv- N
FCell Vpv- 2 Epv 1
.model D_CELL D IS=IS
.param Rs = 0.0042
*.param N=37
*.param N=60
.param N=54
.param TEMP 298
.Param TR = 273 + 25
.Param DT = TEMP - TR
.param Isc = 8.78
.param Vmp = 30.1
*.param Vmp = 18.56
*.param Vmp = 28
.param Imp = 8.31
.param n =1.2
.param Irs_T = 2.6908e-10
```

```
.param a = EXP((12997.03006/n) * ( (1/TEMP) - (1/TR)) )
.param IS = a*Irs_T* PWR((TR/TEMP),(3/n))
.param Vt = (n*1.3805e-23/1.602e-19)*TR
.param b = (Vmp - Imp*Rs)*(8.78-Imp)-n*Vt*Imp
.param c = (Vmp- Imp*Rs)*(Vmp-Rs*(8.78-Imp)-n*Vt)
.param Rp = c/b
.ends pv
.model D D
.lib C:\Users\dukju1\Documents\LTspiceXVII\lib\cmp\standard.dio
.tran 0 12000 0 1 UIC
.model SWOC SW(Ron= 10000G Roff =50m Vt=16.5 Vh=4.5)
.model SWOD SW(Ron= 50m Roff =10000G Vt=16.5 Vh=4.5)
.model SWOC1 SW((Ron= 10000G Roff =50m Vt=16.5 Vh=4.5)
*.model SWOD1 SW(Ron= 50m Roff =10000G Vt=16.5 Vh=4.5)
*.model SWOC SW(Ron= 10000G Roff =50m Vt=11.5 Vh=2.5)
*.model SWOD SW(Ron= 50m Roff =10000G Vt=11.5 Vh=2.5)
*.model SWOC1 SW((Ron= 10000G Roff =50m Vt=11.5 Vh=2.5)
*.model SWOD1 SW(Ron= 50m Roff =10000G Vt=11.5 Vh=2.5)
.backanno
.end
```


MATLAB codes

C.1 Loss circumvention concept

```

1 k=0:0.1:1;
2 m=1:0.1:10;
3 [k,m]= meshgrid(k,m);
4 eta = 100*(1+k)./(2*m);
5 eta1 = 100*(1+k+2*m)./(4*m);
6 eta2 = 100*(1+k+18*m)./(20*m);
7
8 figure3 = figure;
9 colormap(jet);
10 axes1 = axes('Parent',figure3,...
11     'Position',[0.110190476190476 0.13079101837096 0.656904761904762 0.79420898162904]);
12 hold(axes1,'on');
13
14 surf(k,m,eta,'Parent',axes1);
15 surf(k,m,eta1,'Parent',axes1);
16 surf(k,m,eta2,'Parent',axes1);
17 % Create xlabel
18 xlabel('\bf Charging Efficiency \% ','FontSize',12,'Interpreter','latex');
19 % Create ylabel
20 ylabel('\bf m ','FontSize',12,'Interpreter','latex');
21 % Create xlabel
22 xlabel('\bf k ','FontSize',12,'Interpreter','latex');
23 grid on;
24 zoom on;
25 view(axes1,[115.559761484099 34.3131736526947]);
26 grid(axes1,'on');
27 % Create colorbar
28 colorbar(axes1,'Position',...
29     [0.908166666666665 0.118886256466198 0.0380952380952385 0.794208981629041]);
30 % Create textarrow
31 annotation(figure3,'textarrow',[0.744642857142854 0.673214285714283],...
32     [0.672809523809525 0.607142857142858],'String',{'\bf r_{lp} : R.L = 1:1'});
33
34 % Create textarrow
35 annotation(figure3,'textarrow',[0.7625 0.696428571428571],...
36     [0.510904761904764 0.435714285714288],'String',{'\bf r_{lp} only'});
37
38 % Create textarrow
39 annotation(figure3,'textarrow',[0.742857142857142 0.63392857142857],...
40     [0.889476190476192 0.773809523809525],'String',{'\bf r_{lp} : R.L = 1:9'});
41 %print('LCC','-dpdf','-r300');

```


References

- [1] A. Finkel, “The AC/DC current wars make a comeback Online at:<https://cosmosmagazine.com/technology/tesla-vs-edison-the-ac-dc-current-wars-make-a-comeback/>.”
- [2] E. Nix, “How Edison, Tesla and Westinghouse Battled to Electrify America Online at:<https://www.history.com/news/what-was-the-war-of-the-currents>.”
- [3] P. Asmus, “Why Thomas Edison Was Both Right—and Wrong—about Direct Current Distribution Networks Online at:<https://www.tdworld.com/transmission-reliability/article/20971865/why-thomas-edison-was-both-rightand-wrongabout-direct-current-distribution-networks>.”
- [4] L. Beiler, “The War of the Electric Currents Online at:<https://www.paradisolarenergy.com/blog/the-war-of-the-electric-currents>.”
- [5] Wikipedia, “War of the currents Online at: <https://en.wikipedia.org/wiki/War-of-the-currents>.”
- [6] R. Singh, G. F. Alapatt, and G. Bedi, “Why and how Photovoltaics will Provide Cheapest Electricity in the 21st Century,” *Electronics and Energetics*, vol. 27, no. 2, pp. 275–298, June 2014.
- [7] EIA, “Renewable Sources, Online at: <https://www.eia.gov/energyexplained/solar/>, Accessed on: 2016-10-16.”
- [8] —, “Concentrating solar power technologies offer utility-scale power production, Online at:<https://www.eia.gov/todayinenergy/detail.php?id=530>, Accessed on: 2019-10-16.”
- [9] EECA, “Renewable Energy Sources, Online at: <https://www.eeca.govt.nz/energy-use-in-new-zealand/renewable-energy-resources/>, Accessed on: 2016-10-16.”
- [10] —, “Solar in New Zealand, Online at: <https://www.eeca.govt.nz/energy-use-in-new-zealand/renewable-energy-resources/solar/>, Accessed on: 2019-10-16.”
- [11] M. A. Green, K. Emery, Y. Hishikawa, W. Warta, and E. D. Dunlop, “Solar cell efficiency tables (Version 45),” *Progress in photovoltaics: research and applications*, vol. 23, no. 0, pp. 1–9, 2015.
- [12] —, “Solar cell efficiency tables (version 48),” *Progress in Photovoltaics: Research and Applications*, vol. 24, no. 57, pp. 905–913, 2016.
- [13] V. Khanna, B. K. Das, and D. Bisht, “Matlab/simelectronics models based study of solar cells,” *International Journal of Renewable Energy Research (IJRER)*, vol. 3, no. 1, pp. 30–34, 2013.

- [14] M. A. Islam, N. Mohammad, and P. S. Khan, "Modeling and performance analysis of a generalized photovoltaic array in matlab," in *2010 Joint International Conference on Power Electronics, Drives and Energy Systems & 2010 Power India*. IEEE, 2010, pp. 1–5.
- [15] M. Bouzguenda, T. Salmi, A. Gastli, and A. Masmoudi, "Evaluating solar photovoltaic system performance using matlab," in *2012 First International Conference on Renewable Energies and Vehicular Technology*. IEEE, 2012, pp. 55–59.
- [16] R. Krishan, Y. R. Sood, and B. U. Kumar, "The simulation and design for analysis of photovoltaic system based on matlab," in *2013 International Conference on Energy Efficient Technologies for Sustainability*. IEEE, 2013, pp. 647–651.
- [17] F. F. Muhammad, M. Y. Yahya, S. S. Hameed, F. Aziz, K. Sulaiman, M. A. Rasheed, and Z. Ahmad, "Employment of single-diode model to elucidate the variations in photovoltaic parameters under different electrical and thermal conditions," *PLOS ONE*, vol. 12, no. 8, pp. 1–20, 08 2017. [Online]. Available: <https://doi.org/10.1371/journal.pone.0182925>
- [18] M. Wolf and H. Rauschenbach, "Series resistance effects on solar cell measurements," *Advanced energy conversion*, vol. 3, no. 2, pp. 455–479, 1963.
- [19] N. Kularatna, "Supercapacitor Assisted Low Dropout Regulators (SCALDO) for high efficiency DC-DC converters for DC microgrid applications," in *2015 IEEE First International Conference on DC Microgrids (ICDCM)*, June 2015, pp. 333–338.
- [20] R. Singh, "Report of DC Energy Efficiency Committee," IEEE Power and Energy Society, DC at Home Committee Report Washington DC, 29 July 2014, Washington DC.
- [21] D. Kumar, F. Zare, and A. Ghosh, "DC Microgrid Technology: System Architectures, AC Grid Interfaces, Grounding Schemes, Power Quality, Communication Networks, Applications, and Standardizations Aspects," *IEEE Access*, vol. 5, pp. 12 230–12 256, 2017.
- [22] V. Vossos, K. Garbesi, and H. Shen, "Energy savings from direct-DC in U.S. residential buildings," *Energy and Buildings*, vol. 68, pp. 223–231, 2014.
- [23] S. Backhaus, G. W. Swift, S. Chatzivasileiadis, W. Tschudi, S. Glover, M. Starke, J. Wang, M. Yue, and D. Hammerstrom, "DC Microgrids Scoping Study: Estimate of Technical and Economic Benefits," Los Alamos National Laboratory, Los Alamos National Laboratory Report New Mexico, March 2015, New Mexico.
- [24] N. Ayai, T. Hisada, T. ShibaTa, H. Miyoshi, T. Iwasaki, and K. Tayama, "DC Micro Grid System," SEI Technical Review, Electric Wire & Cable ,Energy, October 2012.
- [25] A. T. Elsayed, A. A. Mohamed, and O. A. Mohammeda, "DC microgrids and distribution systems: An overview," *Electric Power Systems Research*, vol. 2, pp. 407–417, 2014.
- [26] P. Loomba, S. Asgotraa, and R. Podmore, "Supercapacitors for distributed energy storage in DC microgrids and loads," in *2016 IEEE PES Power Africa Conference*, 2016, pp. 204–208.
- [27] S. Kouro, J. I. Leon, and L. G. F. Dmitri Vinnikov, "Grid-Connected Photovoltaic Systems: An Overview of Recent Research and Emerging PV Converter Technology," *IEEE Industrial Electronics Magazine*, March 2015.
- [28] S. Babaa, M. Armstrong, and V. Pickert, "Overview of Maximum Power Point Tracking Control Methods for PV systems," *Power and Energy Engineering*, vol. 2, pp. 59–72, 2014.

- [29] N. Kularatna, *Energy Storage Devices for Electronic Systems: Rechargeable Batteries and Supercapacitors*. ELSEVIER, November 2013.
- [30] Y. Liang, C.-Z. Zhao, H. Yuan, Y. Chen, W. Zhang, J.-Q. Huang, D. Yu, Y. Liu, M.-M. Titirici, Y.-L. Chueh *et al.*, “A Review of Rechargeable Batteries for Portable Electronic Devices,” *InfoMat*, vol. 1, no. 1, pp. 6–32, 2019.
- [31] M.-S. Balogun, H. Yang, Y. Luo, W. Qiu, Y. Huang, Z.-Q. Liu, and Y. Tong, “Achieving High Gravimetric Energy Density for Flexible Lithium-ion Batteries Facilitated by Core–Double-Shell Electrodes,” *Energy & Environmental Science*, vol. 11, no. 7, pp. 1859–1869, 2018.
- [32] I. Buchmann, “Bu-107: Comparison table of secondary batteries, Online at: <https://batteryuniversity.com/learn/article/secondarybatteries>.”
- [33] L. SAMWHA Capacitor Co., *ESD-SCAP Catalogue, SAMWHA Capacitor Co.,Ltd., 2018*, 2018.
- [34] A. Dolara, R. Faranda, and S. Leva, “Energy comparison of seven MPPT techniques for PV systems,” *Journal of Electromagnetic Analysis and Applications*, vol. 1, no. 3, pp. 152–162, 2009.
- [35] M. A. G. de Brito, L. P. Sampaio, L. G. Junior, and C. A. Canesin, “Evaluation of mppt techniques for photovoltaic applications,” in *2011 IEEE International Symposium on Industrial Electronics*, June 2011, pp. 1039–1044.
- [36] M. A. G. de Brito, L. P. Sampaio, G. Luigi, G. A. e Melo, and C. A. Canesin, “Comparative analysis of mppt techniques for pv applications,” in *2011 International Conference on Clean Electrical Power (ICCEP)*, June 2011, pp. 99–104.
- [37] M. Adly, M. Ibrahim, and H. El Sherif, “Comparative study of improved energy generation maximization techniques for photovoltaic systems,” in *2012 Asia-Pacific Power and Energy Engineering Conference*, March 2012, pp. 1–5.
- [38] B. Subudhi and R. Pradhan, “A comparative study on maximum power point tracking techniques for photovoltaic power systems,” *IEEE Transactions on Sustainable Energy*, vol. 4, no. 1, pp. 89–98, Jan 2013.
- [39] M. A. G. D. Brito, L. Galotto, L. P. Sampaio, G. de Azevedo e Melo, and C. A. Canesin, “Evaluation of the main MPPT techniques for photovoltaic applications,” *IEEE transactions on industrial electronics*, vol. 60, no. 3, pp. 1156–1167, 2013.
- [40] D. Linzen, S. Buller, E. Karden, and R. W. De Doncker, “Analysis and evaluation of charge-balancing circuits on performance, reliability, and lifetime of supercapacitor systems,” *IEEE Transactions on Industry Applications*, vol. 41, no. 5, pp. 1135–1141, Sep. 2005.
- [41] J. Tabuchi, T. Saito, Y. Kibi, and A. Ochi, “Large capacitance electric double layer capacitor using activated carbon/carbon composite,” *IEEE Transactions on Components, Hybrids, and Manufacturing Technology*, vol. 16, no. 4, pp. 431–436, June 1993.
- [42] L. Zhang, J. Y. Songi, J. Y. Zou, and N. Wang, “High voltage supercapacitors for energy storage devices applications,” in *Symposium on Electromagnetic Launch Technology*, June 2008, pp. 1–4.

- [43] R. L. Spyker and R. M. Nelms, "Classical equivalent circuit parameters for a double-layer capacitor," *IEEE Transactions on Aerospace and Electronic Systems*, vol. 36, no. 3, pp. 829–836, July 2000.
- [44] H. Douglas and P. Pillay, "Sizing ultracapacitors for hybrid electric vehicles," in *31st Annual Conference of IEEE Industrial Electronics Society, 2005. IECON 2005.*, Nov 2005, pp. 6 pp.–.
- [45] M. Pasquali, P. Tricoli, and C. Villante, "Testing methodologies of supercapacitors for load-leveling purposes in industrial applications," in *2011 International Conference on Clean Electrical Power (ICCEP)*, June 2011, pp. 395–399.
- [46] R. L. Spyker and R. M. Nelms, "Evaluation of double layer capacitor technologies for high power and high energy storage applications," in *Proceedings of the IECON'97 23rd International Conference on Industrial Electronics, Control, and Instrumentation (Cat. No.97CH36066)*, vol. 3, Nov 1997, pp. 1086–1091 vol.3.
- [47] P. Harrop, F. Gonzalez, J. Armstrong, and K. Greaves, "Supercapacitor/ Ultracapacitor Strategies and Emerging Applications 2013-2015," IDTechX Ltd, Technical Report, 2013.
- [48] A. Yoshida, K. Imoto, H. Yoneda, and A. Nishimo, "An electric double-layer capacitor with high capacitance and low resistance," *IEEE Transactions on Components, Hybrids, and Manufacturing Technology*, vol. 15, no. 1, pp. 133–138, Feb 1992.
- [49] M. Jayalakshmi and K. Balasubramaniam, "Simple capacitors to supercapacitors - an overview," *International Journal of Electrochemical Science*, vol. 3, pp. 1196–1216, 2008.
- [50] A. G. Pandolfo and A. F. Hollenkamp, "Carbon properties and their role in supercapacitors," *Journal of Power Sources*, pp. 11–27, 2006.
- [51] A. Yoshida, I. Tanahashi, and A. Nishino, "Aluminium collector electrodes formed by the plasma spraying method for electric double-layer capacitors," *IEEE Transactions on Components, Hybrids, and Manufacturing Technology*, vol. 11, no. 3, pp. 318–323, Sep. 1988.
- [52] K. Gunawardane, "Analysis on Supercapacitor Assisted Low Dropout (SCALDO) Regulators," Ph.D. dissertation, University of Waikato, 2014.
- [53] R. Ramachandran and F. Wang, "Electrochemical capacitor performance: Influence of aqueous electrolytes," in *Supercapacitors-Theoretical and Practical Solutions*. IntechOpen, 2017.
- [54] L. Weii and G. Yushin, "Nanostructured activated carbons from natural precursors for electrical double layer capacitors," *Nano Energy*, vol. 1, no. 4, pp. 552–565, 2012.
- [55] S. S. I. W. K. N. H. Itagaki and M. Suzuki, "Impedance analysis of electrical double layer capacitor with transmission line model," *Journal of Power Sources*, vol. 64, pp. 415–424, 2007.
- [56] L. Palma, P. Enjeti, and J. W. Howze, "An approach to improve battery run-time in mobile applications with supercapacitors," in *IEEE 34th Annual Conference on Power Electronics Specialist, 2003. PESC '03.*, vol. 2, June 2003, pp. 918–923 vol.2.
- [57] D. B. Murray and J. G. Hayes, "Cycle testing of supercapacitors for long-life robust applications," *IEEE Transactions on Power Electronics*, vol. 30, no. 5, pp. 2505–2516, May 2015.

- [58] P. Barrade, "Series connection of supercapacitors: Comparative study of solutions for the active equalization of the voltages," in *International Conference on Modeling and Simulation of Electric Machines, Converters and Systems*, June 2008, pp. 1–6.
- [59] A. Muzaffar, M. B. Ahamed, K. Deshmukh, and J. Thirumalai, "A review on recent advances in hybrid supercapacitors: Design, fabrication and applications," *Renewable and Sustainable Energy Reviews*, vol. 101, pp. 123–145, 2019.
- [60] K. Gunawardane and N. Kularatna, "Supercapacitor-Assisted Low dropout Regulator Technique: A new design approach to achieve high-efficiency linear DC-DC converters," *IET Power Electronics*, pp. 1–10, Sep 2017.
- [61] ABB, "PCS100 MV UPS technical specifications, Online at: <https://new.abb.com/ups/systems/medium-voltage-ups/pcs100-mv-ups/technical-data>, Accessed on: 2017."
- [62] N. Kularatna, "Supercapacitors improve the performance of linear power-management circuits: Unique new design options when capacitance jump from micro-farads to farads with a low equivalent series resistance," *IEEE Power Electronics Magazine*, vol. 3, no. 1, pp. 45–59, March 2016.
- [63] N. Kularatna and J. Fernando, "High current voltage regulator, US 9707430B2, US Patent," 15.03.2011.
- [64] K. Kankanmge and N. Kulatana, "Supercapacitor assisted LDO (SCALDO) techniquean extra low frequency design approach to high efficiency DC-DC converters and how it compares with the classical switched capacitor converters," in *2013 Twenty-Eighth Annual IEEE Applied Power Electronics Conference and Exposition (APEC)*, March 2013, pp. 1979–1984.
- [65] K. Kankanmge and N. Kularatna, "Improving the End-to-End Efficiency of DC-DC Converters Based on a Supercapacitor-Assisted Low-Dropout Regulator Technique," *IEEE Transactions on Industrial Electronics*, vol. 61, no. 1, pp. 223–230, Jan 2014.
- [66] N. Kularatna, *DC Power Supplies Power Management and Surge Protection for Power Electronic Systems*. CRC Press, Tylor and Francis Group, 6000 Broken Sound Parkway NW, Suite 300, Boca Raton: CRC Press, September 2012.
- [67] J. Fernando, N. Kularatna, H. Round, and S. Tálele, "Implementation of the supercapacitor-assisted surge absorber (SCASA) technique in a practical surge protector," in *IECON 2014 - 40th Annual Conference of the IEEE Industrial Electronics Society*, Oct 2014, pp. 5191–5195.
- [68] J. Fernando and N. Kularatna, "Supercapacitor assisted surge absorber (scasa) technique: Selection of supercapacitor and magnetic components," in *2014 IEEE Energy Conversion Congress and Exposition (ECCE)*, Sep. 2014, pp. 1992–1996.
- [69] —, "A supercapacitor based enhancement technique for stand-alone surge protection circuits," in *2013 IEEE International Symposium on Industrial Electronics*, May 2013, pp. 1–6.
- [70] N. Kularatna, D. A. Steyn-Ross, J. Fernando, and S. James, *Design of transient protection systems – Including the supercapacitor based design approaches for surge protectors*. Elsevier Cambridge, MA: Elsevier Cambridge, MA, December 2018.

- [71] N. Gurusingham, N. Kularatna, W. H. Round, and D. A. Steyn-Ross, "Energy-limited transient-mode fast supercapacitor charger topology," *IEEE Transactions on Power Electronics*, vol. 32, no. 2, pp. 911–914, Feb 2017.
- [72] —, "Single-stage fast supercapacitor charger with inherent power factor correction for energy-limited applications," in *IECON 2016 - 42nd Annual Conference of the IEEE Industrial Electronics Society*, Oct 2016, pp. 1412–1416.
- [73] T. Ariyaratna, D. Jayananda, N. Kularatna, and D. A. Steyn-Ross, "Potential of supercapacitors in novel power converters as semi-ideal lossless voltage droppers," in *IECON 2017 - 43rd Annual Conference of the IEEE Industrial Electronics Society*, Oct 2017, pp. 1429–1434.
- [74] N. Kularatna and D. Jayananda, "Supercapacitor Based Long Time Constant Circuits: A Unique Design Opportunity for New Power Electronic Circuit Topologies," *Industrial Electronic Magazine*, vol. to be published, 2020.
- [75] K. Kankanamge, N. Kularatna, and D. Steyn-Ross, "Laplace transform-based theoretical foundations and experimental validation: low-frequency supercapacitor circulation for efficiency improvements in linear regulators," *IET Power Electronics*, vol. 5, pp. 1785–1792, November 2012.
- [76] N. Kularatna, J. Fernando, A. Pandey, and S. James, "Surge capability testing of supercapacitor families using a lightning surge simulator," *IEEE Transactions on Industrial Electronics*, vol. 58, no. 10, pp. 4942–4949, Oct 2011.
- [77] J. Fernando, "Supercapacitor Assisted Surge Absorber (SCASA) and Supercapacitor Surge Modelling," Ph.D. dissertation, University of Waikato, 2016.
- [78] D. Jayananda, N. Kularatna, and D. A. Steyn-Ross, "Design Approach for Supercapacitor Assisted LED lighting (SCALED) technique for DC-microgrids," in *2018 IEEE International Conference on Industrial Electronics for Sustainable Energy Systems (IESES)*, Jan 2018, pp. 27–31.
- [79] —, "Powering 12-V LED luminaires with supercapacitor-based energy storage in DC-microgrid systems," in *44th Annual Conference of the IEEE Industrial Electronics Society 2018 (IECON)*, Oct 2018, pp. 1922–1927.
- [80] D. Jayananda, N. Kularatna, and D. A. Steyn-Ross, "Performance characteristics of energy-efficient led lamps leading to supercapacitor assisted led (scaled) technique for dc-microgrid applications," in *2019 IEEE International Conference on Industrial Technology (ICIT)*, Feb 2019, pp. 515–520.
- [81] —, "A validity of mppt technique using supercapacitors as energy storage devices: Example of the scaled converter technique," in *IECON 2019 - 45th Annual Conference of the IEEE Industrial Electronics Society*, vol. 1, Oct 2019, pp. 2301–2306.
- [82] D. Jayananda, N. Kularatna, and D. A. Steyn-Ross, "Supercapacitor Assisted LED lighting (SCALED) for DC-micro grids," in *2019 IEEE Third International Conference on DC Microgrids (ICDCM)*, 2019, p. to be published.
- [83] —, "Supercapacitor Assisted LED (SCALED) technique for renewable energy systems: A very low frequency design approach with short-term DC-UPS capability eliminating battery banks," *IET Renewable Power Generation Journal*, vol. to be published, 2020.

- [84] E. Star, "Lighting technologies: A guide to energy-efficient illumination."
- [85] BP, "BP Statistical Review of World Energy 2019," BP Cooperation, Tech. Rep., 2019.
- [86] EA, "Electricity in New Zealand," Electricity Authority (EA) New Zealand, Tech. Rep., 2017.
- [87] C. NZ, "LED bulb buying guide @Online," 2013.
- [88] Stardust, "Light Bulbs Online at: www.stardust.com/bulb.html."
- [89] T. H. Kim, W. Wang, and Q. Li, "Advancement in materials for energy-saving lighting devices," *Frontiers of Chemical Science and Engineering*, vol. 6, no. 1, pp. 13–26, 2012.
- [90] Diodes Incorporated, "Cost Effective LED Driver Online at: <https://www.diodes.com/design/support/led-partners/cree/>."
- [91] O. Ayan and B. E. Turkay, "Comparison of lighting technologies in residential area for energy conservation," in *2017 2nd International Conference Sustainable and Renewable Energy Engineering (ICSREE)*, May 2017, pp. 116–120.
- [92] R. Matulka and D. Wood, "The history of the light bulb Online at: energy.gov/articles/history-light-bulb," 2013.
- [93] M. N. Khan, *Understanding LED illumination*. CRC Press, 2013.
- [94] Littlefuse, "LED Design Guide," Littlefuse, Inc, Littlefuse LED design guide USA, 2016, United States.
- [95] D. Mccallum, "LED Watt Conversion and Light Replacement Guide Online at: idavidmcallen.wordpress.com/2014/05/05/led-watt-conversion-light-replacement-guide/," 05.05.2014.
- [96] N. Kularatna and D. Jayananda, "Supercapacitor-based long time-constant circuits: A unique design opportunity for new power electronic circuit topologies," *IEEE Industrial Electronics Magazine*, vol. 14, no. 2, pp. 40–56, June 2020.
- [97] D. Jayananda, N. Kularatna, and D. A. Steyn-Ross, "Supercapacitor assisted led (scaled) technique for renewable energy systems: A very low frequency design approach with short-term dc-ups capability eliminating battery banks," *IET Renewable Power Generation*, vol. 14, no. 9, pp. 1559–1570, July 2020.
- [98] V. K. Thawani and A. Reghunathan, "Fully integrated signal and power isolation – applications and benefits," Texas Instruments, Application note, 2017.
- [99] V. C. Valchev and A. Van den Bossche, *Inductors and transformers for power electronics*. CRC press, 2018.
- [100] S. Maniktala, *Switching power supply design & optimization*. McGraw-Hill, Inc., 2004.
- [101] I. Magnetics, "Ferrite core material selection guide," Magnetics Inc, Application note, 2000.
- [102] —, "Ferrite core catalogue."
- [103] L. CSUN Solar Tech Co., "Csun250-60p standard solar products."
- [104] P. Mars, "Coupling a supercapacitor with a small energy-harvesting source," *EDN-Electronic Design News*, vol. 57, no. 11, p. 39, 2012.
- [105] D. Analogue, "Printed Circuit Board (PCB) Design Issues , Online at: <https://www.analog.com/media/en/training-seminars/design-handbooks/Basic-Linear-Design/Chapter12.pdf>."

- [106] V. Spataro, "Counting squares: A method to quickly estimate pcb trace resistance," *EDN*, vol. 58, no. 6, pp. 31–+, 2013.
- [107] S. A. Chowdhury and M. Mourshed, "Off-grid electrification with solar home systems: An appraisal of the quality of components," *Renewable Energy*, vol. 97, pp. 585–598, 2016.
- [108] P. Li and B. Lehman, "Performance prediction of DC-DC converters with impedances as loads," *IEEE Transactions on Power Electronics*, vol. 19, no. 1, pp. 201–209, 2004.
- [109] Y. Panov and M. Jovanovic, "Practical issues of input/output impedance measurements in switching power supplies and application of measured data to stability analysis," in *Twentieth Annual IEEE Applied Power Electronics Conference and Exposition, 2005. APEC 2005.*, vol. 2. IEEE, 2005, pp. 1339–1345.
- [110] CharlesZhang, "Analysis and Design of Input Filter for DC-DC Circuit," Texas Instruments, Tech. Rep., November 2017.
- [111] F. Hämmerle, "Input Impedance Measurements for Stable Input-Filter Design," Omicron Lab, Tech. Rep., 2017.
- [112] M. Panizza, "Input Source Impedance and Its Effects on DC-DC Converter Performance and Characteristics ," Vicor Corporation, Tech. Rep., November 2009.
- [113] R. D. Middlebrook, "Input filter considerations in design and application of switching regulators," *IAS 76*, 1976.
- [114] M. Panizza, "Input Source Impedance and Its Effects on DC-DC Converter Performance and Characteristics ," Vicor Corporation, Tech. Rep., November 2009.
- [115] L. SunnyTech Distributor Co., *Operating Instruction Manual BC-50 DC12-24*, 2017.